This is to certify that the

dissertation entitled

Experimental Development of Microwave Cavity Plasma Reactors for Large Area and High Rate Diamond Film Deposition

presented by

Jie Zhang

has been accepted towards fulfillment
of the requirements for

Ph.D. degree in Electrical Engineering

Major professor

Date 1/12/92

DATE DUE	DATE DUE	DATE DUE
SEP 23 1994	MAR 2 3 2006	
JAN 11 1996		
SEP 23 1997		
MAY 27 1999		
NOV 1 1 2000		
JAN 1 0 2011		

EXPERIMENTAL DEVELOPMENT OF MICROWAVE CAVITY PLASMA REACTORS FOR LARGE AREA AND HIGH RATE DIAMOND FILM DEPOSITION

By

Jie Zhang

A DISSERTATION

Submitted to

Michigan State University

in partial fulfillment of the requirements

for the degree of

DOCTOR OF PHILOSOPHY

Department of Electrical Engineering

1993

ABSTRACT

EXPERIMENTAL DEVELOPMENT OF
MICROWAVE CAVITY PLASMA REACTORS FOR
LARGE AREA AND HIGH RATE DIAMOND FILM DEPOSITION

By

Jie Zhang

Diamond, with its unique mechanical, thermal, chemical, optical and electrical properties, is an attractive material in applications ranging from wear-resistant coatings for mechanical and optical components to substrates for advanced semiconductor devices. This research concerns the experimental investigation and development of microwave cavity plasma reactors for large area and high rate diamond film deposition.

The research and development have lead to the successful creation of a new improved prototype reactor. Diamond films with uniformities better than 2% have been deposited on 3" and 4" silicon wafers with this prototype reactor. The linear growth rates obtained are 0.89 μm/hour on 2" silicon wafers, 0.67 μm/hour on 3" silicon wafers and 0.43 μm/hour on 4" silicon wafers. The performance "figures of merit" were developed to quantitatively compare diamond film deposition reactors in terms of linear growth rate, weight gain rate, deposition area, energy efficiency, gas flow efficiency and carbon conversion efficiency. Three generations of microwave cavity plasma reactors have been investigated and/or

developed for diamond film deposition over larger substrate areas. The new prototype reactor employs an end feed coupling concept which enables the reactor to accept high microwave power input (from 1.5 kW to 4.5 kW) and create discharges up to 12.5 cm in diameter. Three generations of microwave cavity jet reactors have also been developed and/or designed. These reactors have the potential to deposit diamond films with higher growth rates. A method to obtain the operational characteristics of the microwave cavity plasma reactors was developed. The reactor was characterized by a set of input, internal and output experimental parameters. The relationship between the internal and input experimental parameters was established to locate the required experimental conditions when diamond films with desired properties, such as film thickness, morphology, and uniformity, etc. are deposited. The diamond films deposited in the prototype reactor were investigated with respect to their growth rate and morphology as the input experimental parameters were varied. The electric fields in the reactor were also measured to develop a better understanding of the electromagnetic field/plasma interactions during the diamond film deposition process. It was found that the tangential component of the electric field is the main discharge excitation field.

To my parents

Zu-Di Zhang and Xin-Xuan Wu

ACKNOWLEDGMENTS

The author wishes to thank Dr. Jes Asmussen, Jr. for his encouragement, guidance and support throughout this research. Special thanks is extended to Dr. Donnie Reinhard, Dr. Timothy Grotjohn and Dr. Chow Ling Chang of Norton for their valuable discussions. Additional thanks is given to Mr. Jeron Campbell for his experimental laboratory help and to Dr. Aslam for his comments on the manuscript.

This research was supported in part by grants from Norton, Corp., Wavemat, Corp., and Michigan Research Excellence fund.

TABLE OF CONTENTS

Chapter Three
The Microwave-Cavity Plasma Reactors (MCPR)

Chapter Four
The Microwave-Cavity Jet Reactors (MCJR)

Chapter Five
Microwave Electric Fields in the MCPR

Chapter Six
Diamond Film Deposition in the MCPR

Chapter Seven
Conclusions and Recommendations

LIST OF TABLES

LIST OF FIGURES

CHAPTER ONE

INTRODUCTION

1.1 Introduction

The beauty, hardness and rarity of diamond have made it an object of fascination for nearly as long as recorded history. The mechanical, electrical, optical, chemical, and thermal properties of diamond make it attractive in applications ranging from wear-resistant coatings for mechanical and optical components to substrates for advanced semiconductor devices. Ever since Tennant discovered that diamond is simply made of carbon in 1797[1], synthesis of diamond has long been a goal of numerous research efforts of both individuals and organizations.

The diamond-cubic lattice consists of two interpenetrating face-centered cubic lattices, displaced by one quarter of the cube diagonal. Each carbon atom is tetrahedrally coordinated, making strong, directed σ bonds to its neighbors using hybrid sp^3 atomic orbitals. The lattice can also be visualized as planes of six-membered saturated carbon stacked in an ABCABC... sequence along <111> directions.[2]

Figure 1.1 summarizes the diamond properties and its engineering applications.[3]

Diamond is most noted for its mechanical hardness which gives it great promise for a wide range of mechanical coating applications where

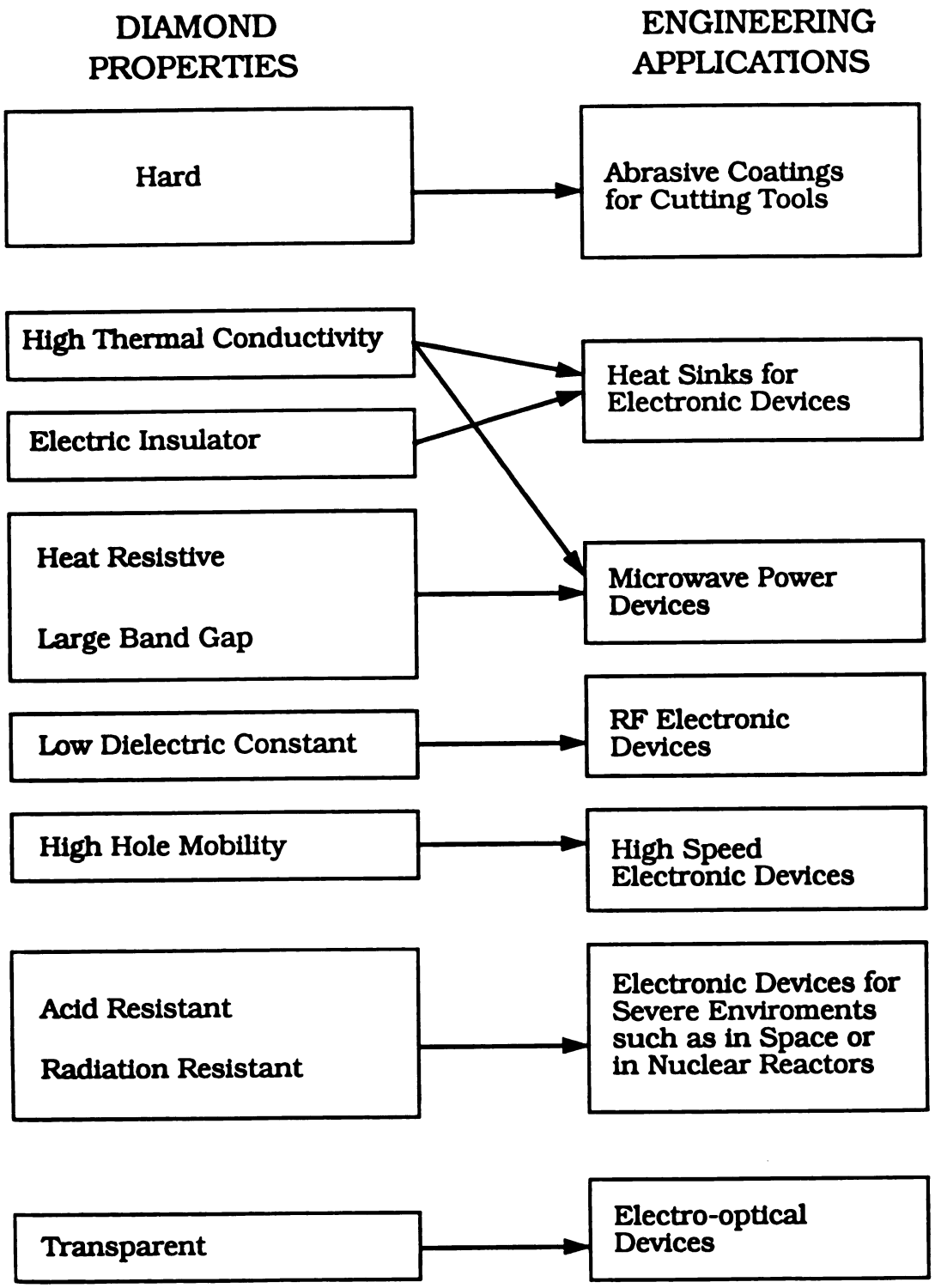

Figure 1.1 Diamond Properties and Its Engineering Applications [3]

resistance to abrasive phenomenon is desired. Diamond coated cutting tools will provide significant productivity improvements for machining super-hard materials, nonferrous refractory metals and superalloys.

At room temperature and above, the thermal conductivity of diamond is greater than that of any other known material, including copper and silver. Thermal transport in diamond is accomplished by phonon mechanisms, whereas in a metal, thermal conduction is by electron transport. Diamond is unique in that no other known material is simultaneously a superb thermal conductor, optically transparent and electrically insulating. With this combination of properties, diamond will be a excellent material for many engineering systems. Diamond's relatively low thermal expansion coefficient makes it ideal for microelectronic circuit boards and semiconductor substrates since large thermal expansion substrates create micro-cracks in the device circuitry resulting in open circuits in high-power, high-temperature electronic applications.

Diamond offers significant promises for high power and high temperature semiconductor device applications. The dielectric breakdown electric field is $1x10^7$volts/m, approximately 50 times that of conventional semiconductors such as GaAs. The theoretical power handling capability of diamond is a factor of 2500 greater than silicon. The bandgap of diamond is 5.45 eV which is more than three times that of conventional semiconductor such as Si and GaAs. Diamond's thermal conductivity is approximately five times that of copper and nearly 20 times that of silicon. Diamond's dielectric constant is about half that of GaAs. Diamond semiconductors demonstrate approximately half the capacitive loading of other conventional semiconductors at any given

frequency. Diamond's saturated carrier velocity is 2.7 times that of GaAs. The saturated carrier velocity of diamond is greater than the peak velocity of GaAs.

Ultra-pure diamond probably has the widest electromagnetic band-pass of any known solid material. Diamond is composed of a homogeneous, tetrahedral network of covalently bonded carbon. Diamond's cubic crystal structure makes diamond optically isotropic. The fact that diamond is composed of a single element means that pure diamond has no fundamental infrared absorption modes. Diamond windows can be used in conjunction with optical detection devices for detection of UV, visible and IR radiation.<3>

In 1955, Bundy and co-workers succeeded in the reproducible synthesis of diamond<4> with a molten transition metal solvent-catalyst at pressures and temperatures where diamond is the thermodynamically stable phase of carbon.

Diamond growth at low pressures where graphite is the stable carbon phase can be traced back to W. G. Eversole<5>, Angus et al.<6> and Deryaguin et al.<7>, but the low growth rate (less than 0.1 micrometer per hour) was not of practical commercial importance, and thus at that time it prevented worldwide interest in low pressure diamond growth. The breakthrough in the synthesis of diamond at low pressures came in the late 1970's and early 1980's, when a group of Soviet researchers<8> and Japanese researchers<9> started publishing a series of research papers on diamond film growth at higher growth rates (several micrometers per hour) from hydrocarbon-hydrogen gas mixtures. Since then, great interest and various techniques have been developed for diamond film growth at low pressures.

applications. The success of this dissertation depended upon these earlier experimental and theoretical studies of microwave discharges inside microwave cavities. The theoretical and experimental knowledge used to design, build and understand the diamond film deposition reactors presented in this dissertation relied on knowledge obtained in these earlier experiments.

The research described in this dissertation reflects co-operation with Norton Company and Wavemat, Inc. The first microwave cavity plasma reactor (MCPR) developed for diamond film deposition was designed and built for Norton Co. at MSU by J. Asmussen in 1986. It was experimentally evaluated at Norton Co. in Nov./Dec. of 1987 and immediately diamond films were successfully deposited. This MSU owned and patented technology was exclusively licenced to Wavemat, Inc./ Norton Co., and Wavemat, Inc. then developed a commercial version of this reactor. One of these reactors was put into operation at MSU in 1988. Continued co-operation with Norton Company and Wavemat, Inc. has contributed to the success of the research described in this dissertation.

The research conducted for this dissertation experimentally investigated and developed two different groups of advanced reactors that produce microwave plasma discharges for diamond film growth. The first group of reactors are the microwave cavity plasma reactors. The second group of reactors are the microwave plasma jet reactors. The research described here is primarily experimental. Since there is no theoretical model for the plasma assisted deposition of diamond films, the improvement of reactors was carried out through many experiments. The final experimental designs were achieved through numerous

experimental iterations and by the investigator's best intuition of the deposition process. The results summarized in this dissertation are the results of at least five hundred separate experiments and of thousands of hours of actual experimental time.

This dissertation summarizes the experimental research and development that has lead to the successful creation of a working prototype of an improved microwave cavity plasma reactor concept. This type of reactor is already being used to deposit diamond films over larger surface areas at Norton Co.. It has made an impact on the commercial production of low pressure diamond coated commercial products by increasing the productivity by more than three times over earlier microwave diamond film deposition reactors. The reactor developments described in this dissertation were continuously monitored by Wavemat, Inc. and Norton Co. and as new reactor concepts were developed and tested at MSU, the successful concepts were almost immediately incorporated into commercial diamond film deposition reactor designs. Some of the research described in this dissertation has already been published in scientific publications and international scientific conferences<14-16> and in patent disclosures<17>. However, much of the results on diamond film deposition on three and four inch silicon wafers using the advanced reactor concept has not been submitted for publication. It is expected that in the near future, these results will also be published.

Diamond films were deposited under various experimental conditions and characterized with respect to the film quality, growth rate and uniformity. Diamond Film quality was characterized by Scanning Electron Microscopy and Raman Spectroscopy. Diamond film growth rate

was characterized by weight gain and Scanning Electron Microscopy. Diamond film uniformity was characterized by Laser Interference/ Reflection Measurement. Electromagnetic field pattern measurements were conducted to develop better understanding of the electromagnetic field/plasma interactions.

1.4 Dissertation Outline

This dissertation is organized as follows. Chapter two presents a generic low pressure diamond deposition reactor concept and briefly reviews the state-of-the-art of other diamond film deposition reactors. The performance of these reactors is compared with respect to the diamond film quality, growth rate, growth efficiency, surface area, and uniformity whenever possible. Chapter three describes a series of microwave cavity plasma reactors that were developed and tested as part of this dissertation research. Chapter four summaries the experimental development of three generations of microwave plasma jet reactors for diamond film growth at high growth rates. Chapter five presents an investigation of the electromagnetic filed patterns in the microwave cavity plasma reactor while operating under diamond film deposition conditions. The purpose of this study was to develop a better understanding of the electromagnetic field/plasma interactions during film deposition process. Chapter six presents a new method that experimentally characterizes the operational characteristics of prototype reactors. Parametric studies of diamond film deposition on three and four inch silicon wafers conducted in the new prototype reactor were also described. Chapter seven presents the conclusions and some

speculations on future research and development of diamond film deposition using microwave technology.

CHAPTER TWO

DIAMOND FILM DEPOSITION REACTORS: A REVIEW

2.1 Introduction

2.1.1 A Generic Diamond Film Deposition Reactor

A generic reactor for low pressure diamond film growth by chemical vapor deposition can be illustrated by the diagram displayed in Figure 2.1. Here, the reactive gas input is usually a mixture of hydrogen (H_2), hydrocarbon (CH_4, C_2H_2, etc.) and oxygen or oxides (O_2, CO, CO_2, etc.), etc. The energy input is provided by electrical (DC, low and/or high frequency ac) energy and/or chemical reaction energy. With sufficient energy input, the input reactive gas mixture is dissociated, creating a mixture of dissociated charged species, electrons and neutral gases. A substrate is placed close to the dissociated reactive gas species and its temperature and/or electrical bias may be controlled by external temperature controller and/or dc or RF power supply. With proper choice of input reactive gas mixture, energy input, substrate, substrate temperature and/or bias, etc., a diamond film is deposited on the substrate.

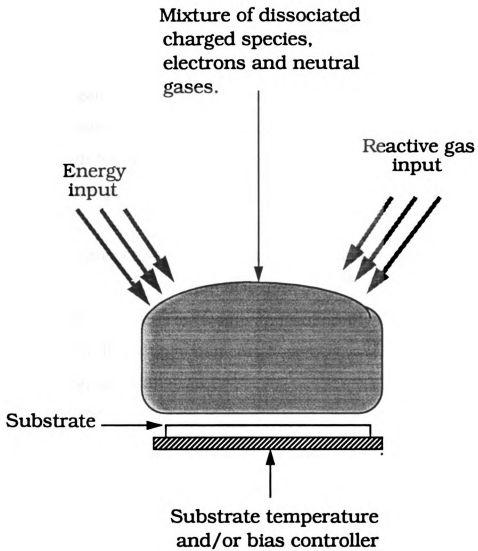

Figure 2.1 A Generic Diamond Film Deposition Reactor

2.1.2 Reactor Categorization

The reactors most frequently used in low pressure diamond film deposition can be divided into five major categories:

(1) Thermally activated (filament) chemical vapor deposition (CVD);

(2) Direct current (DC) discharge assisted CVD;

(3) Combustion flame;

(4) High frequency (RF or microwave) discharge assisted CVD;

(5) Other and hybrid reactors.

2.1.3 "Figures of Merit" of Reactor Performance

In order to quantitatively compare the performance of the reactors, it is necessary to define a set of performance "figures of merit". In this literature review, the following performance "figures of merit" are defined:

(1) Linear growth rate (μm/hour);

It is defined as the diamond film thickness (μm) gain per unit time (hour).

(2) Deposition area A_d (cm^2);

It is defined as the area over which diamond film is deposited.

(3) Weight gain u (mg/hour);

It is defined as the diamond film weight gain (mg) per unit time (hour). Since most literature just report linear growth rate, weight gain is usually calculated from the reported linear growth rate, deposition area and the density of diamond, 3.51 g/cm^3.

(4) Uniformity;

It is defined as the film thickness variation divided by the average film thickness over the deposition area.

(5) Growth Efficiency

(i) Weight gain/power input (mg/kW-hr);

It is defined as the diamond film weight gain (mg) per energy input (kW-hr).

(ii) Weight gain/total flow input (mg/liter);

It is defined as the diamond film weight gain (mg) per total gas input (liters). The total flow input used here is the sum of all input gas flow rates.

(iii) Carbon Conversion Efficiency (%):

It is defined as the percentage of carbon atoms in the input gases that are converted into the diamond film.

2.1.4 Notes on Literature Review

The review described in the following sections is based on experimental data that is published in the open literature. Since diamond film deposition has been used in industrial applications, it is possible that most of the state-of-art deposition information is not available in the open literature.

The performance "figures of merit" described in the following sections are mostly estimated and/or calculated from the best data available in the literature. There are limiting factors on the accuracies of the performance "figures of merit". This is due to that limited data is available in the literature concerning growth rate, deposition area and

uniformity. It is also often not clear how these data are obtained.

Film linear growth rate, for example, is measured differently by different research groups. Some groups use the crystal growth rate (1) as the linear growth rate, i.e., the size of an individual crystal divided by growth time. Some groups determine the film thickness from SEM photographs (2) of the cross-sectional area of a film. The linear growth rate is then obtained from dividing the film thickness by the deposition time. Some groups use weight gain (3) of a substrate after a deposition process along with the deposition area and the density of diamond, $3.51 mg/cm^3$, to determine the film thickness. The linear growth rate is then obtained from dividing the film thickness by the deposition time.

The author believes that the first method, which is frequently used in earlier literature, is not an accurate measure of linear growth rate of a film since it is often possible to grow large individual crystals without forming a complete continuous film. The second method can be an accurate method if the SEM instruments are calibrated and the specimen are photographed directly onto the cross-section. The third method is a simple method and can be an accurate method of evaluating the film thickness provided the deposited film is uniform diamond film. The methods of linear growth rate measurement are indicated whenever available.

Finally in this review, diamond film deposition area is often estimated since film uniformity data are mostly not available in the reviewed literature.

2.2 A Review of Diamond Film Deposition Reactors

2.2.1 Thermally Activated CVD Reactor

A typical thermally activated (hot filament) diamond film deposition reactor is shown in Figure 2.2.[18,19] As shown, in this reactor, the feed gas, which is a mixture of hydrocarbon and hydrogen, dissociates when it is heated by a hot filament. The hot filament is heated by an electric current. The substrate is placed near the hot filament and diamond film is formed on the substrate when the hot dissociated gas species react on its surface.

Variations of this reactor have also been used for diamond film growth. For example, substrate bias and/or substrate heater have been utilized to enhance the growth rate and uniformity of the deposited diamond film[20]. Multiple filaments have been used to scale up the deposition to 4 inch substrate.[21]

Diamond film deposition experiments have been conducted under the following typical experimental conditions [22]: substrate = Si, H_2 flow rate = 100 sccm, C_2H_2 flow rate = 0.5 sccm, CO flow rate = 12 sccm, gas pressure = 50 Torr, total flow rate =100 sccm, temperature of deposition chamber = 890 ^oC, filament temperature = 2400 ^oC, filament voltage = 30 V, filament current = 28 A, heater voltage = 70 V, heater current = 6.5 A.

The "figures of merit" available in the literature are:[22]

(1) Linear growth rate (μm/hour) = 0.6;

(2) Deposition area (cm^2) ~ 6.4;

(3) Weight gain (mg/hour) ~ 1.35;

(3) Uniformity = n/a;

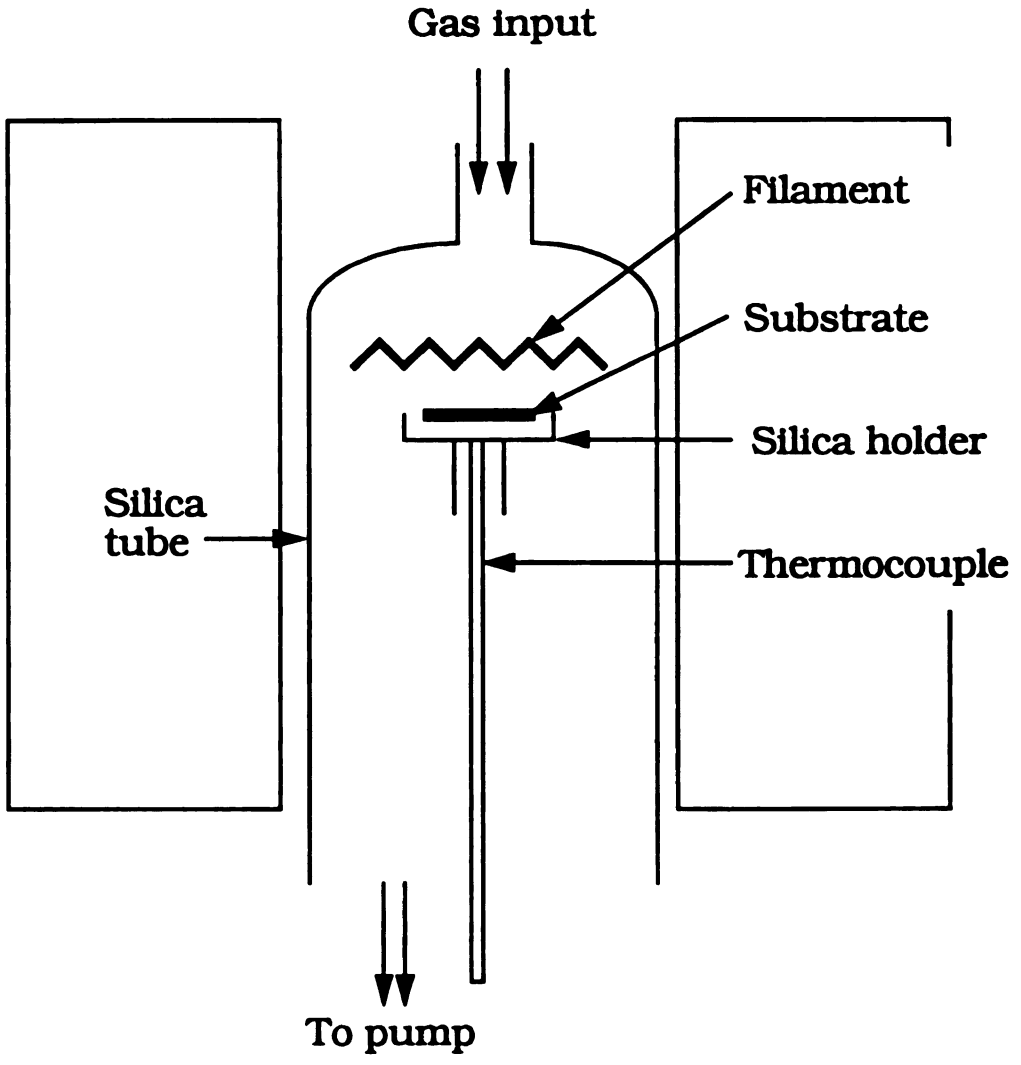

Figure 2.2 Thermally Activated CVD Reactor [18,19]

(4) Growth Efficiencies

(i) Growth rate/power input (mg/kW-hr) ~ 1.04;

(ii) Growth rate/gas input (mg/liter) ~ 0.2;

(iii) Carbon conversion efficiency (%) ~0.32.

The thermally activated diamond film deposition reactor is easy to construct, operate, and scale up. It faces the problem of filament erosion and breakage during the diamond film deposition process.

2.2.2 Direct Current Discharge CVD Reactor

2.2.2.1. Direct Current Discharge Reactor

A schematic drawing of a DC discharge diamond film deposition reactor is shown in Figure 2.3. <23,24> As shown, in this reactor, the input gas which is a mixture of hydrocarbon and hydrogen is dissociated by a DC voltage across the anode and cathode. A DC power supply is used to sustain the DC discharge. The substrate is mounted on the anode and both the anode and cathode can be water cooled. Diamond film is formed on the substrate when the dissociated gas species react on its surface.

Typical experiments have been conducted in this reactor under the following experimental conditions: substrate = Si and Al_2O_3, gas mixture = H_2 and CH_4, CH_4/H_2 = 0.3 - 4%, pressure = over 200 Torr, total flow rate = 20 sccm. anode-cathode separation = 2 cm, substrate temperature = 800 - 850 ^oC, discharge voltage = 1 kV, discharge current = 4A/cm^2, substrate area = 0.25 cm^2.

Notes on reactor operation: The initial stages of diamond particle

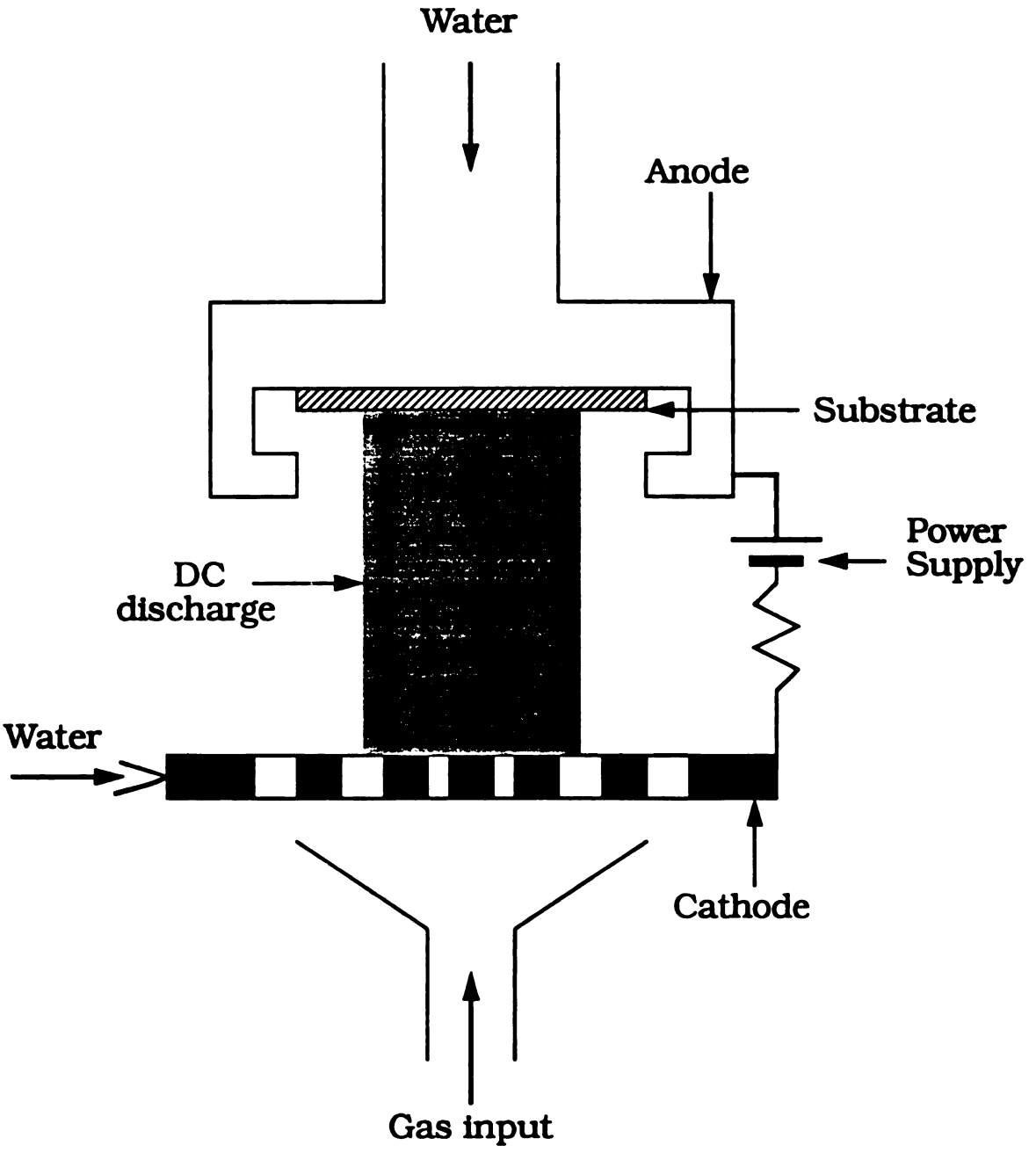

Figure 2.3 DC Discharge Reactor [23,24]

growth at a substrate temperature of 800 °C and CH_4 concentration of 2% indicate that the initial nucleus density of diamond on the mirror polished Si (111) surface is about $10^8/cm^2$. This nucleation density is as large as that on the surface scratched by diamond polishing powder (0.5 μm in diameter). After 30-min of deposition, a continuous film can be obtained in both cases. The growth rate of the films is about 20 μm/hr. Diamond thin films are also formed on Al_2O_3 substrate without surface treatment.<23,24>

Diamond thin films can be obtained at a substrate temperature higher than 600 °C. At a substrate temperature below 600 °C, amorphous carbon films were obtained. If the substrate is mounted on the cathode, the growth of diamond can not be detected and amorphous or graphitic carbon is found over a wide range of experimental conditions.

The "figures of merit" available are:

(1) Linear growth rate (μm/hour) ~ 20;

(2) Deposition area (cm^2) ~ 0.25;

(3) Weight gain (mg/hour) ~ 1.76;

(3) Uniformity = n/a;

(4) Growth Efficiencies

  (i) Growth rate/power input (mg/kW-hr) ~ 0.56;

  (ii) Growth rate/gas input (mg/liter) ~ 1.47;

  (iii) Carbon conversion efficiency (%) ~ 13.7.

2.2.2.2. Direct Current Discharge Jet Reactor

The schematic drawing of a DC discharge jet diamond film reactor is shown in Figure 2.4.[25] As shown, in this reactor, the input gas which is a mixture of Ar, H_2 and CH_4 is dissociated by a DC voltage V_d across the electrodes. A high temperature discharge jet is created and sustained by a DC power supply. The substrate is mounted down stream of the jet stream on a water cooled substrate stage. Diamond film is formed on the substrate when the dissociated gas species react on its surface. The bias voltage V_b is used to enhance the film growth rate.

The typical experimental conditions are: Ar flow rate = 30 l/min, H_2 flow rate = 10 l/min, CH_4 flow rate = 1 l/min, pressure = 140 Torr, discharge voltage = 70 - 76 V, discharge current = 133 - 150 A, bias voltage = 0 - 500 V, bias current = 0 - 5 A, substrate = Mo plate of 20 mm in diameter, distance between the substrate and nozzle = 57 - 102 mm, substrate temperature = 700 - 1100 ^{o}C, deposition time = 10 min, substrate pretreatment = scratched with 5 - 10 μm particle size diamond paste for about 5 min.

Notes on reactor operation: The deposition rate was increased by more than twofold when positive bias was applied to the substrate. The deposition area was also increased but the uniformity of film thickness did not improve. The maximum growth rate obtained was 900 μm/hour.

"Figures of merit" that are available are:

(1) Linear growth rate (μm/hour) ~ 900;

(2) Deposition area (cm^2) ~ 2;

(3) Weight gain (mg/hour) ~ 632;

(3) Uniformity = n/a;

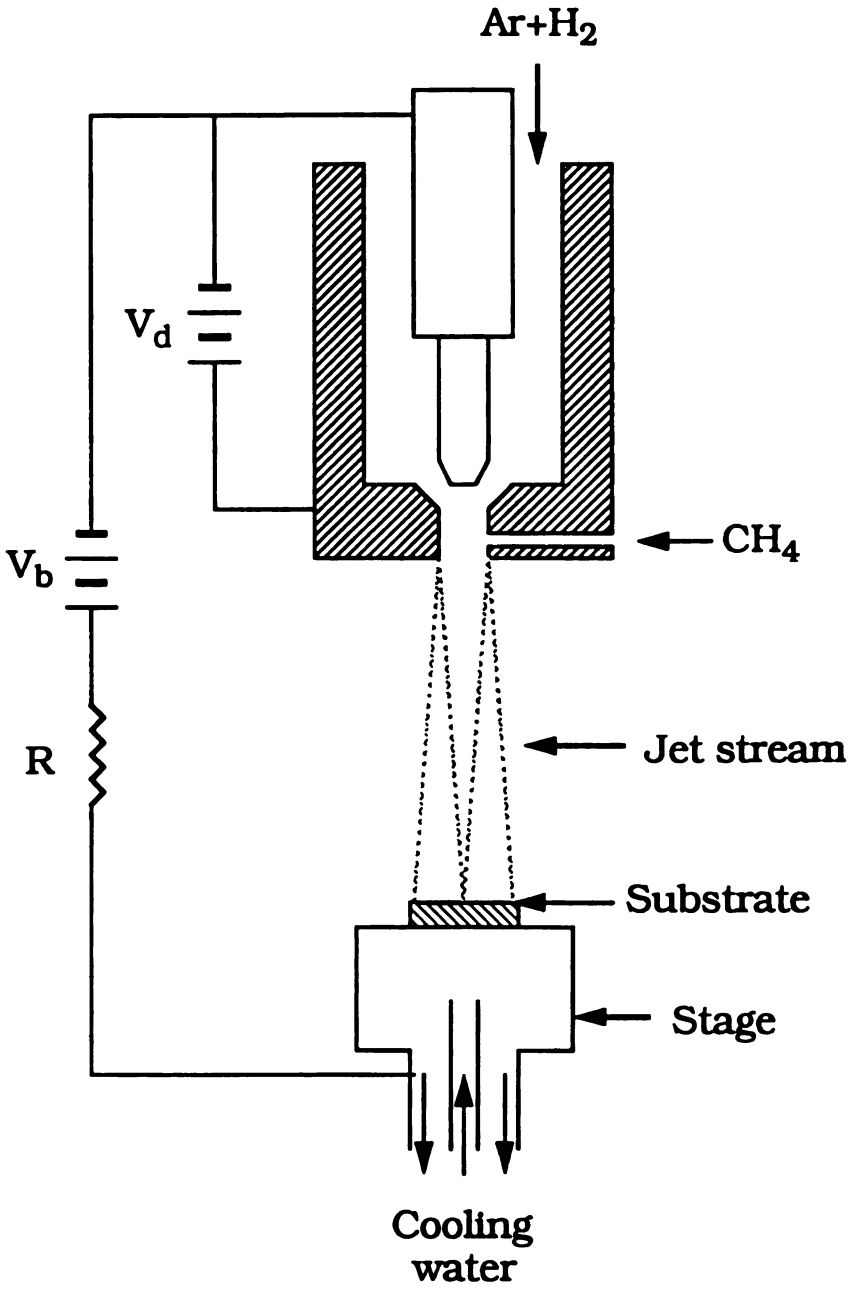

Figure 2.4 DC Discharge Jet Reactor [25]

(4) Growth Efficiencies

(i) Growth rate/power input (mg/kW-hr) ~ 57;

(ii) Growth rate/gas input (mg/liter) ~ 0.26;

(iii) Carbon conversion efficiency (%) ~ 1.97.

2.2.3 Combustion Flame Reactor

The schematic drawing of a typical combustion flame diamond film deposition reactor is shown in Figure 2.5.<26> As shown, in this reactor, the feed gas which is a mixture of acetylene (C_2H_2) and oxygen dissociates by the chemical reaction energy of the gas mixture after a flame is ignited. The combustion flame is self-sustained by the energy released by the chemical reaction of the gas mixture at high temperature. The substrate is placed in the C_2H_2 feather region (see insert in Figure 2.5) and diamond film is formed on the substrate when the dissociated gas species react on its surface.

Typical experimental conditions are as follows<27>: substrate location = in the C_2H_2 feather region of the flame, substrate temperature = 650 - 1050 ^{o}C, gas flow ratio R = O_2/C_2H_2 = 0.9 - 1.2, total flow rate = 2 slm (nozzle dependent). Under these experimental conditions, the feather area is ~ 6 mm in diameter, the growth rate is ~ 60 μm/hour.

The "figures of merit" that are available are:<27>

(1) Linear growth rate (μm/hour) ~ 60;

(2) Deposition area (cm^2) ~ 0.28;

(3) Weight gain (mg/hour) ~ 5.9;

(3) Uniformity = N/A;

(4) Growth Efficiencies

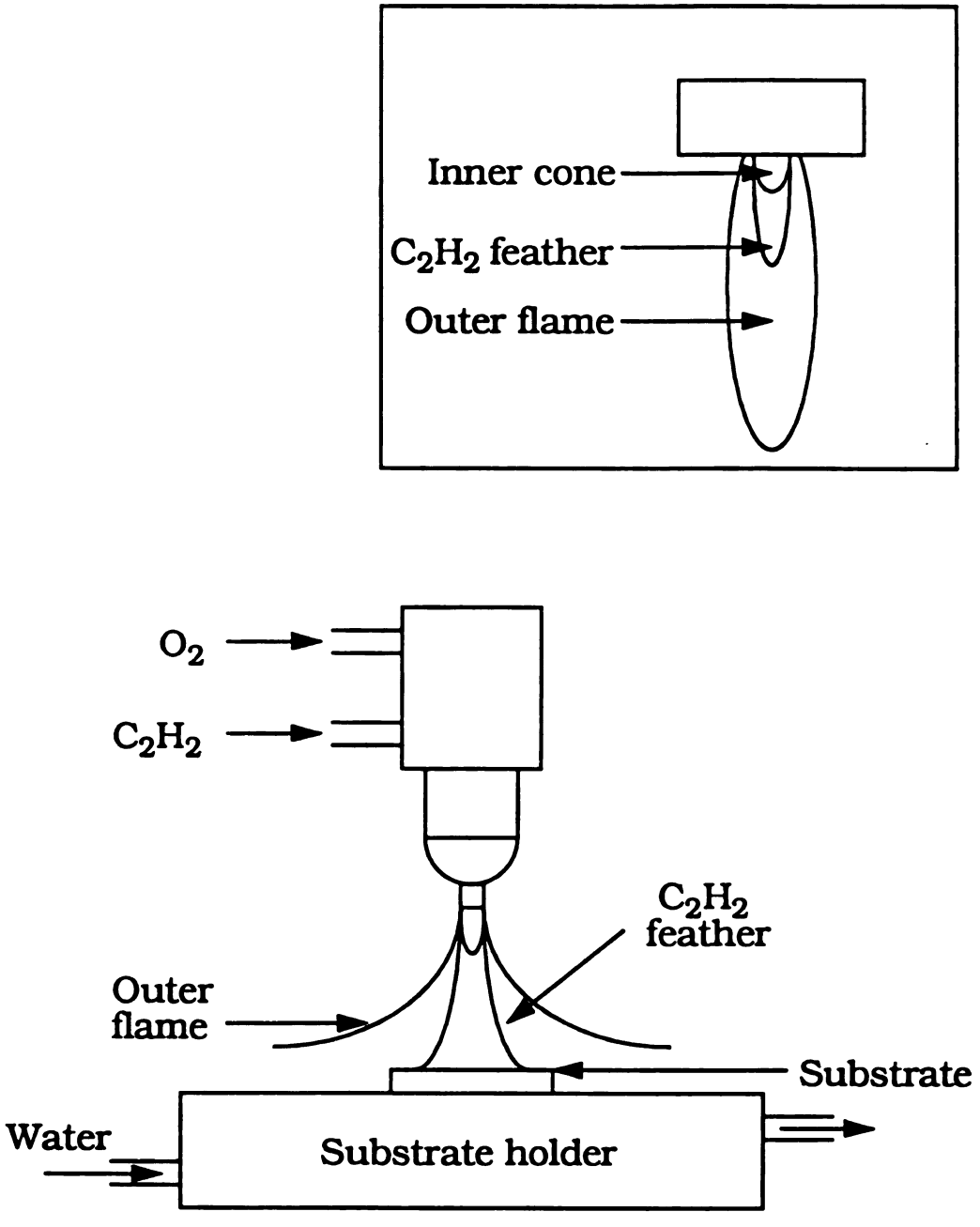

Figure 2.5 Combustion Flame Reactor [26]

(i) Growth rate/power input (mg/kW-hr)= N/A;

(ii) Growth rate/gas input (mg/liter) ~ 0.049;

(iii) Carbon conversion efficiency (%) ~ 0.009

2.2.4 Radio Frequency (RF) Plasma CVD Reactors

2.2.4.1 RF Glow Discharge Reactor

Figure 2.6 displays the schematic drawing a RF glow discharge diamond film deposition reactor<28>. As shown, in this reactor, the input gas, which is a mixture of hydrocarbon and hydrogen, is dissociated by a radio frequency (RF) energy matched into reaction chamber through an impedance matching network. A 13.56 MHz RF power supply is used to sustain the RF discharge. The substrate is placed in the middle of the coil. Diamond film is formed on the substrate when the dissociated gas species react on its surface.

Typical experimental conditions are as follows: substrate = Si or Mo or SiO_2, input gas mixture CH_4/H_2 = 0.2 - 1%, total flow rate ~ 50 sccm, pressure = 3.8 - 22.8 Torr, RF power = 0.5 ~ 1 kW, substrate temperature ~ 950 ^oC, quartz tube geometry = 3 cm in diameter and 1 m long, coil geometry = 4 cm in diameter and 13 cm long, coil material = 13 turns of 6.4 mm diameter copper tube,

Notes on the reactor operation: The substrate temperature could not be determined accurately at low temperatures due to radiation from the discharge. Since there is no external substrate heating, the temperatures of the substrates were raised by inductive heating and energy transfer from the discharge. It is necessary to use high RF power

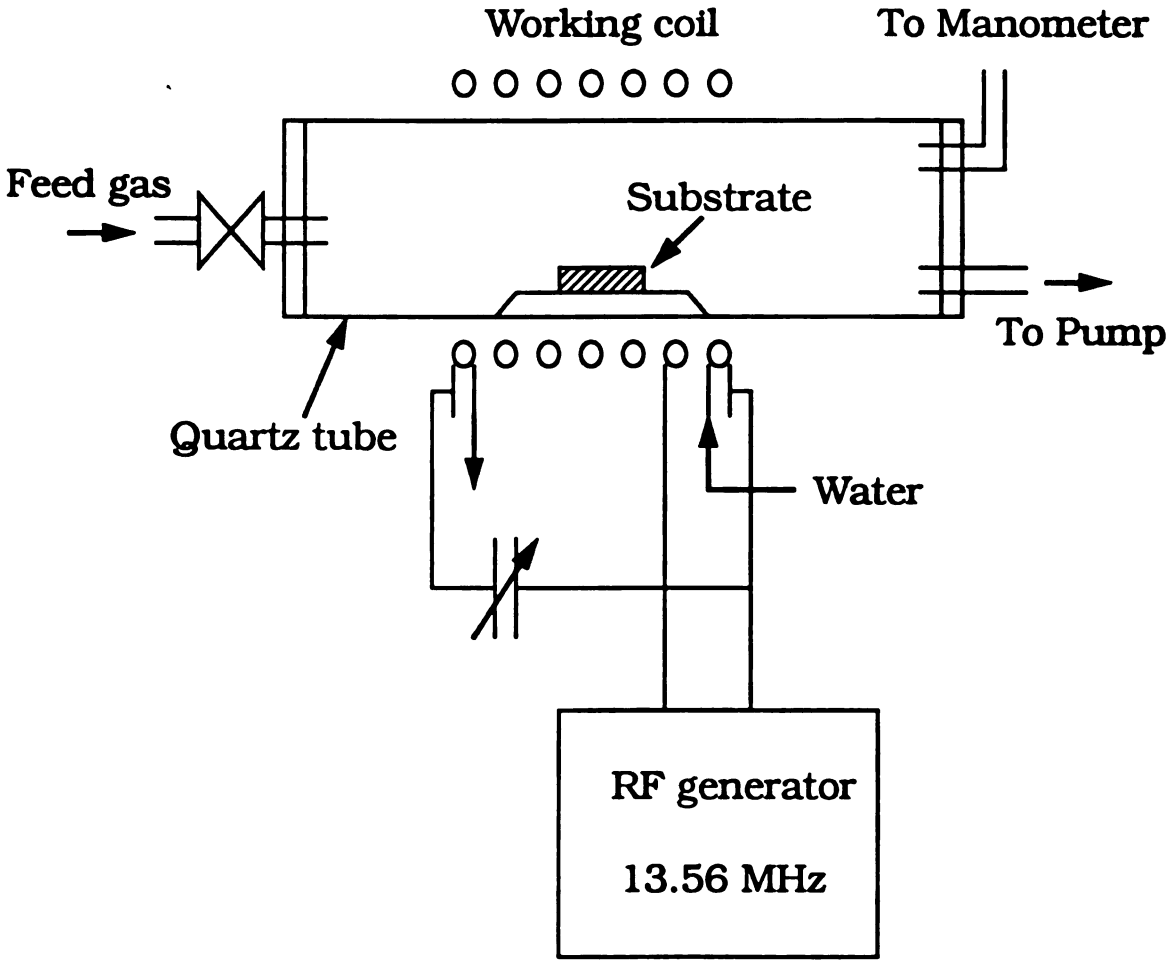

Figure 2.6 RF Glow Discharge Reactor [28]

to create the discharge and the tube wall may be sputtered at low pressures in this reactor.

The "figures of merit" are not obtainable from the literature.

2.2.4.2 RF Induction Thermal Plasma Reactor

The schematic drawing of a RF induction thermal plasma diamond film reactor is displayed in Figure 2.7.[29] As shown, in this reactor, the input gas which is a mixture of Ar, H_2 and CH_4 is dissociated by a radio frequency (RF) energy matched into reaction chamber through an impedance matching network. A 4 MHz 60 kW RF power supply is used to sustain the RF thermal plasma. The substrate is placed within or at the end of the thermal plasma on a water cooled holder. Diamond film is formed on the substrate when the dissociated gas species react on its surface.

Typical experimental conditions are as follows: chamber inside diameter ~ 45 mm, substrate = 20 mm diameter Mo plate, sheath (S) gas flow rate = 35 l/m Ar + 12 l/m H_2, plasma (P) gas flow rate = 17 l/m Ar, carrier (C) gas flow rate = 8 l/m Ar, reactant gas flow rate = 0.1 - 1.2 l/m CH_4, pressure = 760 Torr, RF power = 60 kW, substrate temperature = N/A, substrate pre-treatment = diamond paste polished.

Notes on reactor operation: Pyrometric measurement of substrate temperature was not possible because of the high reflection of plasma emission from the substrate.

The film thickness was not uniform. One of the films was 12 μm thick near the edge and 6 μm thick at the center of the substrate. The growth rate is 60 μm/hour for films with well defined crystal planes. The

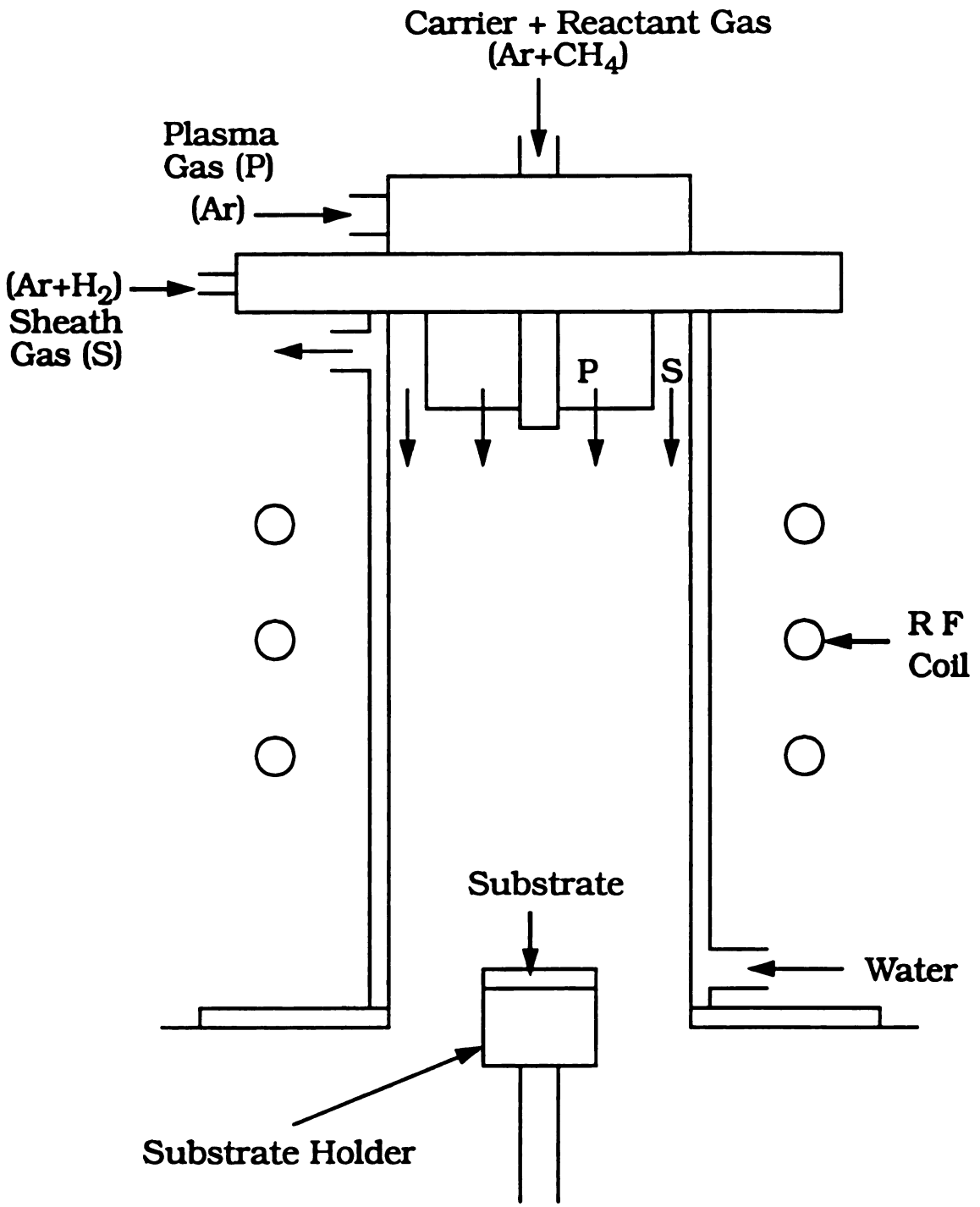

Figure 2.7 RF Induction Thermal Plasma Reactor [29]

essential condition for diamond growth in the present thermal plasma CVD seems to be the cooling of a substrate.

The "figures of merit" that are available are as follows:

(1) Linear growth rate (μm/hour) ~ 60;

(2) Deposition area (cm^2) ~ 3;

(3) Weight gain (mg/hour) ~ 63;

(3) Uniformity ~ 50%;

(4) Growth Efficiencies

  (i) Growth rate/power input (mg/kW-hr) ~ 1.05;

  (ii) Growth rate/gas input (mg/liter) ~ 0.014;

  (iii) Carbon conversion efficiency (%) ~ 0.2

This reactor has the advantage of high growth rate. It has the following disadvantages. Due to the high gas temperature of the thermal plasma, control of substrate temperature is difficult. The films obtained have poor adhesion to the substrates and the film thickness is not uniform.

2.2.5 Microwave Plasma Enhanced CVD Reactors

2.2.5.1 Introduction

Diamond film deposition using microwave plasma has been achieved by several different reactors. Since this dissertation concerns with the development of microwave plasma reactors for the deposition of diamond film, variations of microwave reactors are reviewed in more detail.

2.2.5.2 Tubular Microwave Reactor

A schematic drawing of a typical tubular microwave diamond film deposition reactor is shown in Figure 2.8[<30>]. As shown, in this reactor, the input gas which is a mixture of hydrocarbon and hydrogen is dissociated by the microwave energy coupled into the quartz tube through a set of waveguides, power monitors and tuners. The plasma was adjusted to be at the center of the quartz tube. Microwave power generated by a magnetron is used to sustain the microwave discharge. The substrate is place in the middle of the quartz tube. Diamond film is formed on the substrate when the dissociated gas species react on its surface.

Typical diamond film deposition conditions are as follows: quartz tube diameter = 40 mm, substrate = silicon wafer, gas mixture CH_4/H_2 = 1 - 3%, total flow rate = N/A, pressure = 7.6 - 60.8 Torr, microwave power = 300 - 700 W, substrate temperature ~ 800 - 1000 ^{o}C.

The "figures of merit" that are available are as follows:

(1) Linear growth rate (μm/hour) ~ 3* μm/hour;

(2) Deposition area (cm^2) ~ 3 - 6;

(3) Weight gain (mg/hour) ~ 3 - 6;

(3) Uniformity = n/a;

(4) Growth Efficiencies

  (i) Growth rate/power input (mg/kW-hr) ~ 4.3 - 8.6;

  (ii) Growth rate/gas input (mg/liter) = n/a;

  (iii) Carbon conversion efficiency (%) = n/a.

* It is noted that, in the paper, the author showed the SEM photograph of a film deposited in the reactor for 3 hours. The film

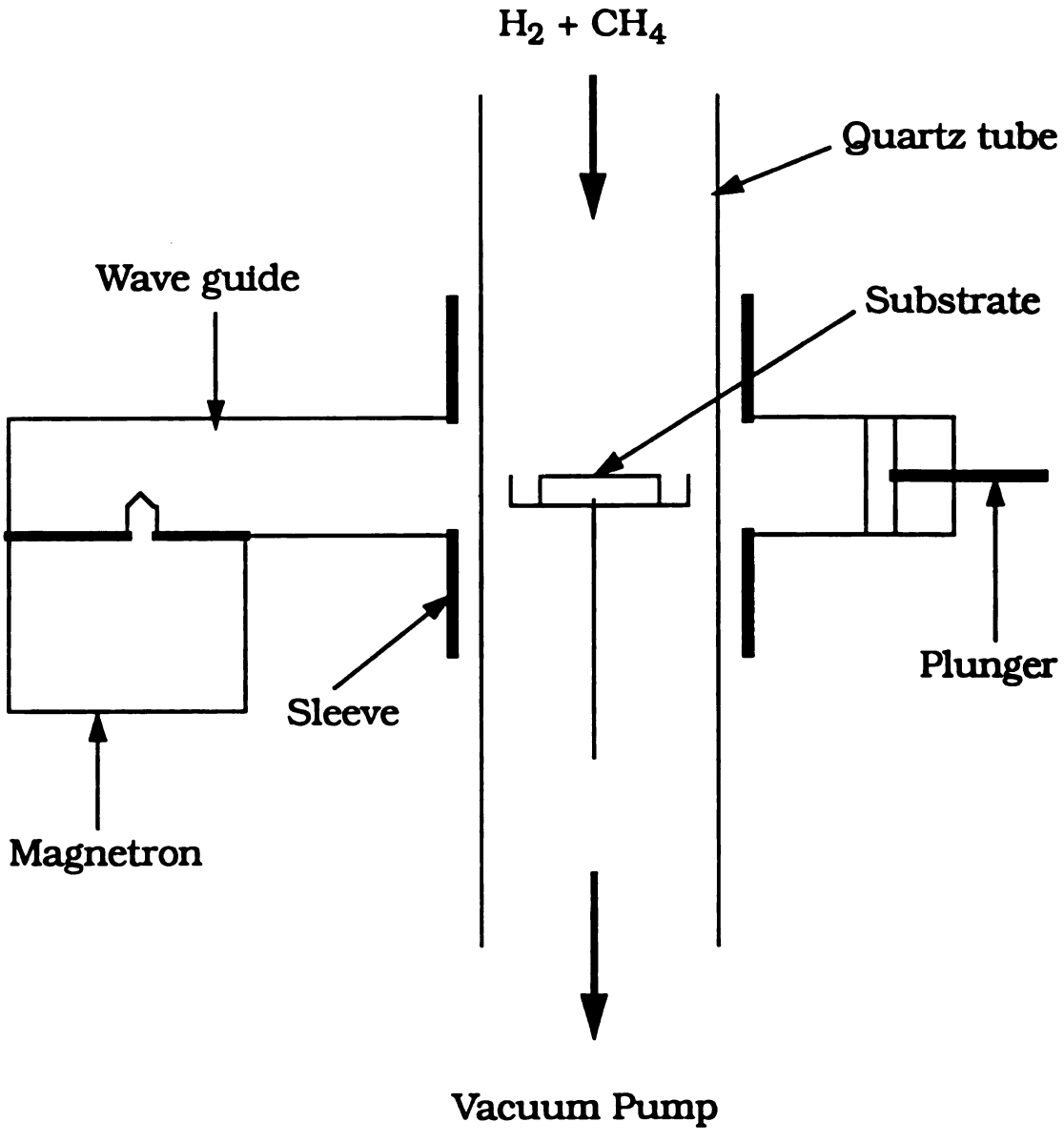

Figure 2.8 Tubular Microwave Reactor [30]

showed discrete particles of ~ 2 μm in diameter and it is not continuous. It is not clear from the paper how the reported growth rate of 3 μm/hour was arrived at and what measurement technique was used to determine that film thickness.

2.2.5.3 Magneto-microwave Reactor

The schematic drawing of a magneto-microwave discharge diamond film deposition reactor is shown in Figure 2.9.<31> As shown, the input gas, which is a mixture of hydrocarbon and hydrogen, is dissociated by the microwave energy coupled into the cylindrical waveguide (discharge area) from a rectangular waveguide. The cylindrical waveguide is excited with TE_{11} mode. The discharge is sustained by the microwave power from a microwave power source. The magnetic field generated by the Helmholtz-type magnetic coils is used to enhance reactive gas dissociation through electron cyclotron resonance (875 Gauss for 2.45 GHz microwave). The substrate is placed near the discharge and the substrate heater is used to control substrate temperature. Diamond film is formed on the substrate when the dissociated gas species react on its surface.

Typical experimental conditions are as follows: cylindrical waveguide inside diameter = 160 mm, substrate = Si, substrate pre-treatment = scratched by 3 mm size diamond paste, gas mixture CH_4/H_2 = 0.5 - 5%, total flow rate = 100 sccm, pressure = 0.1 - 50 Torr, microwave power = 500 - 600 W, substrate temperature = 800 - 900 ^{o}C.

The "figures of merit" are not available in the literature.

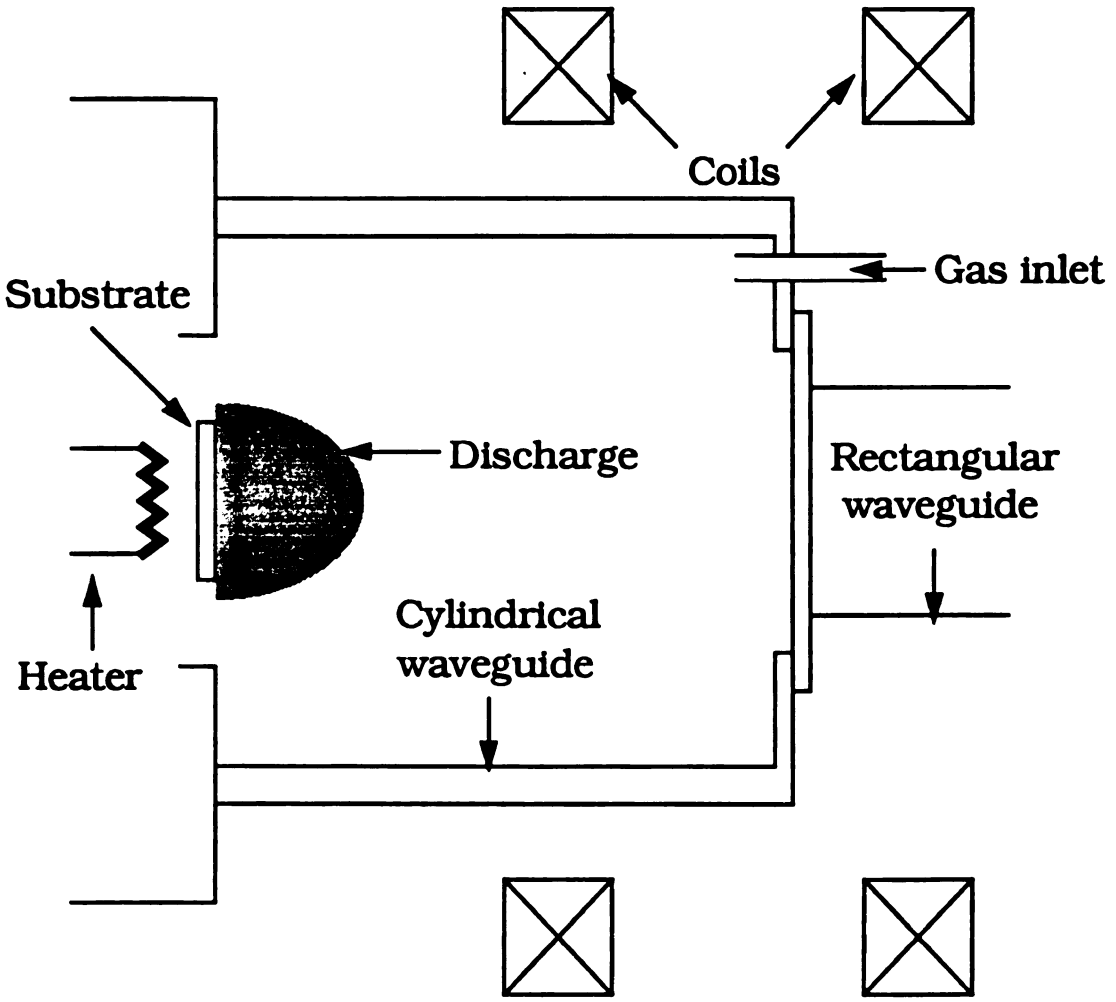

Figure 2.9 Magneto-microwave Reactor [31]

2.2.5.4 Magneto-active Microwave Reactor

The schematic drawing of a magneto-active microwave diamond film deposition reactor is shown in Figure 2.10.<32> As shown, in this reactor, the input gas, which is a mixture of hydrocarbon, hydrogen and oxygen, is dissociated by the microwave energy coupled into the cylindrical process chamber through the quartz window and cylindrical waveguide section. The discharge is sustained by the microwave power from a microwave power source. Electron cyclotron resonance (ECR) is used to enhance the gas dissociation. The ECR magnetic field is provided by the permanent magnet. The substrate is located below the ECR zone and heated during deposition by a tungsten filament located above the substrate. Diamond film is formed on the substrate when the dissociated gas species react on its surface.

Typical experimental conditions: cylindrical chamber diameter = 25 cm, ECR magnet = Nd-Fe-B permanent magnet (15 x 15 x 9 cm^3) with 3250 Gauss at the lower magnet face, ECR zone (875 Gauss) = 8 cm from the lower magnet face, substrate location = 6 cm below the ECR zone, filament temperature = 2040 ^oC, filament-substrate separation = 0.6 cm, substrate pre-treatment = scratched with 1 μm diamond paste, pressure = 2 - 20 Torr, microwave power = 950 W, substrate temperature = 540 - 640 ^oC, CH_4 flow rate = 6 sccm, O_2 flow rate = 2 sccm, H_2 flow rate = 400 sccm.

Notes on reactor operation: The filament is electrically insulated from the chamber wall to eliminate any electron emission current. The substrate temperature is monitored by a thermocouple embedded in the substrate support. The temperature depends mainly on the filament

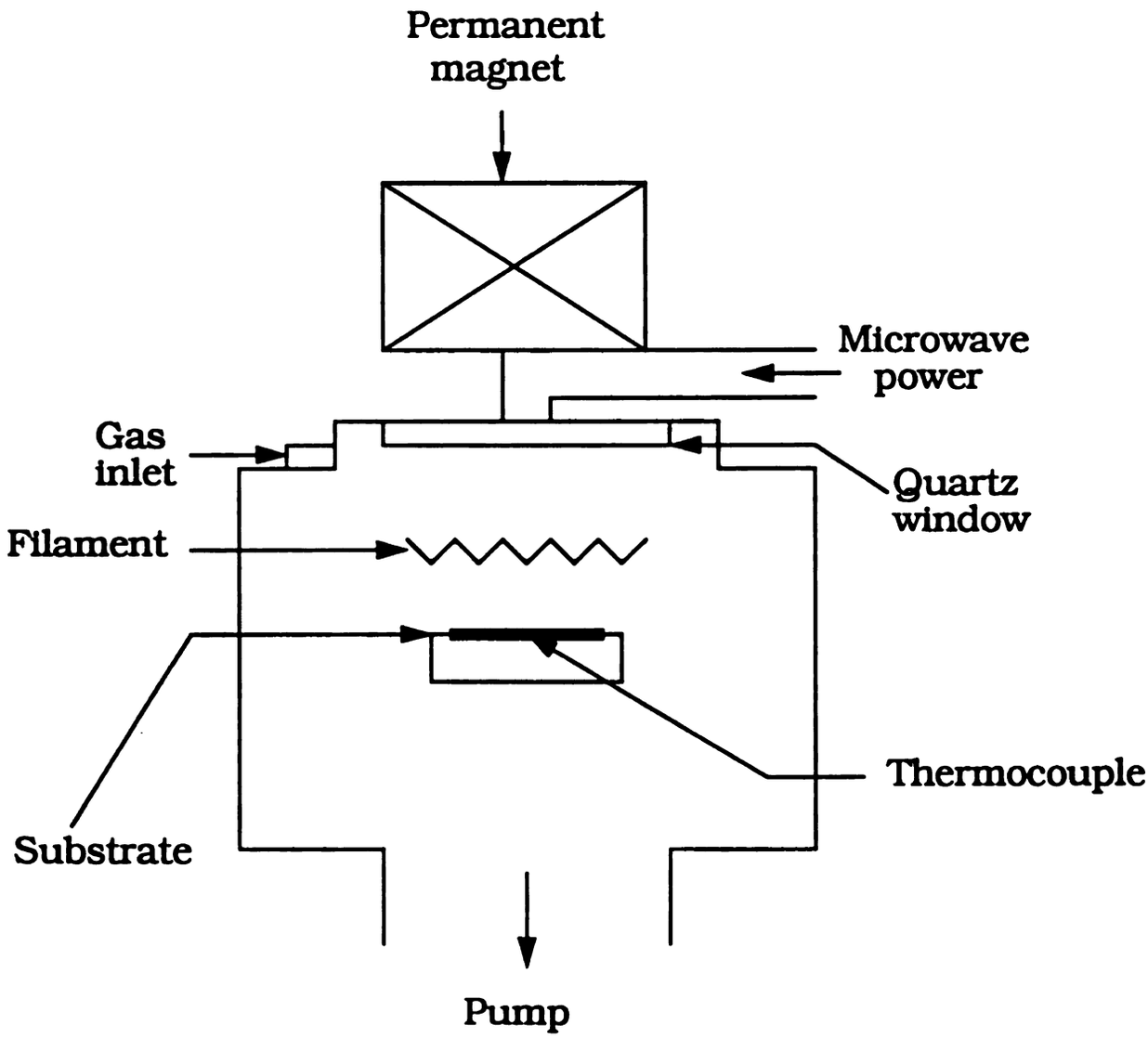

Figure 2.10 Magneto-active Microwave Reactor [32]

temperature, but there is some microwave heating, 250 - 290 °C, for typical input microwave levels of 400 - 1000 W. The pressure range 2 - 20 Torr is low for diamond growth but substantially higher than the sub-Torr pressures typically used with ECR plasmas.

The "figures of merit" that are available are as follows:

(1) Linear growth rate (μm/hour) ~ 2**;

(2) Deposition area (cm^2) ~ 6.45;<33>

(3) Weight gain (mg/hour) ~ 4.5;

(3) Uniformity = n/a;

(4) Growth Efficiencies

  (i) Growth rate/power input (mg/kW-hr) ~ 4.7;

  (ii) Growth rate/gas input (mg/liter) ~ 0.18;

  (iii) Carbon conversion efficiency (%) ~ 2.3.

** It is noted that, in the paper, the author showed the SEM photographs of diamond films which consist of discrete particles of ~ 4.4 - 9.7 μm in diameter. These films are not continuous. It is not clear from the paper how the growth rate of 2 μm/hour mentioned in the paper was calculated and what measurement technique was used to determine that film thickness.

2.2.5.5 Bell-jar Microwave Reactor

The schematic drawing of a bell-jar microwave diamond film deposition reactor is shown in Figure 2.11.<34,35> As shown, in this reactor, the input gas which is a mixture of hydrocarbon, hydrogen and oxygen is dissociated by the microwave energy coupled into the cylindrical cavity through the waveguide and antenna. A ball-shaped

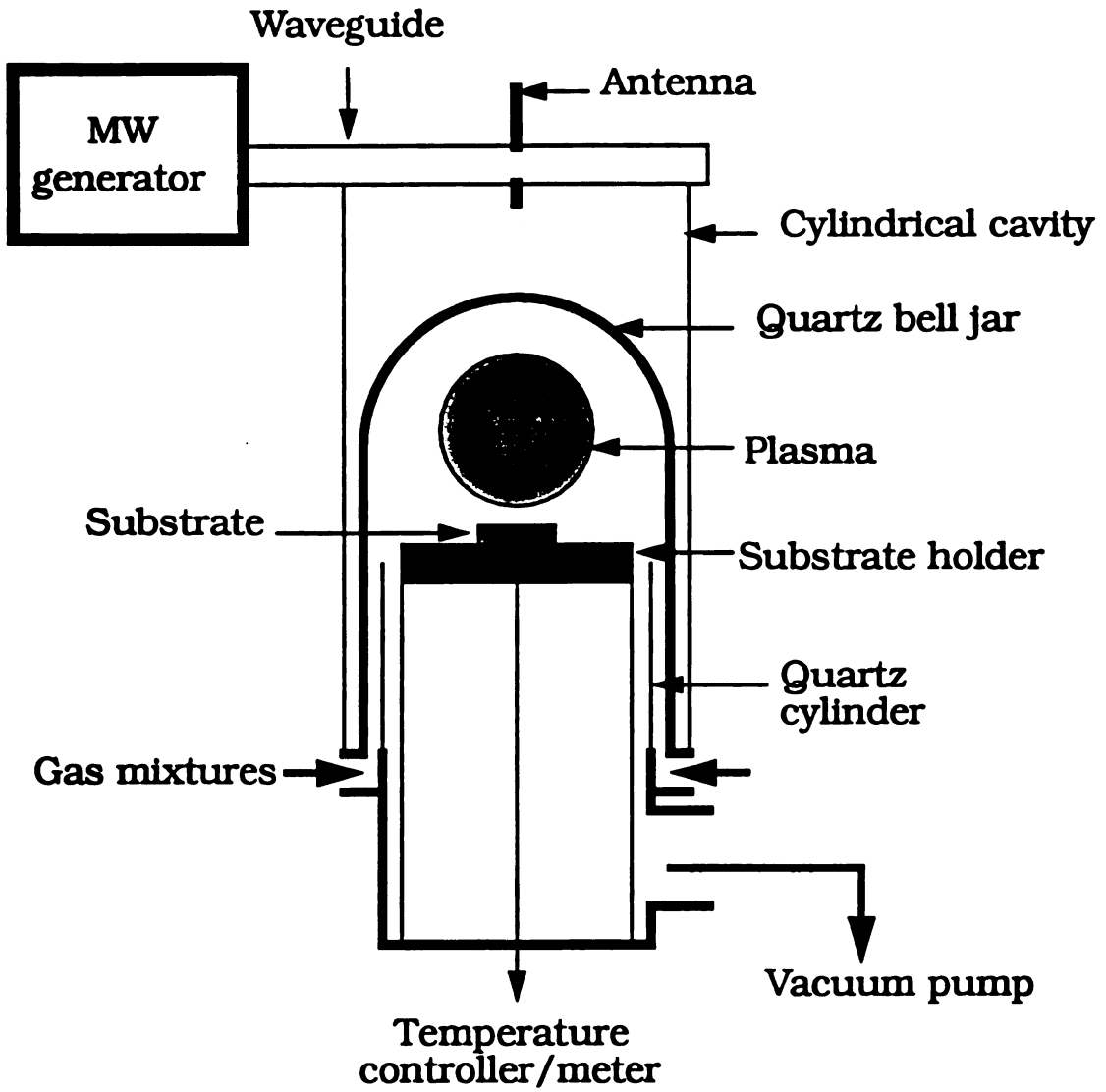

Figure 2.11 Bell-jar Microwave Reactor [34,35]

plasma is formed inside the quartz bell jar and the substrate is placed near the plasma. Diamond film is formed on the substrate when the dissociated gas species react on its surface.

Typical experimental conditions: substrate = Si, pressure = 40 - 70 Torr, substrate temperature = 850 - 1030 ^{o}C, CH_4/H_2 = 0.5%, total flow rate = 200 - 600 sccm.

Notes on reactor operation: Coatings of more than 65 mm (2.75 inch) diameter were deposited on silicon with a separate substrate heater. Pressure variations between 40 and 70 Torr were found to have little effect on the diamond growth rate in this reactor. The variation of the total flow between 200 sccm and 600 sccm (while keeping the methane concentration constant at 0.5%) did not affect the growth rate.

The figures of merit that are available in the literature are:<36>

(1) Linear growth rate (μm/hour) ~ 3.5;

(2) Deposition area (cm^2) ~ 12.5;

(3) Weight gain (mg/hour) ~ 15.4;

(3) Uniformity ~ n/a;

(4) Growth Efficiencies

  (i) Growth rate/power input (mg/kW-hr) ~ 10.3;

  (ii) Growth rate/gas input (mg/liter) ~ 28.5;

  (iii) Carbon conversion efficiency (%) ~ 4.2.

2.2.5.6 Microwave Jet Reactor

The schematic drawing of a microwave jet reactor is shown in Figure 2.12.<37,38> As shown, the input gas, which is a mixture of hydrocarbon, hydrogen and oxygen, is dissociated near the jet nozzle by

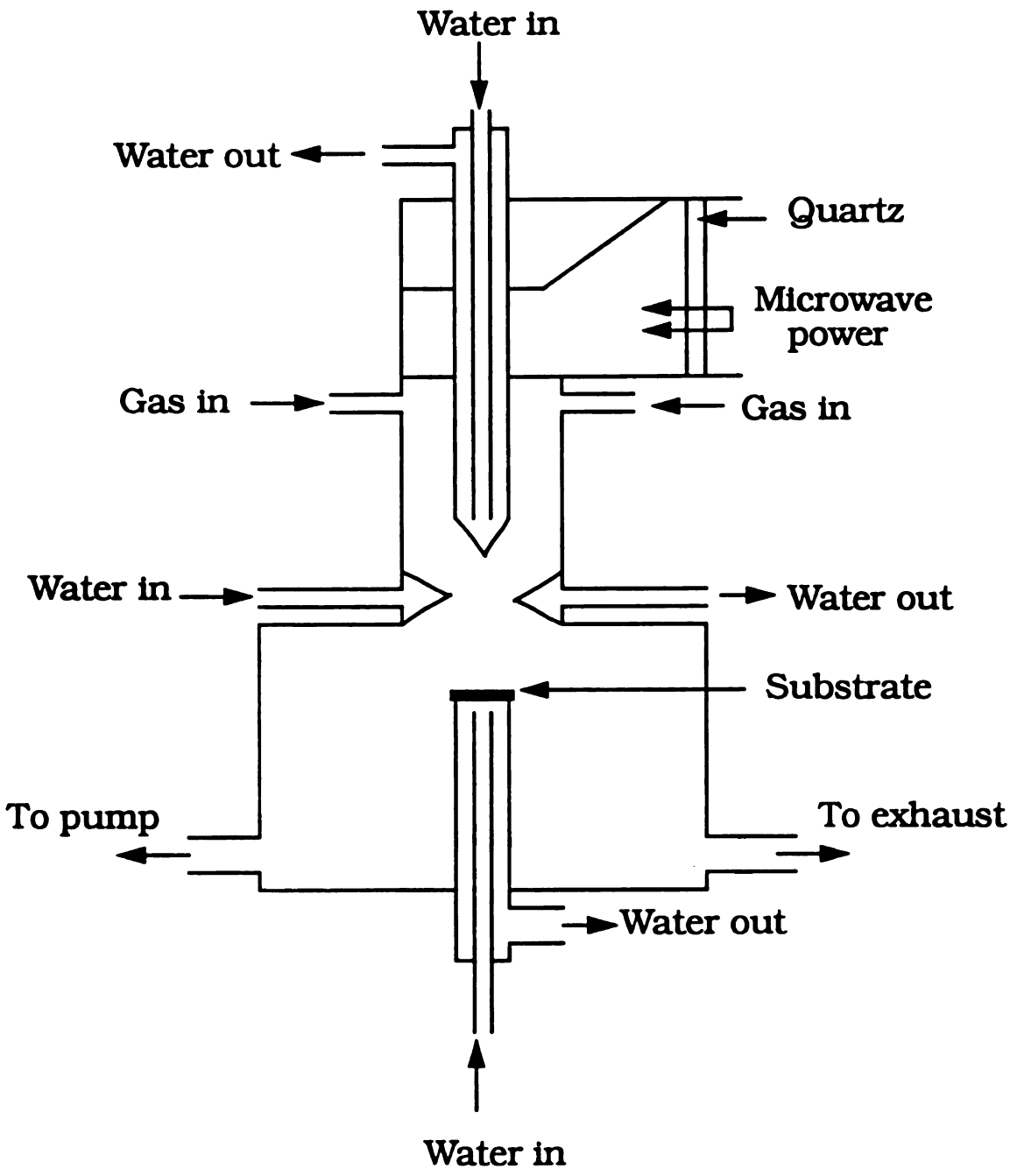

Figure 2.12 Microwave Jet Reactor [37,38]

the microwave energy. Microwave energy is transmitted from the power source to the jet nozzle through TE_{01} mode in the rectangular waveguide, a transition unit and TEM mode in the coaxial waveguide. The plasma jet is generated from the end of the center plasma flow stabilizer and blows into the chamber where the substrate is placed on a water-cooled substrate holder. Diamond film is formed on the substrate when the dissociated gas species react on its surface.

Diamond films have been deposited under the following experimental conditions: substrate = Si, Ar flow rate = 10 l/min, H_2 flow rate = 20 l/min, CH_4 flow rate = 0.6 l/min, O_2 flow rate = 0.15 l/min, total pressure = 760 Torr, substrate temperature = 887 - 927 ^oC, microwave power = 3.8 - 4.2 kW.

Notes on reactor operation: The diameters of the center and outer conductor in the coaxial waveguide are 20 and 57.2 mm, respectively. The conductors taper off and play the roles of plasma flow stabilizers for plasma generation. These stabilizers are made of water-cooled copper in order to prevent thermal evaporation. The edge of the outer electrode (plasma jet nozzle) is 22 mm in diameter, which must be designed properly depending upon the plasma gas composition.

The "figures of merit" that are available are as follows:

(1) Linear growth rate (μm/hour) ~ 12;

(2) Deposition area (cm^2) ~ 2.5;

(3) Weight gain (mg/hour) ~ 10.53;

(3) Uniformity ~ n/a;

(4) Growth Efficiencies

  (i) Growth rate/power input (mg/kW-hr) ~ 2.6;

  (ii) Growth rate/gas input (mg/liter) ~ 0.0057;

(iii) Carbon conversion efficiency (%) ~ 0.055.

2.3 Comparison of Diamond Film Deposition Reactors

A summary of performance "figures of merit" of diamond film deposition reactors is given in Table 2.1.

Since there are no electrodes present in the microwave plasma, the problem of metallic contamination in the process of diamond deposition does not inherently exist. Contamination from reactor walls can be minimized with a proper reactor design. Compared to the erosion of filaments in hot filament reactors, erosion of electrodes in direct current reactors and nozzle erosion in combustion flame reactors, microwave plasma diamond film deposition is a cleaner process. It is also easier to control and optimize the deposition process which makes microwave plasma reactors a promising technique for growing pure, uniform, and high quality diamond films.

To successfully commercialize diamond synthesis at low pressures, diamond growth at high rates and low deposition temperatures on large area substrates is desirable. Each of the microwave reactors described above has its advantages and disadvantages for diamond film deposition. What their disadvantages have in common is that they can not be easily scaled up for large area diamond film deposition.

The tubular reactor has two disadvantages, first, the substrate size is limited by the by the inside diameter of the silica tube, which is 40 mm, and the system is not easily scalable for diamond film growth on a larger surface since the diameter of the silica tube is limited by the size of the rectangular waveguide; second, the plasma generated inside the

Table 2.1 Summary of "Figures of Merit" of Diamond Reactors

	Linear growth rate (μm/hr)	Dep. area (cm^2)	Weight gain (mg/hr)	Energy effic. (mg/ kW-hr)	Gas flow effic. (mg/ liter)	Carbon conv. effic. (%)
Hot filament [22]	0.6	6.4	1.35	1.04	0.2	0.32
DC plasma [23,24]	20	0.25	1.76	0.56	1.47	13.7
DC jet [25]	900	2	632	57	0.26	1.97
Flame [27]	60	0.28	5.9	n/a	0.049	0.009
RF thermal [29]	60	3	63	1.05	0.014	0.2
Tubular MW [30]	3	3 - 6	3 - 5	4.3 - 8.6	n/a	n/a
Mag.-active [32]	2	6.45	4.5	4.7	0.18	2.3
Bell-jar MW [36]	3.5	12.5	15.4	10.3	28.5	4.2
MW jet [37,38]	12	2.5	10.53	2.6	0.0057	0.055

silica tube is very close to the inside walls, under the conditions suitable for diamond deposition, erosion of the silica walls and hence contamination of the diamond film are likely.

The magneto-microwave reactor uses a narrow, electron cyclotron resonance region to generate the high density plasma. Non-uniformity in the deposited film can be expected as an inherent result of the non-uniform distribution of the resonant magnetic field across the substrate surface, especially for diamond film deposition over a larger surface. The reported surface area for diamond growth was 30 mm in diameter. It has a narrow pressure region for diamond film growth, namely from 4 to 50 Torr. At pressures above 50 Torr, the discharge area becomes unstable and below 4 Torr, the products contain graphite or SiC phase and in extreme cases the products are only these phases. The magneto-active microwave reactor uses the same principle as the magneto-microwave reactor. Thus it is expected that it has the same disadvantages as the magneto-microwave reactor.

The bell-jar reactor uses a plasma ball and the substrate is located near the lower pole of the plasma ball. The reactive species distribution over the substrate surface is inherently non-uniform. This is especially true when the substrate surface extends further away from the lower pole of the plasma ball. The reported coating surface area with the plasma is 25 mm in diameter. A separate heater/cooler is needed to coat a surface of 65 mm in diameter. The location of the substrate and substrate holder are fixed in order to generate the ball shaped plasma. External tuning is needed in order to minimize the reflected power from the reactor since there is only one internal adjustment (i.e. the antenna) available for microwave coupling.

The jet reactor uses a small jet nozzle as an exit orifice for the reactive species. It can be used to deposit diamond films with higher growth rates over small areas. But it can not be used to deposit uniform diamond film on large substrates since fine particles of amorphous carbon were deposited on the substrate edge. This came from that the substrate was not heated uniformly, hotter near the center and cooler near the edge.

2.4 Bachmann C-H-O Phase Diagram

A C-H-O phase diagram was introduced by P. K. Bachmann et al. <36> to provide a common scheme for all major diamond chemical vapor deposition (CVD) methods used to date. A schematic drawing of this phase diagram is shown in Figure 2.13. Each side of the equilateral triangle represents the atom fractions of the gas phase composition of one of the binary systems C-H, H-O and O-C, ranging from 0 to 1. Any ternary C-H-O gas compositions are located inside this triangle. There are three regions in this phase diagram, i.e., the non-diamond carbon growth region, the diamond growth domain and the no growth region. In chapter six, the gas compositions used in the deposition experiments are mapped onto this phase diagram.

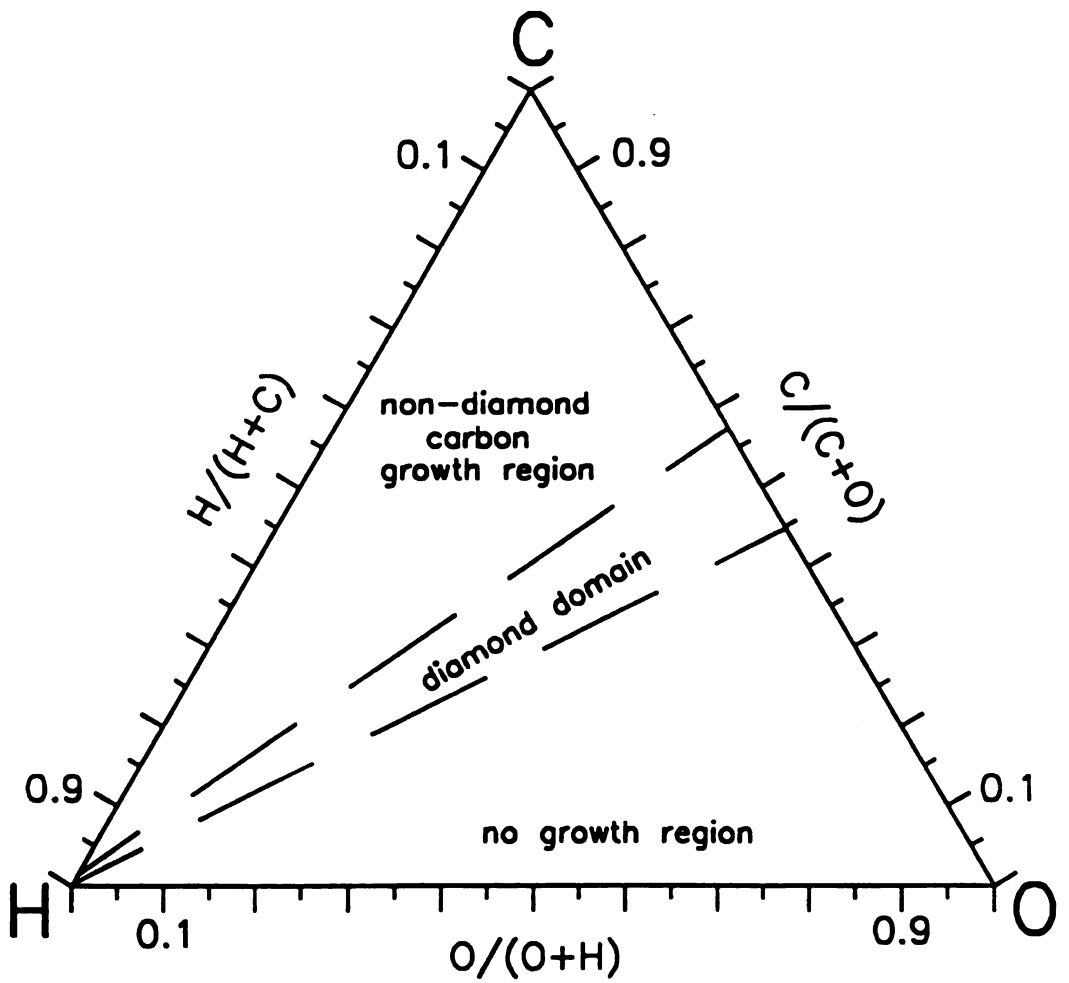

Figure 2.13 Bachmann C-H-O Phase Diagram [36]

CHAPTER THREE

THE MICROWAVE-CAVITY PLASMA REACTORS (MCPR)

3.1 Introduction

In order to deposit diamond films on large substrate surfaces, diamond film deposition reactors that can create large area discharges are needed. These reactors should be designed such that they are easily controllable and the deposition processes can be easily repeated. In this chapter, a series of microwave-cavity plasma reactors (MCPRs) are investigated in order to deposit diamond films uniformly on large substrate surfaces. Cylindrically symmetric cavity applicators which utilize internal matching and which are excited in a single electromagnetic mode are investigated for their ability to deposit diamond films over large surface areas. Earlier work with this type of reactor included the development of plasma ion sources and plasma etching and oxidation reactors.[12,13,39,40] This type of microwave applicator has the advantage of easy operation and adaptability to different substrate sizes and types. High quality diamond film can be produced and easily reproduced in these reactors. The difference between the different reactor concepts investigated here is the size of plasma that can be safely created and the associated substrate area that can be uniformly covered with diamond films.

There are a number of reactor geometry parameters in the plasma reactor design. These parameters include: (1) cavity shape and size, (2) power coupling method and (3) base-plate design, etc. All these reactor geometry parameters have a strong influence on the reactor performance. In the research described in this chapter, a number of these parameters are investigated. They include: (1) 7", 14" and 18" inside diameter cylindrical cavities, (2) probe side and end coupling, and loop side coupling, (3) different size and shape quartz domes and their associated base-plates. These reactors are described below in the order in which they were experimentally investigated. The experimental microwave power supply, reactive gas supply and vacuum pump systems used in the investigation of these reactors are first reviewed in Section 3.2. The computer monitor system used in the experiments described in chapter 6 is also described in section 3.2.

3.2 Experimental Systems

3.2.1 Introduction

All the microwave-cavity plasma reactors that are described in this dissertation use microwave power as their energy source and a single vacuum pump system was used for reactive gas supply and operating pressure control. The microwave power supply, gas flow and vacuum pump system used in the experimental evaluation of MCPRs are described below in sections 3.2.2 and 3.2.3. The computer monitor system used in the experiments described in chapter 6 is described in section 3.2.4.

3.2.2 Microwave Power Delivery Systems

The experimental microwave circuit used to deliver power into the microwave applicators is similar to those described in earlier work <12,13,39,40>. Thus only a brief description is given here. A schematic drawing of the microwave power supply circuit is shown in Figure 3.1. It consists of a 2.45 GHz or 915 MHz, variable power source (1), circulator (2) and matched dummy load (3), dual-directional coupler (4) and associated incident and reflected power meters (5) and (6), and microwave cavity applicator (7). The microwave power supplied by the power source (1) propagates through the circulator (2) and the dual-directional power coupler (4) and is incident on the microwave cavity applicator (7). In the case of any mismatch between the impedances of the waveguide and the cavity applicator (7), some of the incident power will be reflected back from the cavity applicator. This reflected power travels in the opposite direction from the incident power. It propagates through the dual-directional coupler (4) and is directed by the circulator (2) into the matched dummy load (3), where it is absorbed and dissipated as thermal energy. The circulator (2) and its matched dummy load (3) permit the propagation of the microwave energy into the cavity applicator (7) and prevent the propagation of the reflected power back into the power source (1) where it may cause damage to the power source. The incident power P_i is measured by the incident power meter (5) attached to the incident power sampling port of the dual-directional coupler (4) and the reflected power P_r is measured by the reflected power meter (6) attached to the reflected power sampling port. The microwave power absorbed by the cavity applicator (7) is given by $P_t = P_i - P_r$.

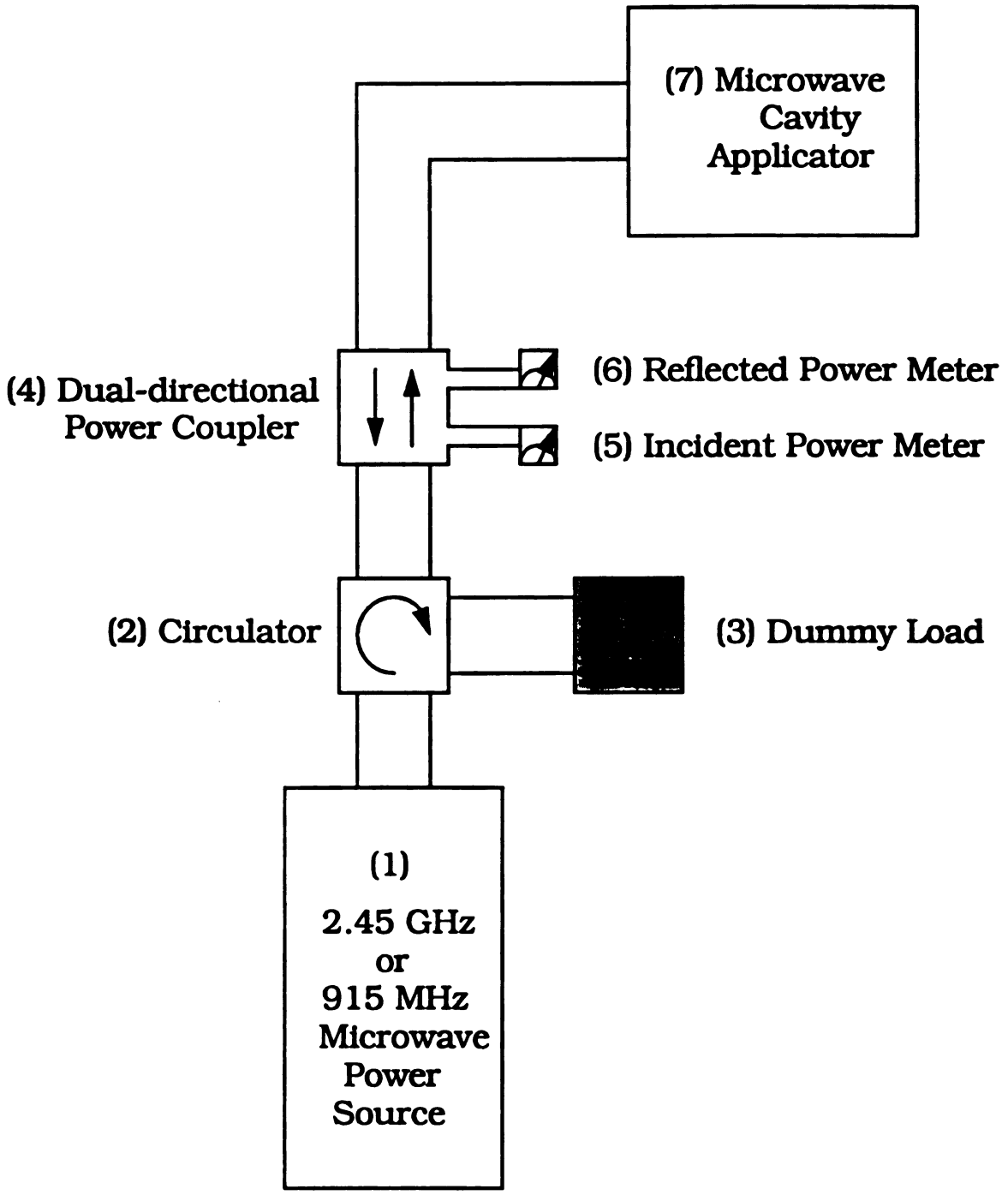

Figure 3.1 Microwave Power Supply Circuit

Four microwave power sources have been used during the research described in this dissertation. The first one is the Chuang (Model No. CA2450-1200CW) 2.45 GHz, 1.2 kW power source. It was used in the experiments conducted in the first generation MCPR, the 2.45 GHz experiments conducted in the 18 and 14 inch MCPRs and the low power experiments conducted in the second generation MCPR. The second power source used is the Chuang (Model No. MPS915-500) 915 MHz, 500 W power source. It was the only 915 MHz power source available in our laboratory and was used in the 915 MHz experiments conducted in the 18 inch MCPR. Due to its low power capacity, it did not find much use in diamond film deposition process. The third power source used is the Gerling (Model No. GL119) 2.45 GHz, 3 kW power source. It was used in the high power (1.1 - 1.7 kW) experiments conducted in the second generation MCPR and the low power (1.5 - 3 kW) experiments conducted in the third generation MCPR. The fourth power source used was the Cober (Model No. S6F/4503) 2.45 GHz, 6 kW power source which was used in the high power (3 - 4.5 kW) experiments conducted in the third generation MCPR. Among the 2.45 GHz power sources available, the Gerling 3 kW power source had the narrowest and most stable frequency spectrum and thus was the "cleanest" power source.

3.2.3 Flow Control and Vacuum Pump Systems

A schematic drawing of the gas flow control and vacuum pump systems is shown in Figure 3.2. As shown, the source gases, H_2 (1), CH_4 (2) and CO_2 (3), are supplied by cylinder tank gases of high purity (99.99% purity or better). The gas flows are controlled by three MKS type

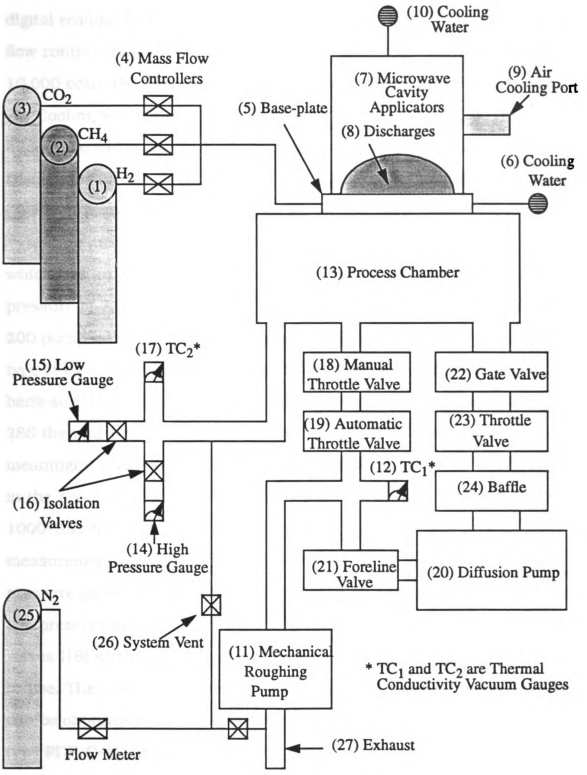

Figure 3.2 Flow Control and Vacuum System for MCPRs

1159A mass flow controllers along with a MKS type 247C power supply/ digital readout/set point source (4). The flow control ranges of the mass flow controllers are 0 - 7.2 sccm CH_4, 0 - 7.4 sccm CO_2, 0 - 500 and 0 - 10,000 sccm H_2. The gases are mixed before they reach the base-plate (5). Cooling water (6) was also supplied to the base-plate (5). The microwave cavity applicator (7) sits on top of the base-plate (5). Discharges (8) are confined in the lower section of the cavity applicator (7) which is usually cooled by both air (9) and water (10)

The mechanical roughing pump (11) is the ALCATEL 2033 pump which has an air pumping speed of 10.9 l/s (23 cfm). It has a base pressure of 7.5×10^{-2} mTorr (1×10^{-4} mbar) when used with ALCATEL 200 pump oil which is a type of mineral oil distilled under vacuum. This type of oil can be used to pump corrosive products and provides reduced back-streaming. The pump base pressure is measured by a MKS type 286 thermal conductivity vacuum gauge TC_1 (12) which has a meaningful pressure measurement range of 5 - 200 mTorr. The pressure in the process chamber (13) is measured by a MKS Baratron type 122A 1000 Torr full scale high pressure gauge (14) for process pressure measurement and a MKS Baratron type127A 0.1 Torr full scale low pressure gauge (15) for the chamber base pressure measurement. These two pressure gauges are connected to the chamber (13) through isolation valves (16) so that they can be isolated from the chamber whenever not in use. The isolation valves (16) ensure that accurate pressure readings can be obtained by stabilizing the zero point of the pressure gauges. MKS type PDR-C-1C and type PDR-D-1 power supplies/digital readouts are connected to these two pressure gauges and display the pressure readings. A MKS type 286 thermal conductivity vacuum gauge TC_2 (17)

with meaningful pressure measurement range of 5 - 200 mTorr is used for general indication of the pressure in the process chamber. It is quite useful during the chamber initial pump down after the chamber is vented to the atmospheric pressure for cleaning, sample loading and/or unloading, etc.

The pressure in the process chamber (13) is controlled by throttle valves between the chamber (13) and the mechanical pump (11). A Varian manual throttle valve (18) was used to control the chamber pressure in the experiments conducted in the first and second generation MCPRs and some of the earlier experiments conducted in the third generation MCPR. A MKS type 253A 20 mm sealing butterfly throttling valve with MKS type 252 exhaust valve controller (19) was used to control the chamber pressure in the later experiments conducted with the third generation MCPR.

A lower pressure pumping system is also part of the vacuum system. It was used to calibrate the zero point of the low pressure gauge (15) and check vacuum tightness of the vacuum system in the experiments described in this dissertation. A Varian VHS-6 (Model No. 0184) 6 inch diffusion pump (20) provides the lower pressure pumping capacity to the vacuum system. This diffusion pump has an optimum operating pressure range of 1×10^{-3} to 1×10^{-9} Torr with an air pumping speed of 2400 l/s. The fore-line valve (21) connects or isolates the diffusion pump (20) from the mechanical pump (11). A Varian 8 inch viton-sealed swing gate valve (22) provides the isolation or connection of the process chamber (13) to the diffusion pump (20). The process chamber pressure is controlled by a MKS 6 inch throttle valve (23). A Varian low profile water cooled baffle (24) is used to prevent the diffusion

pump oil from back streaming into the process chamber (13). By closing the manual valve (18) and/or the 20 mm throttle valve (19) on the chamber direct roughing line, and opening the gate valve (22) and fore-line valve (21), the lower pressure pumping system can be used. By closing the gate valve (22) and the fore-line valve (21), the lower pressure pumping system is isolated from the rest of the vacuum system.

Nitrogen (25) is used for system vent (26) and exhaust (27) purge, because flammable gases H_2 (1) and CH_4 (2) are used in the experiments described in this dissertation. Nitrogen with flow rate of twenty (or more) times of the total flow rates of flammable gases is used to dilute the exhaust gas mixture in the exhaust (27) pipe so that the resultant exhaust gas mixture is no longer flammable. Nitrogen is also used to vent the process chamber (13) during cleaning, sample loading and unloading, etc. It helped to minimize the out-gassing from the chamber walls during chamber pump down.

3.2.4 Computer Monitor System

A computer safety monitor system[41] was used to monitor the system operating conditions and control the shut down procedure in the experiments described in Chapter 6. A block diagram of this computer monitor system is shown in Figure 3.3. The primary task of this computer monitor system is to control experiment time and shut down sequence. It is also used to ensure the safe operation of the system. As is shown in Figure 3.3, the system operating pressure, reflected microwave power and input microwave power readings are used as input signals for the computer monitor system. The operating status (ON/OFF or OPEN/

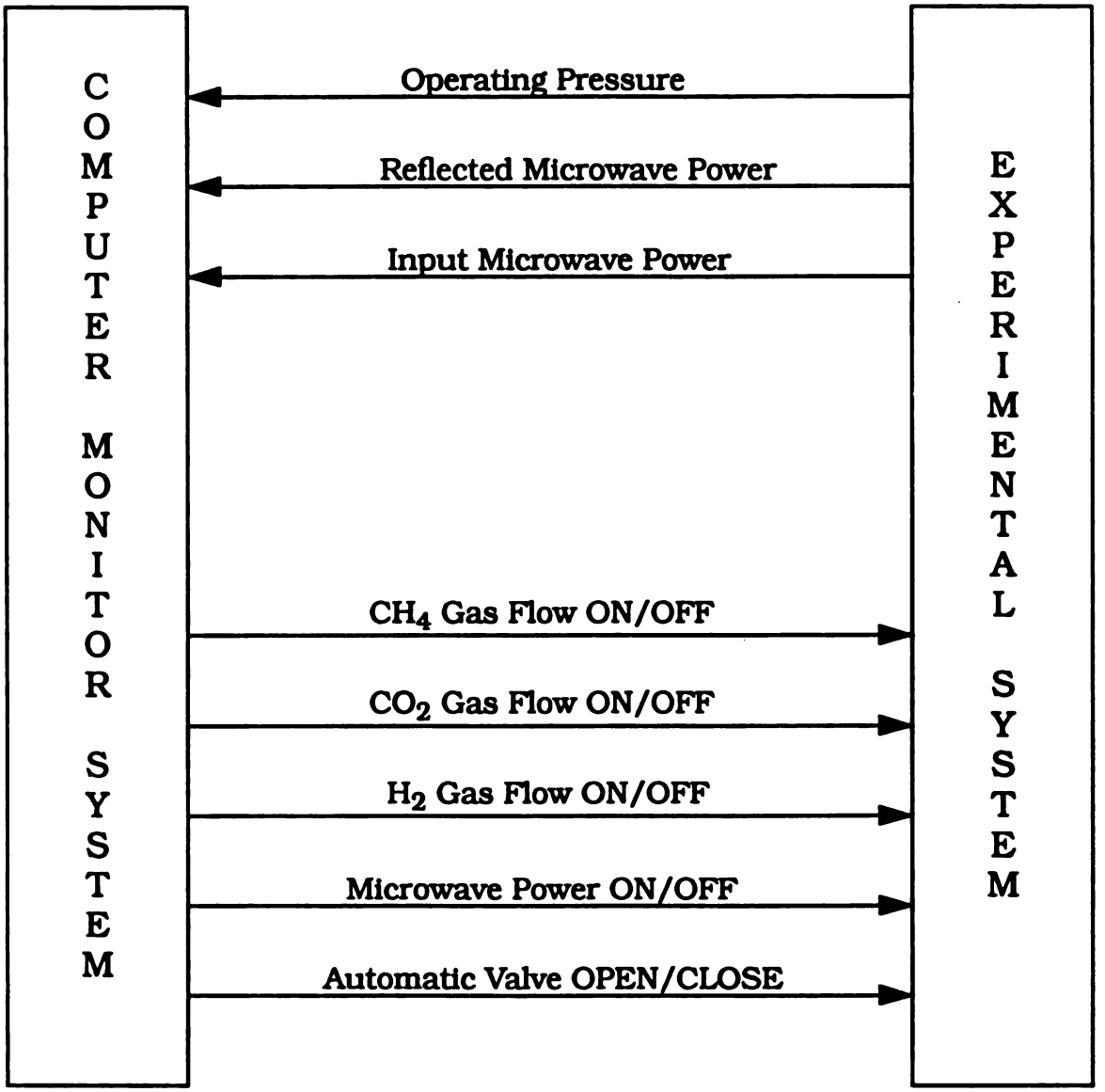

Figure 3.3 Computer Monitor System Block Diagram

CLOSE) of the flow controllers, microwave power source and the automatic throttle valve is controlled by the computer monitor system through a series of relays.

This computer monitor system was designed such that the default state of the experimental system is in a disabled state where the gas flows and microwave power are OFF and the automatic valve is CLOSED. A computer program is needed to enable the experimental system, monitor the experimental conditions and control the shut-down sequence. The flow chart of a computer monitor program[41] is shown in Figure 3.4. As shown, in this program, the operating pressure and reflected microwave power upper limit and the experiment running time are first set. The experimental system is then enabled so that the gas flows and microwave power can be turned on and the automatic throttle valve can operate in an automatic mode to control the system pressure. An experimental start-up procedure (see section 6.3.3.2) follows to start the experiment after which the timer in the computer monitor system is started. During the experiment, a checking loop is used to compare the operating pressure, reflected microwave power and timer with the pre-set values to determine the state of the experiment. If, at any time during the experiment, the operating pressure and/or the reflected microwave power go over the pre-set upper limit, the program directs the experiment into an emergency shut-down sequence. In this sequence, the microwave power is turned off followed by the shut-off of all gas flows. The automatic throttle valve is then closed to isolate the vacuum pump from the process chamber. These three steps follow each other very closely with the speed of the computer. Otherwise the program directs the system into a normal shut-down procedure (see section 6.3.3.2) when the

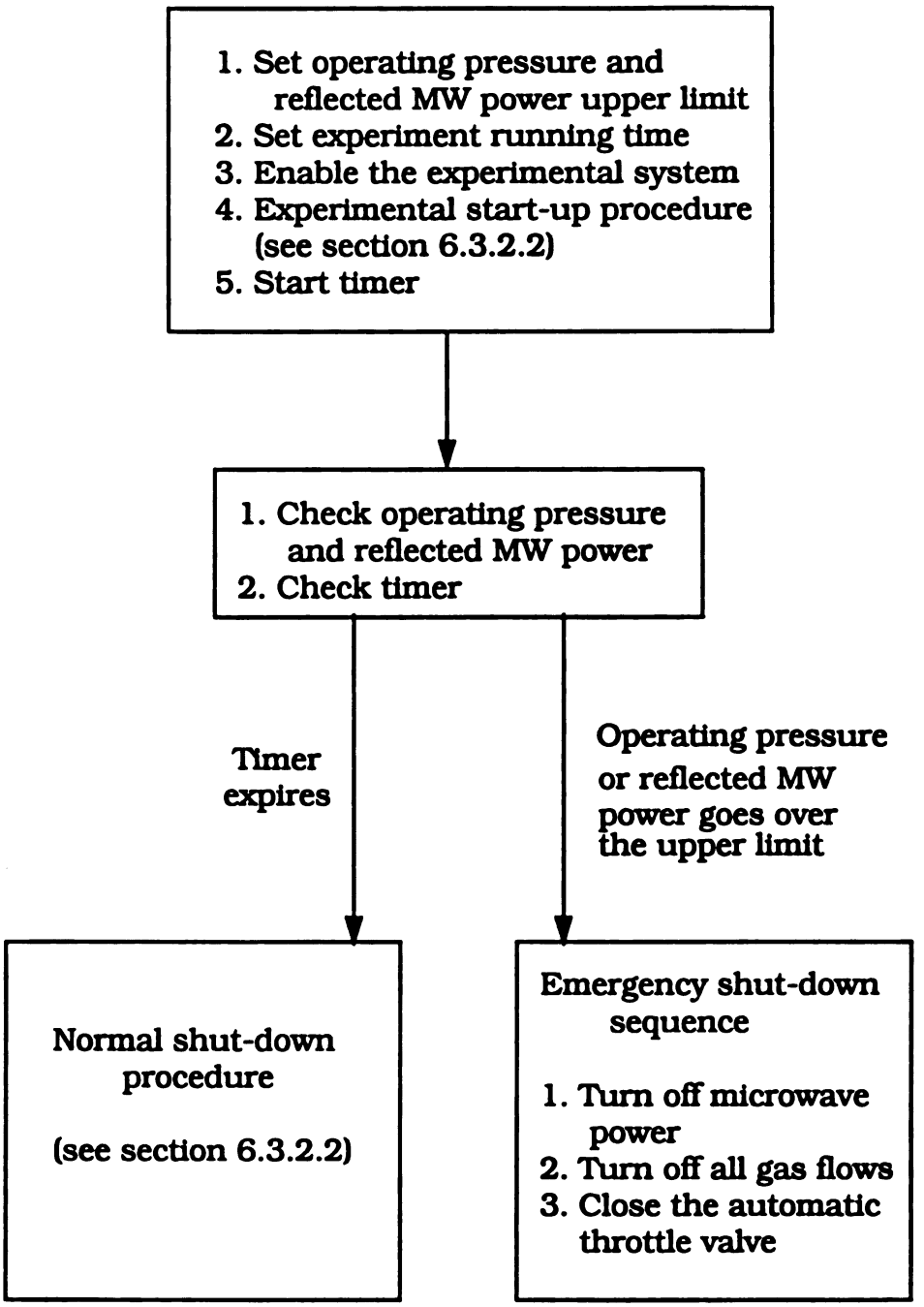

Figure 3.4 Monitor Program Flow Chart

timer expires.

3.3 The First Generation Seven Inch MCPR

3.3.1 Introduction

The first generation seven inch MCPR (MCPR7-1) was the first reactor concept investigated for diamond film growth. It was developed in the Fall of 1986 and built by J. Asmussen and placed into operation in the Fall of 1987 at Norton Company in Salt Lake city, Utah. It was based on a microwave plasma reactor concept invented at Michigan State University and patented by Asmussen et al.<42-50> The technology is licensed to Wavemat, Inc. by Michigan State University. Norton Company has an exclusive sub-license from Wavemat for the application of this technology to diamond film deposition. The reactor used in our investigation is a later version which was commercialized by Wavemat, Inc.

3.3.2 Reactor Geometry

The cross-sectional views of the MCPR7-1 are shown in Figure 3.5. As shown, the reactor consists of the cylindrical cavity walls (1) which form the outer conducting shell of the cavity applicator. The cavity walls are formed from a 7 inch inside diameter, open ended metallic cylinder. A water cooled (41) sliding short (2), which is electrically connected to the cavity walls (1) via the finger stock (3), forms the top end of the cavity. It can be moved back and forth along the longitudinal axis of the

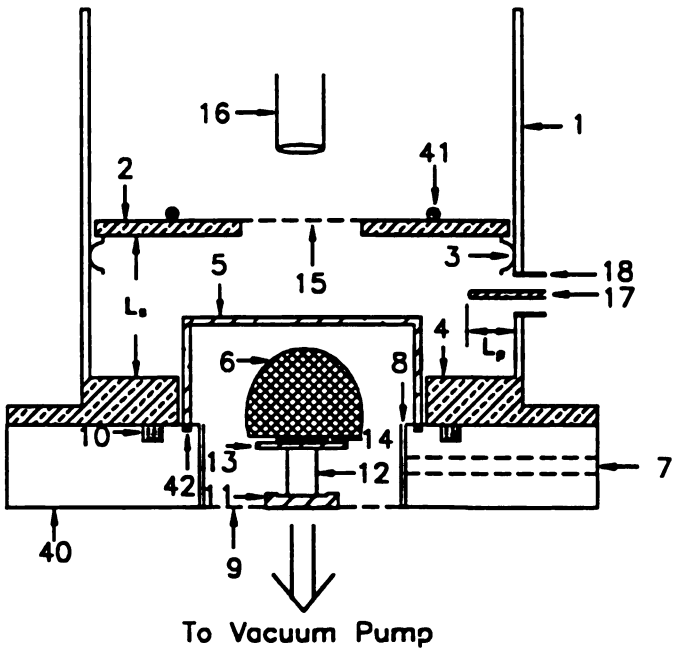

LEGEND

(1) Cavity Walls	(12) Quartz Tube
(2) Sliding Short	(13) Substrate Holder
(3) Finger Stock	(14) Substrate
(4) Cavity bottom surface	(15) Top Window
(5) Quartz Dome	(16) Optical Pyrometer
(6) Discharge Zone	(17) Power Coupling Probe
(7) Gas Input Tunnel	(18) Outer Conductor
(8) Gas Distribution Ring	(40) Base Plate
(9) Metal Screen	(41) Water Cooling
(10) Cooling Water Tunnel	(42) O-ring
(11) Graphite Base	

Figure 3.5 Schematic Drawing of MCPR7-1

cylindrical cavity walls (1) to change the electrical and physical height of the cavity applicator. The cavity bottom surface (4) and the water-cooled (10) base-plate (40) form the lower end of the cavity applicator. Microwave power is coupled into the cavity applicator through an adjustable coaxial power input port which is comprised of the power coupling probe (17) and its outer conductor (18).

Reactive gases flow into the discharge zone (6) via the gas input tunnel (7) inside the base-plate (40). The 9.25 cm i.d. quartz dome (5) confines the working gas to the lower section of the cavity applicator where the microwave fields produce a plasma discharge adjacent to the substrate (14). A metal screen (9), which is attached to the bottom of the base-plate (40), allows gases to flow into the vacuum pump system but prevents microwave energy from radiating out of the applicator. The substrate (14) and substrate holder (13) are placed on top of a quartz tube (12). The quartz tube (12) stands on a graphite base (11) which in turn sits on the metal screen (9). A plasma discharge is ignited in the dome-shaped zone (6) by exciting the cavity in a single discharge loaded resonant mode. The plasma discharge can be viewed through the top screened window (15), through which the substrate temperature can also be measured using a optical pyrometer (16).

3.3.3 Reactor Operation

The general experimental operation of this type MCPR has been described in detail elsewhere <51-55>. Thus, only a brief description is given here. Differences from earlier work <51-55> are operation at high pressure (30 - 80 Torr) and without a static magnetic field. The ignition,

matching, and internal cavity tuning are similar to that reported earlier for microwave electrothermal thrusters [56] and microwave broad beam ion sources[51].

This MCPR can create a microwave discharge when excited in a single cavity electromagnetic mode. The mode diagram of an ideal 7" cavity is shown in Figure 3.6.[57] Each mode was experimentally evaluated for its potential to deposit diamond films at discharge pressure of 30 - 80 Torr. A discharge was started by reducing the H_2/CH_4 gas pressure to 5 -10 Torr, and applying microwave power which would then ignite a discharge that entirely filled the quartz chamber. The discharge pressure was then increased to an operating condition of 30 - 80 Torr while length and probe tuning the cavity to a matched condition.

At ignition the discharge completely filled the quartz tube, but as pressure increased to 30 - 80 Torr, the discharge contracted and separated from the surrounding quartz walls and assumed a shape related to the field pattern of the exciting electromagnetic mode. That is, the discharge became "arc like" and its shape and position varied with cavity mode excitation. This arc like behavior became particularly evident at the 40 - 80 Torr pressures.

Experiments demonstrated that one particular mode was superior to all others for diamond film deposition. This particular mode was identified as the TM_{011} mode by electromagnetic field pattern measurements. A detailed description of field pattern measurements is provided in chapter 5. A schematic drawing of the field pattern of the TM_{011} mode in a discharge loaded cavity is shown in Figure 3.7. As shown in Figure 3.5, when excited in this mode, the discharge hovered over and was in direct contact with the substrate which was placed along

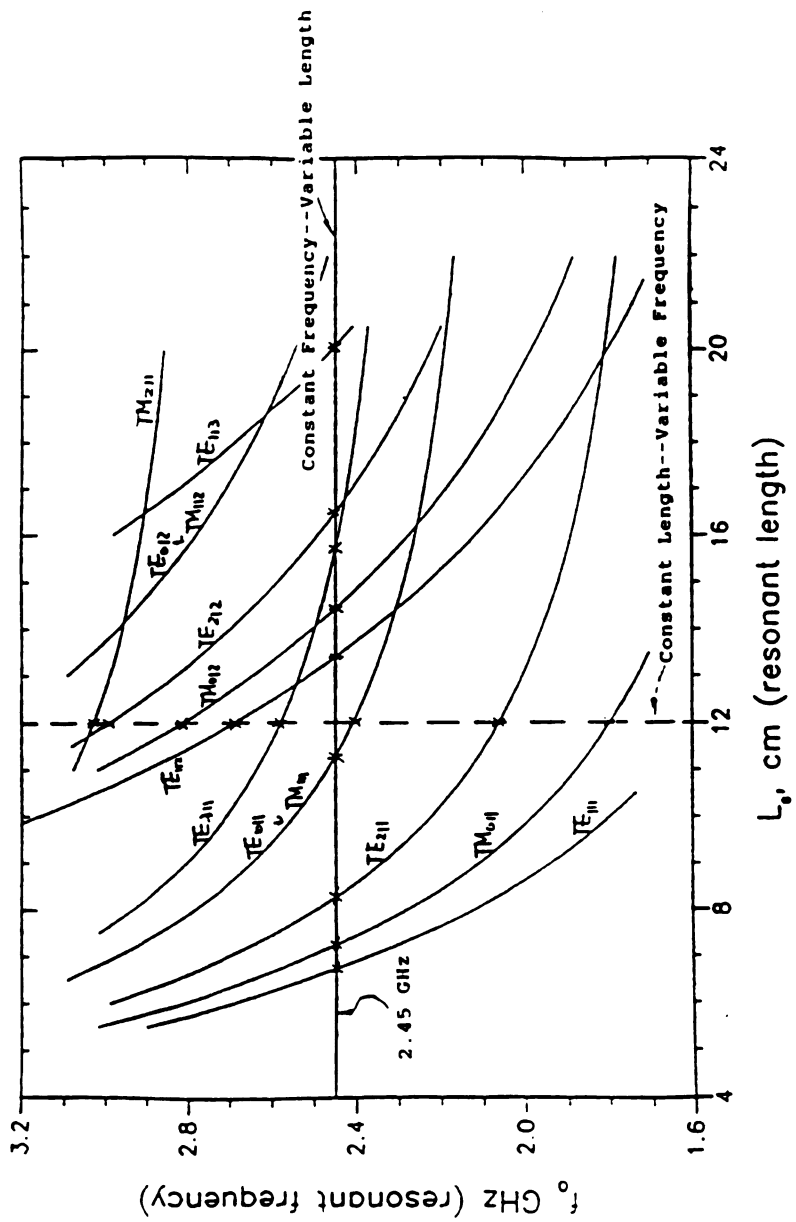

Figure 3.6 Mode Diagram of an Ideal 7" Cavity

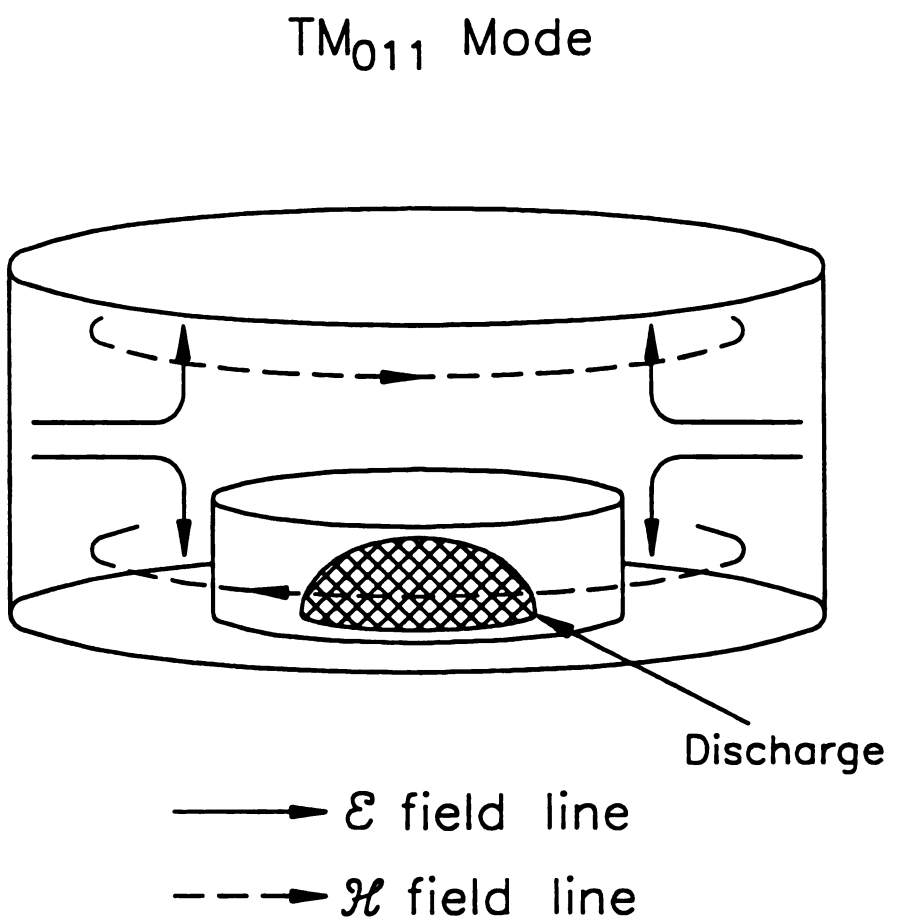

Figure 3.7 Field Pattern of Discharge Loaded TM_{011} Mode

the cavity axis. Under discharge loaded deposition conditions, the cavity length, L_s, was set at approximately 7.2 cm and the probe position, L_p, was adjusted to about 1.8 cm. Deposition experiments were performed with this electromagnetic mode.

3.3.4 Substrate Holder and Quartz Domes

A variety of substrate (14) materials have been used for diamond film deposition in this reactor. These materials include silicon wafers, silicon nitride, carbide drill bits, tungsten wires, etc. The most frequently used substrate materials are silicon wafers since they are readily available, common substrate materials in integrated circuits and bench mark materials for reactor performance determination.

The substrate holders (13) were usually made of graphite, amorphous carbon or boron-nitride. In most holders, recess areas are made on the top surface to accommodate the substrate (14) materials to prevent them from moving during the deposition processes. The typical substrate holder (13) size had a diameter of 5 cm or smaller.

The cylindrical quartz tubes (12) were cut from a quartz tube with an outside diameter of about 1". Typical quartz tube (12) length ranges from 2.5 to 4 cm, depending on the experimental conditions, substrates and substrate holders.

Besides holding the quartz tube (12), the graphite base (11) also helps to attract the plasma discharge (6) to the substrate (14) so that reactive species in the plasma discharge (6) can be effectively utilized for diamond film growth.

The optimum substrate (14) and substrate holder (13) position was

found empirically by numerous experimental runs. The location varied with substrate size and type, gas pressure and flow, input power, etc.

This reactor is designed to accept several height, 9.25 cm i.d. quartz domes (5). There is a range for the optimum quartz dome (5) height and this optimum range depends slightly on substrate size and location. For quartz dome height below this optimum range, the hot plasma used for diamond film growth makes contact with the quartz dome top surface. Film deposition on the quartz dome and in extreme cases quartz dome overheating and melting may result. For quartz dome height above this optimum range, a second plasma appears in direct contact with the quartz dome top surface, weakening the intensity of the plasma in direct contact with the substrate. Again, film deposition on the quartz dome and in extreme cases quartz dome overheating and melting may result. The heights of the quartz domes used in most diamond film deposition experiments described in this dissertation are 4.35 cm and 6 cm. The O-ring groove (42) of the quartz domes is 2 cm below the cavity bottom surface (4). Thus, the top of the domes is located 2.35 cm and 4 cm above the cavity bottom surface (4).

3.3.5 Reactor Performance

Good quality diamond films have been deposited using this reactor on a variety of substrate materials. The actual thin film deposition performance of this reactor have been described in detail elsewhere[58]. Thus, only a brief description is given here.

Typical experimental pressures vary from 30 Torr to 80 Torr using mixtures of hydrogen (50 sccm - 400 sccm) and methane (0.5 sccm to 3

sccm). Under these conditions, absorbed 2.45 GHz power varied from 250 W to 800 W. The substrate area is generally 4 cm by 4 cm or smaller. The linear growth rate is in the range of 0.4 to 0.8 μm/hour.

A typical Raman spectrum of a diamond film (WDF08) deposited in this reactor under the following experimental conditions is shown in Figure 3.8.

CH_4 flow rate = 2.16 sccm

H_2 flow rate = 175 sccm

Pressure = 72.5 Torr

Microwave Power absorbed = 440 W

Though good quality diamond films can be deposited in this reactor, it has the following limitations. First, the vacuum o-ring seal is located close to the hot plasma/substrate region. The substrate has an operating temperature of the order of 700 - 1100 ^{o}C. Hence for any specific operating pressure, there is a limit on the absorbed power level and substrate area to prevent the o-ring failure. Second, the power input comes from the side of the cavity walls and produces an inherent non-uniform electromagnetic "near" field close to the excitation probe. For a small area substrate (5 cm in diameter or smaller), the effect is not significant. But as the substrate area and/or input power level is increased, this "near" field effect gets stronger. The discharge is attracted by the probe's strong "near" field onto the quartz dome walls, creating a non-uniform plasma, causing non-uniform film deposition on the substrate and heating up the quartz walls.

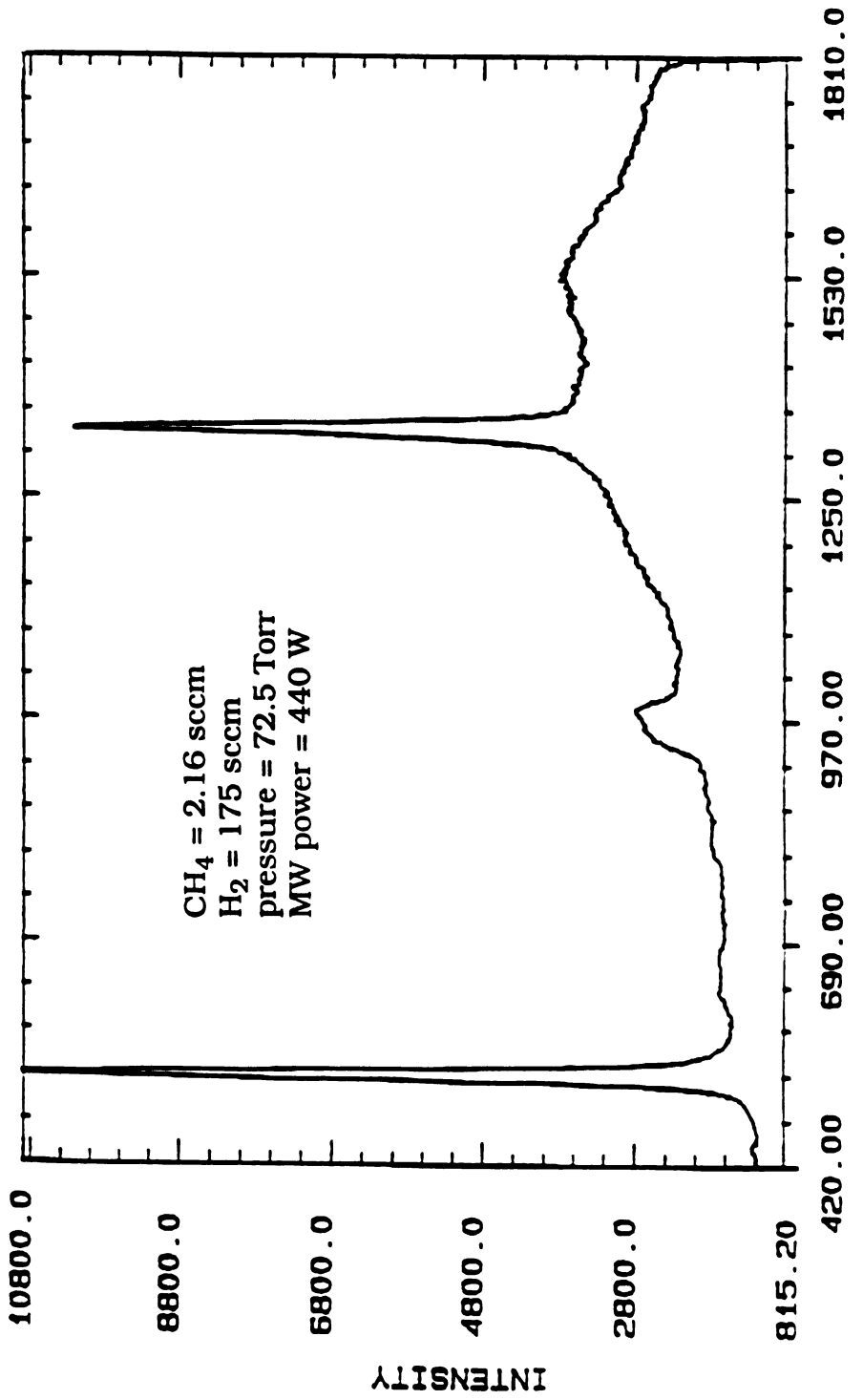

Figure 3.8 Raman Spectrum of a Diamond Film Deposited in MCPR7-1

3.4 The Second Generation Seven Inch MCPR

3.4.1 Introduction

In order to solve the near field problem faced in the MCPR7-1, several versions of second generation MCPR were investigated for diamond film growth.

3.4.2 Reactor Geometry

The second generation MCPR, called the MCPR7-2 in short, is schematically shown in Figure 3.9. As shown, the difference between this MCPR and the MCPR7-1 is that the power probe coupling (19) is now located at the top end of the cavity, instead of on the side of the cavity.

The sliding short (2) and coupling probe (19) adjustments, L_s and L_p, provide the internal cavity impedance tuning mechanism to minimize the reflected power.

New 7" cylindrical cavity walls (1) were designed and built which did not have the side feed port that existed in the conventional 7 inch cavities. This cavity was designed to be longer than the conventional cavity so that TM_{012} and TM_{013} modes can be excited. There are two windows/ports (22a,22b) on the new cavity. The cooling air inlet (22a) is for air input to cool the cavity and quartz dome (5). The window/air outlet (22b) serves as the exhaust port for the cooling air and also as a viewing port through which the substrate temperature is measured by an optical pyrometer.

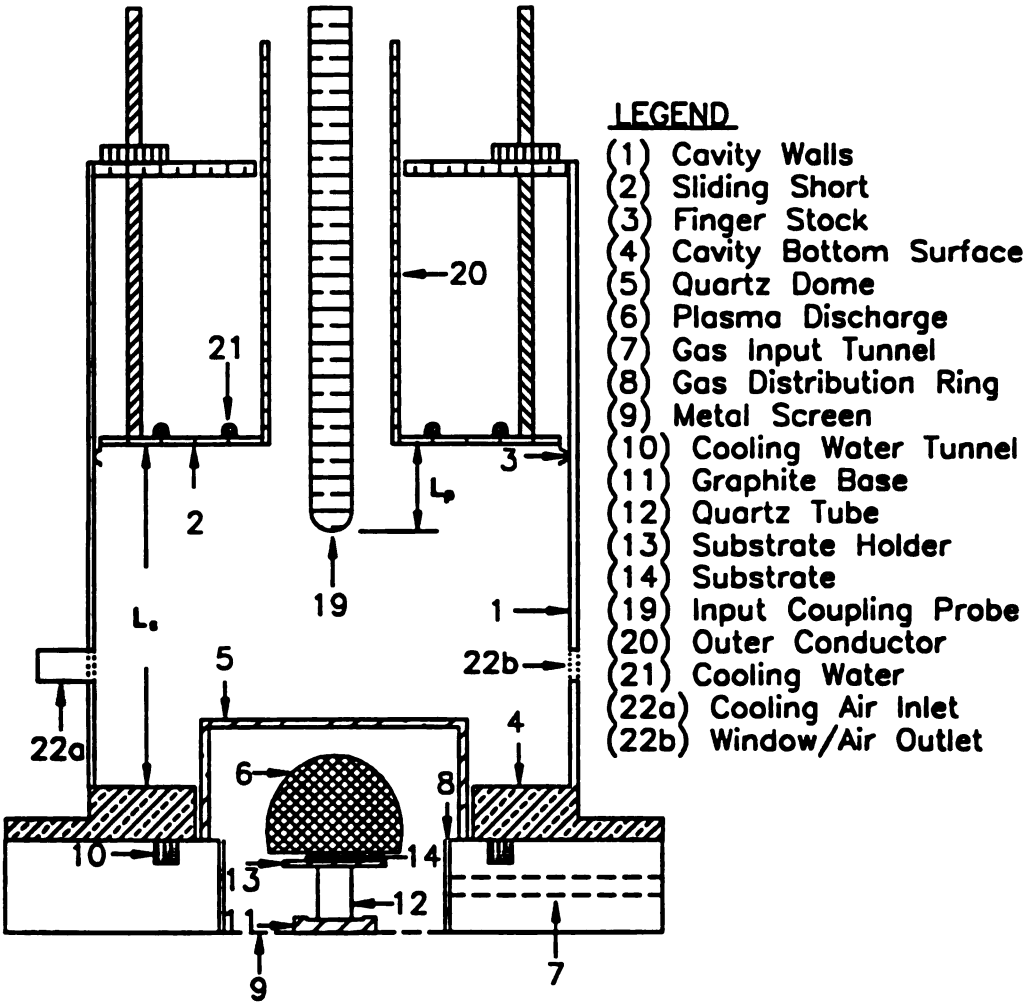

Figure 3.9 Schematic Drawing of MCPR7-2

3.4.3 TM_{01n} Modes Excitation

The experimental operation of this reactor is similar to the MCPR7-1. It uses the same mode diagram of an ideal 7" cavity shown in Fig. 3.6. and follows a similar starting procedure as that of MCPR7-1. The difference between the this reactor and MCPR7-1 is the mode that is used in diamond film deposition.

TM_{011} mode can be easily excited in this reactor. The plasma discharge (6) created is symmetric with respect to the axis of the cavity walls (1). But the probe near field effect still exists in this reactor with TM_{011} mode excitation. Under high input power conditions, the plasma discharge (6) is attracted to the top surface of the quartz dome (5) since the coupling probe (19) is located close to the top surface of the quartz dome with TM_{011} mode excitation.

To eliminate the near field effect, this reactor is excited using either the discharge loaded TM_{012} or TM_{013} mode. The field patterns of TM_{012} and TM_{013} modes are shown in Figure 3.10. With TM_{012} or TM_{013} mode excitation, the cavity length L_s is either doubled or tripled from that of TM_{011} mode excitation. Hence the near field of the coupling probe (19) is moved away from the quartz dome region and now has little effect on the geometry of the plasma discharge (6) that is created. Under discharge loaded TM_{012} mode excitation, the cavity length, L_s, was set at approximately 14.4 cm and the probe position, L_p, was adjusted to about 3.2 cm. Deposition experiments with this reactor (MCPR7-2) were performed with this electromagnetic mode. Under discharge loaded TM_{013} mode excitation, the cavity length, L_s, was set at approximately 21.6 cm and the probe position, L_p, was adjusted to about 3.2 cm. TM_{013}

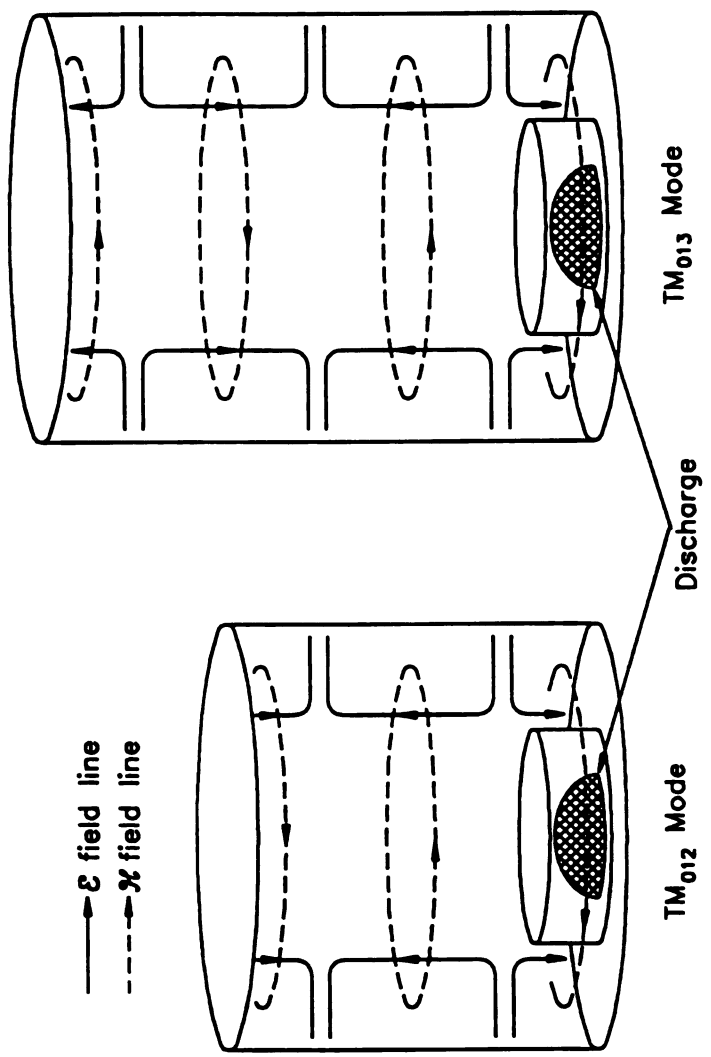

Figure 3.10 Field Patterns of Discharge Loaded TM_{012} and TM_{013} Modes

mode was used in the later part of the experiments conducted in the third generation MCPR (MCPR7-3) which is described in section 3.6.

Another advantage of this reactor over the MCPR7-1 is its reliable operation. In the side feed configuration used in MCPR7-1, since competing degenerate and near degenerate TM and TE modes can all be excited, there exists interference from degenerate and near degenerate dipole modes to the symmetric mode excitation that is desirable for diamond film deposition. But in the end feed configuration used in this reactor, only symmetric TM modes are excited. Hence, the mode excitation zone in the cavity are better separated and the interference from degenerating TE modes is eliminated. This makes the operation of this reactor easier and more reliable under all the substrate operating conditions than MCPR7-1.

3.4.4 End Feed Assembly

Initially, end feed assembly with 7/8" inside diameter probe sleeve (20) and 0.35" diameter coupling probe (19)[59] was tested for diamond film growth in February, 1991. Good quality diamond films were deposited on silicon wafers. After a few experiments, it was noted that the finger stock (3) on the sliding short (2) became fragile. It was over heated since the sliding short (2) to which the 7/8" end feed assembly is attached and the cavity walls (1) do not have water cooling to cool the finger stock (3) in the high input power conditions required for diamond film deposition. Also, the 7/8" coaxial cable was too small to handle the high power (over 1 kW) required for diamond film deposition on larger surface areas (5 cm in diameter or larger).

To solve the over heating and power handling problems, a new end feed with 1 5/8" inside diameter probe sleeve (20) and 5/8" diameter coupling probe (19) was designed and built. It was designed to be attached to a water cooled (21) sliding short (2). This new end power feed assembly has been used to operate at 4 kW over 20 hours in continuous experiments and over 2000 hours in total running time without any noticeable damage.

Air cooling is used to cool the cavity walls (1) and quartz dome (5) under high power input conditions. The cooling air inlet (22a) was initially designed and built to be 0.5" in diameter and compressed air was used as the cooling air supply. It was a noisy and unreliable air cooling system since it sometimes overloaded the air compressor in the Engineering Research Complex. That air cooling system was replaced by a new design. In the new design, the cooling air inlet (22a) was enlarged to 2" in diameter and double screened window was soldered onto the cavity walls (1) to ensure good electrical continuity of the cavity walls (1). A Dayton (model No. 4C443A) air blower with free air delivery speed of 100 cfm is used to supply the cooling air through the enlarged cooling air inlet (22a). This new system is a much quieter and more reliable air cooling system.

3.4.5 Reactor Performance

This reactor has been used to deposit diamond films over larger areas than that in MCPR7-1. The largest area covered was 5.7 cm in diameter. The linear growth rates are in the same range as in MCPR7-1, namely, 0.4 - 0.8 μm/hour.

The 7/8 inch coaxial power end feed system was used for diamond film growth on 3 cm x 3 cm square silicon substrates with the following typical experimental conditions:

CH_4 flow rate = 2 sccm

H_2 flow rate = 300 sccm

absorbed microwave power = 620 Watts

Pressure = 45 Torr

The 1 5/8 inch coaxial power end feed system was used for diamond film growth on 5.7 cm diameter silicon substrates with the following typical experimental conditions:

CH_4 flow rate = 3 sccm

H_2 flow rate = 300 sccm

absorbed microwave power = 1600 Watts

pressure = 40 Torr

A typical Raman spectrum of a diamond film (EDF-2) deposited in this reactor under the following experimental conditions is shown in Figure 3.11.

CH_4 flow rate = 2 sccm

H_2 flow rate = 300 sccm

absorbed microwave power = 560 Watts

pressure = 50 Torr

With the end feed, this reactor design solves the non-uniformity problem caused by the probe "near" field, but the o-ring over-heating problem that existed in MCPR7-1 was still a problem and limited the performance of this reactor.

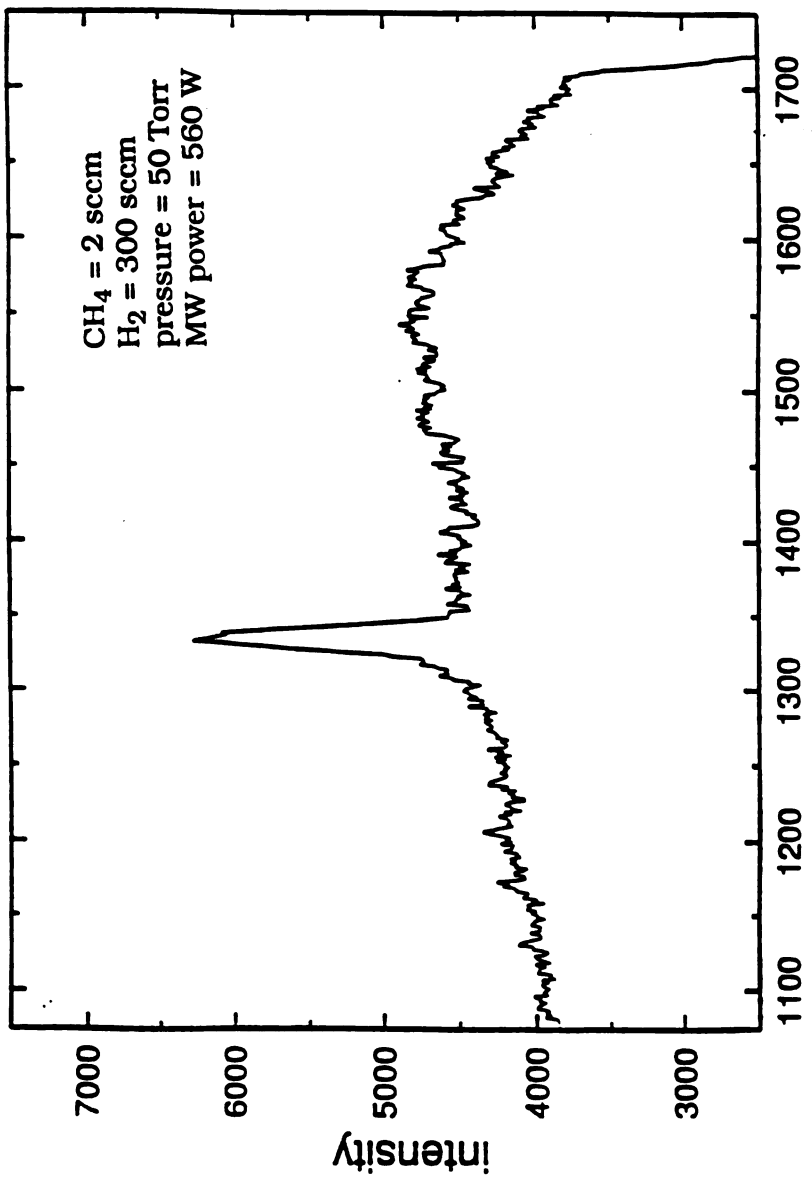

Figure 3.11 Raman Spectrum of a Diamond Film Deposited in MCPR7-2

3.5 Microwave Coupling Methods

3.5.1 Introduction

A series of experiments were performed to find the optimum configuration for the excitation of microwave discharges for diamond film deposition over large surface areas. The following excitation variations were compared: (I) loop and probe coupling, (II) cavity end feed and side feed, and (III) TM_{011}, TM_{012}, TM_{013} and TE_{011}modes excitation.

3.5.2 Loop Coupling and Probe Coupling

In an attempt to excite TE_{011} mode, whose field pattern is shown in Figure 3.12, a loop coupling system was designed. It is schematically shown in Figure 3.13. The loop coupling system was realized by first designing and constructing a series of open loops (arc) (35) from small brass rods. The probe in the side feed was taken out and replaced by these open loops. The open loop was attached at one end to the end of the center conductor of the power input port and pressed against the outer conductor (18) wall at the other end. The loop can be moved horizontally to change the area of the loop and rotated to change the orientation of the loop inside the cavity. A new outer conductor tube for the power input port was designed and built. To eliminate microwave radiation leakage during the linear movement and rotation of the loop, this outer conductor tube did not have the narrow opening machined on the original outer conductor tube for the indication of probe length in the probe coupling.

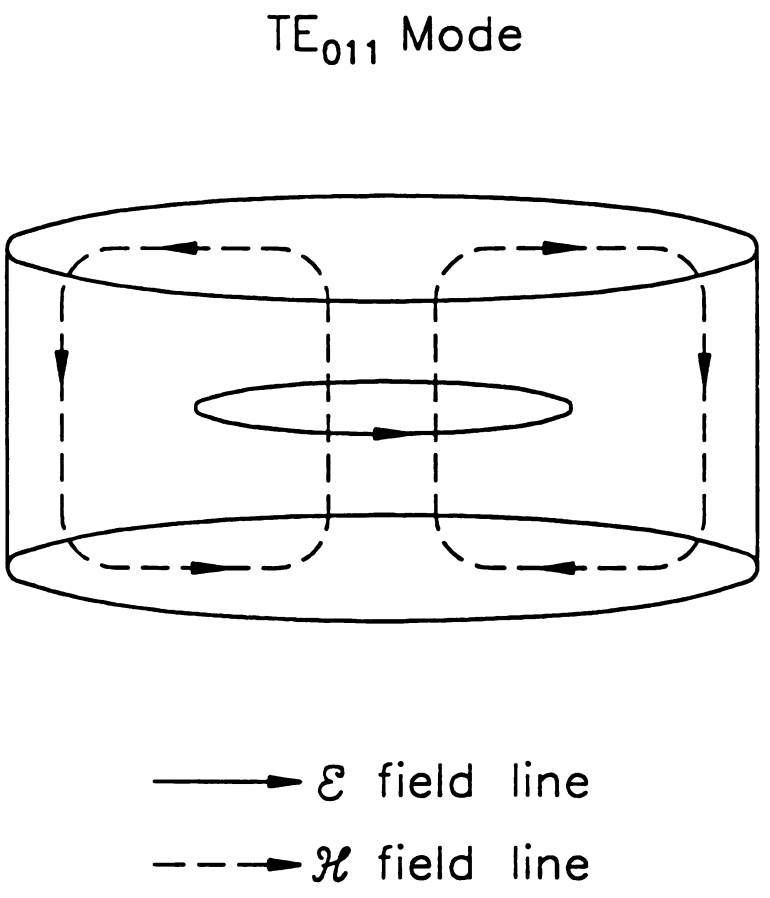

Figure 3.12 Field Pattern of TE_{011} Mode

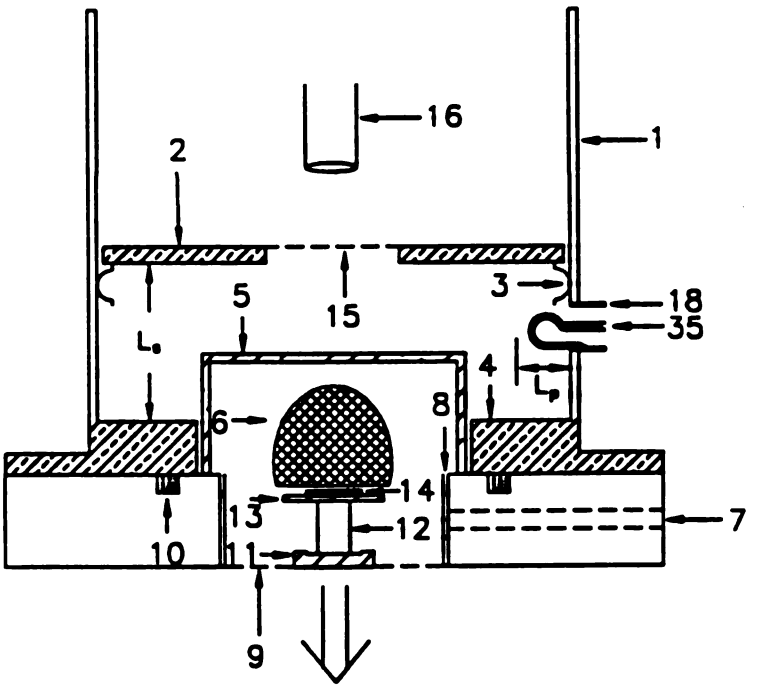

LEGEND

(1) Cavity Walls	(10) Cooling Water Tunnel
(2) Sliding Short	(11) Graphite Base
(3) Finger Stock	(12) Quartz Tube
(4) Cavity bottom surface	(13) Substrate Holder
(5) Quartz Dome	(14) Substrate
(6) Plasma Discharge	(15) Top Window
(7) Gas Input Tunnel	(16) Pyrometer Sensor
(8) Gas Distribution Ring	(18) Outer Conductor
(9) Metal Screen	(35) Power Coupling Loop

Figure 3.13 Schematic Drawing of a Loop Coupling System

The cavity short length L_s, loop area and loop orientation were the three parameters varied to excite loaded cavity modes and match microwave power into the loaded cavity. It was found that the TM_{011} mode was the easiest mode to be excited and the associated plasma was produced. The TE_{011} mode was not excited using this loop. When the TM_{011} mode was excited with the loop, the coupling was not efficient, possibly due to the loose contact between the outer conductor (18) wall and the open loop (35). This loose contact problem can not be easily solved since the loop is rotated and also moved linearly in order to match the input power into the cavity. Arcing takes place at the loose contacts at high input power conditions. Hence, loop coupling can not be easily used at high input power conditions which are required for diamond film growth over larger surface areas.

Compared with loop coupling, probe coupling does not have the loose contact and arcing problems. Thus it became the favorable choice for the excitation of plasma for diamond film deposition.

3.5.3 End Coupling and Side Coupling

An end feed can excite symmetric TM modes and keep the near field away from the plasma/substrate region by exciting higher order modes in diamond film growth process. These are advantages over the side feed where the probe is located on the cavity side wall and a non-symmetric field is always produced. At high input power conditions, a reactor using side feed faces the problem caused by near field if it is to be operated at lower order modes. It also faces the competing excitation problem caused by degenerating or closely degenerating dipole TE and

TM modes if it is to be operated at higher order modes. By contrast, the end feed excitation makes the operation of the diamond film deposition reactor easy and reliable by selective excitation of symmetric TM modes. It is a favorable choice for the excitation of microwave plasma for uniform diamond film deposition on larger surface areas.

3.5.4 Mode Excitation

The mode patterns of TM_{011}, TM_{012}, TM_{013}, and TE_{011} are shown in Figures 3.7, 3.10, and 3.12. In side feed probe coupling and loop coupling, TM_{011} mode is the easiest mode to be excited but the near electromagnetic fields attract the plasma to the side walls in the case of high power input. In end feed probe coupling, TE_{011} mode can not be easily excited and TM_{011}, TM_{012} and TM_{013} modes are easily excited. But in the case of TM_{011} mode excitation, the near fields attract the plasma to the quartz disk top wall and limit high power input. The TM_{012} or TM_{013} mode is the ideal mode to be used for plasma excitation for diamond film deposition in the end feed probe coupling configuration, since the near field effect can be reduced by keeping the probe away from the quartz disk, and high power can be input to produce a large cylindrically symmetric plasma.

3.6 The Third Generation Seven Inch MCPR

3.6.1 Introduction

In order to be able to deposit diamond film uniformly on large surface areas, a new 7 inch microwave plasma disk reactor was designed and built. It was first tested for diamond film growth in May, 1991.

3.6.2 Reactor Configuration

3.6.2.1 Introduction

This reactor was designed to operate in various configurations. These configurations include the basic configuration, forced flow configuration, jet configuration, lower cavity resonance configuration and down stream configuration, etc. A detailed description of each configuration is provided in following sections. Preliminary versions of these configurations have been investigated for diamond film growth.

3.6.2.2 The Basic Configuration

The principle components of the basic configuration reactor are displayed in the cross-sectional view of Figure 3.14. This reactor uses the optimized end feed probe coupling. The power feed is the 1 5/8 inch coaxial power input assembly (19, 20). The end feed assembly (19,20) along with the sliding short (2) form top end of the cavity. The lower section of the cavity consists of the bottom surface (4), the base-plate

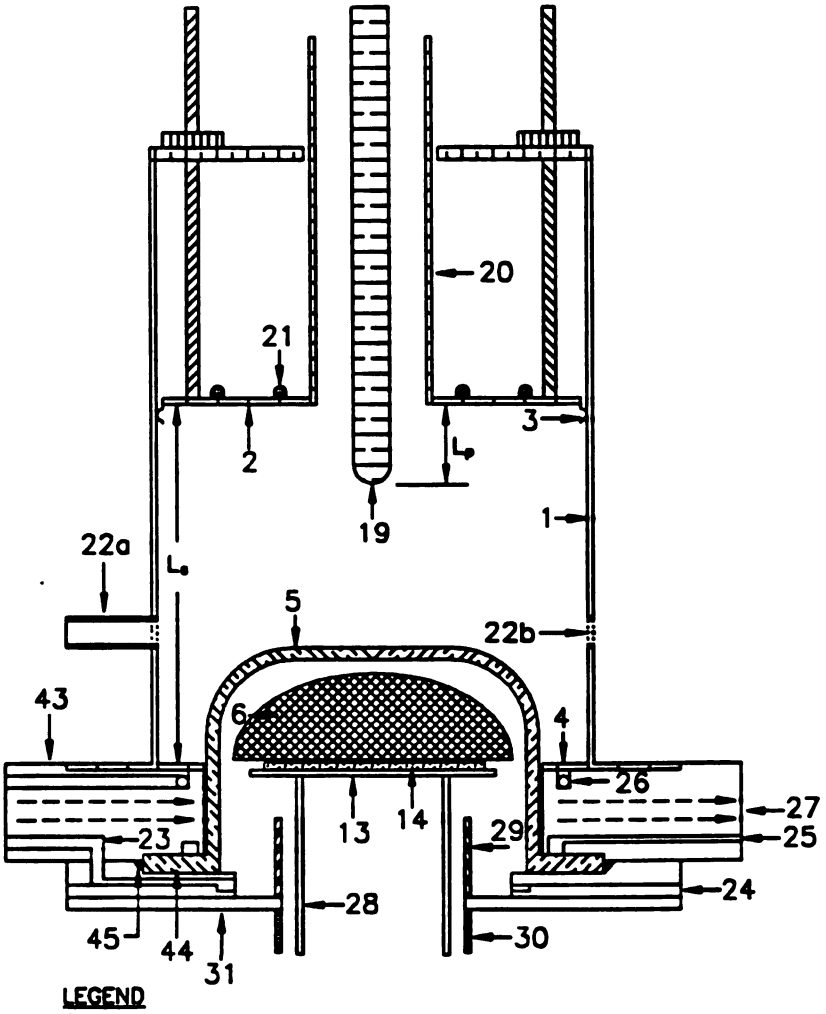

LEGEND

(1) Cavity Walls
(2) Sliding Short
(3) Finger Stock
(4) Cavity Bottom Surface
(5) Quartz Dome
(6) Plasma Discharge
(13) Substrate Holder
(14) Substrate
(19) Power Coupling Probe
(20) Probe Sleeve
(21) Cooling Water
(22a) Cooling Air Inlet
(22b) Window/Air Outlet
(23) Gas Input Tunnel
(24) Distribution Plate
(25) Air Cooling Tunnel
(26) Cooling Water Tunnel
(27) Laser Port
(28) Quartz Tube
(29) Metal Tube
(30) Metal Choke
(31) Metal Plate
(43) Base Plate
(44) Quartz Flange
(45) O-ring Seal

Figure 3.14 The Basic Experimental Configuration

(43), a metal tube (resonance breaker) (29), a metal plate (31) and a metal choke sleeve (30).

The reactive gases, which are supplied through the source gas input tunnel (23) and annular source gas ring on the gas distribution plate (24), is confined at the lower section of the cavity by the quartz dome (5). The quartz dome (5) is enlarged in both diameter and height. Water cooling is incorporated in the sliding short (2) and the base plate (43) by using annular water cooling tunnels (21, 26). There is also a air cooling tunnel (25) built in the base plate (43) for the cooling of the quartz dome walls under high input power operations. Windows (27) are incorporated in the base plate for laser induced fluorescence diagnosis of the microwave plasma under diamond film deposition conditions. A top/ cross-sectional view of the base plate (43) is shown in Figure 3.15.

The substrate (14) to be coated with diamond film lays on top of a substrate holder (13) which is supported by a quartz tube (28). Different height quartz tubes (28) were used to change to the position of the substrate with respect to the plasma discharge (6). If available, a mechanical moving stage can be used to change the substrate position. The metal tube (29) was a 3 inch outside diameter stainless steel tube. It functioned as a resonance breaker. It ensured that the plasma discharge (6) stayed on top of the substrate by breaking the cavity resonance and the discharge excitation condition in the smaller cavity underneath the substrate. By ensuring that the plasma discharge (6) is only created above the substrate, the resonance breaker (29) improves the efficiency of the microwave input power. It also improves the reliability and repeatability of the experimental results and the area on a substrate that can be uniformly coated with diamond film. The metal choke (30) sleeve

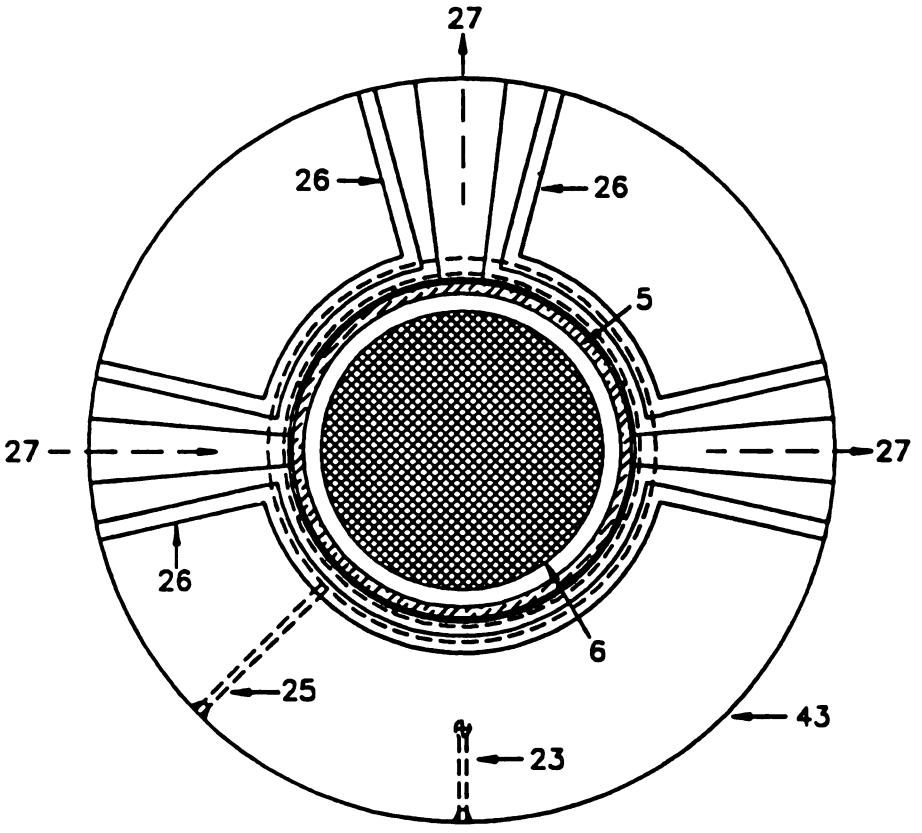

LEGEND
(5) Quartz Dome
(6) Plasma Discharge
(23) Gas Input Tunnel
(25) Air Cooling Tunnel
(26) Cooling Water Tunnel
(27) Laser Port
(43) Base Plate

Figure 3.15 The Base-plate of MCPR7-3

provides a floating end of the cavity and a choke of the microwave radiation.

This design minimizes the plasma volume by creating a hemisphere shaped plasma adjacent to the substrate. The cylindrical symmetry of the tuning mechanism and system configuration ensures that the plasma generated has an inherent cylindrical symmetry. This reactor is mounted on a vacuum chamber with chamber walls and a chamber outlet leading to a vacuum pump.

3.6.2.3 The Forced Flow Configuration

Figure 3.16 is a schematic drawing of a forced flow configuration. This configuration is different from the basic configuration by the way the gas flow passage is controlled. In the basic configuration, the gas flow is not controlled, it flows naturally inside the quartz dome (5). Whereas in this forced flow configuration, a metal plate (31) and a quartz tube (28) are put together to force the gas to flow through a flow pattern regulator (32). The flow pattern regulator (32) is a plate with a series of holes, directing the way that the gas flows through the plasma and the substrate. This configuration increases not only the efficiency of the source gas but also the uniformity of the coating by influencing the shape of the plasma discharge (6) through changing the flow pattern into the plasma discharge (6).

Figure 3.17 (a) shows one example of flow regulator, where a number of smaller substrates are being coated. Variation of input power, pressure and flow rates along with the flow pattern regulator produces uniform plasma over the smaller substrates and ensures uniform

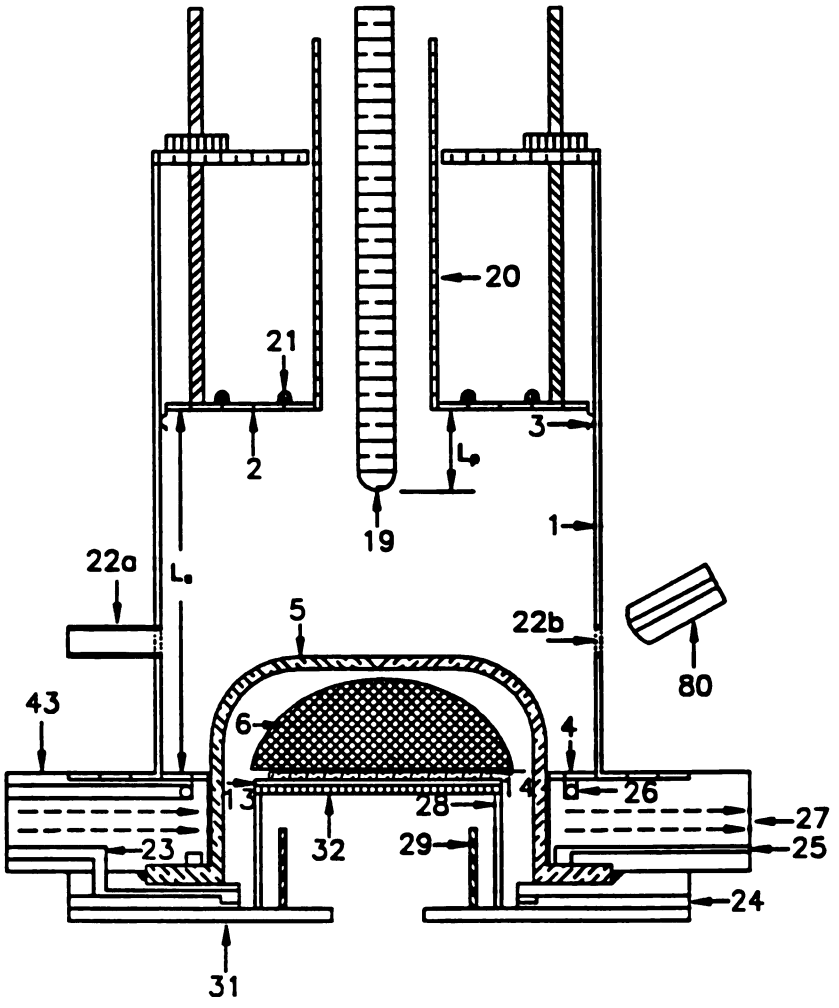

LEGEND

(1) Cavity Walls
(2) Sliding Short
(3) Finger Stock
(4) Cavity Bottom Surface
(5) Quartz Dome
(6) Plasma Discharge
(13) Substrate Holder
(14) Substrate
(19) Power Coupling Probe
(20) Probe Sleeve
(21) Cooling Water
(22a) Cooling Air Inlet
(22b) Window/Air Outlet
(23) Gas Input Tunnel
(24) Distribution Plate
(25) Air Cooling Tunnel
(26) Cooling Water Tunnel
(27) Laser Port
(28) Quartz Tube
(29) Metal Tube
(31) Metal Plate
(32) Flow Regulator
(43) Base Plate
(80) Optical Pyrometer

Figure 3.16 The Forced Flow Experimental Configuration

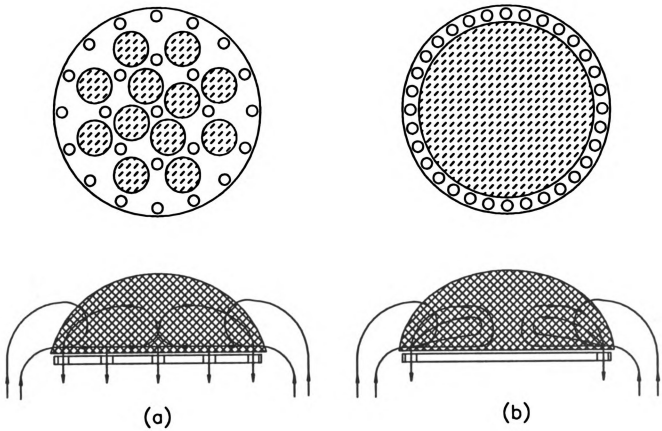

Figure 3.17 Flow Pattern Regulators

coatings on them. Figure 3.17 (b) shows another example of flow pattern regulator, where a large piece of substrate is being coated. Variation of input power, pressure and flow rates along with the flow pattern regulator produces a uniform plasma over the substrate so that a uniform diamond coating can be obtained.

3.6.2.4 The Jet Configuration

Figure 3.18 is a schematic drawing of a jet configuration where the substrate (14) and substrate holder (13) are located in a region separated from the plasma discharge (6). The metal plate (31) and quartz tube (28) are put together to force the gas flow through the jet grid (33) which is an electrically conducting plate with a series of holes. The size of the holes, the flow rate and the vacuum pump's pumping speed determine the pressure difference between the plasma discharge (6) region and chamber region wherein the substrate (14) is located. In this configuration, the reactive species are forced to flow at a higher speed over selected areas so that the deposition rates at the selected areas are increased.

3.6.2.5 The Lower Cavity Resonance Configuration

Figure 3.19 shows a lower cavity resonance configuration where the substrate (14) is located at the lower section of the cavity without the use of metal resonance breaker (29) shown in Figure 3.14. This was the first configuration used for diamond film growth in the third generation MCPR.

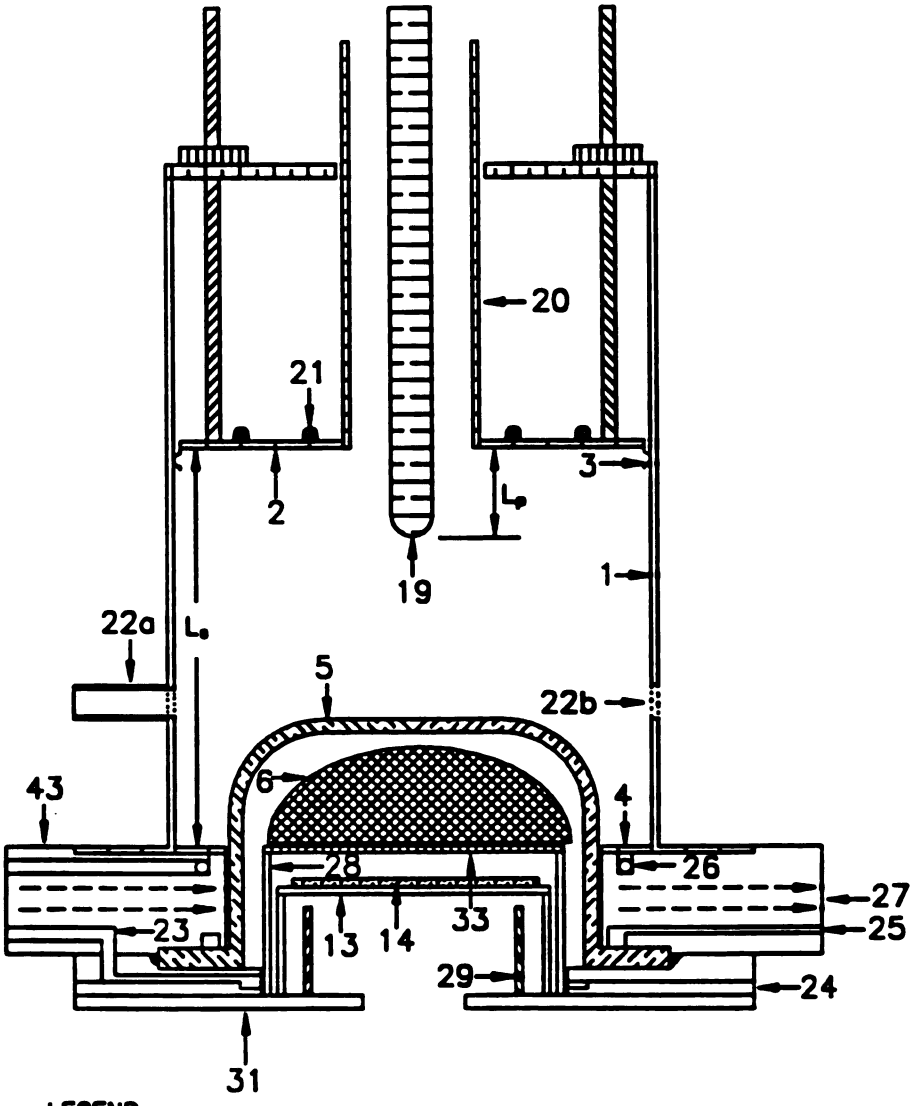

LEGEND

(1) Cavity Walls
(2) Sliding Short
(3) Finger Stock
(4) Cavity Bottom Surface
(5) Quartz Dome
(6) Plasma Discharge
(13) Substrate Holder
(14) Substrate
(19) Power Coupling Probe
(20) Probe Sleeve
(21) Cooling Water
(22a) Cooling Air Inlet
(22b) Window/Air Outlet
(23) Gas Input Tunnel
(24) Distribution Plate
(25) Air Cooling Tunnel
(26) Cooling Water Tunnel
(27) Laser Port
(28) Quartz Tube
(29) Metal Tube
(31) Metal Plate
(33) Jet Grid
(43) Base Plate

Figure 3.18 Jet Experimental Configuration

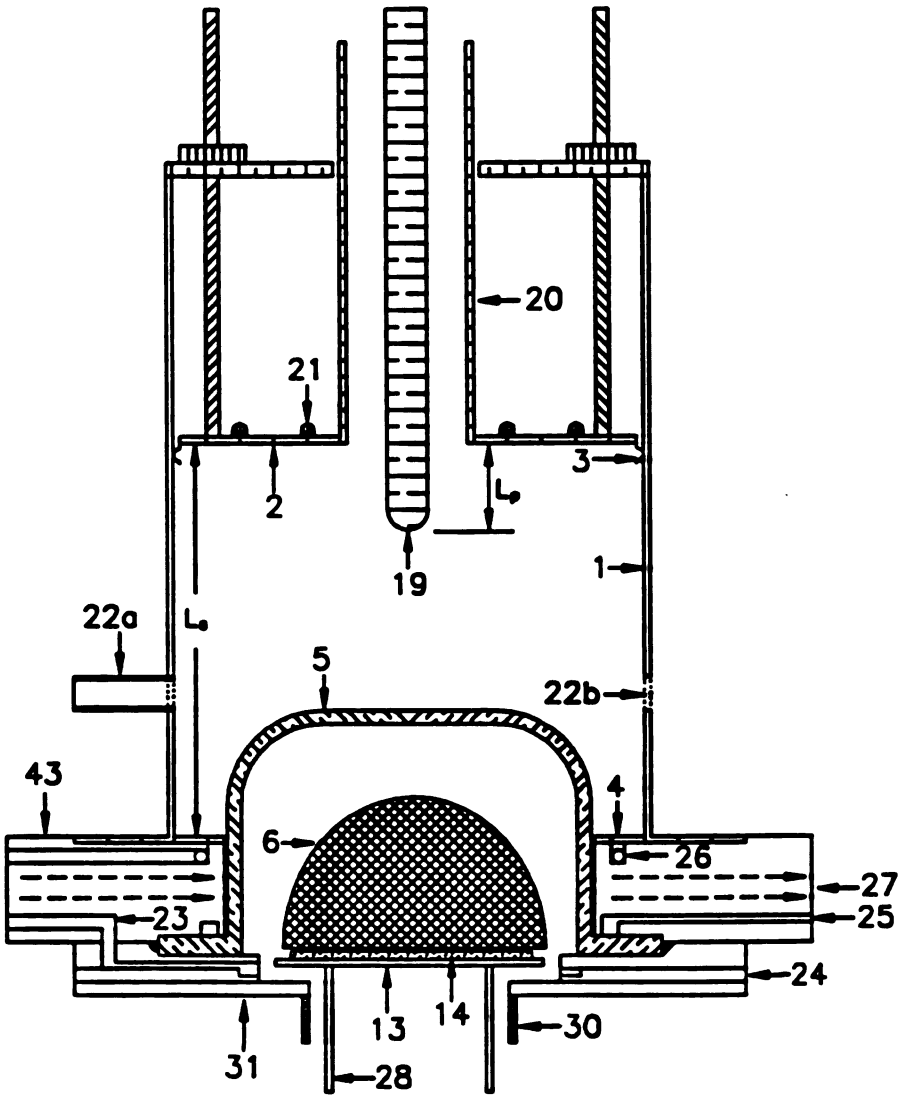

LEGEND

(1) Cavity Walls	(22a) Cooling Air Inlet
(2) Sliding Short	(22b) Window/Air Outlet
(3) Finger Stock	(23) Gas Input Tunnel
(4) Cavity Bottom Surface	(24) Distribution Plate
(5) Quartz Dome	(25) Air Cooling Tunnel
(6) Plasma Discharge	(26) Cooling Water Tunnel
(13) Substrate Holder	(27) Laser Port
(14) Substrate	(28) Quartz Tube
(19) Power Coupling Probe	(30) Metal Choke
(20) Probe Sleeve	(31) Metal Plate
(21) Cooling Water	(43) Base Plate

Figure 3.19 Lower Cavity Resonance Configuration

3.6.2.6 The Down-stream Configuration

Figure 3.20 shows a down-stream configuration where the substrate (14) is located outside the cavity and plasma discharge (6) region.

The substrate can be biased with a voltage during the deposition. The temperature of the substrate can be adjusted by a heater or cooling tunnels. Permanent magnets can be placed in the base-plate (43) around the plasma discharge (6) region to enhance plasma formation at low deposition pressures.

3.6.3 Reactor Operation

The reactor operation of the third generation 7" MCPR (MCPR7-3) is similar to that of MCPR7-2. The main difference is that TM_{013} mode is used in later part of the experiments conducted in MCPR7-3 where the cavity length, L_s, was set at approximately 21.6 cm and the probe length, L_p, was adjusted to about 3.2 cm.

3.6.4 Reactor Performance

3.6.4.1 Introduction

Preliminary versions of the five operating configurations have been investigated for diamond film growth. A summary of the reactor performance in the preliminary versions of is given below. Detailed description of reactor performance in the force flow configuration is given

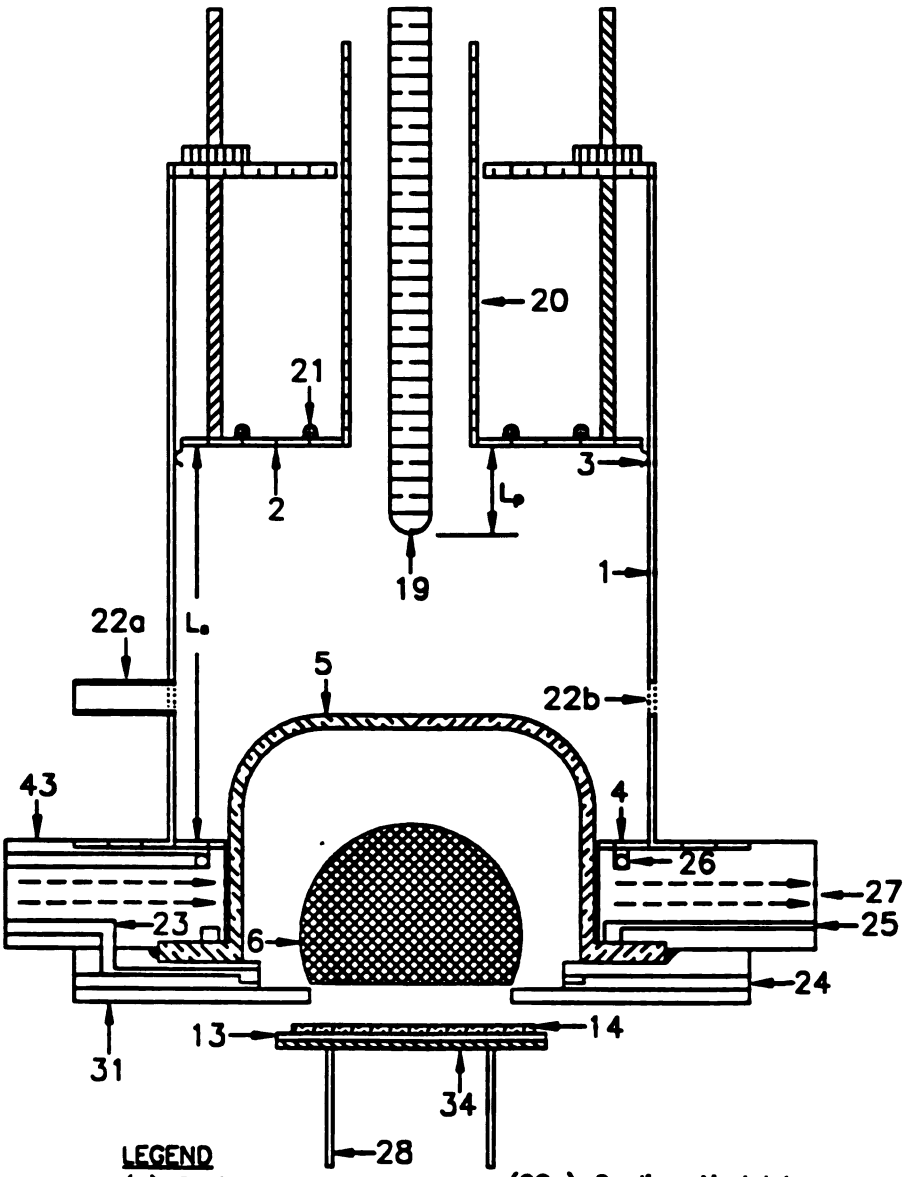

Figure 3.20 Down-stream Experimental Configuration

in chapter 6.

3.6.4.2 The Basic Configuration

Diamond film was deposited on 4" silicon wafer under the following experimental conditions:

H_2 gas flow = 300 sccm

CH_4 gas flow = 3 sccm

Pressure = 20 Torr

MW power absorbed = 2 kW

Seeding: scratched with 1 μm diamond powder.

The resultant diamond film deposition rate was slow (~ 3 mg/hr), possibly due to low operating pressure and power. Both graphite and amorphous carbon substrate holders were used in diamond film deposition processes in this configuration. It was found that higher film growth rates were obtained with the amorphous carbon substrate holders, possibly due to easier carbon dissolution from the amorphous carbon holder into the reactive gas mixture. The amorphous carbon holders were distorted in the high temperature deposition processes.

3.6.4.3 The Forced Flow Configuration

Using the forced flow configuration, a 12 cm diameter discharge was created with 200 sccm hydrogen and 2 sccm methane gas flow at 40 Torr with 4 kW 2.45 GHz absorbed power. The discharge area produced is larger than any discharge area reported in the open literature. The discharge created had a symmetric, hemisphere shape over the substrate

surface. Diamond films have been deposited uniformly on 4 inch diameter silicon wafers. The uniform coated area is larger than any coated area reported in the open literature. A detailed description of the reactor performance in this configuration is provided in chapter 6.

3.6.4.4 The Jet Configuration

A preliminary version of this configuration was used for diamond film deposition. It is schematically shown in Figure 3.21. In this preliminary version, gas was forced to flow through the center hole on the graphite grid. The center hole is 0.5 inch in diameter and the substrate was located approximately 1 cm below the graphite grid. Without using any cooling mechanism, increased deposition rate (~ 1 μm/hr) over 1.5 cm diameter area had been achieved. Typical experimental conditions are as follows:

H_2 flow rate = 400 sccm

CH_4 flow rate = 6 sccm

CO_2 flow rate = 2 sccm

pressure = 95 Torr

absorbed microwave power = 1.67 kW

The deposition rate was limited because of substrate melting at high pressure and temperature conditions. It is expected that by adding cooling tunnels underneath the substrate to control the substrate temperature, higher pressure and power can be used to further increase the deposition rates.

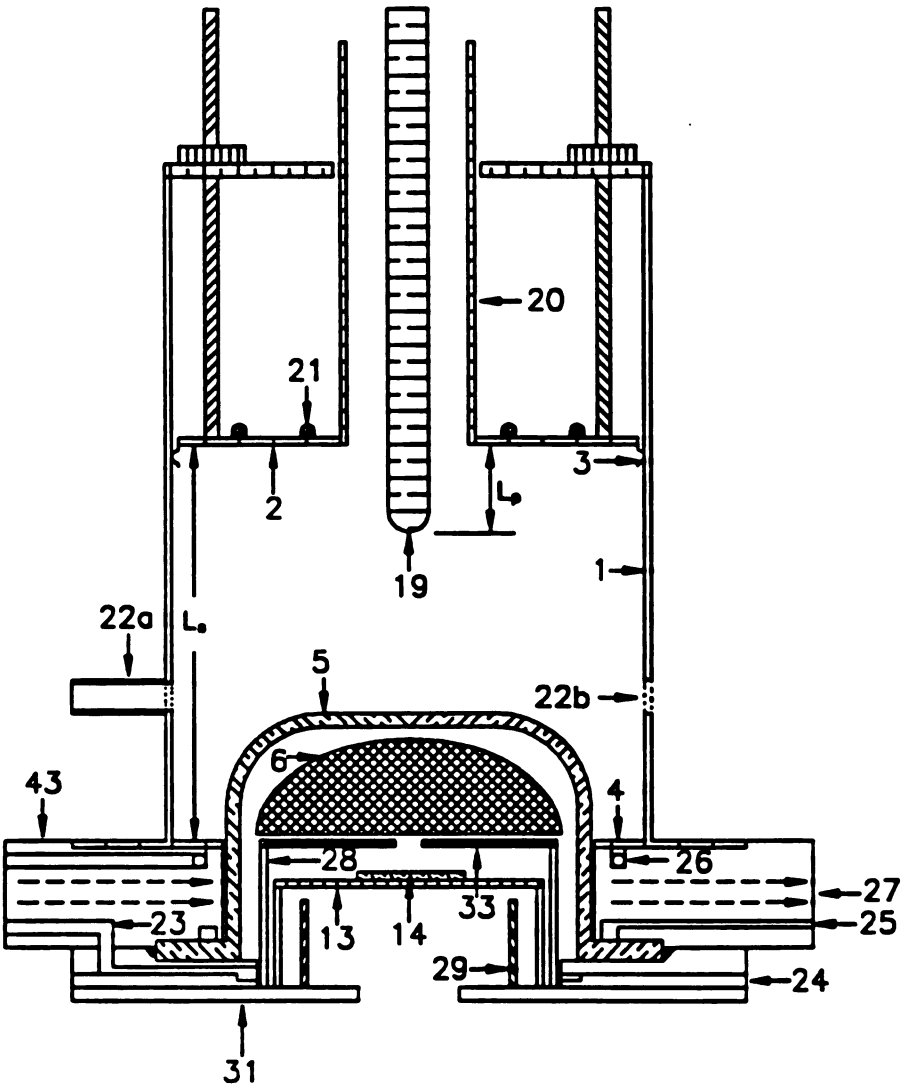

LEGEND

(1) Cavity Walls
(2) Sliding Short
(3) Finger Stock
(4) Cavity Bottom Surface
(5) Quartz Dome
(6) Plasma Discharge
(13) Substrate Holder
(14) Substrate
(19) Power Coupling Probe
(20) Probe Sleeve
(21) Cooling Water
(22a) Cooling Air Inlet
(22b) Window/Air Outlet
(23) Gas Input Tunnel
(24) Distribution Plate
(25) Air Cooling Tunnel
(26) Cooling Water Tunnel
(27) Laser Port
(28) Quartz Tube
(29) Metal Tube
(31) Metal Plate
(33) Jet Grid
(43) Base Plate

Figure 3.21 Preliminary Jet Experimental Configuration

3.6.4.5 The Lower Cavity Resonance Configuration

Diamond film was deposited on a 3 inch silicon wafer under the following experimental conditions:

H_2 gas flow = 200 sccm

CH_4 gas flow = 2 sccm

Pressure = 30 Torr

MW power absorbed = 2 kW

The resultant diamond film was fairly uniform. The deposition rate was ~ 3.56 mg/hr. It was found that a plasma discharge (6) generated in this configuration had to compete with a discharge generation process underneath the substrate holder (13). The competing process made the starting procedure complicated and unreliable.

3.6.4.6 The Down-stream Configuration

A preliminary experiment with this configuration was conducted in which a 3 inch substrate heater (34)<60> was used to control the substrate temperature.

A schematic drawing of the heater is shown in Figure 3.22.<60> As shown, it is a resistant heater and consists of three layers, a top boron-nitride (BN) (46), a pyrolytic graphite (47) and a lower boron-nitride (BN) (48) layer where the pyrolytic graphite layer is the middle layer. The exposed pyrolytic graphite areas (49) at the two ends are electrical contacts. This heater was specified to meet the following heating requirements, namely, it (a) has a 3" heating zone, (b) can achieve temperatures up to 1500 ^{o}C, (c) can achieve temperature uniformity of $\pm$

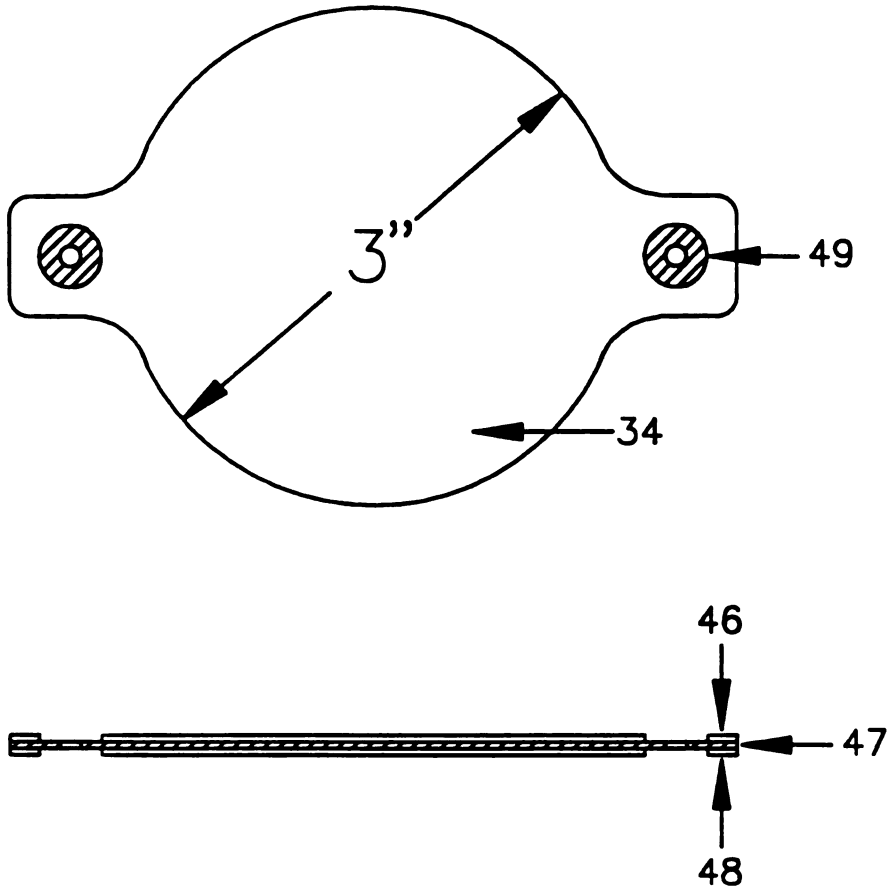

LEGEND
(34) Heater
(46) Top BN layer
(47) Pyrolytic Graphite
(48) Lower BN layer
(49) Contacts

Figure 3.22 Schematic Drawing of a 3" Substrate Heater

10 °C over the heating zone, (d) operates with 60 Hz, 0 - 200 Volts AC power, (e) draws a maximum current of 15 A and (f) can be used at pressures from 1 mTorr to 100 Torr in H_2/CH_4 gas mixture environment.

The experimental conditions were:

H_2 gas flow = 400 sccm

CH_4 gas flow = 4 sccm

Pressure = 15 Torr

MW power absorbed = 1.5 kW

Heater voltage = 100 Volts, 60 Hz

The resultant film growth rate was low and the film uniformity was poor.

3.7 Comparison of Seven Inch MCPRs

This third generation MCPR offer advantages over the reactors described in chapter two and the first two generations of MCPRs in that it creates a large symmetric, disk to hemisphere shaped discharge for uniform diamond film deposition over large surface areas. The symmetry of the plasma discharge is ensured by the symmetric, end feed power input configuration. The power input system, excitation probe and probe sleeve, have large dimensions so that high microwave power (2 to 5 kilowatts) can be delivered into the cavity. High input power, low near field effects, a large quartz disk and the design configuration of keeping the vacuum seal away from the heated areas ensure that a large diameter plasma can be created. The equator plane of the hemispherical shaped discharge is created and defined by the cavity bottom surface with the help of a metallic step near the outside surface of the quartz

disk and the lower cavity resonance breaker. The quartz disk ensures only the plasma adjacent to the substrate is produced and the efficiency of the absorbed power is maximized. The substrate is located near the equator of the hemisphere, hence the spacial uniformity of the distribution of reactive species and the thickness of deposited diamond film is ensured.

This reactor employs some of the basic features of the conventional microwave-cavity plasma reactors (MCPR). They are: (1) cylindrical cavity, (2) internal matching, i.e., sliding short and variable probe; (3) excitation of TM_{01n} modes for deposition of films. However, there are some important differences between the MCPR7-3 and the conventional microwave reactors. They are: (1) the probe is mounted on the sliding short, not on the cavity side walls, thus all the internal cavity adjustments take place on the sliding short; (2) the probe is located at the center of the short and thus only TM modes are easily excited; (3) the probe is located far away from the discharge region so that the probe near field does not interfere with the TM_{01n} mode electromagnetic fields within the discharge region; (4) larger diameter quartz disk can be used and (5) much higher microwave power can be delivered to the reactor to create a larger diameter plasma; (6) with the help of the lower cavity resonance breaker, the cavity bottom surface and the metallic step defines the equator of the symmetric, disk-like or hemisphere shaped plasma when the cavity is excited in TM_{01n} modes; (7) the substrate holder is adjustable in that it can be moved up and down independently, this feature together with the independent sliding short and excitation probe movement allow the movement of the relative position of the substrate with respect to the plasma so that the optimum deposition

conditions can be reached; (8) the forced reactive gas flow through the plasma near the substrate improves the efficiency of the reactive gases, and the uniformity of the deposited film; (9) film deposition down stream from the plasma; (10) independent and selected area substrate heating or cooling increases the deposition areas and film uniformity.

3.8 Fourteen and Eighteen Inch MCPRs

3.8.1 Introduction

The feasibility of diamond film growth over larger surface areas using larger diameter cavity MCPRs was investigated using 14" and 18" side feed MCPRs with 2.45 GHz and 915 MHz power. The test results are described in sections 3.8.2 and 3.8.3.

3.8.2 Fourteen Inch MCPR

The feasibility of diamond film growth using a side power feed 14" MCPR[<61>] and 2.45 GHz power was tested using the Chuang 1.2 kW 2.45 GHz power source. The schematic drawing of the experimental set-ups are shown in Figure 3.23 for substrate supported by a quartz tube and Figure 3.24 for substrate supported by a metal tube. As shown, these schematic drawings are similar to that shown in Figure 3.5. The main differences are that (a) the cavity inside diameter is now 14", (b) the vacuum seal is placed away from the discharge zone and (c) the quartz dome is 10" in diameter and 3.5" in height.

It was possible to couple microwave power into the cavity and a

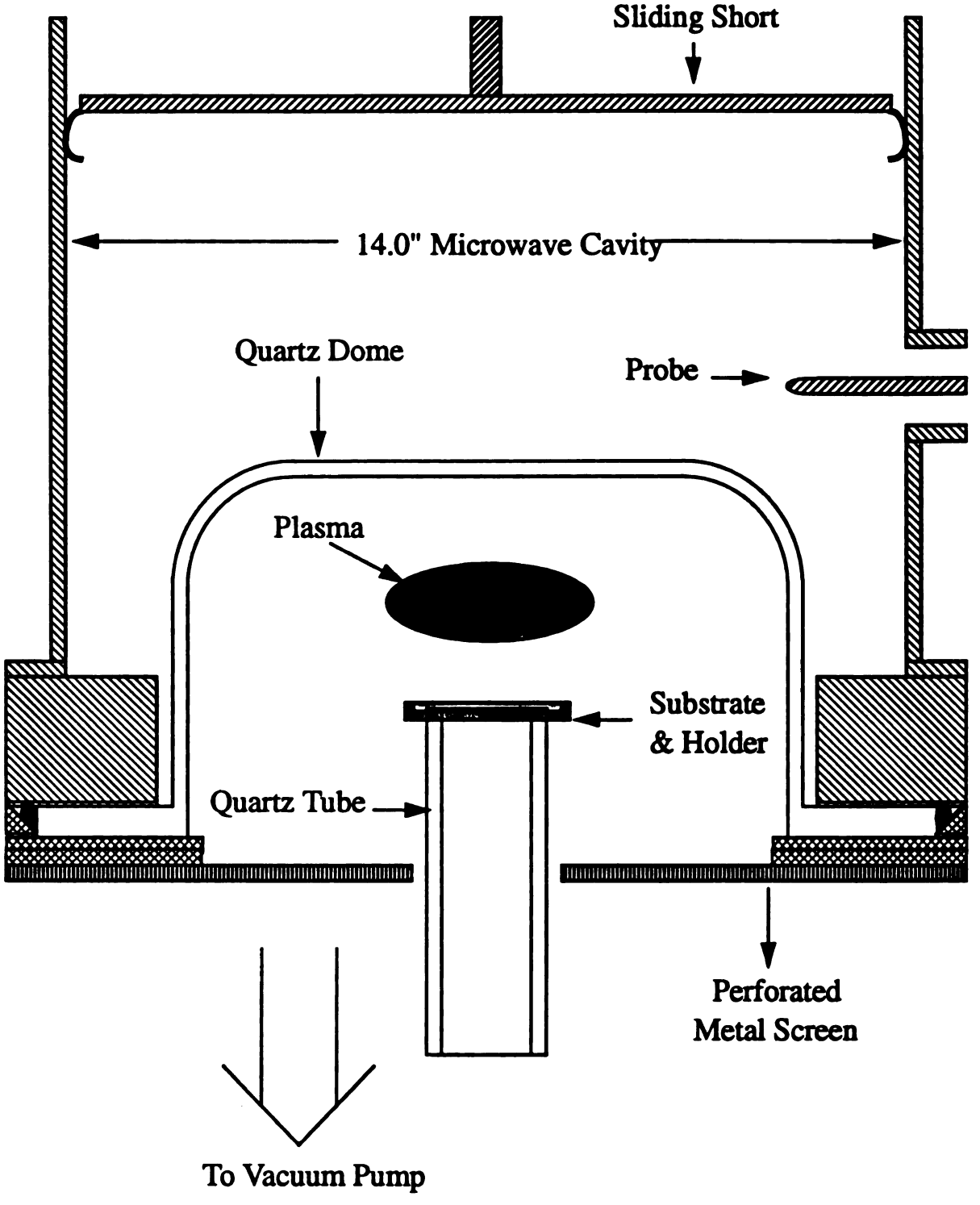

Figure 3.23 Substrate Supported by a Quartz Tube in 14" Cavity

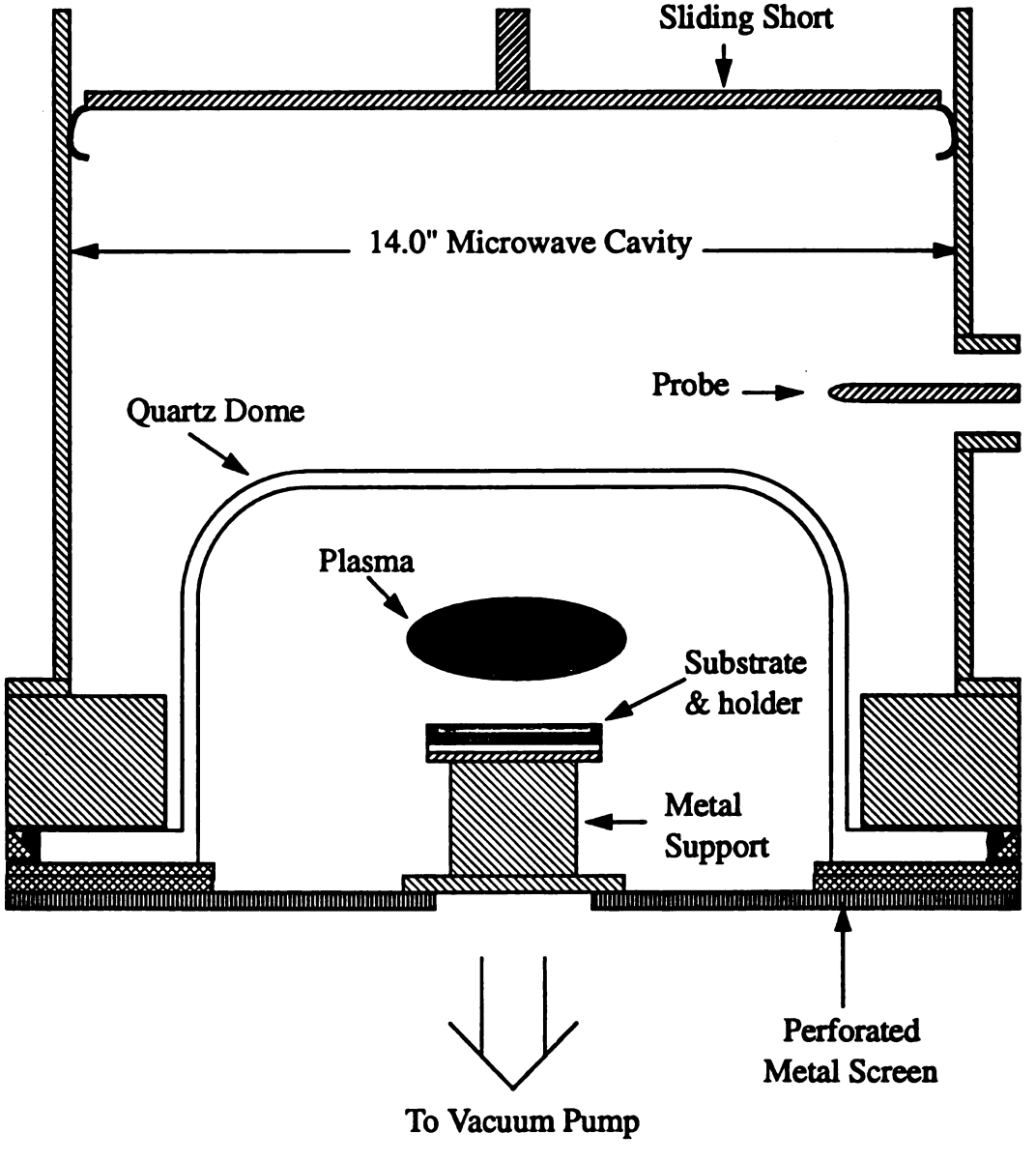

Figure 3.24 Substrate Supported by a Metal Tube in 14" Cavity

plasma disk can be produced. The plasma disk was approximately 3 inch in diameter at 20 Torr with 700 Watts power input. The plasma disk was suspended above the substrate surface.

From the resonant cavity lengths for the TM modes displayed in Figure 3.25 and Table 3.1, it is expected that TM_{012} mode can be excited in a 14 inch cavity without much interference from the other TM modes. With an end feed and a properly designed base plate, it is expected that discharge loaded TM_{012} mode can be excited in a 14" MCPR. Diamond film may be deposited in this reactor with a substrate moving stage and sufficient microwave power (3 - 15 kW).

3.8.3 Eighteen Inch MCPR

The concept of plasma discharge generation over larger surface area using 915 MHz power in a larger cavity was proposed by J. Asmussen.

To test this concept, an 18" MCPR[62] with side feed coupling was used with a 500 W, 915 MHz power supply. The schematic drawing of the 18" MCPR is similar to that shown in Figure 3.5. The cavity inside diameter is 18". The side feed probe sleeve has an inside diameter of 1 5/8" and the coupling probe has an outside diameter of 5/8".

After a series of experiments, it was found that the plasma discharge loaded TM_{011} mode can be easily excited. But the available power level was too low to be used for actual diamond film growth over a significant area.

The feasibility of diamond film growth using the 18" MCPR and 2.45 GHz power was tested using the Chuang 2.45 GHz 1.2 kW power

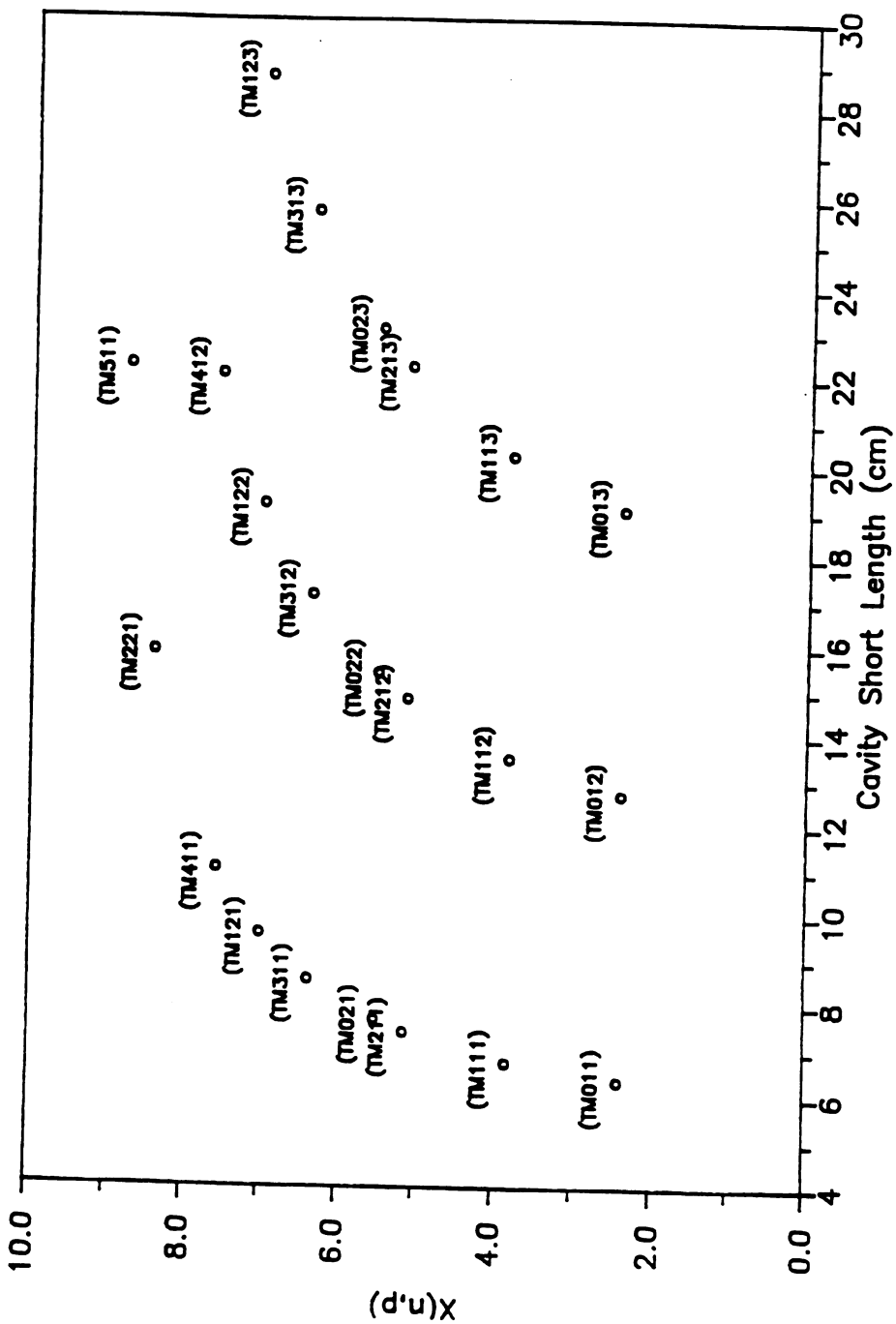

Figure 3.25 Resonant Cavity Lengths of TM Modes in 14" Cavity

Table 3.1 Resonant Cavity Lengths of TM Modes in 14" Cavity

X(n,p)	Cavity Mode	Cavity Length (cm)
2.405000	(TM011)	6.346941
2.405000	(TM012)	12.69388
2.405000	(TM013)	19.04082
3.832000	(TM111)	6.746388
3.832000	(TM112)	13.49278
3.832000	(TM113)	20.23916
5.136000	(TM211)	7.407754
5.136000	(TM212)	14.81551
5.136000	(TM213)	22.22326
5.520000	(TM021)	7.689620
5.520000	(TM022)	15.37924
5.520000	(TM023)	23.06886
6.380000	(TM311)	8.564938
6.380000	(TM312)	17.12988
6.380000	(TM313)	25.69481
7.016000	(TM121)	9.577787
7.016000	(TM122)	19.15557
7.016000	(TM123)	28.73336
7.588000	(TM411)	11.02720
7.588000	(TM412)	22.05441
7.588000	(TM413)	33.08161
8.417000	(TM221)	15.86860
8.417000	(TM222)	31.73721
8.771000	(TM511)	22.24383
8.771000	(TM512)	44.48766

source. It was found that it was difficult to couple the 2.45 GHz power into the cavity efficiently to create a centered plasma. This could be due to the large number of degenerate and nearly degenerate modes present. The instability of the power source may have also contributed to this inefficient power coupling problem.

CHAPTER FOUR

THE MICROWAVE-CAVITY JET REACTORS (MCJR)

4.1 Introduction

Diamond film deposition with high growth rates is desirable in many applications. One method to increase the growth rate is to increase the reactive species concentrations over the growth surface. The microwave cavity jet reactor (MCJR) is one type of plasma reactor that may be able to deposit diamond films with high growth rates. In the microwave cavity jet reactor, the excited species from the microwave discharge are directed through a nozzle onto a substrate. Since the microwave discharge can be maintained at high pressure (100 Torr to 1 atmosphere), the number of active species available for diamond film growth is high. Thus higher growth rates are expected. One advantage that the MCJRs have over some other types of jet reactors, such as DC arc jet reactors, is that MCJRs do not have electrodes, thus eliminating the possible contamination from the electrodes. The MCJR was originally developed at MSU as microwave electrothermal thrusters[10,11].

In this chapter, three microwave cavity jet reactors, the first, second and third generations of microwave cavity jet reactors, MCJR-1, MCJR-2 and MCJR-3, are described. The MCJR-1 and MCJR-2 have been developed and investigated for diamond film growth. The MCJR-3

was designed but has not been built due to lack of funding.

The experiments described in this chapter are preliminary experiments in investigating the potential of microwave cavity jet reactors in diamond film deposition. Diamond films have been deposited with a different type of microwave jet reactor[37,38] which was reviewed in chapter 2. Linear growth rates in the order of 12 μm/hour have been reported with that reactor.[37,38]

4.2 Experimental Systems

4.2.1 Introduction

All the microwave cavity jet reactors that are described in this dissertation use microwave power as their energy source and vacuum pumping system is used for reactive gas supply and operating pressure control. The microwave power supply, gas flow and vacuum pump system used in the MCJRs are described below in Sections 4.2.2 and 4.2.3.

4.2.2 Microwave Power Delivery System

The microwave circuit used to deliver microwave power to the jet reactors is similar to that described in Section 3.2.2. The only difference was the microwave power source that was used. In the experiments described in this chapter, a Thermex (Model No. 4074) 2.45 GHz, 2.5 kW power source was used.

4.2.3 Flow Control and Vacuum Pump Systems

A schematic drawing of the gas flow control and vacuum pump system is shown in Figure 4.1. As shown, the reactive gases, high purity (99.99% or better) H_2 and CH_4, are supplied by cylinder gas tanks (1) and (2). The gas flow rates are measured by mass flow meters (3) and controlled by needle valves (4). The flow meters measure flow rates with full scale flow ranges of 10 sccm (CH_4) and 500 sccm (H_2). The reactive gases are combined and mixed and as they flow into the quartz tube (5) which extends into the microwave cavity applicator (6). They flow through the cavity applicator (6) and the base plate (7) into the process chamber (8). A mechanical roughing pump (10) pumps the reactive gases through a manual valve (9) and out into the exhaust (11). The flow rate of purge gas supplied by nitrogen gas cylinders (12) is measured by a tube flow meter (13) and controlled by needle valves (14). It is added to the exhaust (11) to dilute the flammable reactive gases.

The pressure in the process chamber region is measured by a Hastings thermal conductivity vacuum gauge (15) with meaningful pressure measurement range of 5 - 200 mTorr and a MKS type 220B 10,000 Torr full scale baratron pressure gauge (16). The thermal conductivity vacuum gauge (15) was used to monitor chamber base pressure and the MKS pressure gauge was used to measure the process pressure. The chamber pressure is controlled by the gas flow rates and the manual throttle valve.

The instrumentation feed through port (17) on top of the process chamber is used for heater power supply and thermal couple electrical signal transmission. With this instrumentation feed through, the

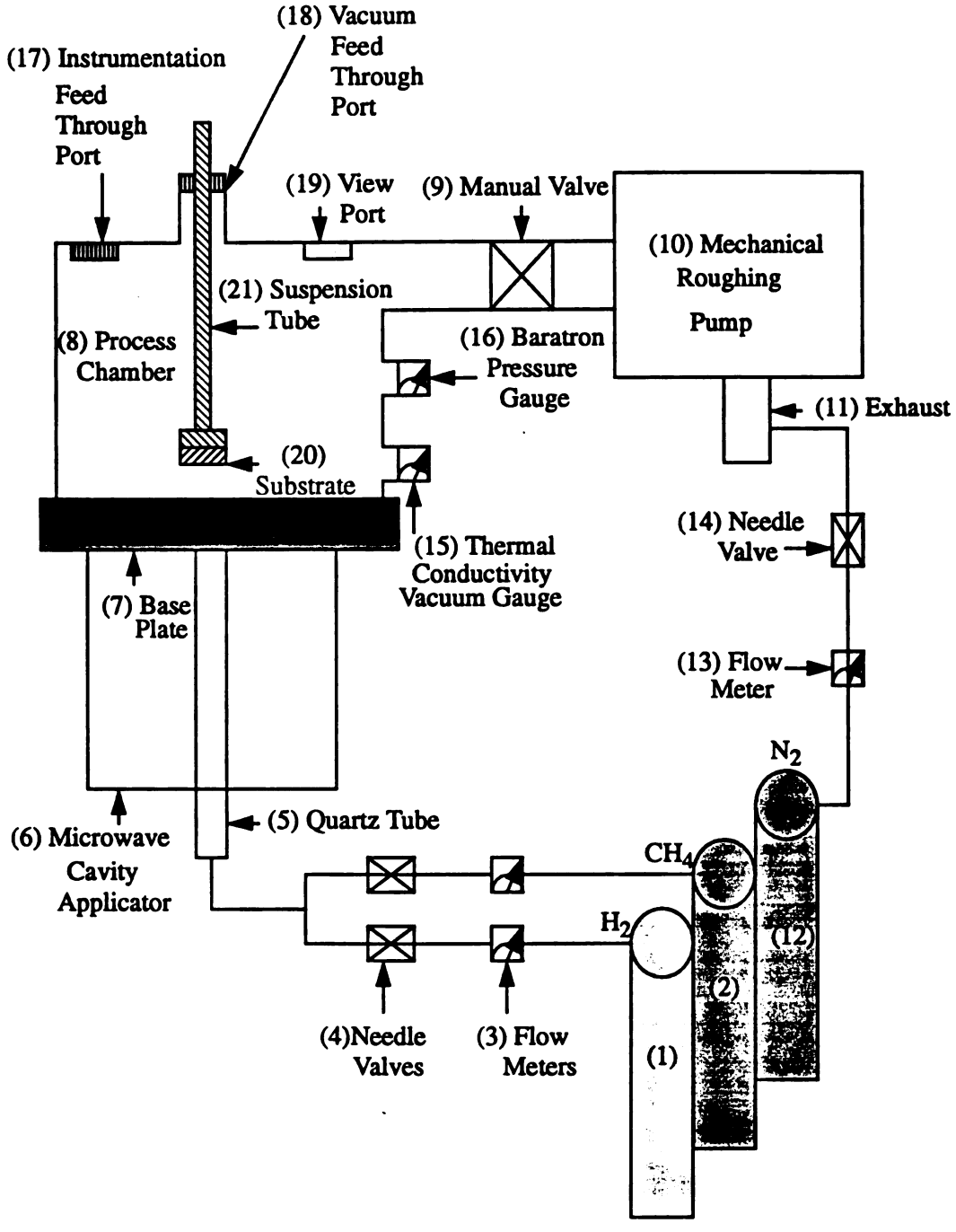

Figure 4.1 Flow Control and Vacuum System for MCJRs

temperature of the substrate can be measured and an independent substrate heater can be used to vary the substrate temperature.The vacuum feed through port (18) is used to suspend the substrate (20) and change its position via the suspension tube (21). The downward facing substrate (20) is mounted on the lower end of the suspension tube (21). The upper end of the suspension tube (21) is a half inch stainless steel tube which can be sealed by a half inch ultra-torr compressed o-ring vacuum fitting (18) welded to the center of the process chamber (8) top surface. When cooling liquid or gas flows inside a hollow suspension tube (21), the substrate (20) can be cooled. Part of the process chamber can be viewed through the view port (19).

4.3 The First Generation MCJR

4.3.1 Introduction

The first generation MCJR (MCJR-1) was the first jet reactor investigated for diamond film growth. It was developed in 1988 and was built from an existing microwave cavity and an existing stainless steel chamber.

4.3.2 Reactor Geometry

A schematic drawing of this reactor is shown in Figure 4.2. As shown. This reactor has a cylindrical side-wall (1) which forms the outer conducting shell of the cavity applicator. A water-cooled (21) sliding short (2) forms the lower end of the cavity applicator. The sliding short (2) can

First Generation MCJR (MCJR-1)

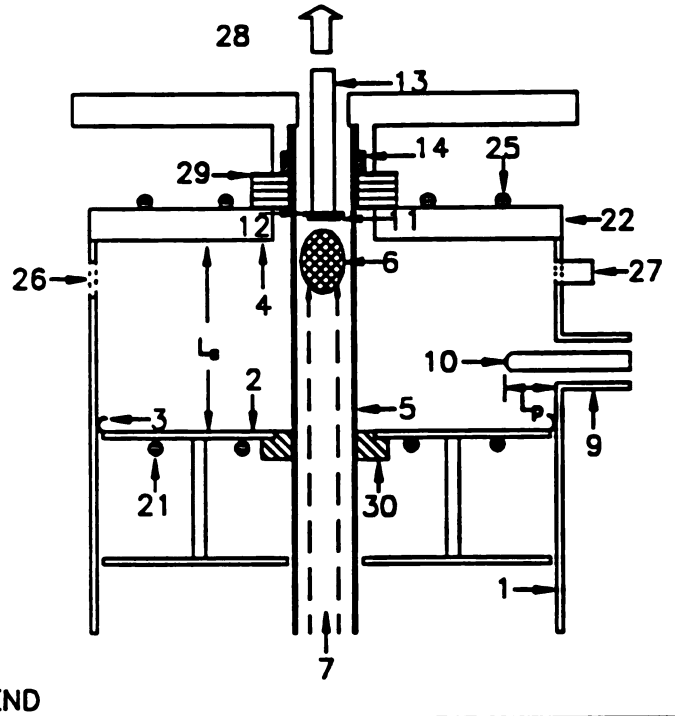

LEGEND

(1) Cavity Walls	(13) Linear Feed Through
(2) Sliding Short	(14) O-ring Seal
(3) Finger Stock	(21) Cooling Water
(4) Cavity Top Surface	(22) Brass Top Plate
(5) Quartz Tube	(25) Cooling Water
(6) Plasma Discharge	(26) Window/Air Outlet
(7) Gas Input	(27) Cooing Air Inlet
(9) Outer Conductor	(28) Process Chamber
(10) Power Input Probe	(29) Ultra-Torr Fitting
(11) Substrate	(30) Brass Collar
(12) Substrate Holder	

Figure 4.2 Schematic Drawing of MCJR-1

be moved along the cylindrical axis of the cavity wall (1) to change the position of the lower end of the cavity applicator. A water cooled (25) brass top plate (22) with the cavity top surface (4) form the top end of the cavity applicator. The brass top plate (22) and the cavity wall (1) are soldered together. Microwave energy is coupled into the applicator through the power input probe (10) and its coaxial outer conductor (9).

Reactive gas mixture enters the cavity applicator from the gas input port (7) where it is contained inside the 1" outside diameter quartz tube (5). The gas mixture flows upward, it is heated, ionized and dissociated inside the cavity applicator. The microwave discharge then flows over and around the substrate (11) and substrate holder (12) into the stainless steel process chamber (28) after which it is pumped out by a vacuum pump.

The "ultra-torr" vacuum fitting (29) near the bottom of the stainless steel process chamber (28) serves as a vacuum seal port to the quartz tube through the compressed o-ring seal (14). The quartz tube inner space near the "ultra-torr" vacuum fitting (29) functions as the nozzle for this jet reactor. Two inch diameter openings exist at the center of the sliding short (2) and the brass top plate (22) so that quartz tubes of less than 2 inch in outside diameter can extend through the center of the microwave applicator. Brass collars (30) are used to reduce the size of the opening to fit smaller quartz tubes and to reduce the microwave radiation leakage from the cavity applicator. The "ultra-torr" vacuum fitting (29) on the stainless steel chamber is an 1 inch ultra-torr fitting, hence quartz tubes (5) of 1 inch in outside diameter and brass collars (30) of 1 inch in inside diameter were used when experimenting with this reactor concept.

Besides being cooled by the water cooling tubing (21) on the sliding short (2) and the water cooling tubing (25) on the brass top plate (22), this reactor is also cooled by cooling air. The cooling air entered the cavity applicator through the cooling air inlet (27) and exited through the screened window/air outlet (26) which also served as a viewing port.

4.3.3 Reactor Operation

The experimental operation of this MCJR has been described in detail else where <10,11,63,64>. Thus, only a brief description is given here. Differences from earlier work <10,11,63,64> are operation at lower pressure (30 - 80 Torr) and lower flow rates (100 - 400 sccm). The ignition, matching, and internal cavity tuning are similar to that reported earlier for microwave electrothermal thrusters <11>.

The mode diagram of an ideal 7" cavity is shown in Figure 3.6. This MCJR can create a microwave discharge when excited in a single cavity electromagnetic mode. A discharge was started by reducing the H_2/CH_4 gas pressure to 5 -10 Torr, and applying microwave power which would then ignite a discharge that filled the quartz tube. The discharge pressure was then increased to an operating condition of 30 - 80 Torr while adjusting the length, L_s, and the probe, L_p, tuning the cavity to a matched condition.

When the sliding short length L_s is adjusted to about 7.45 cm and the probe length L_p to 8.1 mm, the discharge loaded TM_{011} mode is excited. A schematic drawing of the field pattern of the TM_{011} mode in a discharge loaded cavity is shown in Figure 3.7. As shown in Figure 4.2, with the help of the brass collar (30), the substrate (11) and substrate

holder (12), only the plasma near the top of the cavity applicator is excited. With this excitation configuration, the plasma is brought close to the substrate so that the reactive species can efficiently flow over the substrate. Deposition experiments were performed with this excitation configuration.

Comparing this microwave plasma reactor with the other microwave cavity plasma reactors (MCPR) described in chapter 3, the structure of this reactor has interesting features. Referring to Figure 4.2, the MCJR is mounted upside down compared with MCPR. This idea was brought up by J. Asmussen in 1986. In this MCJR, the reactive gases flow upward and are heated and dissociated by absorbing microwave energy in the cavity applicator. The reactive species generated in a hot discharge (6) naturally flows upward towards the substrate (11). This is due to the fact that under the same pressure and for the same gas, higher temperature gas has a lower density and tends to flow naturally upward in a cooler, higher density gas environment. Therefore, reactive species are effectively utilized for diamond film growth. Another interesting feature about this configuration is that the input reactive gases are drawn toward the hot discharge (6) when the reactive species generated in the hot discharge (6) flows up and around the substrate (11) toward the pump. Hence, the input reactive gases are efficiently utilized for diamond film growth in this mounting and gas flow configuration.

4.3.4 Reactor Performance

The first generation MCJR has been tested in diamond film growth experiments from September, 1988 to February, 1989 in more than 17

experiments. When the substrates (11) were lowered until they were in contact with the discharge (6), diamond films were grown on the substrates. The substrates used were typically 1 cm x 1 cm silicon wafers and silicon nitride.

A typical experiment (DTF04) was conducted under the following experimental conditions:

CH_4 flow rate = 1 sccm

H_2 flow rate = 120 sccm

pressure = 50 Torr

cavity short length L_s = 7.45 cm

probe length L_p = 8.1 mm

absorbed microwave power = 300 Watts

There are a few limitations in the first generation MCJR. First, it is not a "true" jet reactor since the "nozzle" diameter is the inside diameter of the quartz tube (5), which is close to 1 inch. Second, because of the long "neck" in the ultra-torr fitting (29), the discharge (6) is usually located far below the open area of the stainless steel chamber and the substrate (11) is usually lowered into the "neck" area for diamond film deposition. This configuration puts a limit on the size of the substrate to be smaller than the inner area of the quartz tube, which in the present reactor is less than 1" in diameter. Third, there are severe limitations on the input power level and operating pressure in the operation of this reactor. Since the discharge is in close contact with the quartz walls which has a melting temperature in the same range as the temperature of reactive gases in a discharge (6) suitable for diamond film growth, the deposition pressure was limited to less than100 Torr and the power input was limited to less than 500 Watts so that the quartz tube walls

would not melt. And finally, the experimental reproducibility in this reactor was poor because materials were deposited on the quartz tube walls.

4.4 The Second Generation MCJR

4.4.1 Introduction

To reduce the nozzle size and scale up the substrate area, the second generation jet reactor (MCJR-2) was developed in 1989. New top end plate of the cavity applicator and lower end plate of the stainless chamber were designed and built. Diamond film deposition experiments were conducted with this reactor.

4.4.2 Reactor Geometry

A schematic drawing of this reactor is shown in Figure 4.3. As shown, the new end plate (23) of the cavity applicator is machined from a brass plate. It has an 1.1 inch diameter opening at the center. A water cooling tunnel (16) is incorporated in the plate which is located close to the discharge (6) zone so that efficient cooling can be achieved. The O-ring spacer (18) functions primarily as a shock resist mechanical support to the quartz plate (32). A new cavity shell which does not have an end plate soldered onto it is used as the cavity walls (1). Finger stock (8) is used to electrically connect the brass end plate (23) to the cavity walls (1).

The lower end of the stainless steel chamber which was used in

Second Generation MCJR (MCJR-2)

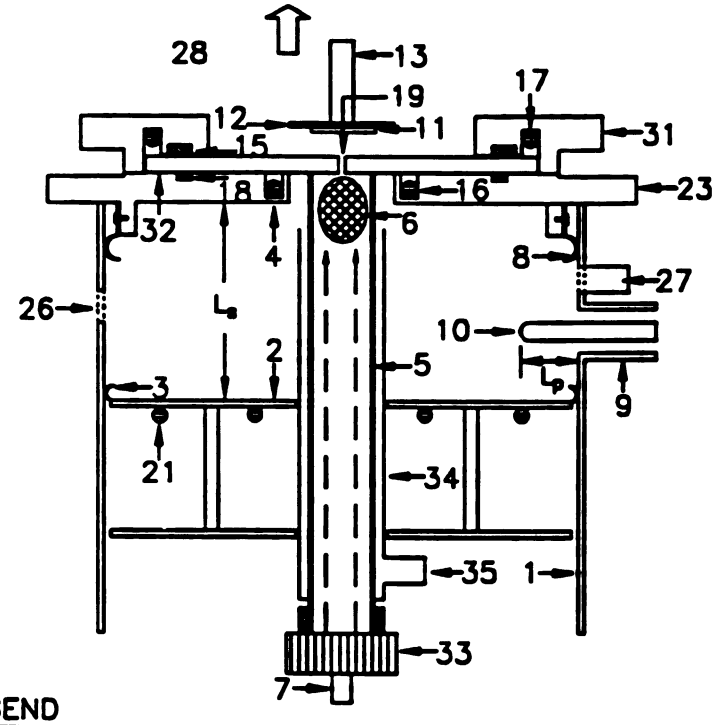

LEGEND

(1) Cavity Walls	(16) Cooling Water
(2) Sliding Short	(17) Cooling Water
(3) Finger Stock	(18) O-ring Spacer
(4) Cavity Top Surface	(19) Jet Nozzle
(5) Quartz Tube	(21) Cooling Water
(6) Plasma Discharge	(23) Brass End Plate
(7) Gas Input	(26) Window/Air Outlet
(8) Finger Stock	(27) Cooling Air Inlet
(9) Outer Conductor	(28) Process Chamber
(10) Power Input Probe	(31) S.S. End Plate
(11) Substrate	(32) Quartz Flange
(12) Substrate Holder	(33) Ultra-Torr Fitting
(13) Linear Feed Through	(34) Outer Quartz Tube
(15) O-ring Seal	(35) Cooling Gas Inlet

Figure 4.3 Schematic Drawing of MCJR-2

MCJR-1 was cut off and a Varian 8 inch diameter stainless steel Conflat flange with 6 inch opening near the center was welded onto the stainless steel chamber. This welded plate serves as a vacuum bolt joint between the stainless steel chamber (28) and the stainless steel end plate (31). The stainless steel end plate (31) is made from a Varian 8 inch stainless steel Conflat blank flange. There is a 3.8 inch opening near the center so that substrates up to 3.8 inch in diameter can be used in the stainless steel chamber. A water cooling tunnel (17) is incorporated in the plate for the chamber cooling. The O-ring seal (15) on this plate serves as the vacuum seal between the stainless steel end plate (31) and the quartz plate (32).

The jet assembly is made of an one inch quartz tube (5) welded to the center of a quartz plate (32), which is 5.5 inches in diameter and 0.25 inch thick. A 1/32 inch diameter hole was drilled at the center of the quartz plate (32). It serves as the jet nozzle (19). The one inch quartz tube (5) passes through the cavity applicator while the quartz plate (32) is sandwiched between the brass end plate (23) and stainless steel end plate (31). Ultra-torr fitting (33) seals the lower end of the quartz tube and makes the gas flow transition from stainless steel tubing to the quartz tube (5). On the outside of the 1 inch quartz tube (5), another quartz tube (34) of 1.5 inch in inside diameter is used to transport the safety and cooling N_2 gas to the discharge (6) region. This outer quartz tube (34) is sealed to the inner quartz tube (5) near the lower end of the sliding short (2) and left open near the discharge region (6). N_2 gas enters this outer quartz tube (34) from the gas inlet (35) and exits into the cavity applicator near the discharge zone (6). This double tube cooling mechanism is efficient since it forces the cooling gas to flow close to the

hot discharge zone (6).

4.4.3 Reactor Performance

This second generation MCJR has been investigated for diamond film growth from November, 1989 to January, 1990. More than 17 experiments were performed with this reactor. Diamond-like films have been grown on silicon substrates. The operation of this reactor is similar to that of the MCJR-1.

The Raman spectrum of a typical film (JDF-10) deposited under the following experimental conditions is shown in Figure 4.4:

CH_4 flow rate = 3.5 sccm

H_2 flow rate = 504 sccm

Ar flow rate = 252 sccm

pressure = 84 Torr

cavity short length L_s = 7.12 cm

probe length L_p = 3 cm

absorbed microwave power = 350 W

The discharge generated in this reactor was almost in direct contact with the quartz tube walls. The pressure was limited to 100 Torr and the power input was limited to 500 Watts so that the quartz tube walls would not melt. It was not possible to generate a high temperature discharge to pass through the nozzle (19) to achieve the substrate (11) temperature required for diamond film growth. The reproducibility was poor because materials were deposited on the quartz tube walls.

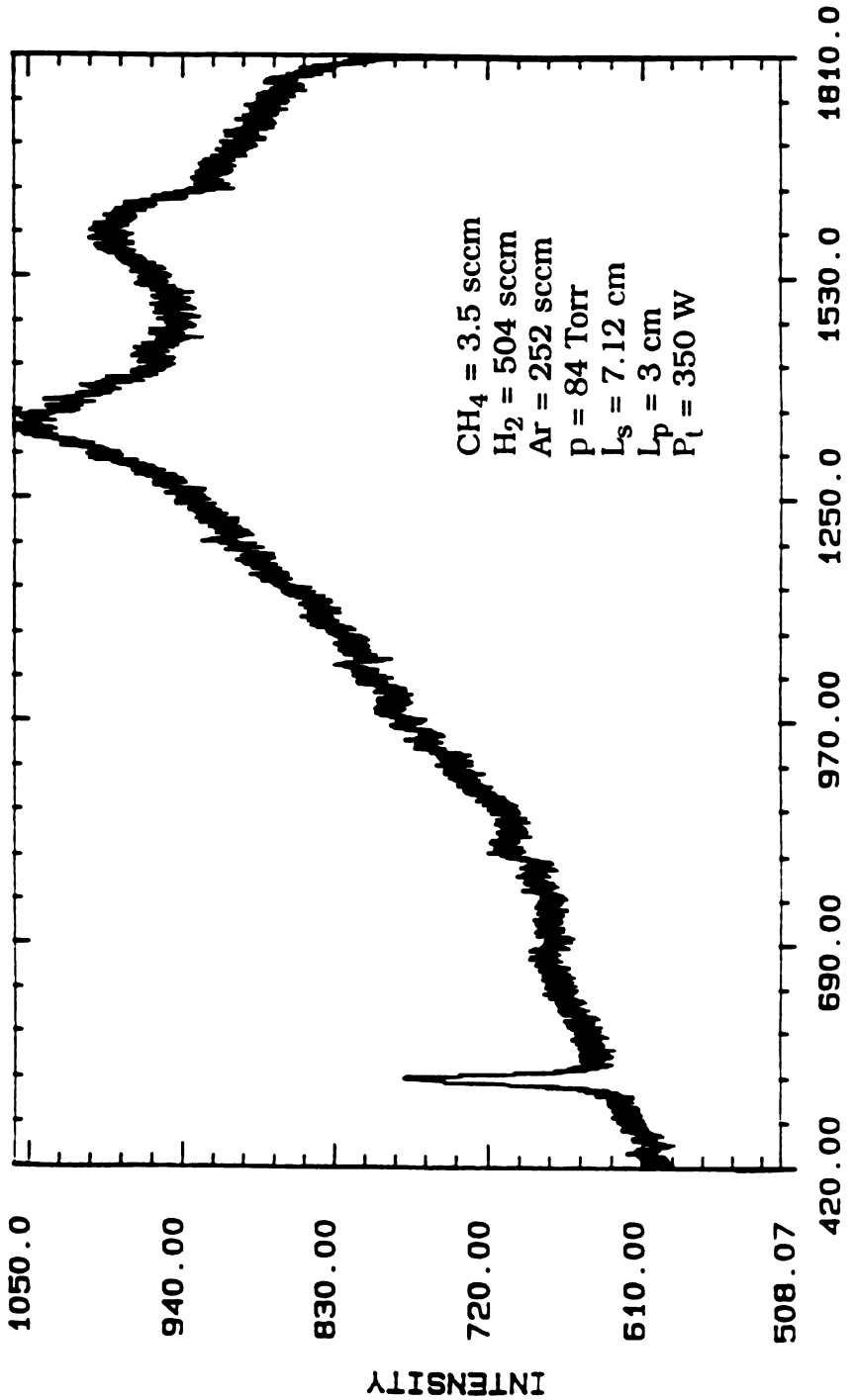

Figure 4.4 Raman Spectrum of a Film Deposited in MCJR-2

4.5 The Third Generation MCJR

4.5.1 Introduction

In order to keep the quartz walls away from the hot plasma discharge zone, the third generation MCJR (MCJR-3) was designed. With this design, the quartz wall erosion and reproducibility problems faced by the previous two generations of MCJR may be solved. Much higher power input and higher operating pressure experiments may be conducted so that higher diamond film growth rates may be achieved.

4.5.2 Reactor Geometry

A schematic drawing of this reactor is shown in Figure 4.5. As shown, new brass end plate (24) of the cavity applicator and new end plate (31) of the stainless steel chamber are designed.

The brass end plate (24) has a 4.62 inch opening near the center. Water cooling tunnels (16) are incorporated in this plate. O-ring spacer (18) is used to support the quartz flange (32). Finger stocks (8) are used to electrically connect the brass end plate (24) to the cavity walls (1).

The stainless steel end plate (31) is designed to be machined from a Varian 8 inch Conflat blank flange. It has a 0.5 inch opening near the center. A series of stainless steel nozzle inserts with different nozzle sizes are designed to be fit into the 0.5 inch opening. An enlarged drawing of the nozzle insert is shown in Figure 4.6. Water cooling (17) is incorporated in this plate and O-ring seal (15) is used to seal the quartz flange (32) to the stainless steel end plate (31).

Third Generation MCJR (MCJR-3)

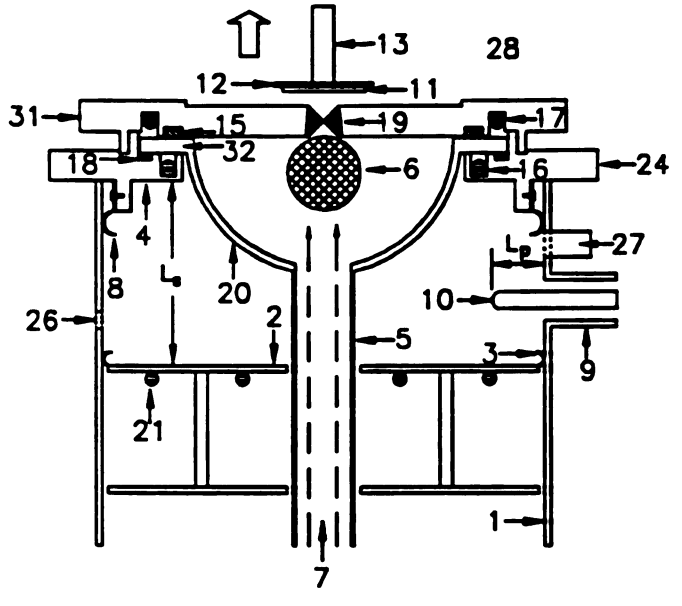

LEGEND

(1) Cavity Walls	(15) O-ring Seal
(2) Sliding Short	(16) Cooling Water
(3) Finger Stock	(17) Cooling Water
(4) Cavity Top Surface	(18) O-ring Spacer
(5) Quartz Tube	(19) Jet Nozzle
(6) Plasma Discharge	(20) Quartz Dome
(7) Gas Input	(21) Cooling Water
(8) Finger Stock	(24) Brass End Plate
(9) Outer Conductor	(26) Window/Air Outlet
(10) Power Input Probe	(27) Cooling Air Inlet
(11) Substrate	(28) Process Chamber
(12) Substrate Holder	(31) S.S. End Plate
(13) Linear Feed Through	(32) Quartz Flange

Figure 4.5 Schematic Drawing of MCJR-3

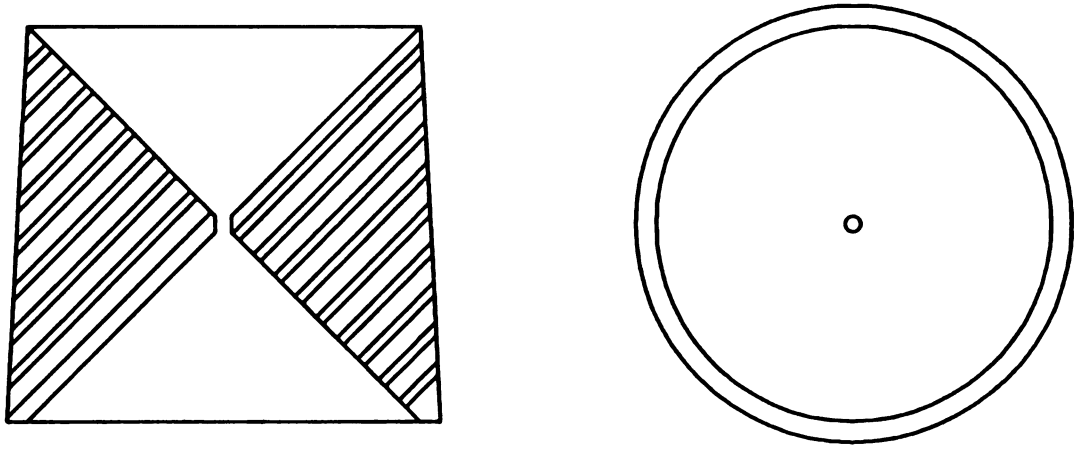

Figure 4.6 Enlarged Drawing of the Nozzle Insert

A quartz assembly is used to transport and confine the reactive gas mixture. The quartz assembly is made of a one inch quartz tube (5) welded to a hemispherical quartz dome (20) which has an inside diameter of 4.25 inches and an outside diameter of 4.5 inches. This hemispherical quartz dome (20) is welded near the equator to a quartz flange (32) of 6 inch in diameter and 0.25 inch thick. The one inch quartz tube (5) passes through the sliding short (2) of the cavity applicator and the quartz dome is housed inside the cavity applicator. The quartz flange (32) is sandwiched between the brass (24) and stainless steel (31) end plates.

4.5.3 Remarks

This third generation MCJR has been designed but has not been built. It is expected that the discharge and quartz wall direct contact problem and the poor reproducibility problem encountered in first and second generation MCJR will be solved with this jet reactor. Higher operating pressure and higher input power which are desirable for diamond film growth at higher growth rates are expected to be achievable with this jet reactor.

CHAPTER FIVE

MICROWAVE ELECTRIC FIELDS IN THE MCPR

5.1 Introduction

In order to develop microwave reactors that can deposit diamond films over large surface areas and at high growth rates, it is important to improve the knowledge of the fundamental plasma/chemical reactions of film deposition and to develop an understanding of the electromagnetic field/plasma interactions.

When an ideal cylindrical cavity of radius a is excited with a resonant mode (TE_{npq} or TM_{npq} modes) at frequency f_o, the cavity lengths L_r are determined by the following equations,[65]

$$(L_r)^{TM}_{npq} = q\pi a\,(4\pi^2 a^2 f_o^2 \varepsilon\mu - x_{np}^2)^{-1/2} \qquad \text{(eq. 5.1)}$$

for TM_{npq} modes, and

$$(L_r)^{TE}_{npq} = q\pi a\,(4\pi^2 a^2 f_o^2 \varepsilon\mu - x'^2_{np})^{-1/2} \qquad \text{(eq. 5.2)}$$

for TE_{npq} modes, where n, p and q are non-negative integers, x_{np} are zeros of the Bessel function, $J_n(x)$, and x'_{np} are zeros of the derivative of the Bessel function, $J'_n(x)$.

Each of these resonant modes, TE_{npq} or TM_{npq}, has well defined electric and magnetic field patterns which are expressed as the analytical solutions to the Maxwell's equations with perfectly conducting cylindrical walls as the boundaries.

When the cavity is excited with a plasma discharge, the electric and magnetic field patterns of these resonant modes are disturbed. The determination of electromagnetic field patterns in a general plasma discharge loaded cylindrical cavity from analytically solving the Maxwell's equations has not been achieved yet. This is due to the fact that plasma discharge can be created at various conditions, such as from sub-mTorr to over 1 atmosphere pressures, with various geometries and various electromagnetic properties. The electromagnetic properties of these plasma discharges as of yet have not been well established. Also, it is still a challenge to obtain solutions to Maxwell's equations in a cavity loaded with electromagnetically lossy material, such as the plasma discharge.

This chapter describes the techniques and results of the measurement of electric field strengths along the cavity inside walls in a plasma discharge loaded cylindrical cavity (MCPR7-1).[10,13,14,70] The electromagnetic (microwave) /plasma conditions required to grow diamond thin film are discussed. Specifically, the (relative) spatial variations of the exciting electromagnetic field patterns are measured. These spatial electric field measurements and intensities are then related to other important experimental parameters such as gas mixture, flow rate, input power, substrate temperature, and discharge pressure, etc.

5.2 Experimental Measurement System

The electromagnetic field pattern measurement system consists of a vertical bar shown in Figure 5.1 and two horizontal cylindrical bars enclosing the cavity as shown in the cross sectional view of Figure 5.2. They are soldered onto the outside surface of the cavity side walls. The top and bottom horizontal cylindrical bars are located at (A) 50 mm and (B) 20 mm from the cavity bottom surface, respectively. A series of holes, about 2.2 mm in diameter, are drilled into the vertical and the horizontal bars and completely through the inside surface of the cavity walls. The spacing between the holes on the vertical bar is 10 mm and the holes on the horizontal circles have an angular spacing of 7.5^{o}.

A semirigid micro-coaxial diagnostic probe is inserted into the holes until the tip of the probe is flush with the inside surface of the cavity side walls (see insert on Figure 5.2). Power readings, which are proportional to the square of the rms electrical field strength normal to the inside cavity walls, are obtained by connecting a power meter to the other end of the micro-coaxial probe during the experiments.[10]

The relationship between the diagnostic probe power reading P_p and the actual rms electrical field strength E, where E is defined by $E^2 = \overline{\vec{E} \cdot \vec{E}}$, was determined by using a 6" diameter empty cylindrical brass cavity.[56,10,70]

The calibration procedure was performed as follows. The empty cylindrical brass cavity was excited with the TM_{011} mode and several 2.45 GHz input power levels were used. The corresponding probe power readings were taken with a power meter attached to the other end of the probe whose tip was set flush with the inside surface of 6" cavity walls.

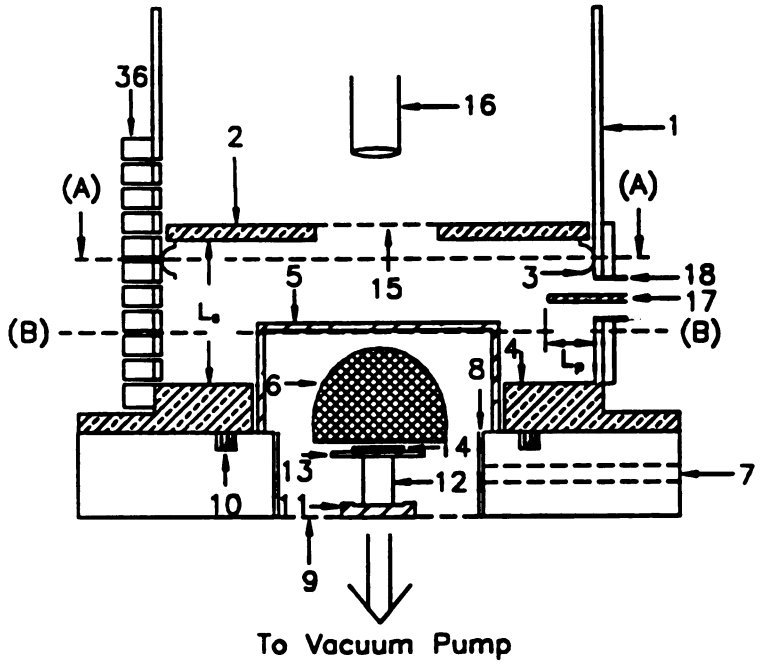

LEGEND

(1) Cavity Walls	(11) Graphite Base
(2) Sliding Short	(12) Quartz Tube
(3) Finger Stock	(13) Substrate Holder
(4) Cavity bottom surface	(14) Substrate
(5) Quartz Dome	(15) Top Window
(6) Plasma Discharge	(16) Pyrometer Sensor
(7) Gas Input Tunnel	(17) Input Coupling Probe
(8) Gas Distribution Ring	(18) Outer Conductor
(9) Metal Screen	(36) Vertical Bar
(10) Cooling Water Tunnel	(A) & (B) Horizontal Rings

Figure 5.1 Electric Field Measurement System

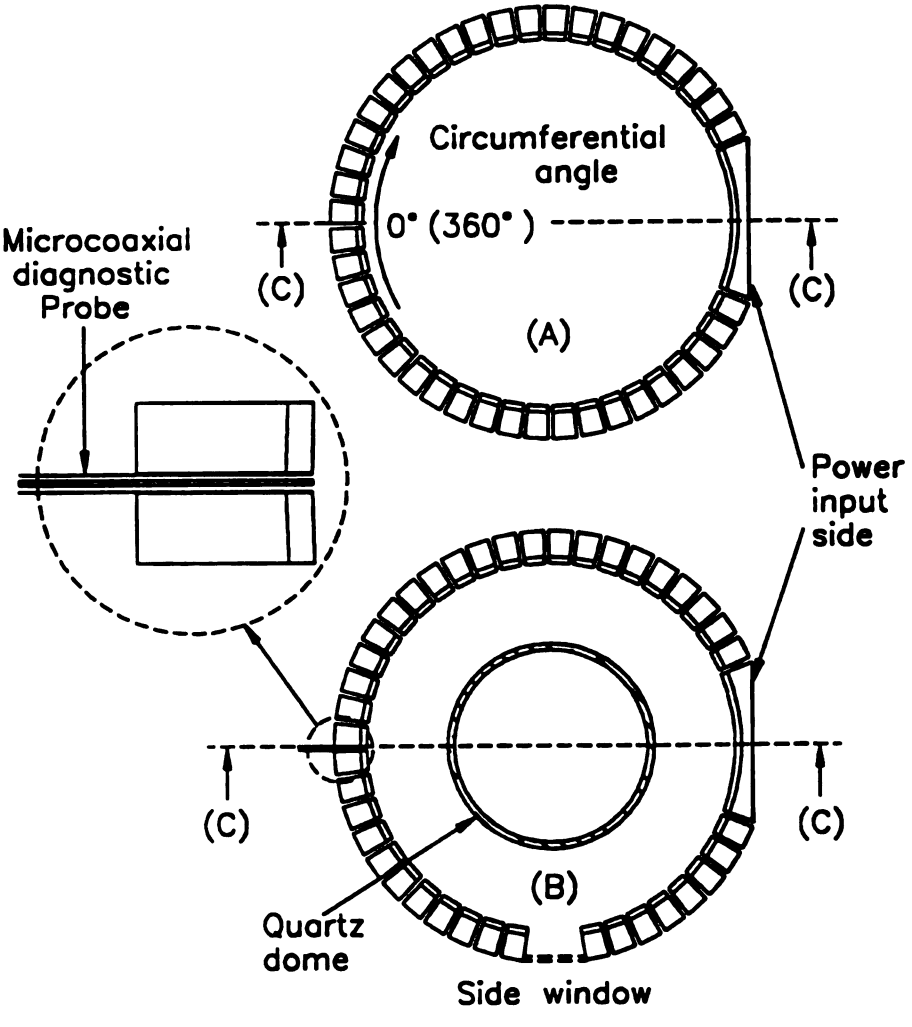

Figure 5.2 Horizontal Cross-sectional View

When the probe was inserted into the probe hole at z = 3.7 cm above the cavity bottom surface and the cavity length d is adjusted to 7.795 cm for TM_{011} mode excitation, the following table of diagnostic probe power reading vs. input power was obtained,

Table 5.1 Diagnostic Probe Power Reading versus Input Power

Incident Power P_i (W)	Reflected Power P_r (W)	Probe Power P_p (μW)
0.8526	0.0229	48
0.5858	0.0134	33
0.3608	0.0046	20.5
0.1093	0.0011	6.3

and the following table of absorbed power $P_d = P_i - P_r$, probe power P_p and their ratio P_d/P_p is generated,

Table 5.2 Absorbed Power and Probe Power Ratio

Absorbed Power P_d (W)	Probe Power P_p (μW)	Power Ratio P_d/P_p
0.8297	48	1.73×10^4
0.5724	33	1.73×0^4
0.3560	20.5	1.74×10^4
0.1082	6.3	1.72×10^4

where we see the power ratio stays constant when the absorbed power is changed, i.e., $P_d/P_p = 1.73 \times 10^4$.

In order to establish the relationship between the electric field strength E near the cavity inside walls and the probe power reading P_p. The relationship between the electric field strength E near the cavity

inside walls and the absorbed power P_d, is first derived. Thereafter, the relationship between E and P_p can be established from $P_d/P_p = 1.73 \times 10^4$.

Using the perturbation theory for lossy conducting surfaces and assuming that the power absorbed by the empty cavity is dissipated on the cavity walls, the following power balance equation is established,<65>

$$P_d = \Re \oint |\vec{H}|^2 ds \qquad \text{(eq. 5.3)}$$

whereas for brass material at $f_o = 2.45$ GHz, $\Re$ is given by,<65>

$$\Re = 5.01 \times 10^{-7} \sqrt{f_o} = 0.0248 \qquad \text{(eq. 5.4)}$$

For TM_{011} mode, $\vec{H}$ field has mainly the ϕ component, which is given by,<65>

$$H_\phi = C\left(\frac{x_{01}}{a}\right) J_1\left(\frac{x_{01}}{a} r\right) \cos\left(\frac{\pi z}{d}\right) \qquad \text{(eq. 5.5)}$$

where $x_{01} = 2.405$, a = 3" = 7.62 cm and C is a constant.

Using equations 5.4 and 5.5, we get, from equation 5.3,

$$P_d = \Re \oint |\vec{H}|^2 ds =$$

$$= C^2 \left(\frac{x_{01}}{a}\right)^2 \Re \left[2\pi a J_1^2(x_{01}) \int_0^d \cos^2\left(\frac{\pi z}{d}\right) dz + 2 \int_0^a 2\pi r J_1^2\left(\frac{x_{01}}{a} r\right) dr \right]$$

$$= C^2 x_{01}^2 \Re J_1^2(x_{01}) \left[\frac{\pi d}{a} + 2\pi \right] \qquad \text{(eq. 5.6)}$$

Since $x_{01} = 2.405$, $J_1(x_{01}) = 0.5191$, $d/a = 7.795/7.62 = 1.02$, $\Re = 0.0248$, we have, from equation 5.6,

$$P_d = 0.367C^2 \qquad \text{(eq. 5.7)}$$

The electric field $\vec{E}$ near the cylindrical cavity inside walls has mainly the component normal to the walls, i.e., $E = |E_r|$, where E_r is given by the following equation,<65>

$$E_r\big|_{r=a} = \frac{Cx_{01}\pi}{j\omega\varepsilon ad} J_1(x_{01}) \sin\left(\frac{\pi z}{d}\right)$$

which leads to,

$$|E_r|^2\big|_{r=a} = \frac{C^2 x_{01}^2 \pi^2}{\omega^2 \varepsilon^2 a^2 d^2} J_1^2(x_{01}) \sin^2\left(\frac{\pi z}{d}\right) \qquad \text{(eq. 5.8)}$$

where $\omega = 2\pi \times 2.45 \times 10^9$, $z/d = 3.7/7.795 = 0.43$. When the other parameters used to obtain equation 5.7 are also used, we obtain, from equation 5.8,

$$|E_r|^2\big|_{r=a} = 2.34 \times 10^7 C^2 \qquad \text{(eq. 5.9)}$$

From equations 5.7 and 5.9, we obtain the following relationship between the electric field strength E near the cylindrical cavity inside walls, $E = |E_r|$, and the absorbed power, P_d,

$$|E_r|^2\big|_{r=a} = 6.37 \times 10^7 P_d \qquad \text{(eq. 5.10)}$$

Using the result from table 5.2, i.e., $P_d/P_p = 1.73 \times 10^4$, we obtain the following relationship between the electric field strength E near the cavity inside walls and the probe power reading, P_p,

$$E^2 = |E_r|^2\Big|_{r=a} = 1.1 \times 10^{12} P_p \qquad \text{(eq. 5.11)}$$

where the unit of E is volt/m and the unit of P_p is W.

5.3 Measurement Results

5.3.1 Electromagnetic Field Patterns

The axial and circumferential electric fields were measured while the MPDR was operating under diamond thin film deposition conditions. An example of a field pattern measurement is displayed in Figure 5.3 for the case of a discharge that is symmetrically centered over the substrate. The experimental conditions were: pressure = 65 Torr, H_2 flow rate = 300 sccm, CH_4 flow rate = 1.5 sccm, absorbed microwave power = 590 W and substrate temperature ~ 975 °C. As shown in Figure 5.3, the electric field at a constant height is nearly independent of circumferential angle ϕ. The slight variation in intensity versus ϕ can be attributed to the near field of the exiting probe. Also shown in Figure 5.3, the axial field was measured and is compared to an empty waveguide TM_{01} standing wave (dashed line).

These field measurements clearly show that the mode is ϕ independent, and indicate that the plasma loaded TM_{011} mode was

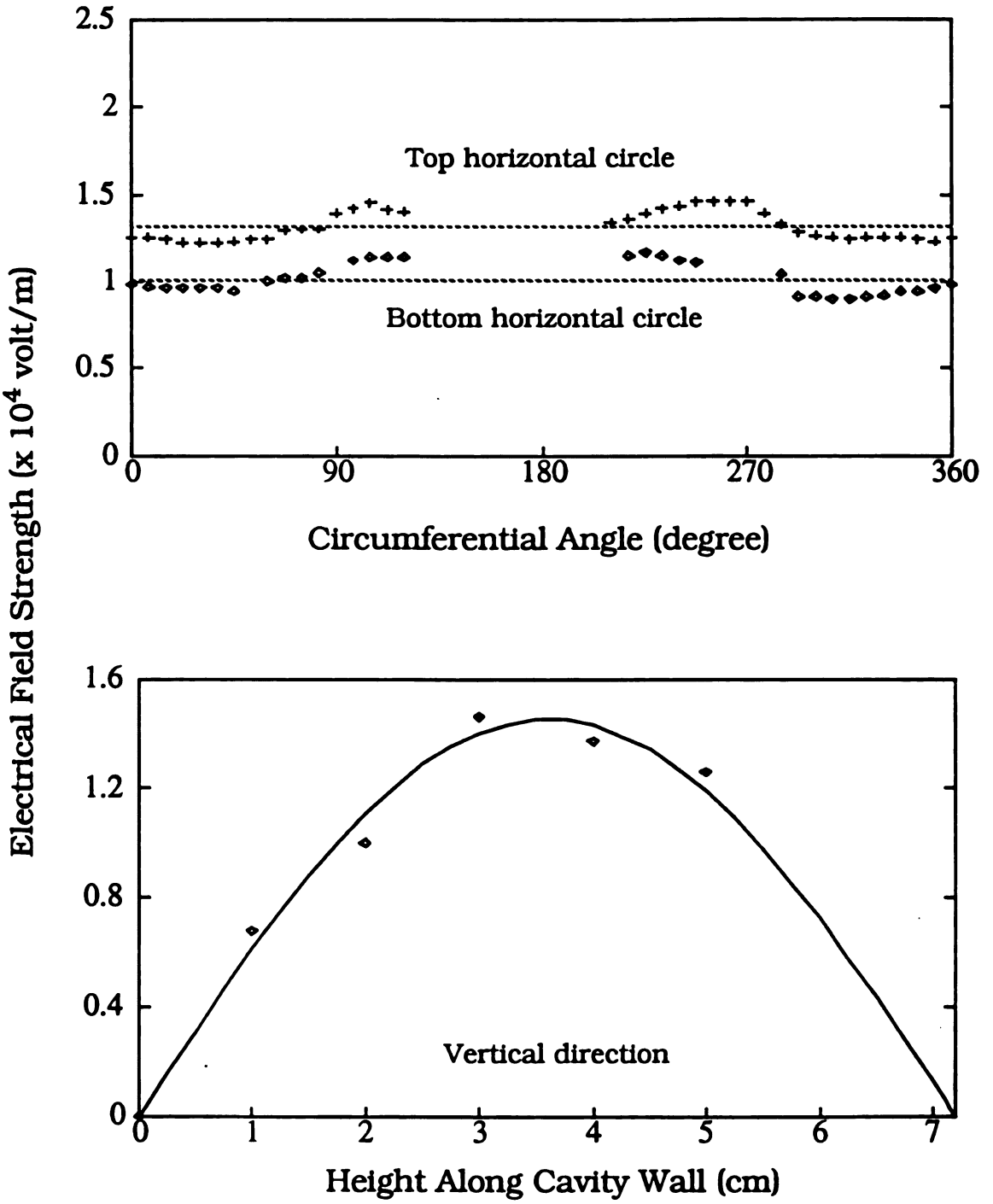

Figure 5.3 Measured Electric Field Strength Distribution

excited during deposition.

The shape of the electric field patterns shown in Figure 5.3 are typical of the electric field measured for a ϕ symmetric, axially centered discharge operating under a wide range of different experimental conditions. As experimental conditions change, i.e., pressure from 30 - 70 Torr, gas flow and input power, only a slight variation of L_s and L_p (less than a few mm) are required to maintain a well matched and centered discharge. However, the discharge can also be maintained in an off-centered and non-symmetrical position if L_s and L_p are changed from the optimal discharge centered conditions and/or if the substrate itself is positioned off the center of the cavity axis. When this occurs, the electromagnetic field patterns are altered. The vertical field intensities retain the standing wave field pattern shown in Figure 5.3, however the circumferential electric field displays a skewed pattern where the electric field intensities are the highest near the coupling probe ($\phi \sim 180^0$) and decrease as ϕ varies form 180^0 to 0 or 360 degrees. Film growth is usually non-uniform and non-symmetric under these experimental conditions.

Figure 5.4 summarizes the measured, plasma loaded TM_{011} mode electric and magnetic field patterns and their relationship to the discharge and substrate. The discharge is formed at the open end of the cavity inside the quartz disk and its length can be as long as a quarter wavelength ~3.6 cm. The most intense electric field components are tangential to the discharge boundary. As shown, the discharge is completely separated from the quartz walls and is in direct contact with the substrate and holder. The metal base-plate walls adjacent to the discharge and the substrate help stabilize the arc. In this configuration

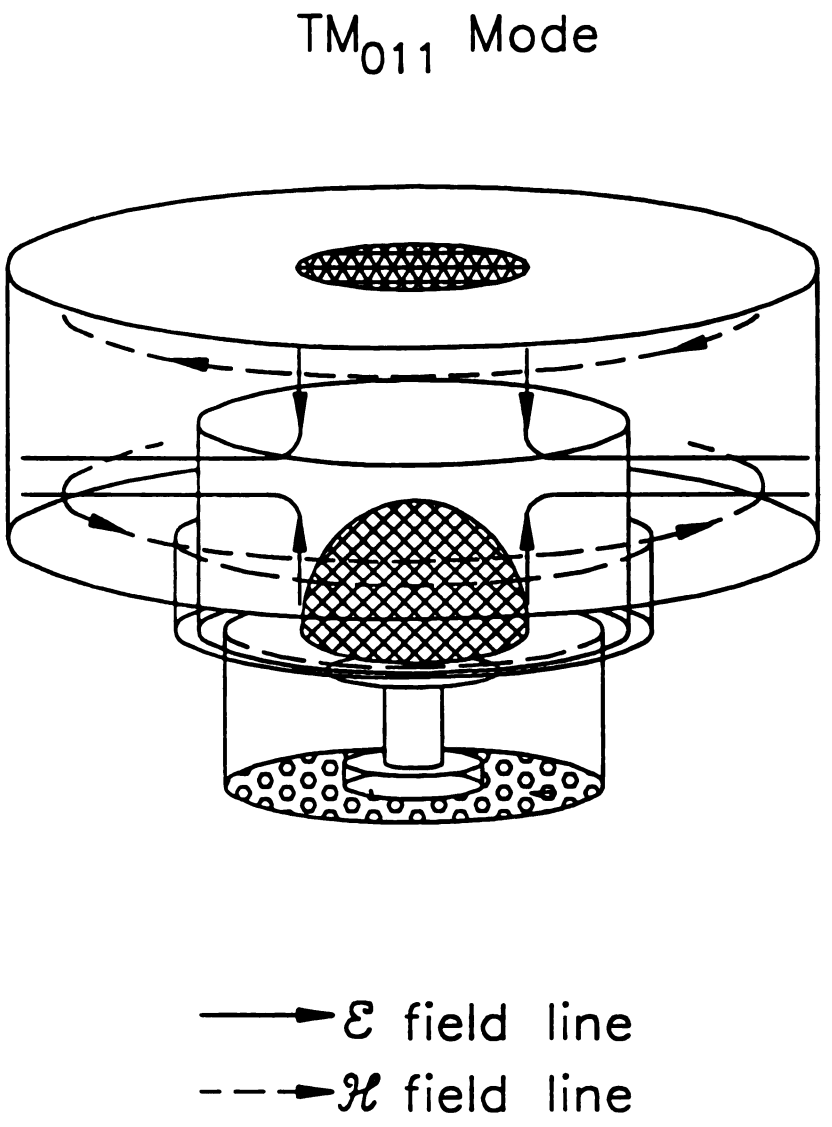

Figure 5.4 Measured Field Pattern in MCPR

ions and free radicals derived from hydrogen and methane impinge directly on the substrate heating the wafer by conduction and convection and provide the necessary species for the appropriate substrate surface chemistry.

To further illustrate the relationship between electric field and discharge boundary, a comparison of plasma discharge excited in a rectangular cavity and that in our cylindrical cavity is shown in Figure 5.5. Since the electric field has different distribution in the two different cavities, the plasma discharge takes on a different shape. What the two different configurations have in common is that the intense electric field adjacent to the discharge are tangential to the discharge boundary. This relationship can serve us as a guide in designing microwave cavities for a specific applications.

5.3.2 Power Balance and Discharge Power Density

The microwave power coupled into the plasma loaded applicator is given by $P_d = P_i - P_r$, where P_i is the incident power and P_r is the reflected power. The power coupled into the applicator P_d divides itself between the power absorbed in the conducting applicator walls P_b, and the power delivered to the discharge load P_a. The exact division of the power P_d between the walls and the discharge load depends on the relative losses in the discharge versus the losses in the applicator walls.

The experimentally measured electric field intensities shown in Figure 5.3 are typical order of magnitude electric field strengths inside the cavity under diamond film thin film deposition conditions. These measured electric field strengths can be used to estimate the power loss

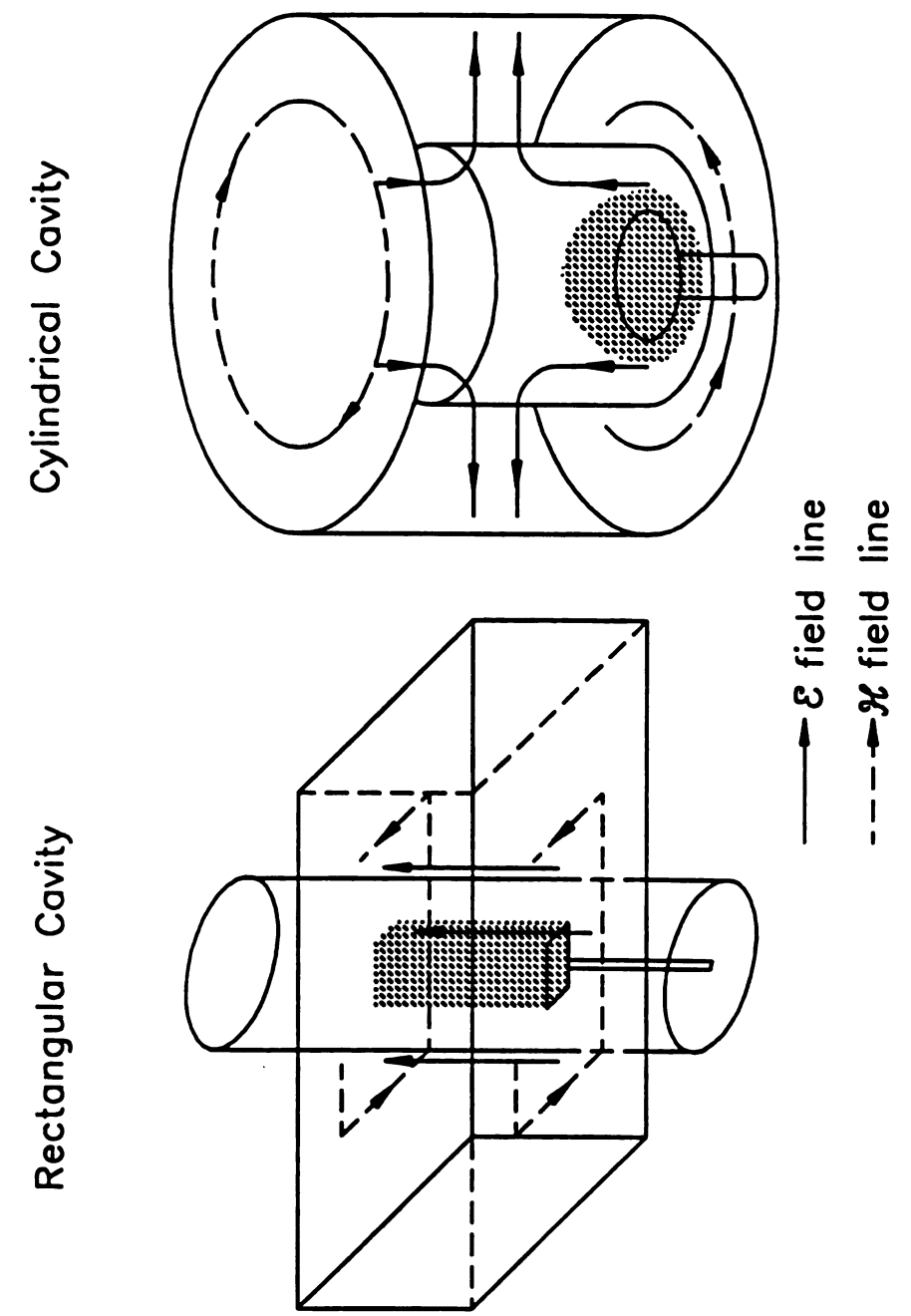

Figure 5.5 Discharge Boundaries and Electric Fields

on the cavity walls and the cavity loaded Q under diamond film deposition conditions.

To estimate the power loss on the cavity walls, the measured electric field strength along the cavity inside walls is first expressed empirically by the following equation, from Figure 5.3,

$$|E_r|\|_{r=a} = 1.45\times 10^4 \sin\left(\frac{\pi z}{d}\right) \qquad \text{(eq. 5.12)}$$

From equations 5.8 and 5.12, we obtain the following equation to determine the constant C,

$$C = 1.45\times 10^4 \frac{\omega\varepsilon a d}{x_{01}\pi J_1(x_{01})} \qquad \text{(eq. 5.13)}$$

where for the MCPR used in the field pattern measurements, a = 3.5" = $8.89\text{x}10^{-2}$ m and d = $7.2\text{x}10^{-2}$ m. Hence, the constant C is given by,

$$C = 3.22 \qquad \text{(eq. 5.14)}$$

From equations 5.6 and 5.14, the power loss on the cavity walls is given by

$$P_b = C^2 x_{01}^2 \Re J_1^2(x_{01})\left[\frac{\pi d}{a} + 2\pi\right] = 3.54\,(\text{W}) \qquad \text{(eq. 5.15)}$$

Therefore, the data shown in Figure 5.3 yields an estimated absorbed wall power of less than 4 W indicating most of the 590 W of absorbed power is coupled to the discharge/substrate holder. The absorbed microwave power efficiency is greater than 99%.

The Q factor of the plasma discharge loaded cavity applicator is estimated by first calculating the energy stored in the cavity applicator.

Assuming that the electromagnetic fields were only slightly altered by the presence of the discharge and that the electromagnetic fields in the discharge were not much different from those when the discharge was not present, the electric field components, E_r, E_ϕ and E_z can be expressed by the following equations,<65>

$$E_r = \frac{Cx_{01}\pi}{j\omega\varepsilon ad} J_1\left(\frac{x_{01}}{a}r\right) \sin\left(\frac{\pi z}{d}\right) \qquad \text{(eq. 5.16)}$$

$$E_\phi = 0 \qquad \text{(eq. 5.17)}$$

$$E_z = \frac{Cx_{01}^2}{j\omega\varepsilon a^2} J_0\left(\frac{x_{01}}{a}r\right) \cos\left(\frac{\pi z}{d}\right) \qquad \text{(eq. 5.18)}$$

The energy stored in the cavity applicator is given by,<65>

$$W = 2\overline{W_e} = \varepsilon\int|\vec{E}|^2 dV = \varepsilon\int|E_r|^2 dV + \varepsilon\int|E_z|^2 dV =$$

$$= \varepsilon\left(\frac{C}{\omega\varepsilon}\right)^2\left(\frac{x_{01}}{a}\right)^2 2\pi\left[\left(\frac{\pi^2}{d^2}\right)\int_0^d \sin^2\left(\frac{\pi}{d}z\right)dz\int_0^a J_1^2\left(\frac{x_{01}}{a}r\right)rdr + \right.$$

$$\left. + \left(\frac{x_{01}^2}{a^2}\right)\int_0^d \cos^2\left(\frac{\pi}{d}z\right)dz\int_0^a J_0^2\left(\frac{x_{01}}{a}r\right)rdr\right] =$$

$$= \frac{C^2\pi d}{2\omega^2\varepsilon}x_{01}^2 J_1^2(x_{01})\left[\left(\frac{\pi}{d}\right)^2 + \left(\frac{x_{01}}{a}\right)^2\right] \qquad \text{(eq. 5.19)}$$

where C is given by equation 5.14. Hence the energy stored in the cavity applicator is,

$$W = 2.3 \times 10^{-6} (J) \qquad \text{(eq. 5.20)}$$

Since the absorbed microwave power by the plasma discharge loaded cavity applicator is P_d = 590 W, the loaded cavity Q factor is given by,<65>

$$Q = \frac{\omega W}{P_d} = 60 \qquad \text{(eq. 5.21)}$$

Thus, the absorbed microwave power is very efficient, i.e., $P_d \sim P_a$.

A visual estimation of the discharge volume is 100 cm^3 at the low pressure of 20 Torr. As pressure increases to 70 Torr, the volume decreases (for a constant power of 590 W) to 30 cm^3. Thus, the discharge absorbed power density varies from approximately 6 W/cm^3 to 20 W/cm^3.

5.3.3 Electric Field Strength

Diagnostic probe power readings were taken when chamber pressure, hydrogen and methane flow rates, and microwave power input were varied. Each set of measurements were taken for a ϕ symmetric, well-centered discharge. The results are summarized in Figures 5.6 and 5.7 in which diagnostic probe power is plotted vs. input power, flow rate, and pressure. The measured diagnostic probe power is proportional to the square of electric field, i.e., it is proportional to the energy stored in the loaded cavity fields. The power absorbed, P_d, is equal to the total power dissipated within the cavity. Thus, the ratio of the probe power to the absorbed power is proportional to the discharge loaded cavity Q.

Figure 5.6 shows under a constant pressure of 70 Torr and three

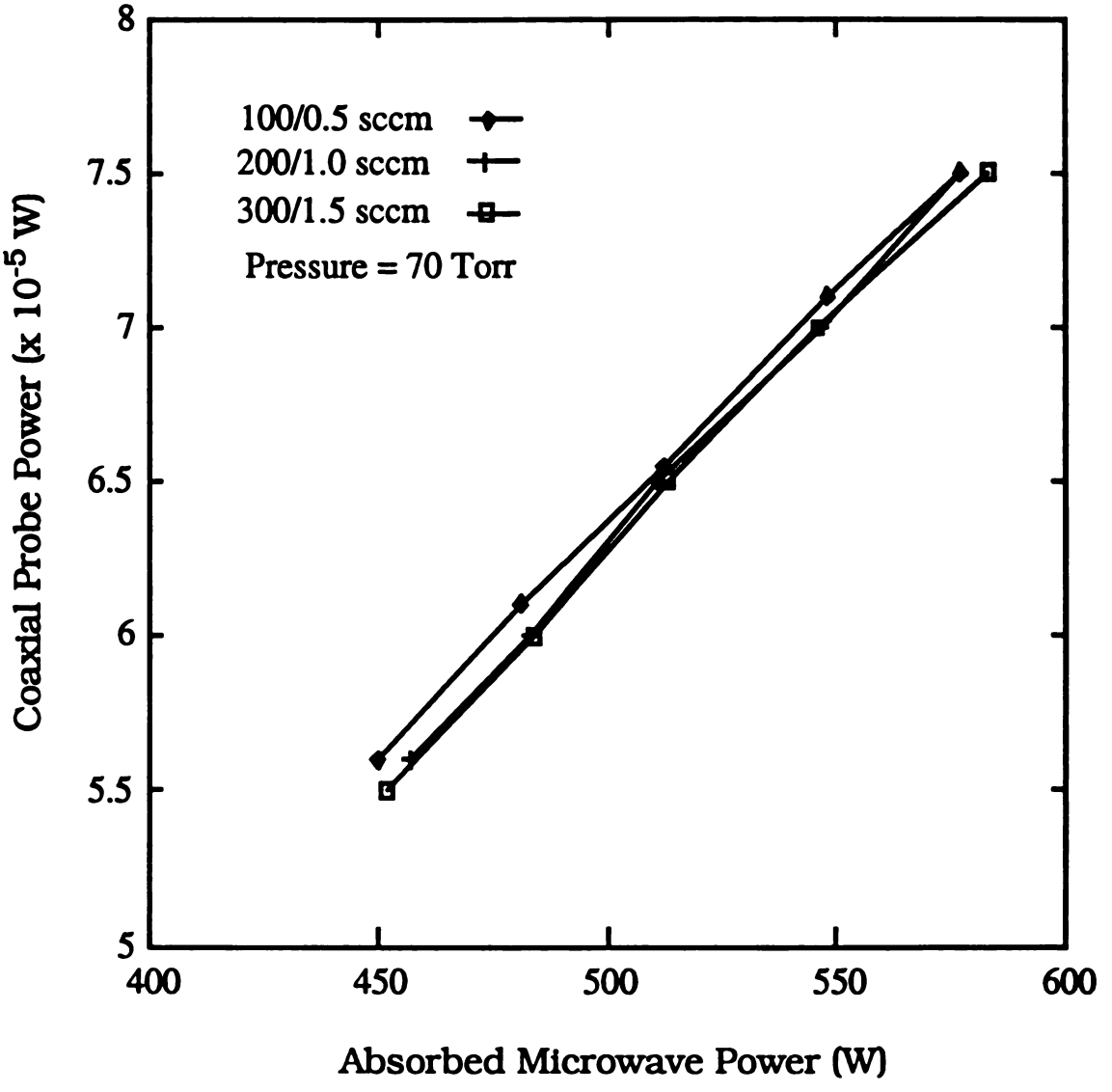

Figure 5.6 Coaxial Probe Power versus Microwave Power and Flow Rate

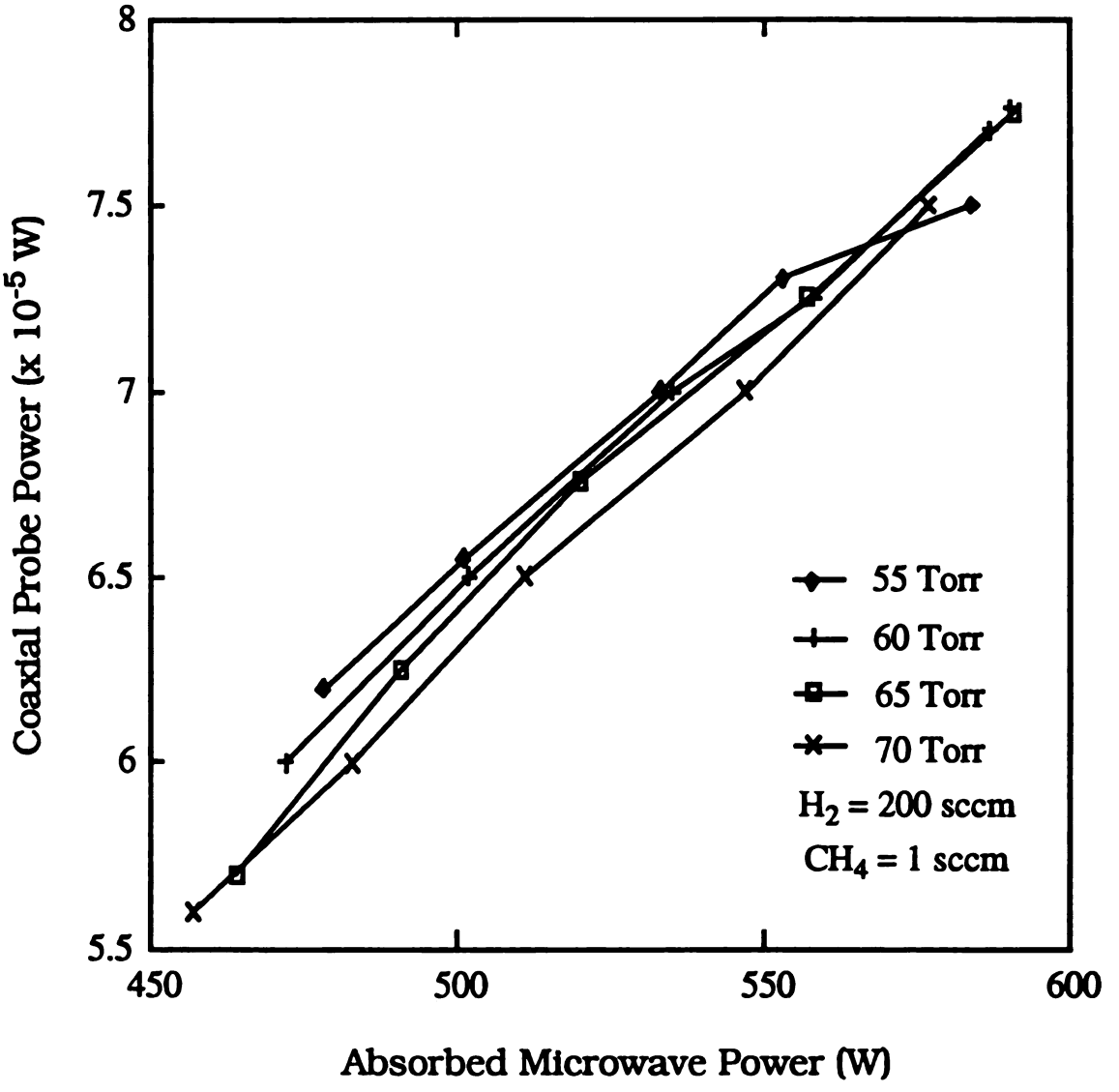

Figure 5.7 Coaxial Probe Power versus Microwave Power and Pressure

different flow rates, the diagnostic probe power, and hence the square of the cavity electric field strength, is approximately proportional to the power input and only slightly influenced by the flow rates.

Figure 5.7 shows for a constant flow of 200 sccm H_2 and 1.0 sccm CH_4, the probe power is approximately proportional to the input power and is only slightly influenced by the variation in pressure.

These measurements demonstrate that the discharge loaded cavity Q varies little (~ 60) over the different flow rates, pressures and input powers. The absorbed microwave power efficiency is high over the wide variations of experimental conditions shown in Figures 5.6 and 5.7. Thus, the power absorbed by the applicator is essentially equal to the power dissipated in the plasma/substrate holder.

5.3.4 Substrate Temperature

Substrate temperature plays important role in diamond film growth process. It affects diamond film growth rate and morphology, two of the leading figures of merit in diamond film growth process. Figures 5.8 and 5.9 show substrate temperature versus absorbed microwave power, flow rates and pressure.

Figure 5.8 shows under a constant pressure of 60 Torr and three different flow rates, the substrate temperature increases as absorbed power is increased and is only slightly influenced by the flow rates in our reactor.

Figure 5.9 shows for a constant flow of 200 sccm H_2 and 1.0 sccm CH_4, the substrate temperature increases when the absorbed power and pressure are increased.

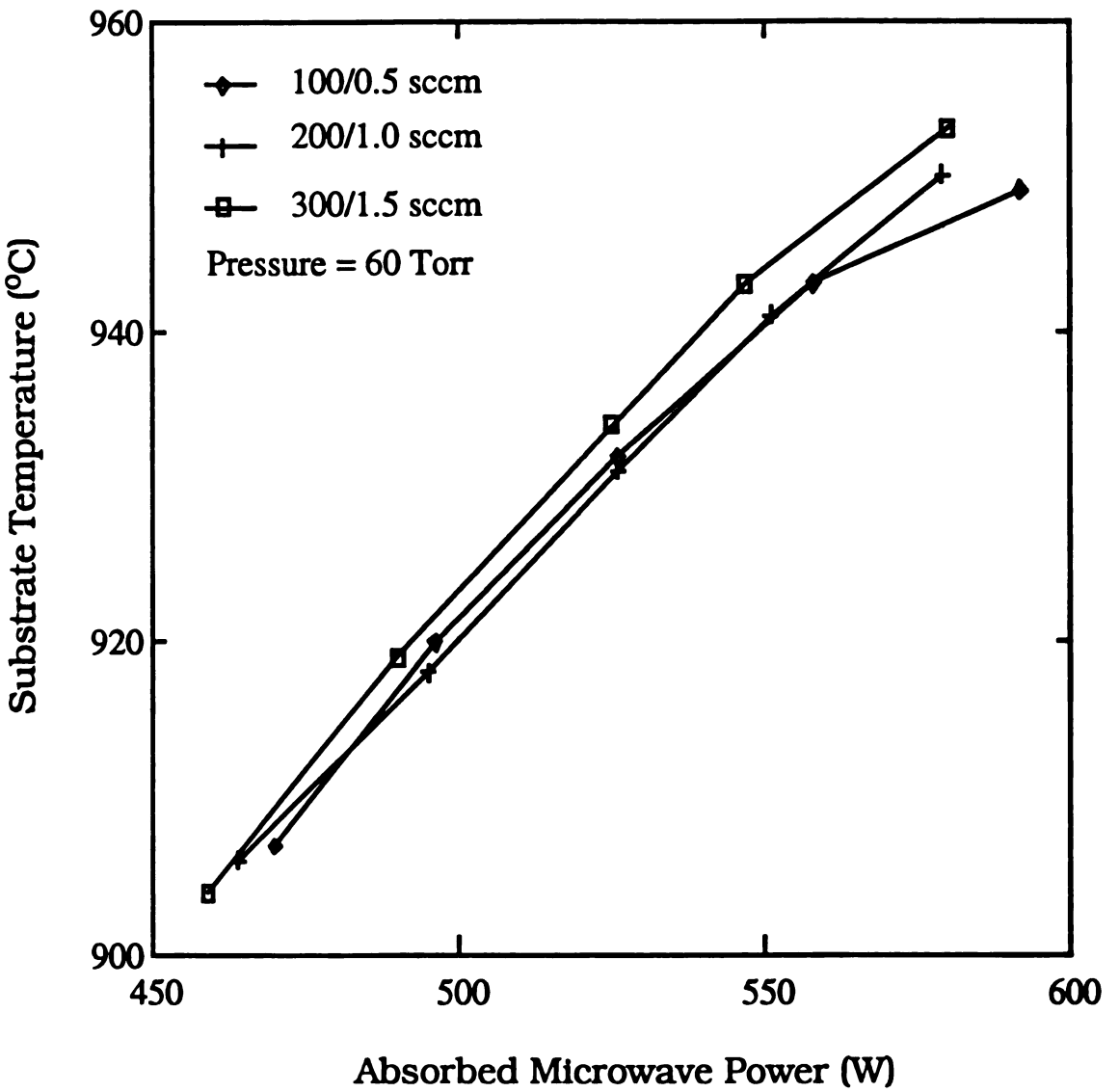

Figure 5.8 Substrate Temperature vs. Microwave Power and Flow Rate

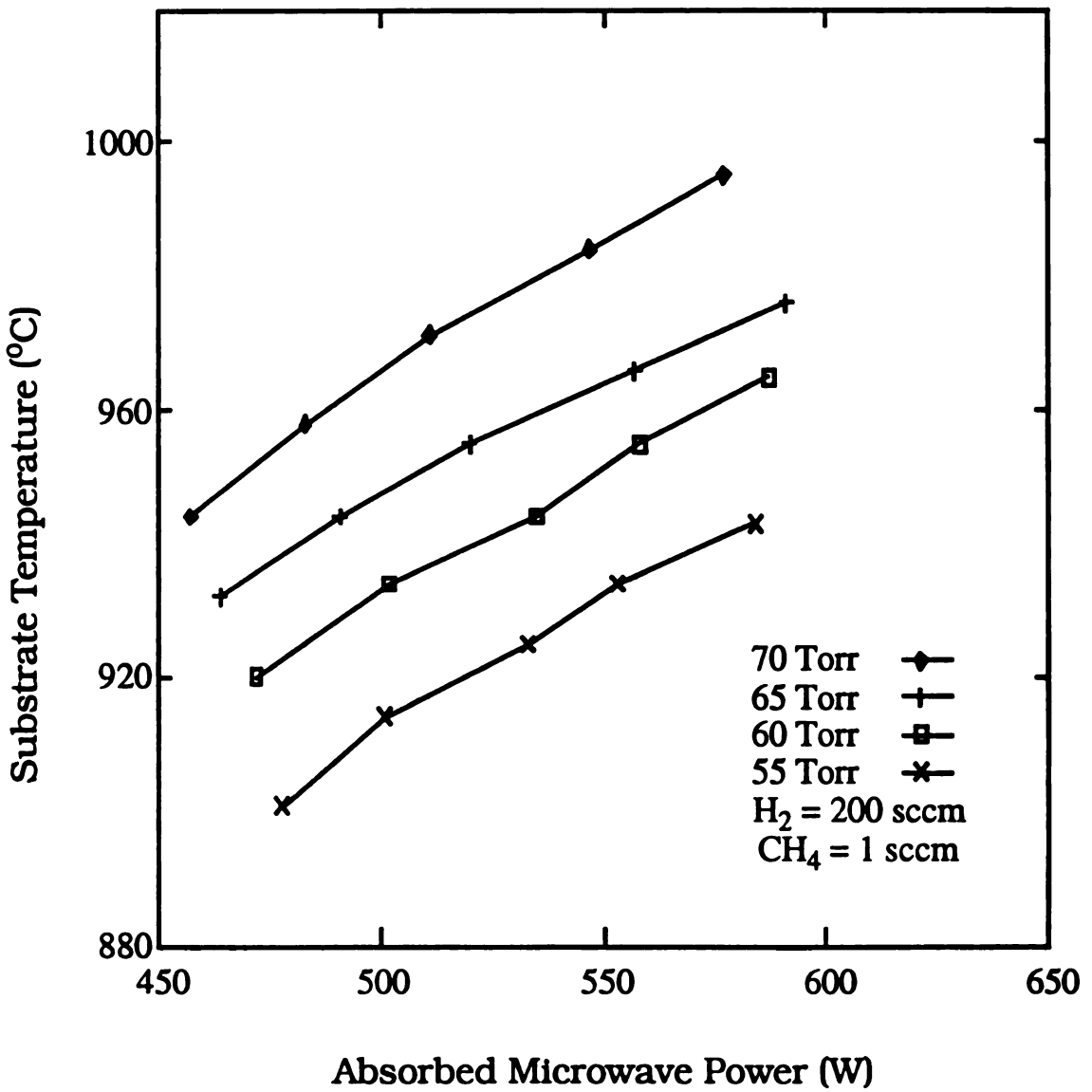

Figure 5.9 Substrate Temperature vs. Microwave Power and Pressure

5.4 Discussion

These experiments indicate that under the diamond thin film deposition conditions of 30 to 80 Torr the microwave discharge is in a transition between an am-bipolar diffusion controlled discharge and a freely floating microwave arc.<56,63,66-68> The discharge is excited by the lossy plasma loaded TM_{011} cylindrical cavity mode where, as shown in Figure 5.4, the most intense electric field adjacent to the discharge is tangent to the discharge boundary. This mode couples to the discharge very efficiently and has been used to excite high pressure "arc like" microwave discharges for other applications.<56,63,66-68> It also has the same relationship between electromagnetic field patterns and the discharge boundaries that was present in the earliest microwave plasma diamond thin film deposition experiments,<30> as shown in Figure 5.5.

Since the microwave arc appears to be fundamental to the observed diamond film deposition, several of its features are briefly discussed here to provide a better understanding of the discharge. The microwave arc, like lower-frequency and DC arcs, is a thermally in-homogeneous discharge. It has a hot central core, and thermal gradients exist between the discharge center and surrounding walls. Microwave energy is readily coupled into the electron gas in the hot discharge center because of its reduced gas density, and because neutral gas species are also readily ionized and excited in the hot discharge region.

Major energy losses form the discharge occur by heat conduction, convection, and radiation. When large temperature gradients are present, heat conduction losses become an important loss process. This loss mechanism includes the contribution to the heat conductivity by

molecules, atoms, electrons, and ions, and also chemical reactions such as the transport of dissociation energy and ionization energy to the arc fringes by free radicals and ions. Owing to the high-pressure environment, electron, ion and free radicals recombine quickly outside the hot central core or on a solid surface in contact with the arc core and thus convert their dissociation, ionization, and excitation energy into thermal energy. The result is a discharge with radially varying gas temperature, ionization rate, and volume recombination rate. Gas temperature, ionization, dissociation, etc., are highest in the center of the discharge, while volume recombination and de-excitation of the different species increase away from the discharge center as the cooler, denser gas regions near the walls are approached. The central discharge core gas temperatures vary with gas type and pressure and can be in excess of 2000 ^{o}K,[66-68] while temperatures external to the discharge are controlled by wall temperatures and the temperatures of the gas flowing around the discharge. If gas temperatures are 2000 ^{o}K or more in hydrogen gas, then atomic hydrogen can be created by thermal dissociation as well as free electron impact.[69]

5.5 Summary

The following conclusions were reached from this study, under diamond film deposition conditions in MCPR7-1:

(1) The excitation mode was identified to be discharge loaded TM_{011} mode.

(2) Maximum electric field intensity in the cavity was ~ 150 V/cm.

(2) Discharge loaded cavity quality factor was ~ 60.

(3) The tangential component of the $\vec{E}$ field is the main discharge excitation field.

(4) Average power density in the discharge was ~ 6 W/cm^3 at 20 Torr and 20 W/cm^3 at 70 Torr.

(5) Under a constant pressure, the square of the cavity electric field strength is approximately proportional to the power input and only slightly influenced by the variation in flow rates.

(6) At a constant gas flow, the square of the cavity electric field strength is approximately proportional to the power input and only slightly influenced by the variation in pressure.

(7) Under a constant pressure, the substrate temperature increases with the power input (~ 0.4 ^{o}C/W) and is only slightly influenced by the variation in flow rates.

(8) At a constant gas flow, the substrate temperature increases with the power input (~ 0.4 ^{o}C/W) under each working pressure. Also, at the constant gas flow and input power, the substrate temperature increases (~ 3.5 ^{o}C/Torr) with increasing pressure.

CHAPTER SIX

DIAMOND FILM DEPOSITION IN THE MCPR

6.1 Introduction

In various practical applications, diamond films with various thicknesses and morphologies are desired. In order to determine the growth rates and morphologies of diamond films deposited under various experimental conditions and hence characterize the performance of the third generation microwave cavity plasma reactor for diamond film growth, diamond films are grown on three and four inch silicon wafers under various experimental conditions. In this chapter, the diamond film growth rates, growth efficiencies and morphologies are presented with respect to variations in substrate temperature, gas composition and flow rate. Typical uniformity profile and Raman spectrum are also presented.

The objective of depositing diamond films on 3" and 4" silicon wafers is to achieve the highest possible growth rate with good uniformity (judged by visual inspection).

The sections in this chapter are arranged as follows. Section 6.2 describes the experimental methodology by which the reactor is characterized. Reactor block diagram and experimental parameters are used to describe the experimental methodology. Section 6.3 describes the experimental configuration and the common experimental procedures

used in the parametric study. The characteristic behaviors of this experimental configuration are described. Section 6.4 describes the results of an experimental parametric study of diamond film deposition on 3" silicon wafers. The goal of this study is to achieve the highest growth rate possible since achieving good uniformity (judged by visual inspection) over 3" silicon wafer is possible under a wide range of experimental conditions in this MCPR. Film growth rates, growth efficiencies and morphologies of the deposited diamond films under various deposition conditions are described. Typical uniformity profile and Raman spectrum are also presented. Section 6.5 describes a study of experimental set-up for diamond film deposition on 4" silicon wafers. Here film uniformity and growth rate are the judging criteria. Section 6.6 describes a parametric study of diamond film deposition on 4" silicon wafers. The goal of this study is to achieve the highest growth rate possible while maintaining good uniformity (judged by visual inspection). There exists a compromise between the uniformity and growth rate in diamond film deposition on 4" silicon wafers in the present reactor. When reasonable uniformity is required, the main limiting factor on the growth rate comes from the safe operating temperature limit and the coating speed of the quartz dome. Film growth rates, growth efficiencies and morphologies of diamond films deposited under various experimental conditions are described. Typical uniformity profile and Raman spectrum are also presented.

6.2 Experimental Methodology

6.2.1 Introduction

In order to orderly investigate the performance of the MCPR, it is essential to identify the experimental parameters and establish a method of evaluating the operational performance of the MCPR. This section describes the various experimental parameters, methods and "figures of merit" used in the evaluation.

The deposition experiments conducted in MCPR have many experimental parameters. The reactor I/O block diagram shown in Figure 6.1 displays the relationship between these experimental parameters. These experimental parameters can be divided into three groups: (1) independent input experimental parameters, (2) internal, dependent experimental parameters, and (3) external, output parameters. Each of them is summarized in more detail below.

I. Independent Input Experimental Parameters
   - (i) Substrate size, shape and other physical properties
   - (ii) Reactor geometry parameters
     - (a) cavity applicator construction
     - (b) quartz dome geometry
     - (c) base-plate design
     - (d) gas flow configuration
     - (e) substrate holder geometry and material
     - (f) substrate location
     - (g) end feed vs. side feed
     - (h) electromagnetic mode excitation and cavity tuning

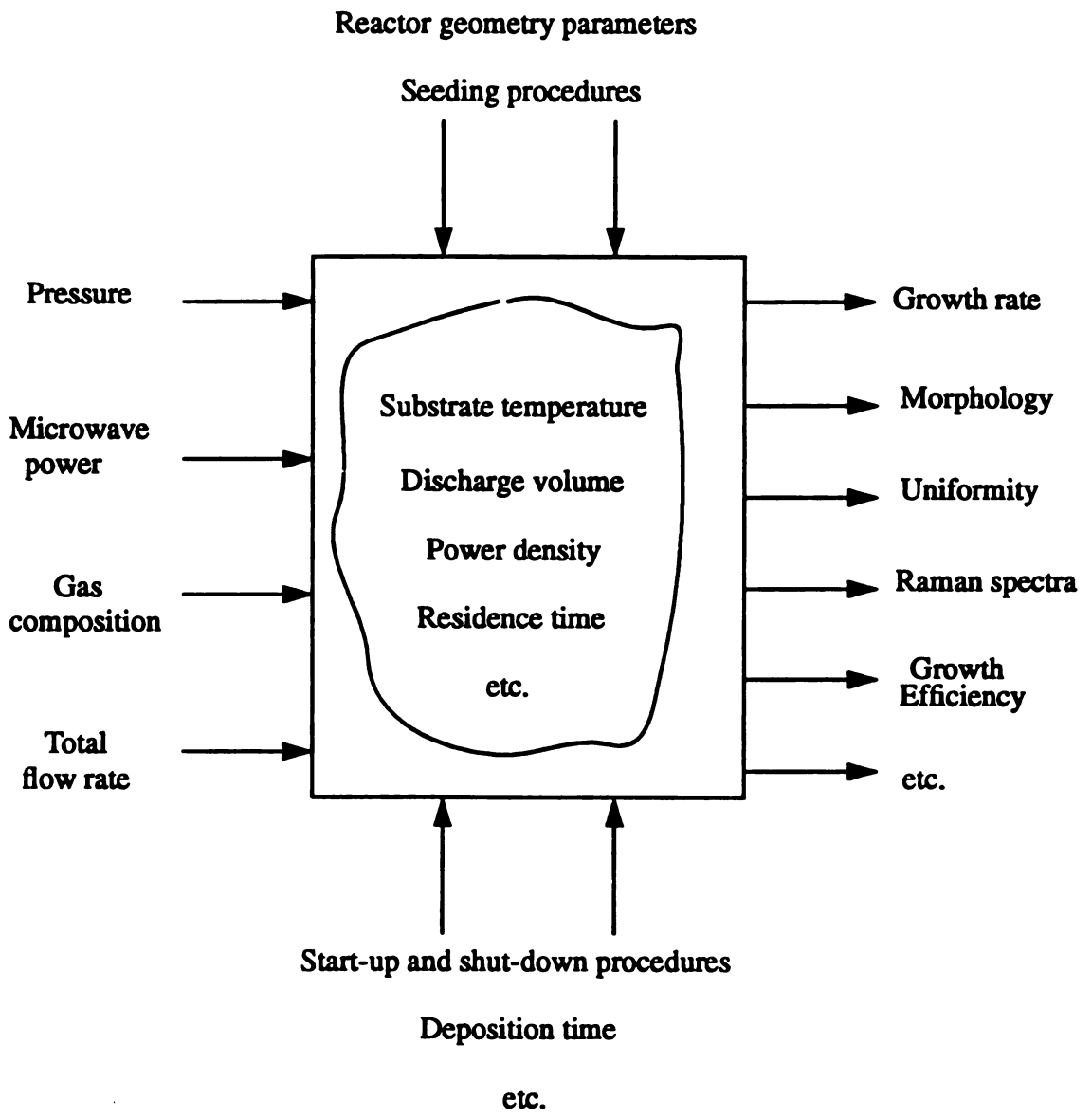

Figure 6.1 Reactor I/O Block Diagram

(j) vacuum system - pumping speed, volume, etc.

(iii) Deposition process parameters

(a) substrate seeding procedure

(b) start-up and shut-down procedures

(c) input power variation vs. time (CW vs. pulsed power, etc.)

(d) deposition time, etc.

(iv) Macroscopic controllable input parameters

(a) operating pressure, p

(b) absorbed microwave power, P_t

(c) gas composition expressed in % of H_2 gas flow, i.e. H_2, CH_4/H_2, CO_2/H_2, etc.

(d) total input gas flow rate, f_t.

II. Internal, Dependent Experimental Parameters

(i) Substrate temperature, T_s

(ii) Discharge volume, V_d, and deposition area, A_d

(iii) Discharge power density, w

(iv) Gas residence time, t_r

(v) Electric field strengths and electromagnetic field distributions within the reactor

(vi) Densities of discharge species

(a) densities of charged species

(b) densities of excited species

(c) densities of atomic and molecular species

(d) variation of these densities within the reactor (especially above the substrate)

(vii) Energy distributions and temperatures of discharge species

(viii) Flow patterns of discharge species within the reactor

(ix) Fluxes of discharge species onto the substrate

III. External, Output Parameters

(i) Film linear growth rate (μm/hr) and weight gain, u (mg/hr)

(ii) Film morphology

(iii) Film uniformity

(iv) Film Raman spectra

(v) Film growth efficiency

(a) growth rate vs. power, P_t

(b) growth rate vs. power density, w

(c) growth rate vs. power flux, P_t/A_d

(d) growth rate vs. total flow rate, f_t

(e) carbon atom conversion efficiency

6.2.2 Independent, Input Experimental Parameters

It is obvious that the experiment here has many independent input parameters. Thus in order to develop an understanding of the operational performance of the reactor, it is best to empirically optimize and fix some of the independent experimental parameters.

The substrate size and physical properties are usually fixed. Three and four inch silicon wafers are used in the experiments described in this chapter. The cavity applicator construction, quartz dome geometry, base-plate design, gas flow configuration, substrate holder geometry and material, substrate location, power feed configuration, and cavity electromagnetic mode excitation are empirically optimized to create the optimum discharge geometry for uniform substrate heating and

minimum quartz dome heating and coating.

Among the deposition process parameters, the seeding and start-up procedures are empirically optimized to generate reproducible and high diamond nucleation density. The shut down procedure is chosen such that the formation of non-diamond carbon on the deposited film surface is minimized. CW power is used in all the experiments described in this chapter. The deposition time is fixed for each set of experiments. More detailed description of these independent parameters is given in relevant sections.

The four macroscopic controllable input experimental parameters, i.e., pressure (p), absorbed microwave power (P_t), gas composition and total gas flow rate (f_t), are varied during the experiments in order to understand the characteristic behavior of MCPR under diamond film deposition conditions and to optimize the diamond film deposition process in MCPR.

6.2.3 Internal, Dependent Experimental Parameters

The internal, dependent experimental parameters vary with changes in the independent experimental parameters. Substrate temperature T_s and discharge volume V_d are two important internal experimental parameters in the diamond film deposition process. The substrate temperature T_s greatly affects the growth rate, morphology and Raman spectra of the deposited film. The discharge volume V_d determines the deposition area and film uniformity.

These internal experimental parameters are determined and/or defined as follows:

substrate temperature T_s is measured by an optical pyrometer,

discharge volume V_d is estimated by visual estimation,

the discharge power density w is defined by

$$w = P_t/V_d$$

where P_t is the absorbed microwave power, and

the gas residence time t_r is defined by

$$t_r = pV_q/f_t \text{ (sec)}$$

where p (expressed in Torr) is the pressure, V_q (expressed in liters) is the quartz dome volume above the substrate and f_t (expressed in Torr-liter/sec, 1 Torr-liter/sec = 79.05 sccm) is the total flow rate.

These dependent internal experimental parameters vary in a non-linear fashion when the input experimental parameters vary. In order to control the deposition process, these parameters must be controlled. It is also often desirable to measure some of these internal experimental parameters in-situ during the deposition process. If these measurements are performed versus time during the deposition process, the understanding of the deposition process can be greatly improved.

The other internal, dependent experimental parameters will not be discussed in this dissertation.

6.2.4 External, Output Experimental Parameters

The reactor performance is evaluated in terms of the external, output experimental parameters. These output parameters can be measured and/or calculated after the film deposition is completed. Film growth rate is expressed in terms of both linear growth rate (μm/hour) and weight gain, u (mg/hour). Weight gain is obtained from the

deposition time and weighing the wafer before and after the deposition process using a weight balance. The linear growth rate is calculated from the weight gain, the area of the wafer and the density of diamond, 3.51 g/cm^3.

The film morphology is obtained from observation under the optical microscope and photographs taken with Scanning Electron Microscope (SEM). The film uniformity is obtained by both visual estimation and laser interference reflection technique.<71> The film quality is characterized by Raman spectroscopy.

The following "figures of merit" are used to quantify the film growth efficiency of the MCPR:

(1) k_1 (mg/kW-hr) = u/P_t: u versus P_t, growth rate versus absorbed microwave power,

(2) k_2 (mg-cm^3/kW-hr) = u/w: u versus w, growth rate versus power density,

(3) k_3 (mg-cm^2/kW-hr) = u/S: u versus S, growth rate versus power flux S. S is defined by $S = P_t/A_d$, where A_d is the area of the substrate,

(4) gas flow efficiency, k_4 (mg/liter) = u/f_t: u versus f_t, growth rate versus total flow rate.

(5) carbon conversion efficiency, k_5 (%): it is defined as the percentage of carbon atoms in the input gases that are converted into the diamond film.

These output parameters allow the MCPR to be compared with other reactors and allow the comparison of the MCPR as experimental input conditions change. It is also noted here that the optimization of one performance criteria, such as uniformity, may not optimize another

performance criteria, such as growth rate.

6.3 Experimental Operational Characteristics

6.3.1 Introduction

In this section, the basic experimental configuration for diamond film deposition on 3" and 4" silicon wafers is described. The common experimental techniques, i.e., seeding, start-up and shut-down procedures, are described in detail. The operational characteristics of this experimental configuration, i.e., internal experimental parameters vs. input experimental parameters, are presented.

6.3.2 Experimental Configuration

The forced flow experimental configuration which was described in detail in chapter 3 is the experimental configuration used for diamond film deposition on 3" and 4" silicon wafers. A schematic drawing of this experimental configuration is displayed in Figure 3.16.

Figures 6.2 and 6.3 display the schematic drawings of two cavity shells used in the experiments. The main difference between the two cavity shells is that there exist four small windows (optical access windows for emission and laser induced fluorescence spectroscopy experiments) in the cavity shell (II). The microwave power coupling efficiency of cavity shell (II) is better than that of cavity shell (I). But the discharge generated with cavity shell (I) is confined to the silicon wafer better than that with cavity shell (II). The differences are especially

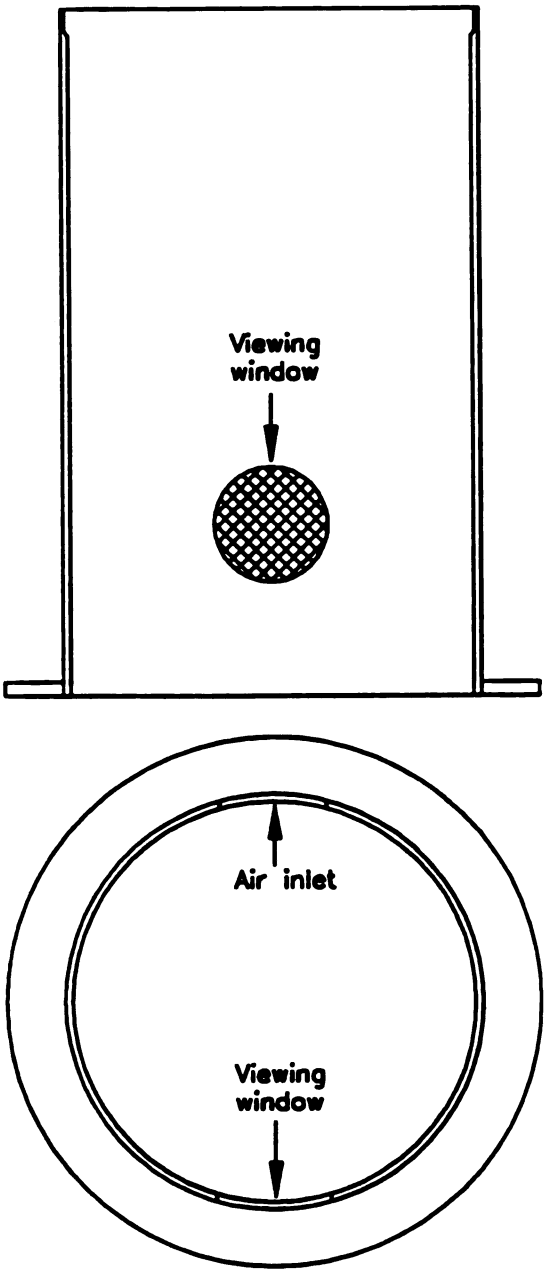

Figure 6.2 Schematic Drawing of Cavity Shell (I)

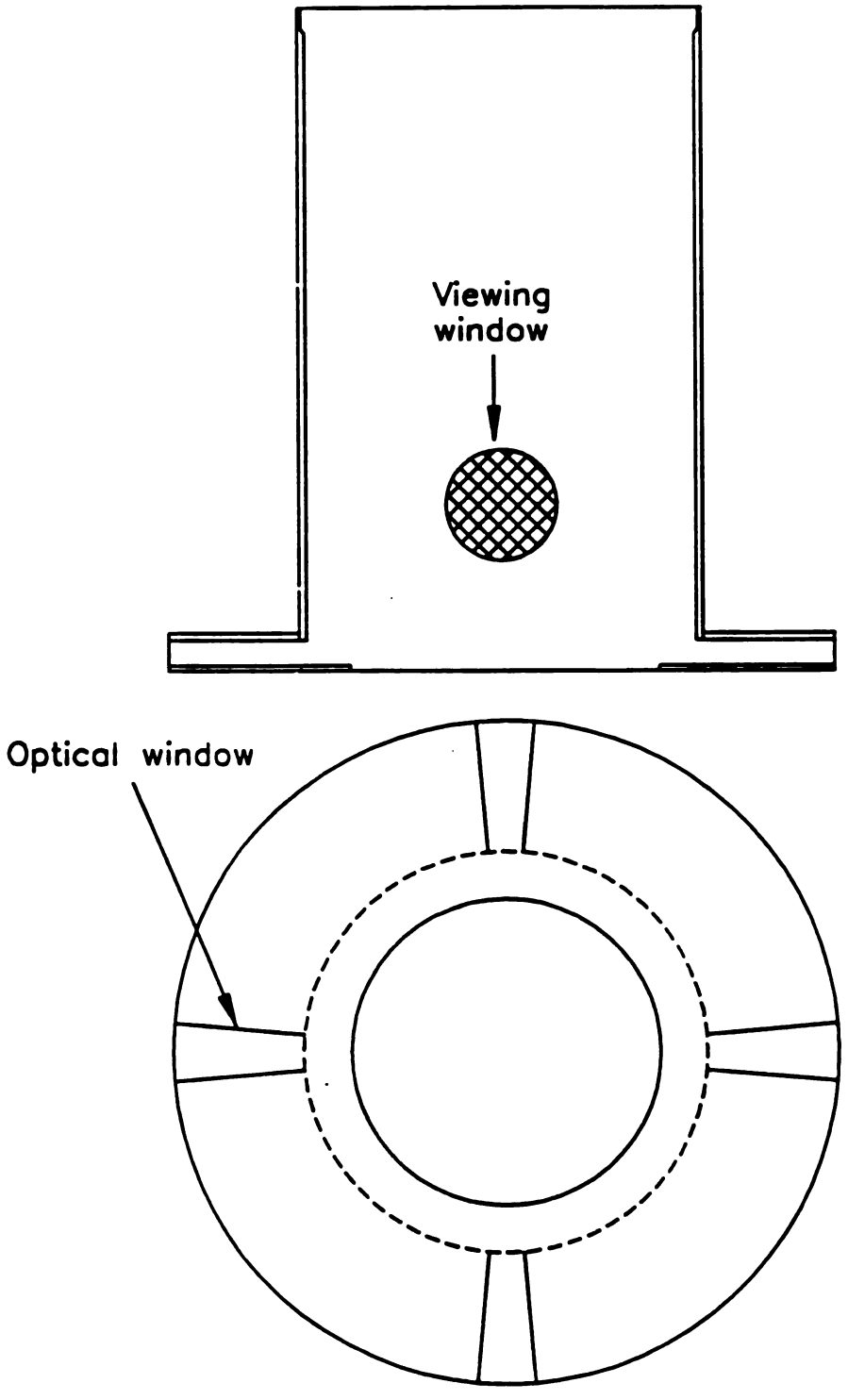

Figure 6.3 Schematic Drawing of Cavity Shell (II)

obvious when diamond films are deposited on 4" silicon wafers. For diamond film deposition on silicon wafers, cavity shell (I) is a more favorable choice.

The quartz domes made by different manufacturers and those constructed at different times by the same manufacturer result in small differences in geometry. These small differences in geometry do not have much effect on diamond film deposition on substrate surfaces which are 3.25" in diameter or smaller. But when diamond films are deposited on 4" silicon wafers, these small differences in geometry influence the optimum deposition condition, cavity tuning and the resulting film morphology, uniformity, and growth rate, etc.

In the present experimental configuration, the substrate holder (13) and flow regulator (32) are combined into one holder (13:32). The metal tube (29) used here has an outside diameter of 3", inside diameter of 2.875" and a length of 1.5".

6.3.3 Common Experimental Procedures

In this section, the common experimental procedures, i.e., seeding, start-up and shut down procedures, which are used in all the experiments discussed in this chapter, are described in detail.

6.3.3.1 Seeding Procedures

Substrate seeding has been used prior to deposition experiment to enhance diamond nucleation density. Three types of seeding procedures have been used in the experiments described in this dissertation. They

include (1) seeding by hand scratching substrate with 0.25 μm diamond paste, (2) seeding by hand scratching substrate with 1 μm diamond powder and (3) seeding by photo resist seeding method[22,72].

The first two methods are self-explanatory. They are simple to perform but the repeatability is poor. The third method is the best in terms of both repeatability and nucleation density and it is the seeding method used in all the experiments described in this chapter.

The photo resist seeding method was derived from the standard photolithography procedure used in integrated circuit fabrication. In this method, diamond powder and photo resist are first mixed ultrasonically. The resulting mixture is then used to cover the entire wafer. The wafer is in turn spined in a spinner which results in a uniform coating on the wafer. Diamond seeds are embedded in this uniform coating.

A standard recipe[73] of the photo resist seeding procedure is as follows:

(a) mix 142 mg Amplex [74] 0.1 μm diamond powder with 16 ml of Shipley[75] type A photoresist thinner,

(b) ultrasonically mix the mixture for 15 minutes,

(c) add 42 ml of Shipley 1470 photo resist,

(d) ultrasonically mix the mixture for 15 minutes,

(e) apply the mixture onto the wafer,

(f) spin the wafer with the following spin speed and time: 0 - 4000 rpm in 10 seconds, stay at 4000 rpm for 30 seconds and slow down to 500 rpm in 5 seconds,

(g) bake the wafer at 135 ^{o}C for 30 minutes.

6.3.3.2 Start-up and Shut-down Procedures

The computer monitor system described in section 3.2.4 is used in the experiments described in this chapter. The following start-up and shut-down procedures are followed.

I. Start-up procedure:

(a) evacuate the system to below 5 mTorr,

(b) turn on H_2, CH_4 and CO_2 gas flow,

(c) turn on 1.5 kW microwave power when pressure reaches 10 Torr,

(d) increase microwave power as pressure increases,

(e) start timing when pressure and microwave power reach set levels.

In the present experimental system, the pressure rise time is about 10 Torr/min with 400 sccm H_2 gas flow.

II. Shut-down procedure:

(a) turn off CH_4 and CO_2 gas flow together,

(b) wait 3 or 5 minutes for process self-cleaning,

(c) turn off microwave power,

(e) turn off H_2 gas flow,

(f) evacuate the experimental system.

6.3.4 Experimental Operational Characteristics

It was shown in section 6.2 that the microwave cavity plasma reactor can be characterized by a set of input. internal and output experimental parameters. As displayed in Figure 6.1, the substrate

temperature, T_s, and discharge volume, V_d, are internal experimental parameters which depend on all independent input experimental parameters. In this section, the characteristic behavior of the internal experimental parameters is investigated as the input experimental parameters, i.e., pressure, microwave power, gas composition and total gas flow rate, are varied.

The forced flow experimental configuration shown in Figure 3.16 is used in all the experiments described in this section. Here, the supporting quartz tube (28) has an inside diameter of 95 mm, an outside diameter of 100 mm and a length of 50 mm.

Three inch silicon wafers are used as substrates in these experiments. They have the following physical properties: prime grade, p-type, Boron doped, <100> orientation, 1 - 10 ohm-cm in resistivity, 76 mm in diameter, and 356 - 406 μm in thickness.

To help describing the characteristic behavior of the experimental reactor, the following nomenclatures are defined:

p <--> Pressure,

P_t <--> Absorbed Microwave Power,

f_t <--> Total Gas Flow Rate,

C_g <--> Gas Composition,

T_s <--> Substrate Temperature,

V_d <--> Discharge Volume.

The experimental procedures to obtain the characteristic behavior of the internal experimental parameters are as follows. A diamond film was deposited on a 3" silicon wafer under the following experimental conditions: H_2 flow rate = 400 sccm, CH_4 flow rate = 6 sccm, CO_2 flow rate = 2 sccm, pressure = 51 Torr, absorbed microwave power = 2.34 kW,

substrate temperature ~ 900 ^{o}C and deposition time = 5 hours. This diamond film was estimated to be more than 2.5 μm thick, judging from previous experiments conducted under similar experimental conditions. All the measurements were conducted after this diamond film had been formed. The substrate temperature, T_s, was measured by an optical pyrometer which was mounted on a tripod and fixed at the same location throughout the entire experiment. The discharge volume, V_d, was estimated by visual estimation. The neighboring substrate temperature readings and discharge volume estimations were recorded by varying a minimum number of input experimental parameters and waiting at least 5 minutes for the experiment to reach steady state.

Figure 6.4 shows the variation of substrate temperature T_s vs. pressure p and absorbed microwave power P_t. As shown, the substrate temperature T_s is very sensitive to variations in pressure p and only varies slowly as the absorbed microwave power P_t is varied.

The discharge volume V_d is sensitive to both the variation in pressure p and absorbed microwave power P_t. Keeping pressure p constant, the discharge volume V_d increases with increasing absorbed microwave power P_t. Keeping the absorbed microwave power P_t constant, the discharge volume V_d decreases with increasing pressure p.

In Figure 6.4, the lower power limit is defined by the minimum power needed to generate a discharge volume $(V_d)_{min}$ that covers a 3" diameter substrate area. The upper power limit is defined by the maximum power that can be used to operate the reactor safely without over-heating the quartz dome. The upper discharge volume limit $(V_d)_{max}$ is the volume of the quartz dome above the substrate.

Figure 6.5 shows the variation of substrate temperature T_s vs. CH_4

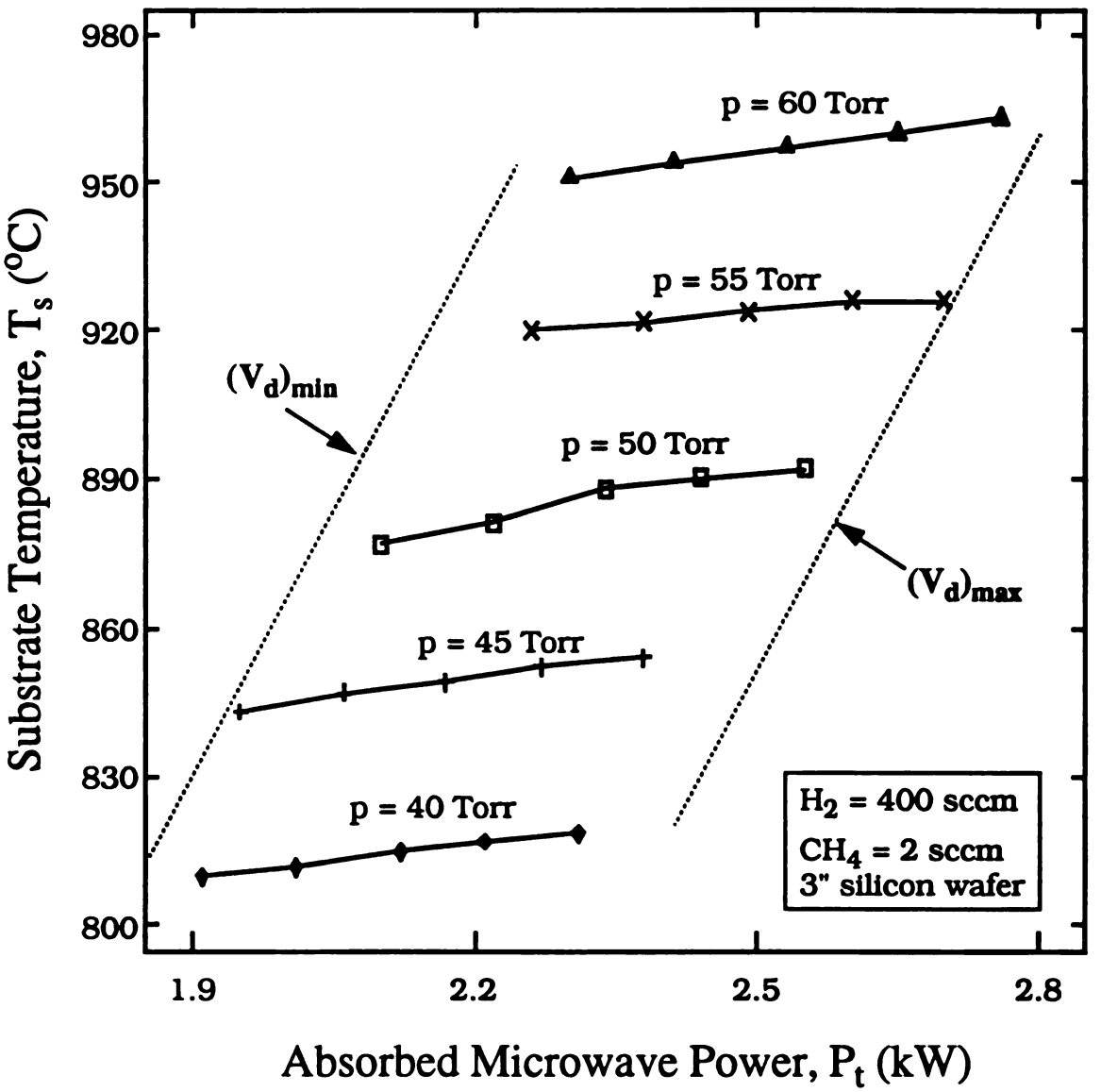

Figure 6.4 Substrate Temperature versus Pressure and Absorbed Microwave Power

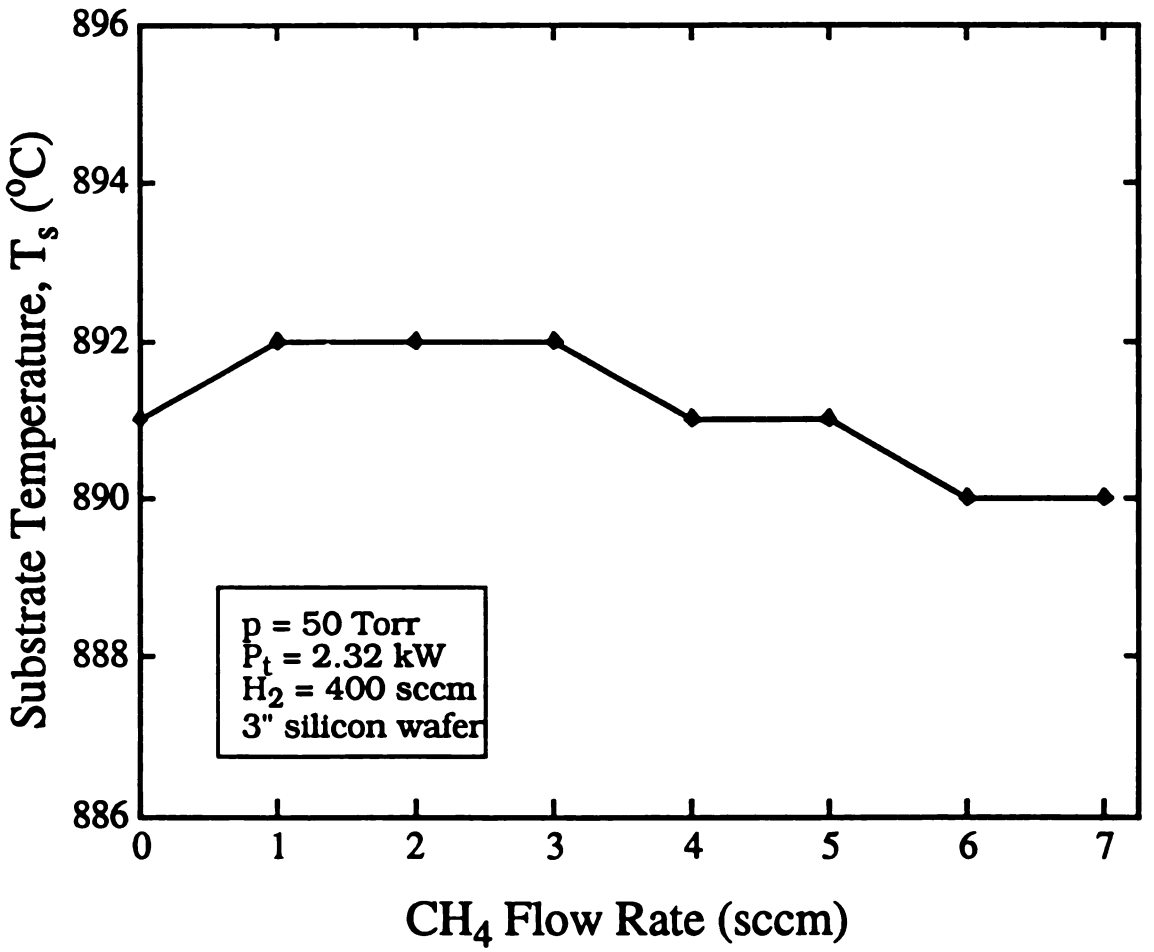

Figure 6.5 Substrate Temperature versus CH_4 Concentration

concentration. As shown, the substrate temperature T_s is not sensitive to variation in CH_4 concentration.

Figure 6.6 shows the variation of substrate temperature T_s vs. CO_2 concentration. As shown, the substrate temperature T_s varies slowly with low CO_2 concentration and decreases when CO_2 concentration is further increased. Low CO_2 concentrations are used in the diamond film deposition experiments described in this chapter. Figures 6.5 and 6.6 show that the substrate temperature T_s is not sensitive to variation in gas composition C_g. It is also found by visual estimation that the discharge volume V_d is not sensitive to variation in gas composition C_g.

Figure 6.7 shows the variation of substrate temperature T_s vs. absorbed microwave power P_t and total flow rate f_t. As shown, the substrate temperature T_s increases gradually when the absorbed microwave power P_t is increased and it is not sensitive to variations in total gas flow rate f_t. It is also found by visual estimation that the discharge volume V_d is not sensitive to variations in total gas flow rate f_t.

6.3.5 Summary

The following conclusions can be drawn from the experiments described in the previous section:

(1) Substrate temperature T_s increases sharply with increasing pressure (~ 6 ^oC/Torr) and at constant pressure, T_s increases gradually (~ 0.02 ^oC/W) with increasing absorbed microwave power. It is not sensitive to variations in gas composition and total flow rate.

(2) Discharge volume V_d decreases with increasing pressure and increases with increasing absorbed microwave power. It is not sensitive

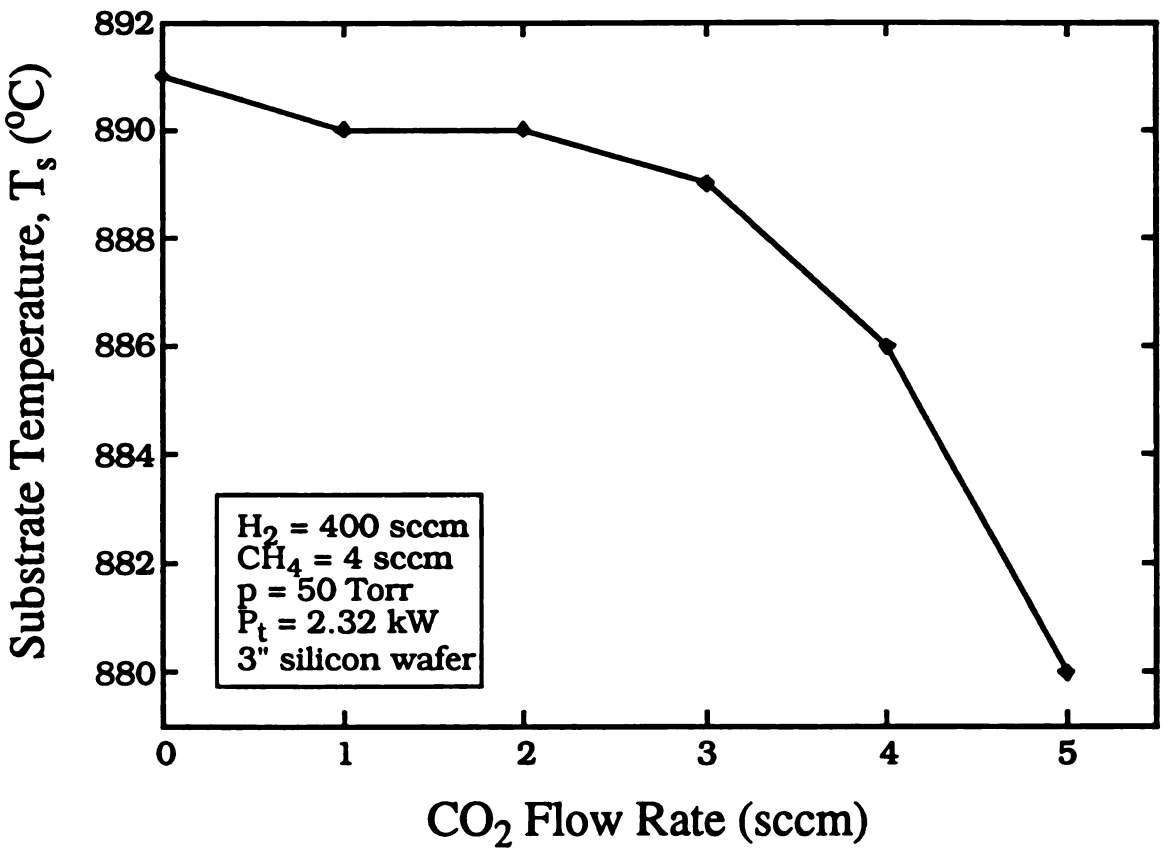

Figure 6.6 Substrate Temperature versus CO_2 Concentration

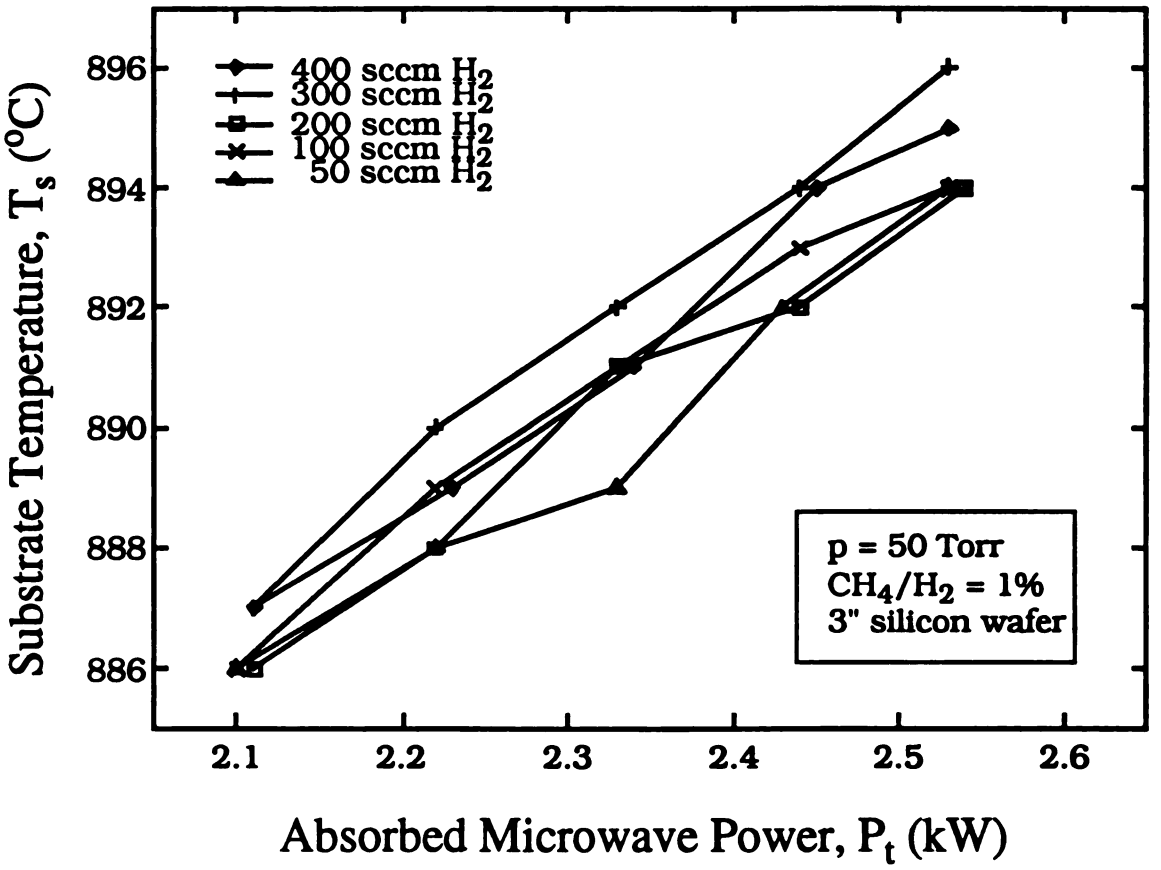

Figure 6.7 Substrate Temperature versus Total Flow Rate and Absorbed Microwave Power

to variations in gas composition and total flow rate.

Using the definitions of discharge power density w and power flux S,

$$w = P_t/V_d$$

$$S = P_t/A_d$$

where A_d is the substrate area, the following additional conclusions can be drawn.

(3) Power density, w, increases with increasing pressure and at constant pressure, it is not sensitive to variation in absorbed microwave power. That is, under a constant pressure, as the absorbed microwave power increases, the discharge volume also increases, resulting in small variation in absorbed power density. Power density is not sensitive to variation in gas composition and total flow rate.

(4) Power flux S increases with increasing absorbed microwave power. It is not sensitive to variation in gas composition and total flow rate.

These results on the characteristic behavior of the MCPR under diamond film deposition conditions demonstrate that the reactor behaves in an unique repeatable fashion. A set of experimental curves can be used to describe the substrate temperature variations as pressure, absorbed microwave power, gas composition and total flow rate vary. This set of curves can be used to understand and describe the experimental behavior of the reactor. The allowable experimental operating space is defined by these curves. If certain substrate temperature conditions are desired, these curves can be utilized to determine the pressure and absorbed microwave power required. These curves serve as the experimental reactor operating energy "road map".

6.4 Diamond Film Deposition on 3" Silicon Wafers

6.4.1 Introduction

Diamond films with various physical properties are deposited on 3" silicon wafers under various experimental conditions. In order to optimize the diamond film deposition process, it is necessary to study the co-relation between the physical properties of the deposited diamond films and the experimental conditions. Hence a parametric study of diamond film deposition on 3" silicon wafers was conducted. In this study, the following experimental parameters are considered:

I The independent input experimental parameters:

- (1) absorbed microwave power, P_t,
- (2) pressure, p,
- (3) gas (H_2, CH_4, CO_2) composition, and
- (4) total flow rate, f_t.

II. The internal experimental parameters:

- (1) substrate temperature T_s, and
- (2) gas residence time, t_r.

III. The output experimental parameters:

- (1) film linear growth rate (μm/hour),
- (2) film weight gain u (mg/hour),
- (3) film growth efficiencies:
  - (i) growth rate vs. power flux, i.e., u vs. S,
  - (ii) gas flow efficiency: k_4 (mg/liter) = u/f_t,
  - (iii) carbon conversion efficiency, k_5 (%).
- (4) film morphology,

(5) typical film uniformity, and

(6) typical film Raman spectrum.

In this study, diamond films are deposited on 3" silicon wafers using the forced flow configuration shown in Figure 3.16. The physical properties of the 3" silicon wafers and quartz tube (28) used in these experiments are the same as that described in section 6.3.4.

Descriptions of relevant experimental operational energy and chemistry space are also included whenever possible.

6.4.2 Film Growth Rate and Growth Efficiency

6.4.2.1 Effects of Substrate Temperature

Substrate temperature is an important internal experimental parameter in diamond film deposition process. In this study, the substrate temperatures are achieved by choosing the appropriate pressures. The absorbed microwave powers are adjusted such that the discharge volumes are large enough to cover the silicon substrates.

Figure 6.8 displays diamond film linear growth rate and weight gain versus substrate temperature and microwave power flux with gas flow rates of 200 sccm H_2 and 4 sccm CH_4. The pressures and absorbed microwave powers used to achieve the three substrate temperatures are shown in Table 6.1 located above Figure 6.8.

Figure 6.9 (a) shows the locations of these substrate temperature conditions on the characteristic energy "map". Figure 6.9 (b) displays the relevant carbon conversion efficiency and gas flow efficiency vs. substrate temperature.

Table 6.1 Substrate Temperature Conditions (I)

Temperature, T_s (°C)	750	850	950
Pressure, p (Torr)	33	45	57
MW power, P_t(kW)	1.47	2.05	2.51

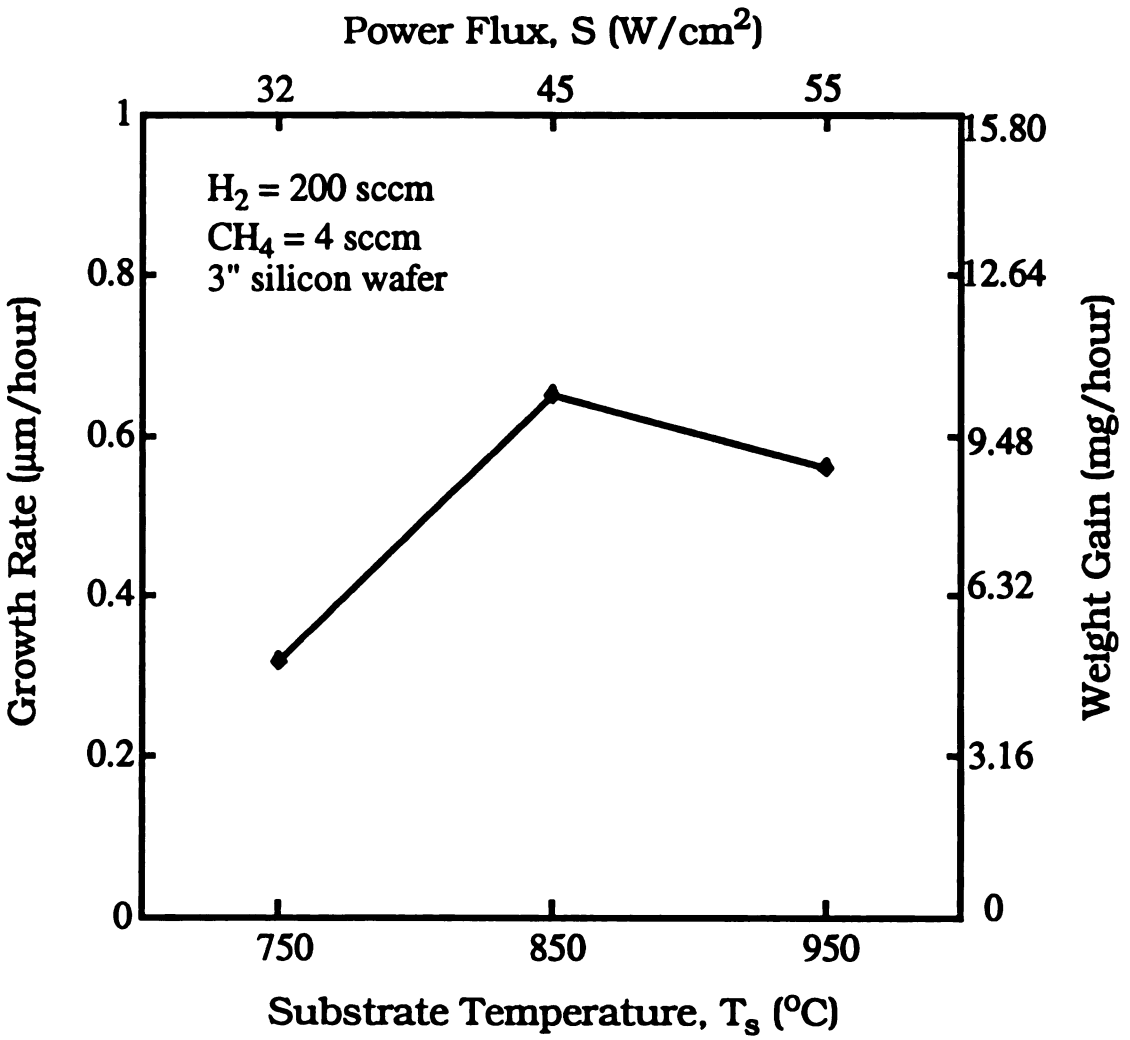

Figure 6.8 Linear Growth Rate and Weight Gain versus Substrate Temperature and Power Flux (I)

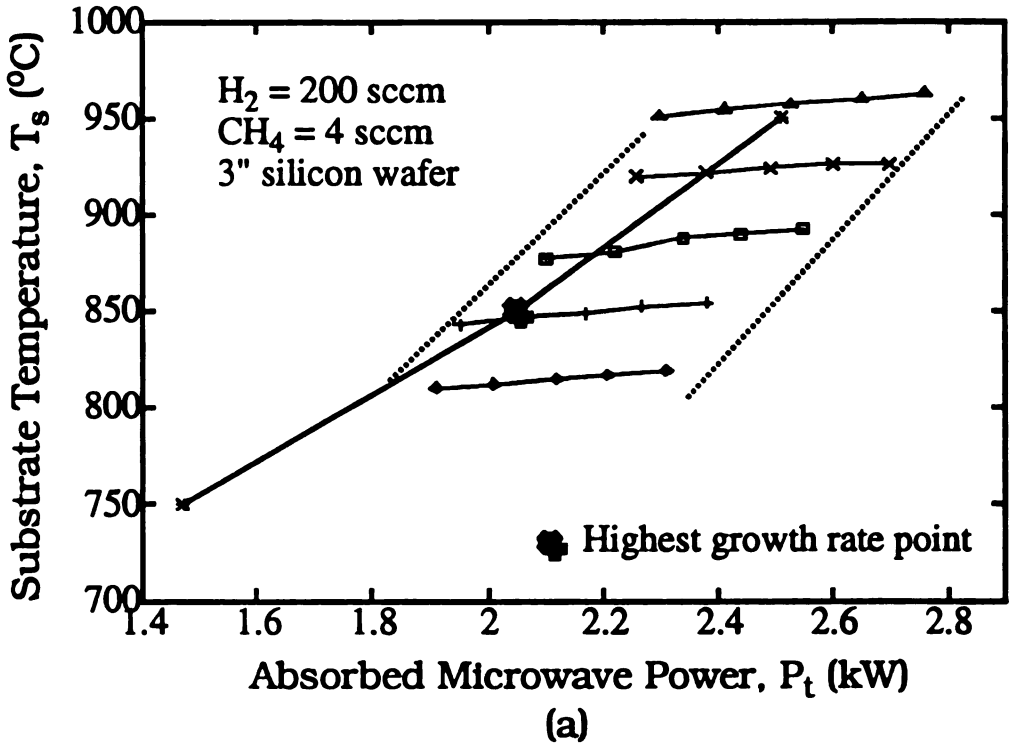

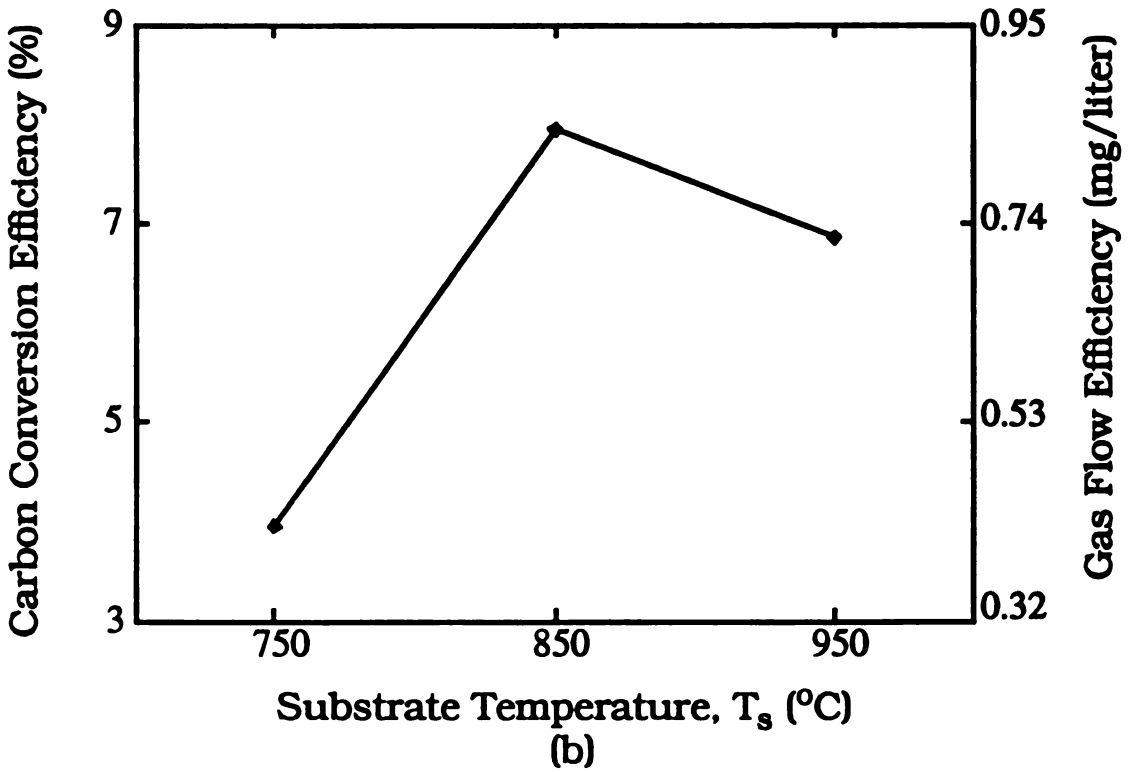

Figure 6.9 (a) Location of Substrate Temperature Conditions on Energy Map and (b) Carbon Conversion Efficiency and Gas Flow Efficiency versus Substrate Temperature (I)

Figure 6.10 displays diamond film linear growth rate and weight gain versus substrate temperature and microwave power flux with gas flow rates of 200 sccm H_2, 2 sccm CH_4 and 2 sccm CO_2. The pressures and absorbed microwave powers to achieve the five temperatures are shown in Table 6.2 located above Figure 6.10.

Figure 6.11 (a) shows the locations of these substrate temperature conditions on the characteristic energy "map". Figure 6.11 (b) displays the relevant carbon conversion efficiency and gas flow efficiency vs. substrate temperature.

Figure 6.12 shows diamond film linear growth rate and weight gain versus substrate temperature and microwave power flux with gas flow rates of 400 sccm H_2, 4 sccm CH_4 and 2 sccm CO_2. The pressures and absorbed microwave powers used to achieve the three temperatures are shown in Table 6.3 located above Figure 6.12.

Figure 6.13 (a) shows the locations of these substrate temperature conditions on the characteristic energy "map". Figure 6.13 (b) displays the relevant carbon conversion efficiency and gas flow efficiency vs. substrate temperature.

As displayed in Figures 6.8 through 6.13, the linear growth rate, weight gain, carbon conversion efficiency and gas flow efficiency generally experience peak values when the substrate temperature is varied between 700 ^{o}C and 1000 ^{o}C. It is also noted from these figures that the peak values are gas composition dependent. The locations of these gas compositions on the Bachmann C-H-O phase diagram are shown in Figure 6.14. It is also shown in Figures 6.9(a), 6.11(a) and 6.13(a) that the combinations of pressures and absorbed microwave powers to achieve these peak values fall within the boundaries of the characteristic

Table 6.2 Substrate Temperature Conditions (II)

Temperature, T_s (°C)	Pressure, p (Torr)	MW power, P_t (kW)
750	33	1.48
800	39	1.76
850	45	2.05
900	51	2.34
950	57	2.64

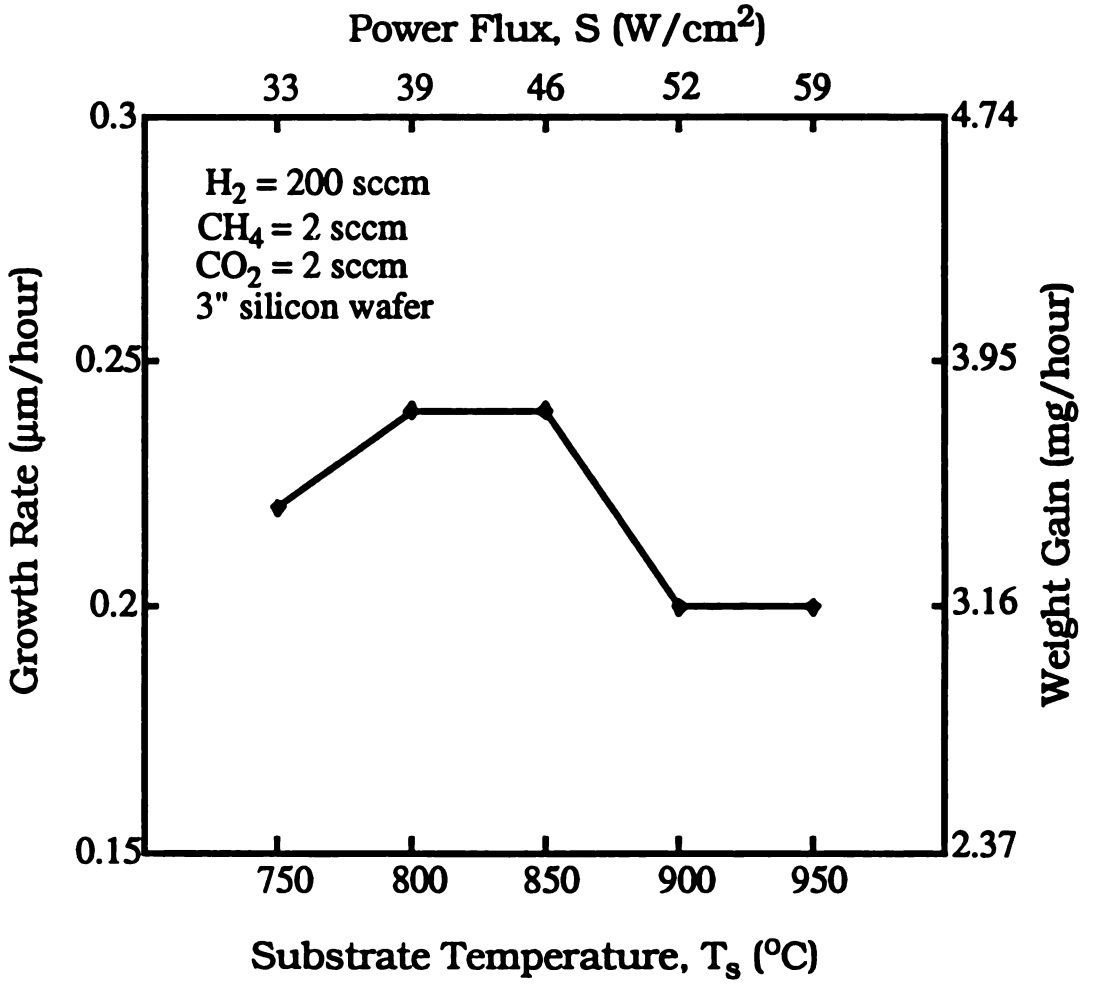

Figure 6.10 Linear Growth Rate and Weight Gain versus Substrate Temperature and Power Flux (II)

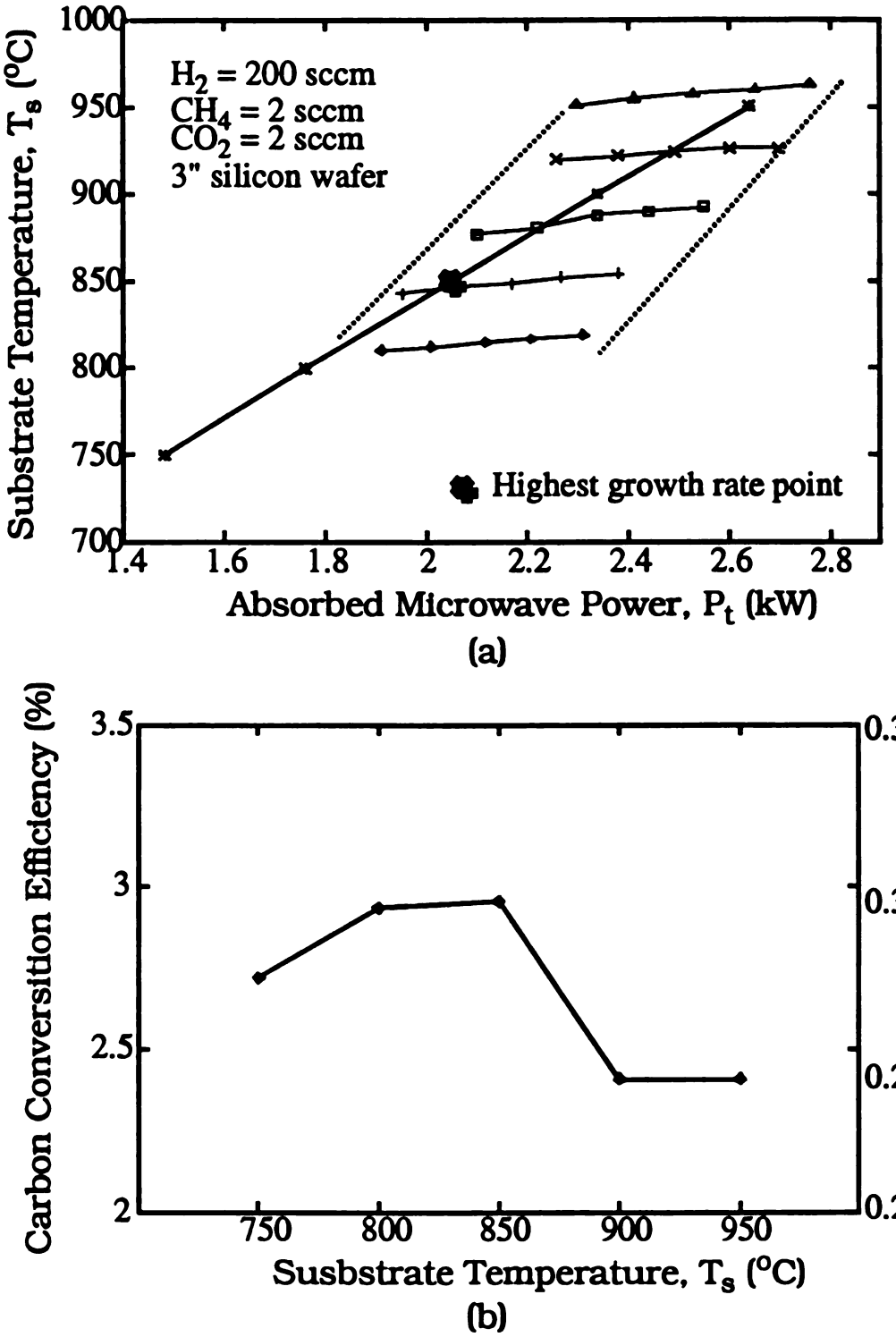

Figure 6.11 (a) Location of Substrate Temperature Conditions on Energy Map and (b) Carbon Conversion Efficiency and Gas Flow Efficiency versus Substrate Temperature (II)

Table 6.3 Substrate Temperature Conditions (III)

Temperature, T_s (°C)	927	964	1001
Pressure, p (Torr)	50	55	60
MW power, P_t (kW)	2.61	2.67	2.74

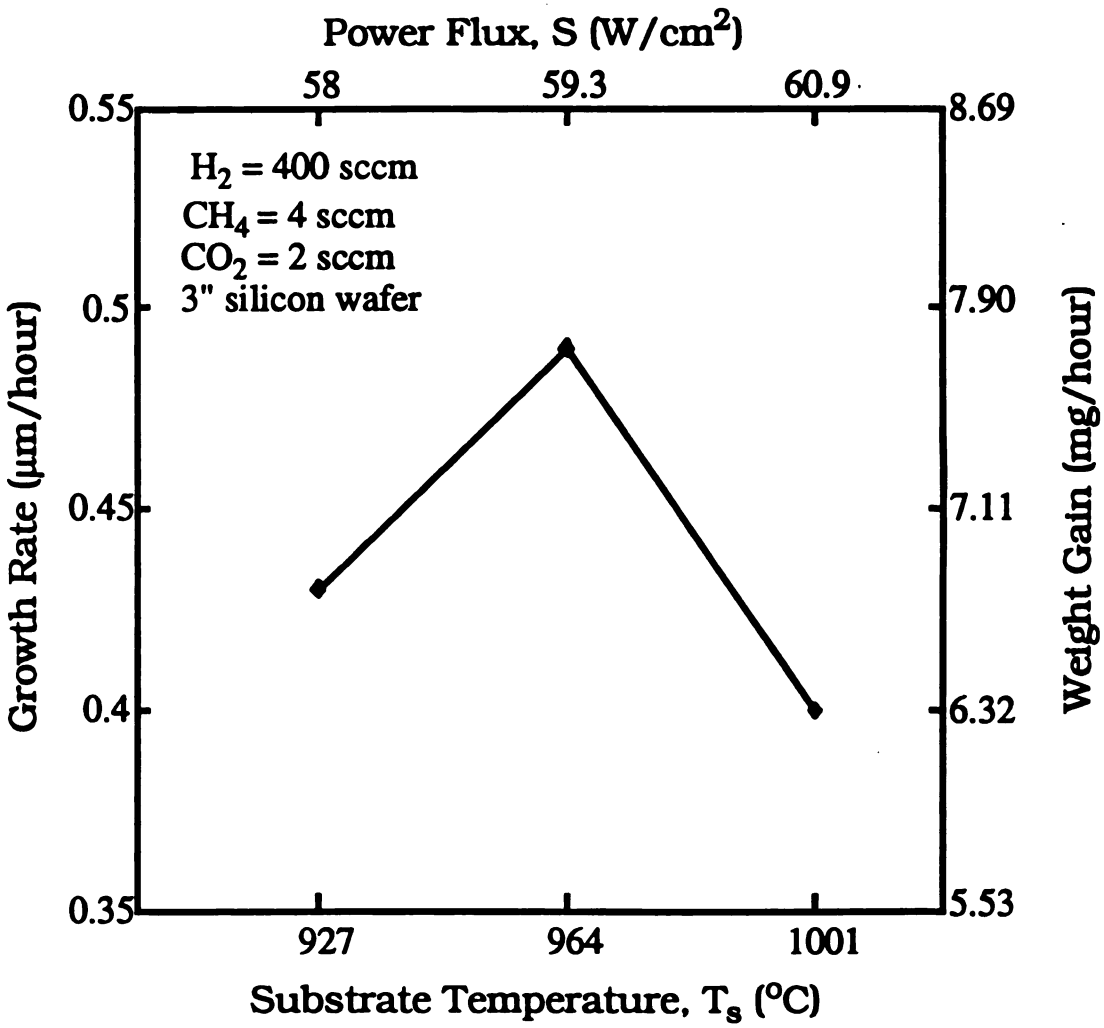

Figure 6.12 Linear Growth Rate and Weight Gain versus Substrate Temperature and Power Flux (III)

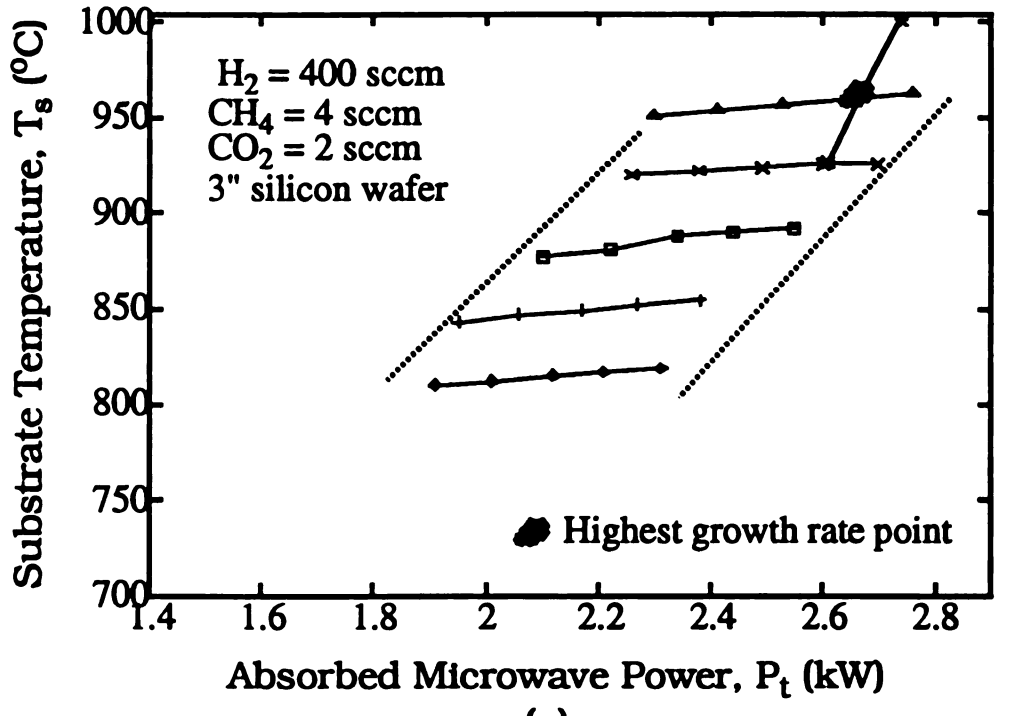

(a)

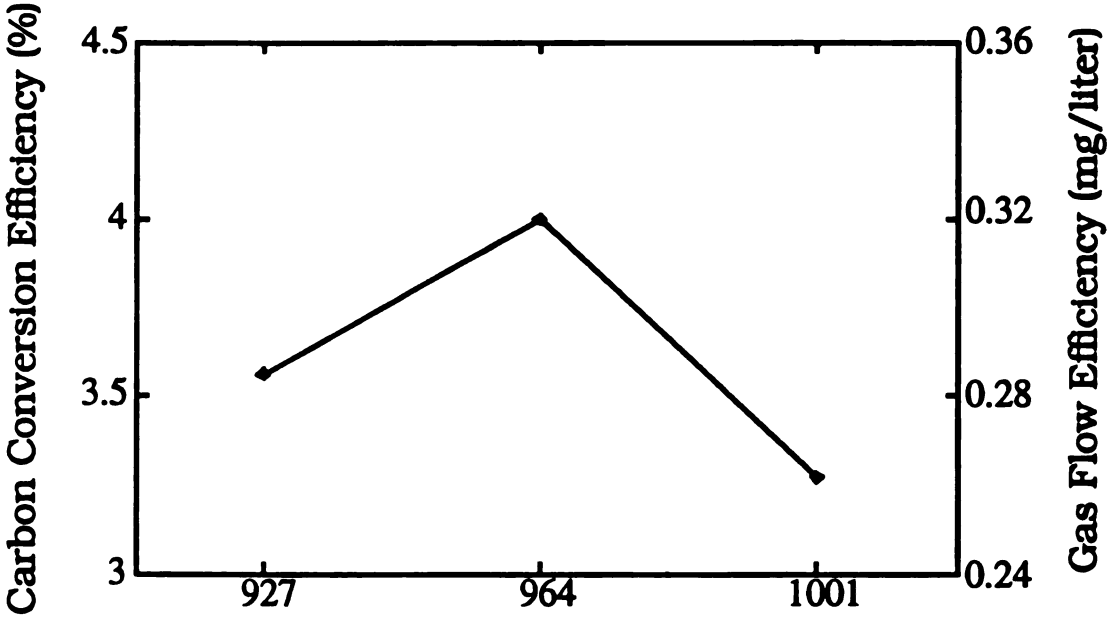

(b)

Figure 6.13 (a) Location of Substrate Temperature Conditions on Energy Map and (b) Carbon Conversion Efficiency and Gas Flow Efficiency versus Substrate Temperature (III)

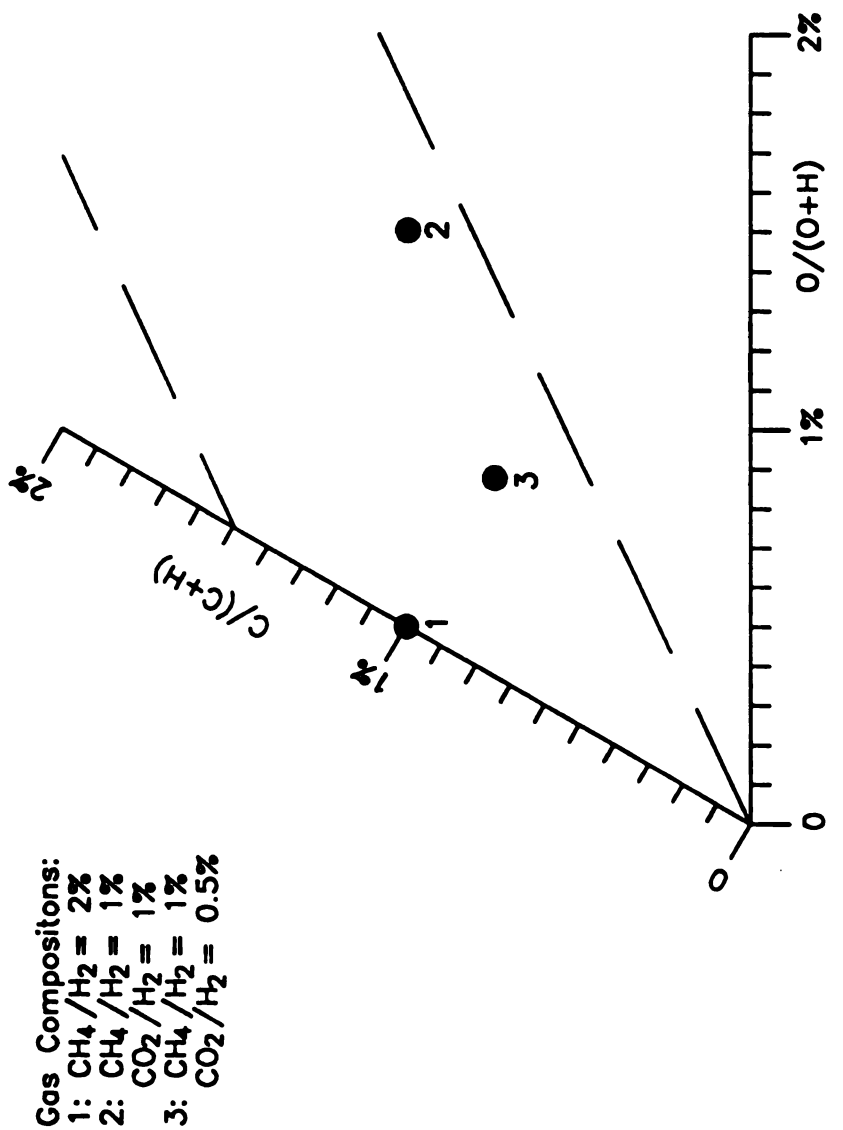

Figure 6.14 Location of Gas Compositions on the C-H-O Phase Diagram (I)

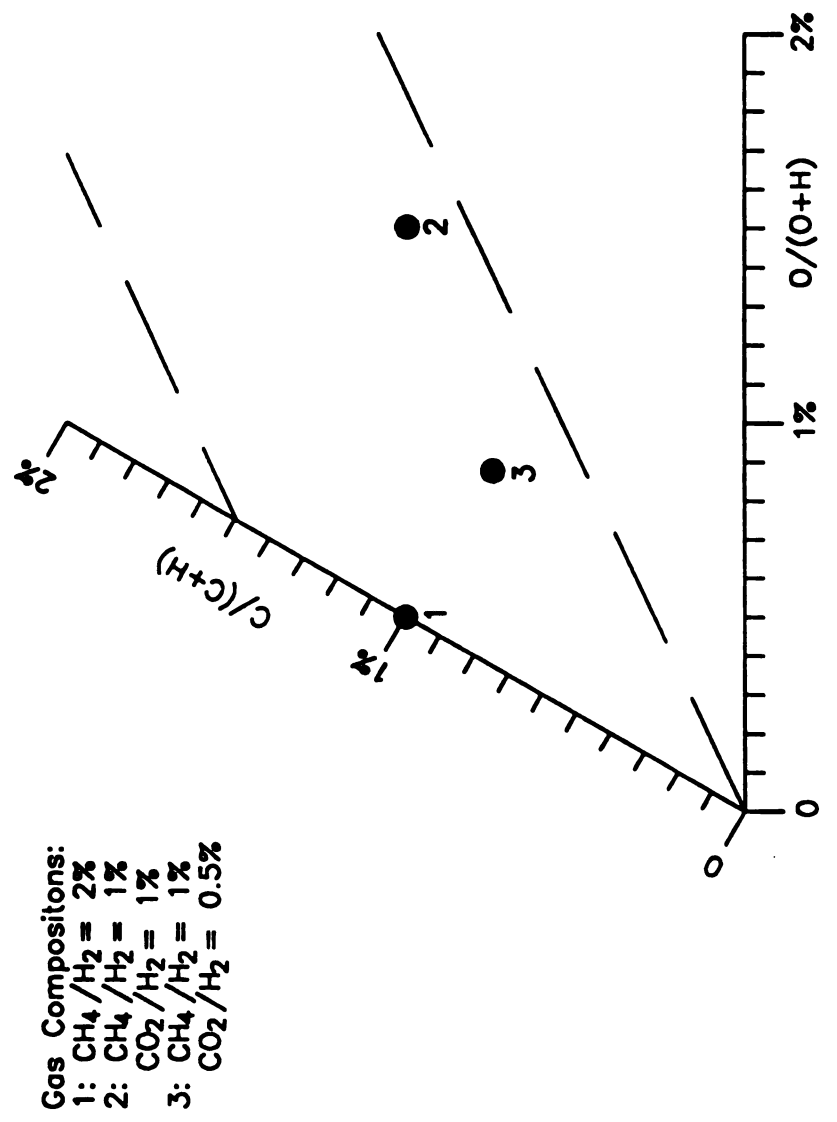

Figure 6.14 Location of Gas Compositions on the C-H-O Phase Diagram (I)

energy "map".

In the growth rate and growth efficiency vs. gas composition and total flow rate experiments that follow, the substrate temperature is chosen to be fixed at either 900 °C or 950 °C. The CH_4 concentration is varied first in the growth rate vs. gas composition experiments.

6.4.2.2 Effects of CH_4 Concentration

Figure 6.15 displays the diamond film linear growth rate, weight gain and carbon conversion efficiency vs. CH_4 gas concentration under the following experimental conditions: H_2 flow rate = 400 sccm, pressure = 51 Torr, absorbed microwave power = 2.34 kW, substrate temperature ~ 900 °C and deposition time = 6 hours.

As shown, the film linear growth rate and weight gain experience peak values with CH_4 to H_2 volume ratio of about 6/400 = 1.5%. The carbon conversion efficiency decreases as CH_4 concentration is increased.

Figure 6.16 displays the diamond film linear growth rate, weight gain and carbon conversion efficiency vs. CH_4 gas concentration under the following experimental conditions: H_2 flow rate = 400 sccm, pressure = 57 Torr, absorbed microwave power = 2.5 kW, substrate temperature ~ 950 °C and deposition time = 6 hours.

As shown, the film linear growth rate and weight gain experience peak values with CH_4 to H_2 volume ratio of about 5/400 = 1.25%. The carbon conversion efficiency decreases when CH_4 concentration is increased beyond this optimum CH_4 concentration.

Figure 6.17 displays the locations of the gas compositions used in

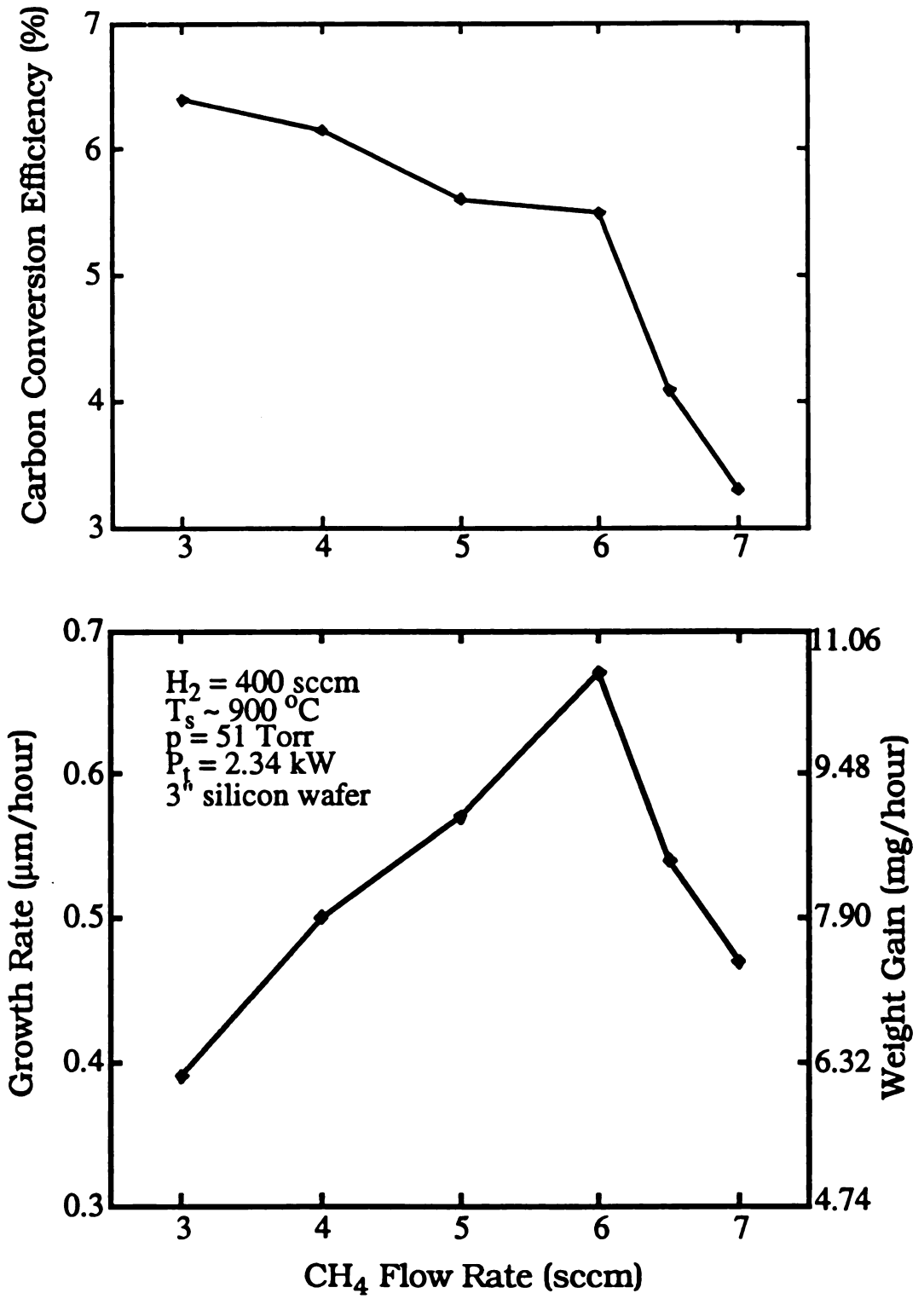

Figure 6.15 Linear Growth Rate, Weight Gain and Carbon Conversion Efficiency versus CH_4 Concentration (I)

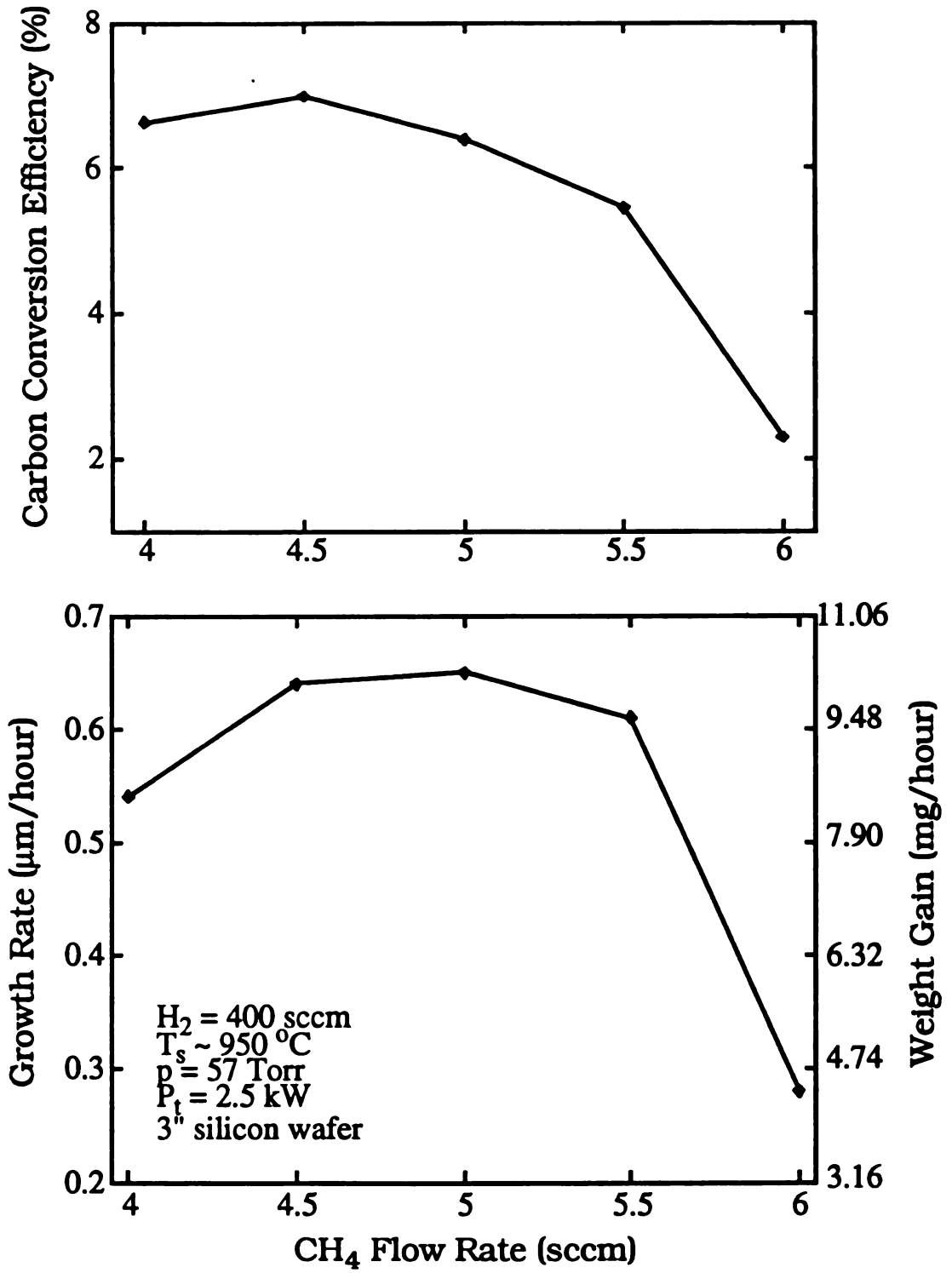

Figure 6.16 Linear Growth Rate, Weight Gain and Carbon Conversion Efficiency versus CH_4 Concentration (II)

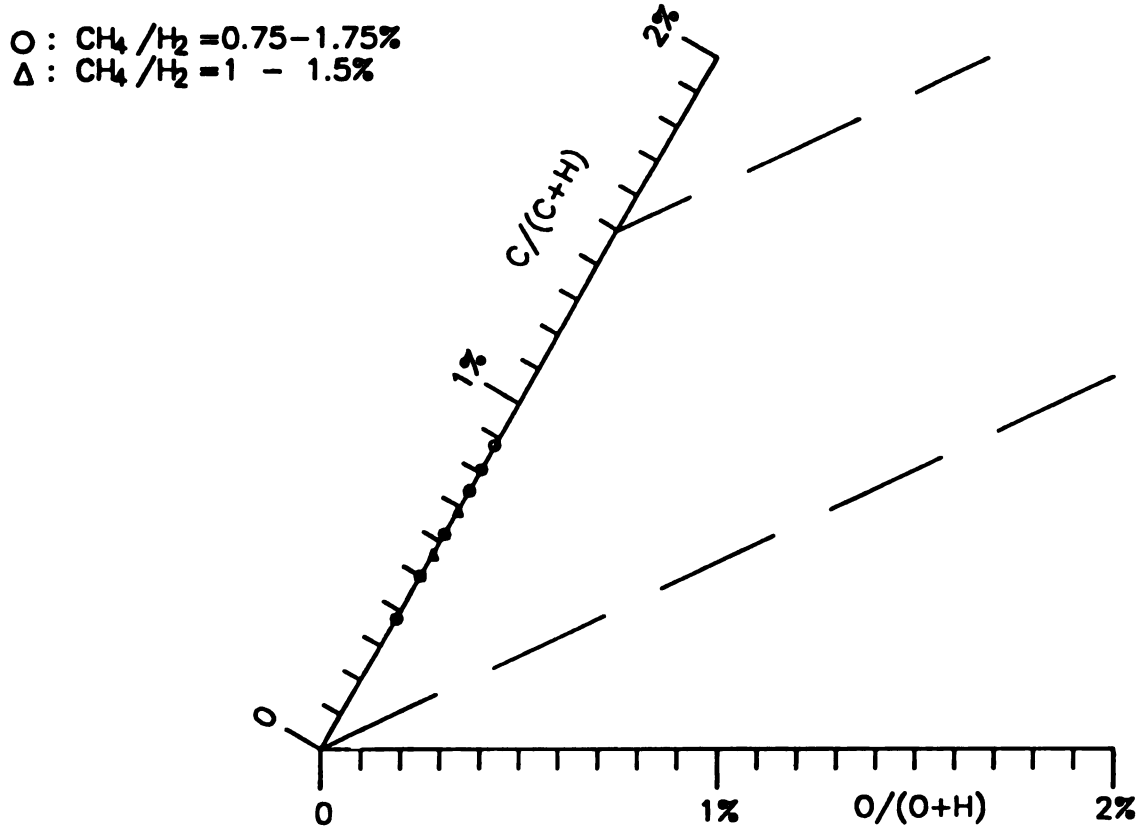

Figure 6.17 Location of Gas Compositions on the C-H-O Phase Diagram (II)

Figures 6.15 and 6.16 on the Bachmann diagram.

The experimental parameters used to obtain the peak growth rate values are used as the starting experimental parameters in the following sections.

6.4.2.3 Effects of CO_2 Concentration

Figure 6.18 displays the diamond film linear growth rate, weight gain and carbon conversion efficiency vs. CO_2 gas concentration under the following experimental conditions: H_2 flow rate = 400 sccm, CH_4 flow rate = 6 sccm, pressure = 51 Torr, microwave power absorbed = 2.34 kW, substrate temperature ~ 900 ^oC and deposition time = 6 hours.

As shown, the film linear growth rate, weight gain and carbon conversion efficiency experience gradual decline as the CO_2 gas concentration is increased. Crystalline diamond films are deposited with these four gas compositions.

Figure 6.19 displays the film linear growth rate, weight gain and carbon conversion efficiency vs. CO_2 gas concentration under the following experimental conditions: H_2 flow rate = 200 sccm, CH_4 flow rate = 6 sccm, pressure = 51 Torr, microwave power absorbed = 2.46 kW, and deposition time = 6 hours.

As shown, the film linear growth rate, weight gain and carbon conversion efficiency experience sharp increases as CO_2 flow rate is increased from 3 to 3.5 sccm, where a dark film is deposited with 3 sccm CO_2 gas flow and a crystalline diamond film is deposited with 3.5 sccm CO_2 gas flow. The film linear growth rate, weight gain and carbon conversion efficiency are decreased as CO_2 gas flow rate is further

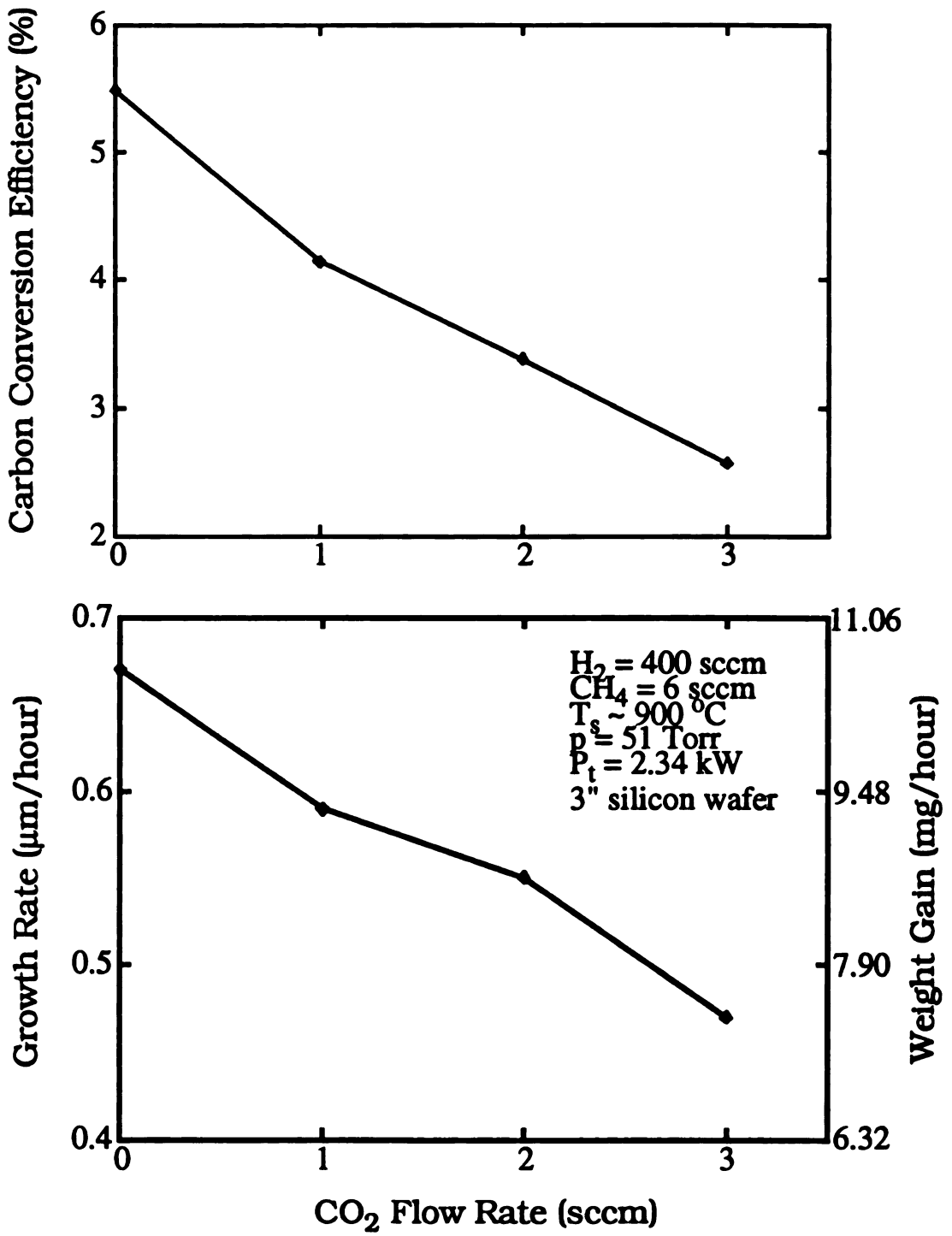

Figure 6.18 Linear Growth Rate, Weight Gain and Carbon Conversion Efficiency versus CO_2 Concentration (I)

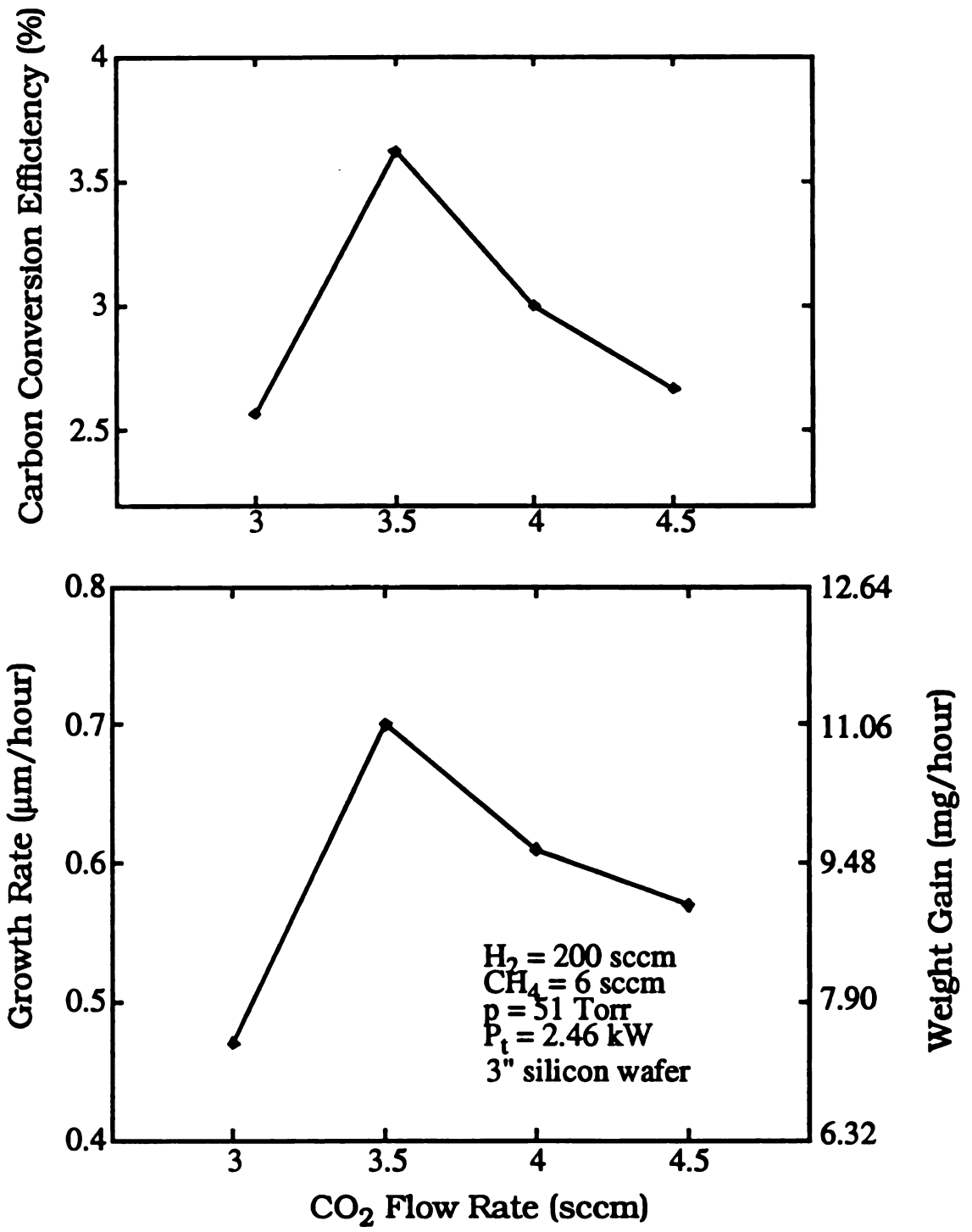

Figure 6.19 Linear Growth Rate, Weight Gain and Carbon Conversion Efficiency versus CO_2 Concentration (II)

increased from 3.5 sccm to 4.5 sccm. Crystalline diamond films are deposited in the later three cases.

Figure 6.20 shows the locations of the gas compositions used in Figures 6.18 and 6.19 on the Bachmann C-H-O phase diagram.

From Figures 6.15 and 6.18, we see the optimum gas composition for high rate diamond film growth at 900 °C is the following: H_2 flow rate = 400 sccm and CH_4 flow rate = 6 sccm. This gas composition is used in the following growth rate versus total flow rate experiments.

6.4.2.4 Effects of Total Flow Rate

Figure 6.21 displays the diamond film linear growth rate, weight gain and carbon conversion efficiency vs. total gas flow rate and gas residence time under the following experimental conditions: CH_4 to H_2 volume ratio = 1.5%, pressure = 51 Torr, absorbed microwave power = 2.34 kW, substrate temperature ~ 900 °C and deposition time = 6 hours.

Figure 6.22 displays the diamond film linear growth rate, weight gain and carbon conversion efficiency vs. total gas flow rate and gas residence time under the following experimental conditions: CH_4 to H_2 volume ratio = 1.25%, pressure = 57 Torr, absorbed microwave power = 2.5 kW, substrate temperature ~ 950 °C and deposition time = 6 hours.

As shown in Figures 6.21 and 6.22, the film linear growth rate and weight gain increase with increasing total flow rate when the total flow rate is low and gas residence time is high. As the total flow rate is further increased and the gas residence time decreases, the linear growth rate and weight gain start to saturate. The carbon conversion efficiency decreases with increasing total flow rate and decreasing gas residence

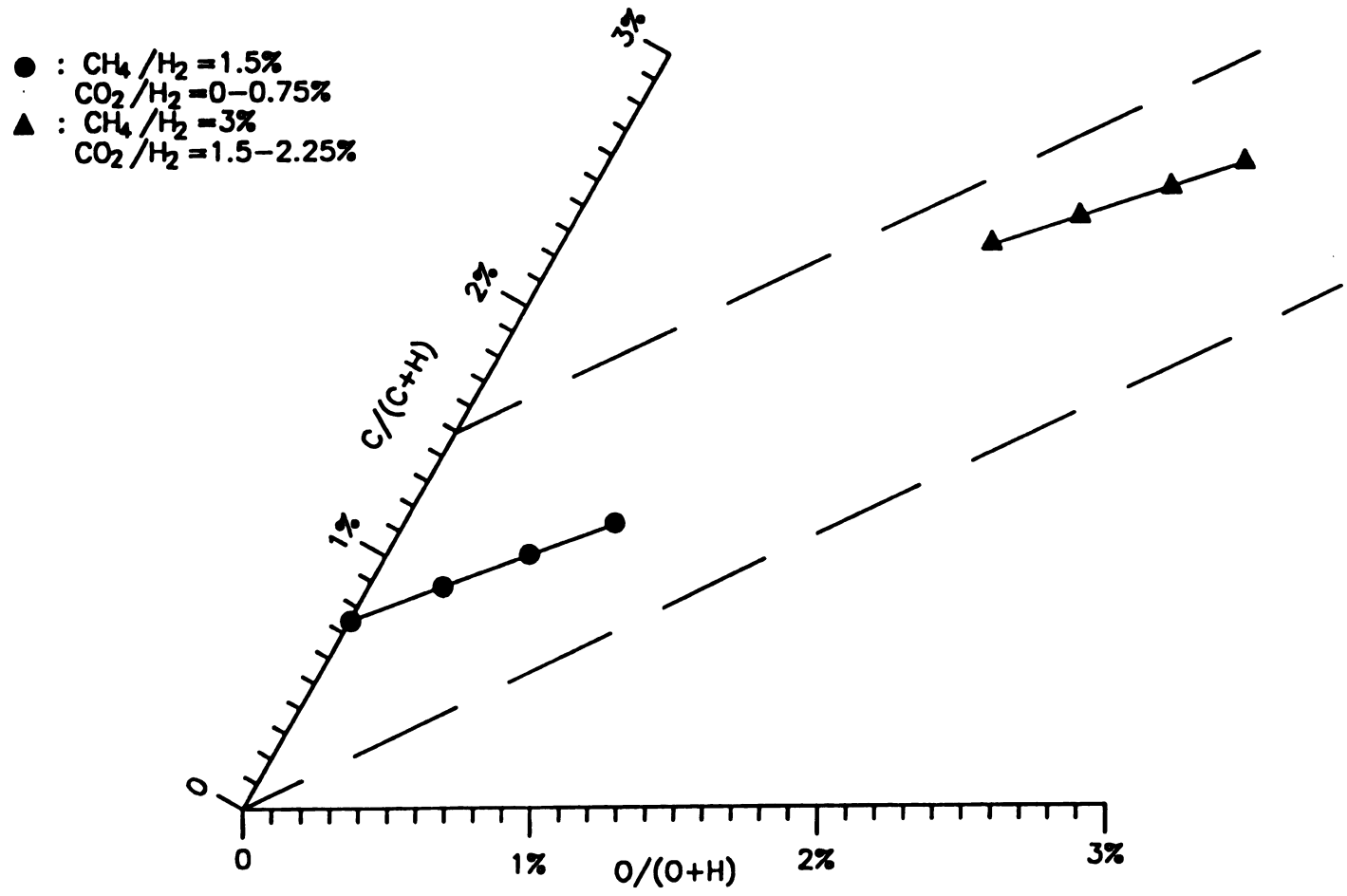

Figure 6.20 Location of Gas Compositions on the C-H-O Phase Diagram (III)

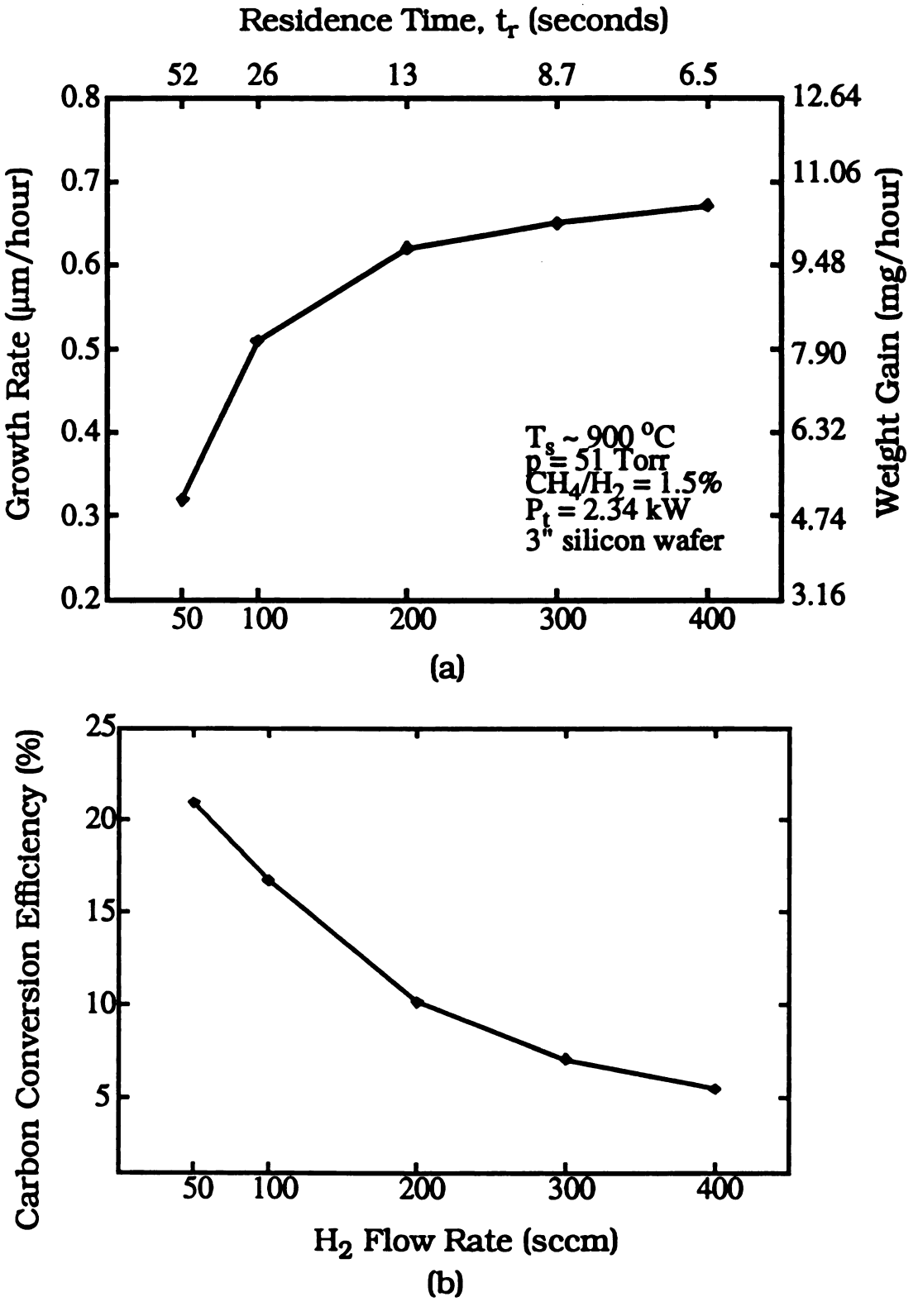

Figure 6.21 (a) Linear Growth Rate, Weight Gain and (b) Carbon Conversion Efficiency versus Total Flow Rate and Gas Residence Time (I)

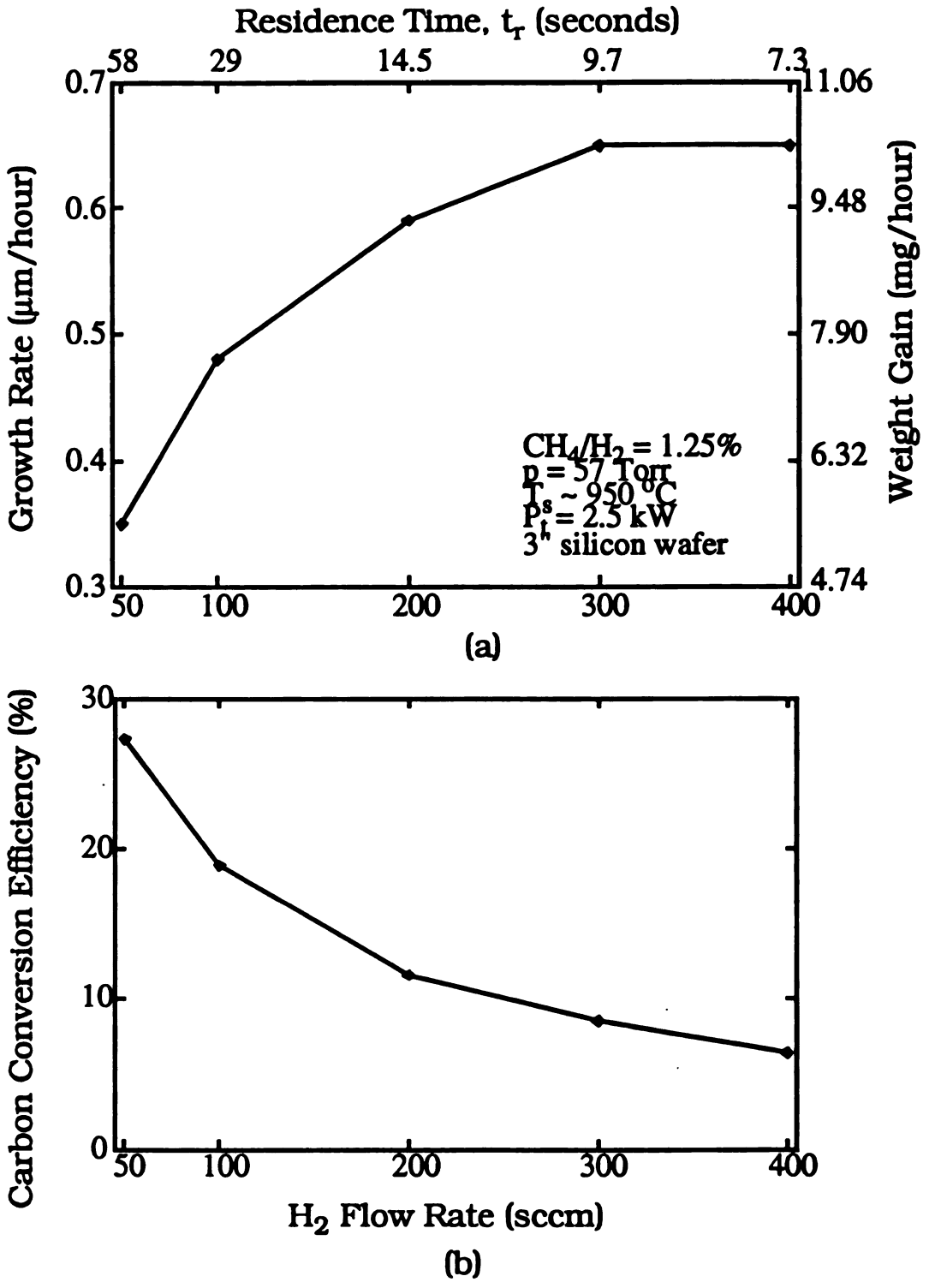

Figure 6.22 (a) Linear Growth Rate, Weight Gain and (b) Carbon Conversion Efficiency versus Total Flow Rate and Gas Residence Time (II)

time.

6.4.3 Film Morphology

6.4.3.1 Introduction

Scanning Electron Microscopy (SEM) is used to identify the morphologies of films deposited under various experimental conditions. The films deposited under the various experimental conditions described in section 6.4.2 are characterized.

6.4.3.2 Effects of Substrate Temperature

Figure 6.23 displays the SEM photographs of three films deposited with substrate temperatures: (a) 750 ^{o}C, (b) 850 ^{o}C and (c) 950 ^{o}C. The pressures and absorbed microwave powers used to achieve these temperatures are listed in Table 6.1 located above Figure 6.8. The other deposition conditions are: H_2 flow rate = 200 sccm, CH_4 flow rate = 4 sccm, and deposition time = 4 hours.

As shown, the deposited films evolve from "cauliflower" film at 750 ^{o}C, to crystalline film at 850 ^{o}C and small grain film at 950 ^{o}C.

Figure 6.24 displays the SEM photographs of five films deposited with substrate temperatures: (a) 750 ^{o}C, (b) 800 ^{o}C, (c) 850 ^{o}C, (d) 900 ^{o}C and (e) 950 ^{o}C. The pressures and absorbed microwave powers used to achieve these temperatures are listed in Table 6.2 located above Figure 6.10. The other deposition conditions are: H_2 flow rate = 200 sccm, CH_4 flow rate = 2 sccm, CO_2 flow rate = 2 sccm, and deposition time = 4

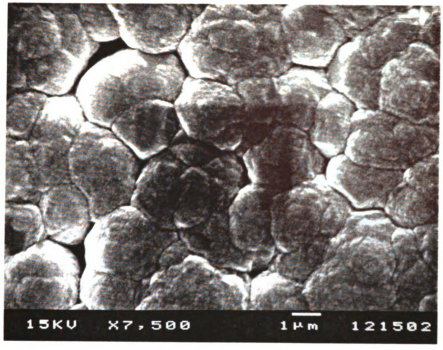

(a)

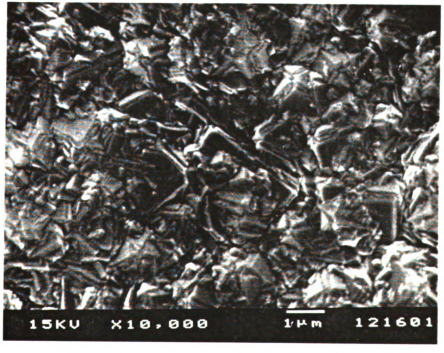

(b)

Figure 6.23 Effects of Substrate Temperature on Film Morphology (I)
H_2 = 200 sccm, CH_4 = 4 sccm and
T_s = (a) 750, (b) 850 and (c) 950 ^oC

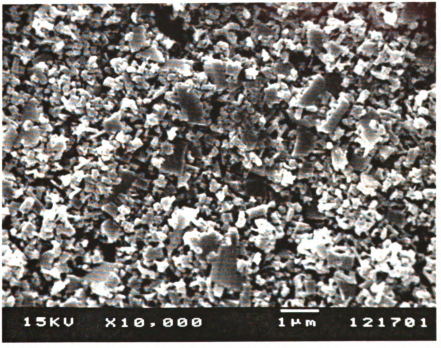

(c)

Figure 6.23 (cont'd)

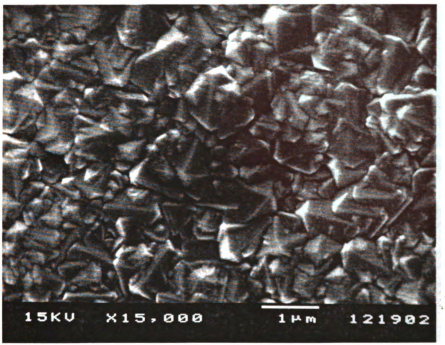

(a)

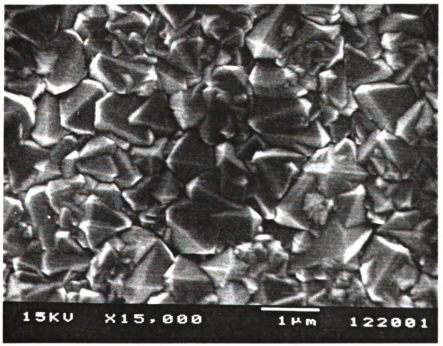

(b)

Figure 6.24 Effects of Substrate Temperature on Film Morphology (II)
H_2 = 200 sccm, CH_4 = 2 sccm, CO_2 = 2 sccm and
T_s = (a) 750, (b) 800, (c) 850, (d) 900 and (e) 950 ^oC

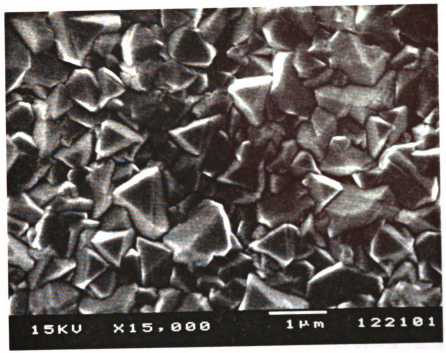

(c)

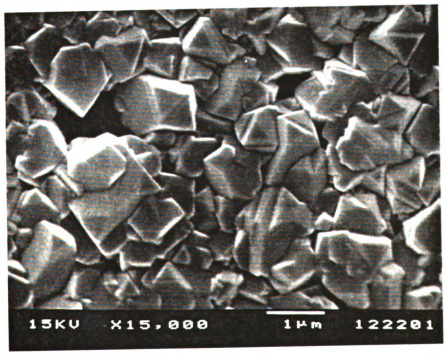

(d)

Figure 6.24 (cont'd)

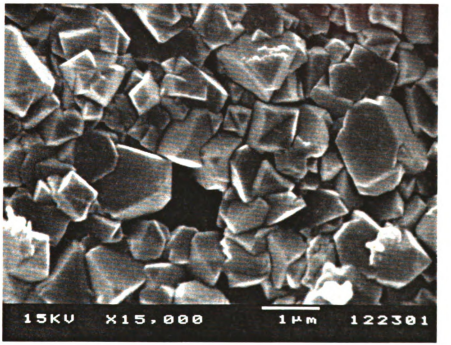

(e)

Figure 6.24 (cont'd)

hours.

As shown, the films deposited under these conditions are crystalline films with slightly different average grain sizes. The average grain size increases gradually as the substrate temperature is increased from 750 °C to 950 °C.

6.4.3.3 Effects of CH_4 Concentration

Film morphology vs. CH_4 concentration is shown in Figure 6.25 where the SEM photographs of six films are shown. These films are deposited under the following experimental conditions: H_2 flow rate = 400 sccm, pressure = 51 Torr, microwave power absorbed = 2.34 kW, substrate temperature ~ 900 °C, deposition time = 6 hours and CH_4 flow rate (a) 3, (b) 4, (c) 5, (d) 6, (e) 6.5 and (f) 7 sccm.

As shown, the average grain size of the films decreases gradually as the CH_4 flow rate is increased from 3 to 7 sccm.

Figure 6.26 displays the SEM photographs of five films deposited under the following experimental conditions: H_2 gas flow = 400 sccm, pressure = 57 Torr, absorbed microwave power = 2.5 kW, substrate temperature ~ 950 °C, deposition time = 6 hours and CH_4 flow rate (a) 4, (b) 4.5, (c) 5, (d) 5.5 and (e) 6 sccm.

As shown, the average grain size of the films decreases gradually also as the CH_4 flow rate is increased from 4 to 6 sccm.

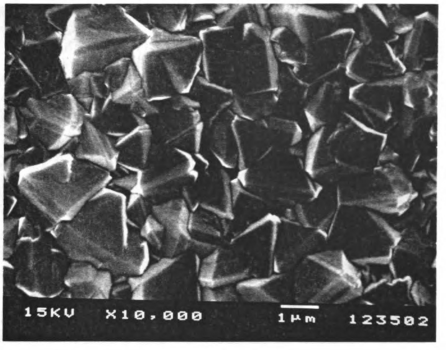

(a)

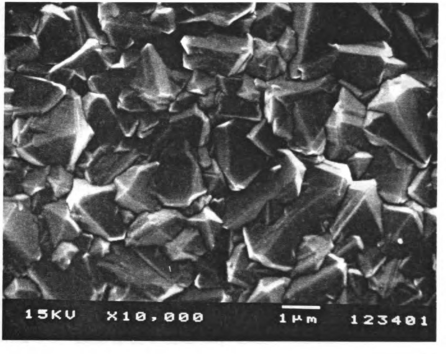

(b)

Figure 6.25 Effects of CH_4 Concentration on Film Morphology (I) H_2 = 400 sccm, p = 51 Torr, P_t = 2.34 kW, T_s ~ 900 ^oC, and CH_4 = (a) 3, (b) 4, (c) 5, (d) 6, (e) 6.5 and (f) 7 sccm

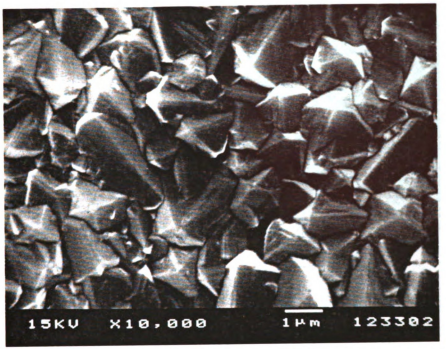

(c)

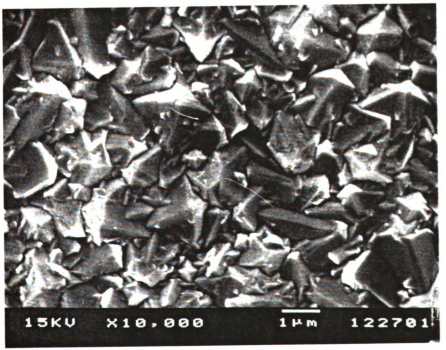

(d)

Figure 6.25 (cont'd)

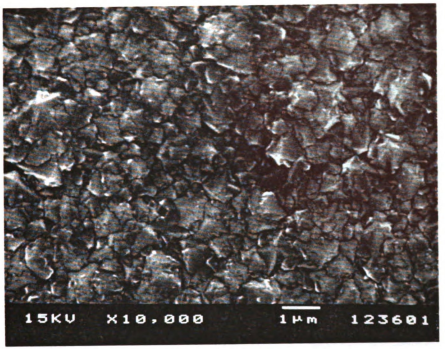

(e)

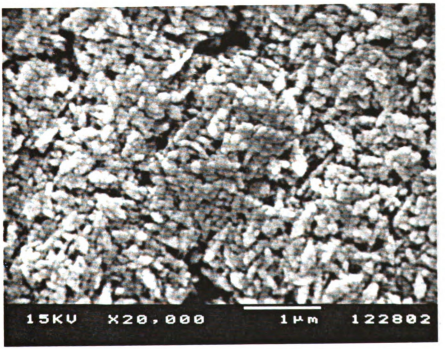

(f)

Figure 6.25 (cont'd)

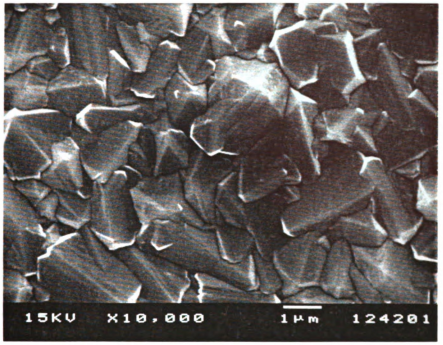

(a)

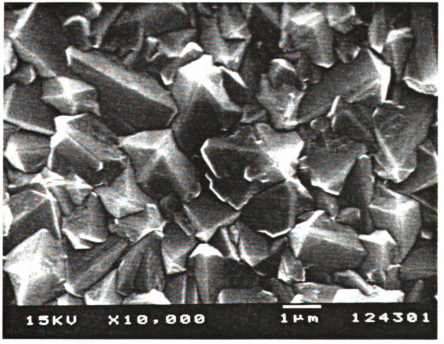

(b)

Figure 6.26 Effects of CH_4 Concentration on Film Morphology (II) H_2 = 400 sccm, p = 57 Torr, P_t = 2.5 kW, T_s ~ 950 ^oC, and CH_4 = (a) 4, (b) 4.5, (c) 5, (d) 5.5 and (e) 6 sccm

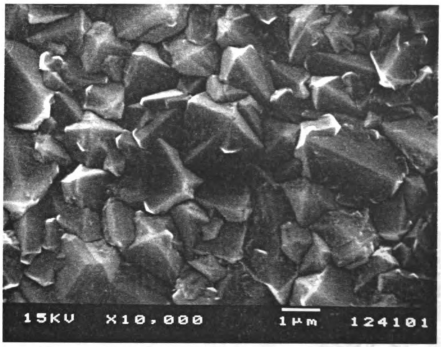

(c)

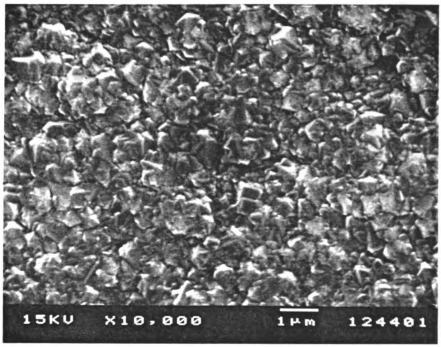

(d)

Figure 6.26 (cont'd)

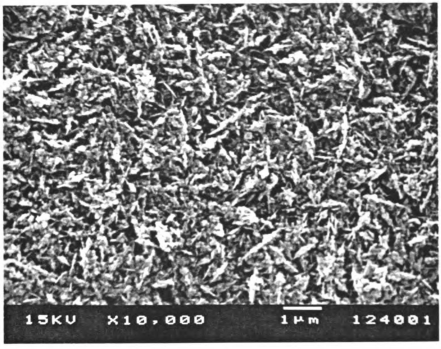

(e)

Figure 6.26 (cont'd)

6.4.3.4 Effects of CO_2 Concentration

Film morphology vs. CO_2 concentration is shown in Figure 6.27 where the SEM photographs of four films are shown. These films are deposited under the following experimental conditions: H_2 flow rate = 400 sccm, CH_4 flow rate = 6 sccm, pressure = 51 Torr, absorbed microwave power = 2.34 kW, substrate temperature ~ 900 ^oC, deposition time = 6 hours and CO_2 flow rate (a) 0, (b) 1, (c) 2, and (d) 3 sccm.

As shown, the average grain size of the films increases gradually as the CO_2 flow rate is increased from 0 to 3 sccm.

Figure 6.28 displays the SEM photographs of four films deposited under the following experimental conditions: H_2 flow rate = 200 sccm, CH_4 flow rate = 6 sccm, pressure = 51 Torr, absorbed microwave power = 2.46 kW, deposition time = 6 hours and CO_2 flow rate (a) 3, (b) 3.5, (c) 4, and (d) 4.5 sccm.

As shown, the average grain size of the films increases gradually also as the CO_2 flow rate is increased from 3 to 4.5 sccm.

6.4.3.5 Effects of Total Flow Rate

Film morphology vs. total flow rate is shown in Figure 6.29 where the SEM photographs of five films are shown. These films are deposited under the following experimental conditions: CH_4 to H_2 volume ratio = 1.5%, pressure = 51 Torr, absorbed microwave power = 2.34 kW, substrate temperature ~ 900 ^oC, deposition time = 6 hours and H_2 flow rate (a) 50, (b) 100, (c) 200, (d) 300 and (e) 400 sccm.

As shown, the average grain size experiences first a slight increase

(a)

(b)

Figure 6.27 Effects of CO_2 Concentration on Film Morphology (I) H_2 = 400 sccm, CH_4 = 6 sccm, p = 51 Torr, P_t = 2.34 kW, T_s ~ 900 oC, and CO_2 = (a) 0, (b) 1, (c) 2 and (d) 3 sccm.

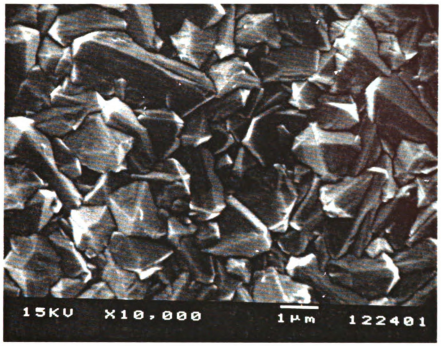

(c)

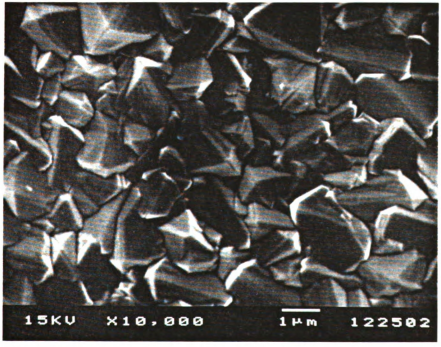

(d)

Figure 6.27 (cont'd)

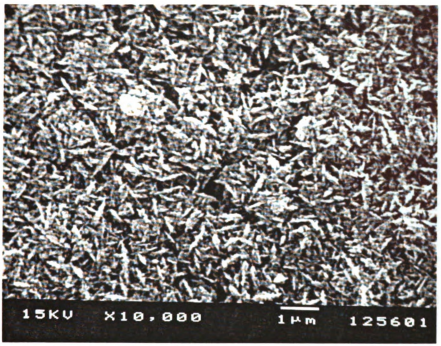

(a)

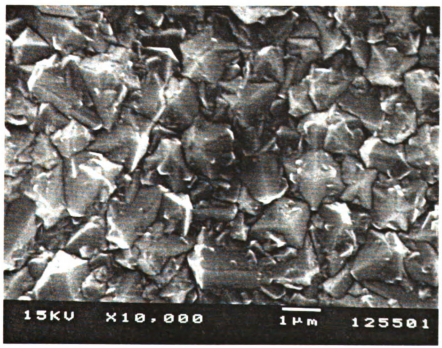

(b)

Figure 6.28 Effects of CO_2 Concentration on Film Morphology (II) H_2 = 200 sccm, CH_4 = 6 sccm, p = 51 Torr, P_t = 2.46 kW, and CO_2 = (a) 3, (b) 3.5, (c) 4 and (d) 4.5 sccm.

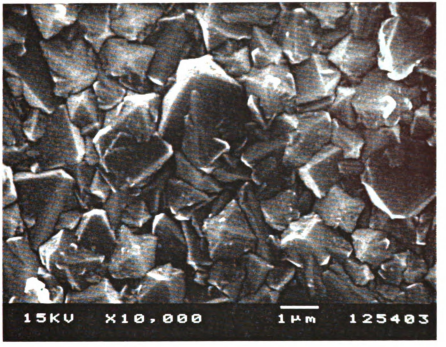

(c)

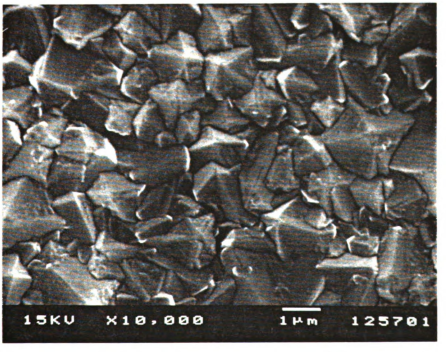

(d)

Figure 6.28 (cont'd)

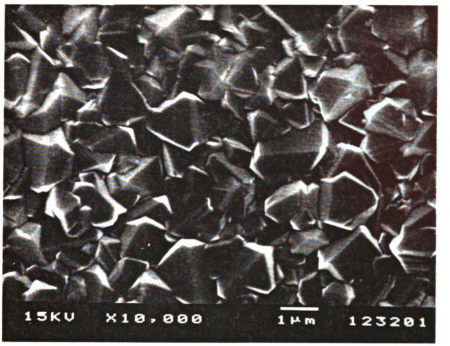

(a)

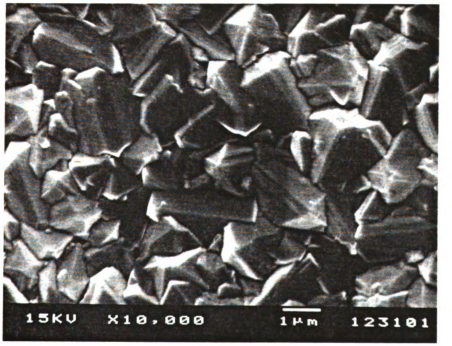

(b)

Figure 6.29 Effects of Total Flow Rate on Film Morphology (I) CH_4/H_2 = 1.5%, p = 51 Torr, P_t = 2.34 kW, T_s ~ 900 °C, and H_2 = (a) 50, (b) 100, (c) 200, (d) 300 and (e) 400 sccm.

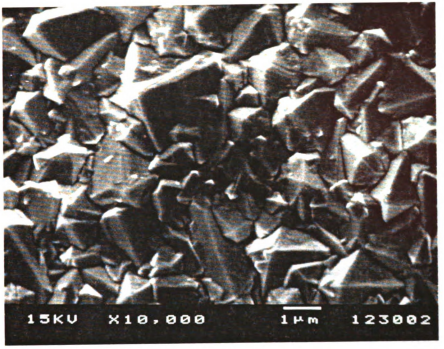

(c)

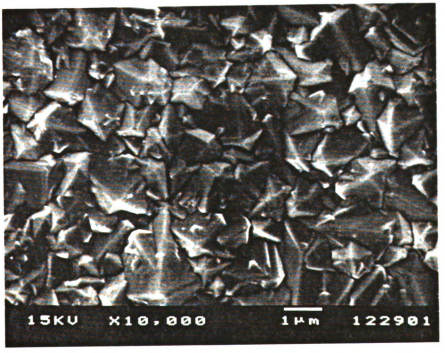

(d)

Figure 6.29 (cont'd)

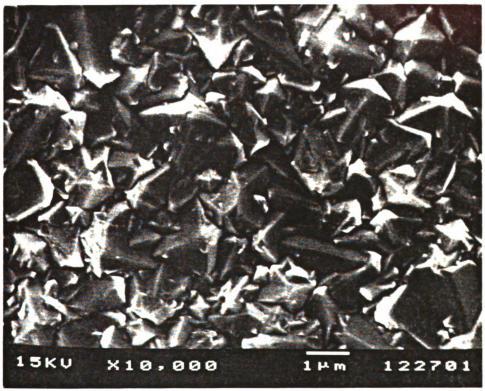

(e)

Figure 6.29 (cont'd)

when the H_2 flow rate is increased from 50 to 100 sccm and then a slight gradual decrease as the H_2 flow rate is further increased toward 400 sccm.

Figure 6.30 displays the SEM photographs of five films deposited under the following experimental conditions: CH_4 to H_2 volume ratio = 1.25%, pressure = 57 Torr, absorbed microwave power = 2.5 kW, substrate temperature ~ 950 ^oC, deposition time = 6 hours and H_2 flow rate (a) 50, (b) 100, (c) 200, (d) 300 and (e) 400 sccm.

As shown, the average grain size experiences first an increase when the H_2 flow rate is increased from 50 sccm to 100 sccm and then a slight gradual decrease as the H_2 flow rate is further increased toward 400 sccm.

6.4.4 Typical Raman Spectrum

Figure 6.31 displays the Raman spectrum[76] of a diamond film deposited on a 3" silicon wafer under the following experimental conditions: H_2 flow rate = 400 sccm, CH_4 flow rate = 4 sccm, CO_2 flow rate = 2 sccm, pressure = 50 Torr, absorbed microwave power = 2.61 kW and substrate temperature ~ 927 ^oC. The sharp peak near 1332 cm^{-1} indicates the excellent quality of the deposited diamond film.

6.4.5 Typical Uniformity Profile

The thickness profiles of a diamond film are displayed in Figures 6.32 and 6.33.[71] They were obtained by laser interference/reflection technique. The diamond film was deposited on a 3" silicon wafer under

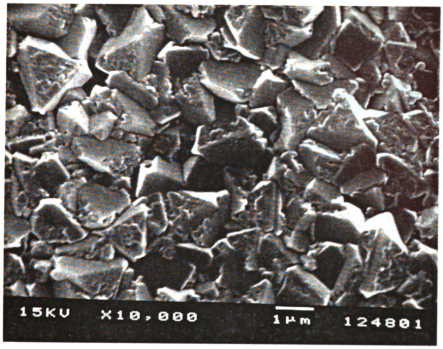

(a)

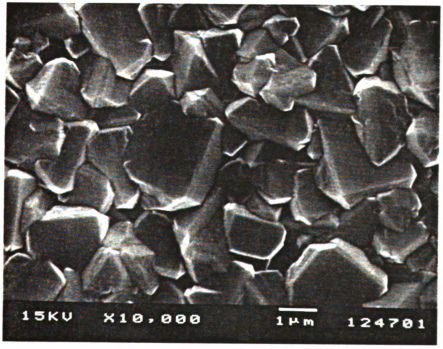

(b)

Figure 6.30 Effects of Total Flow Rate on Film Morphology (II) CH_4/H_2 = 1.25%, p = 57 Torr, P_t = 2.5 kW, T_s ~ 950 °C, and H_2 = (a) 50, (b) 100, (c) 200, (d) 300 and (e) 400 sccm.

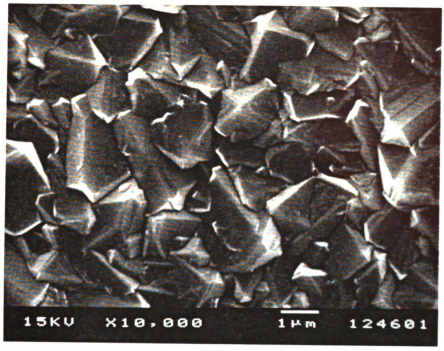

(c)

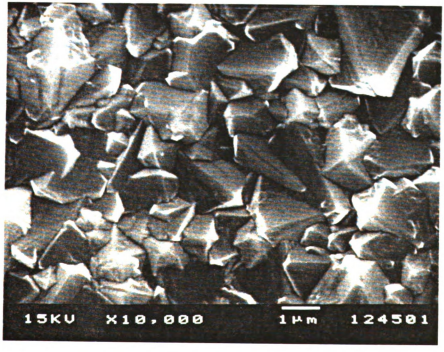

(d)

Figure 6.30 (cont'd)

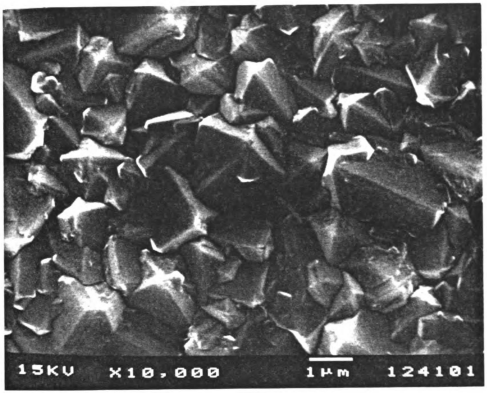

(e)

Figure 6.30 (cont'd)

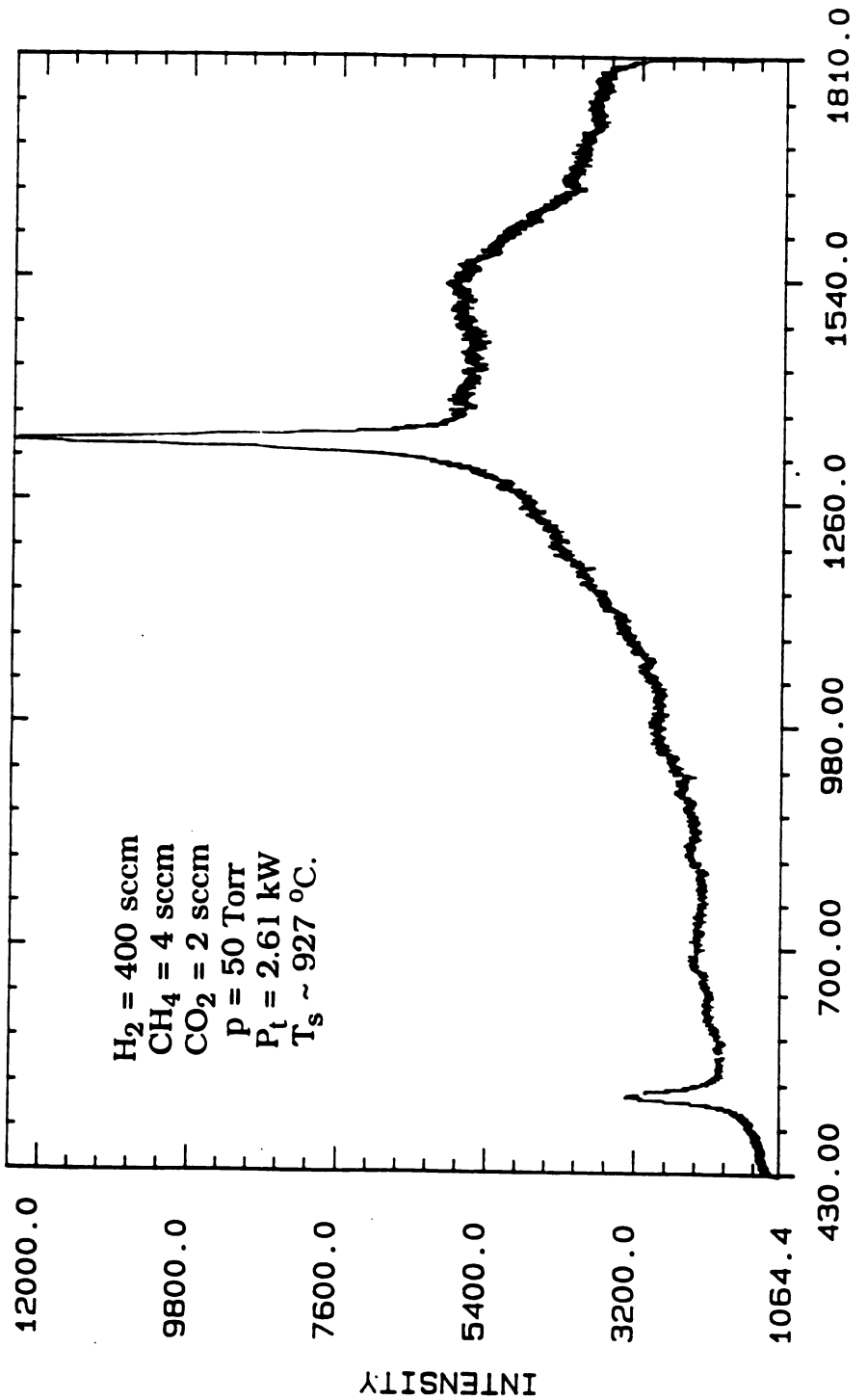

Figure 6.31 Raman Spectrum of a 3" Diamond Film Deposited in MCPR7-3

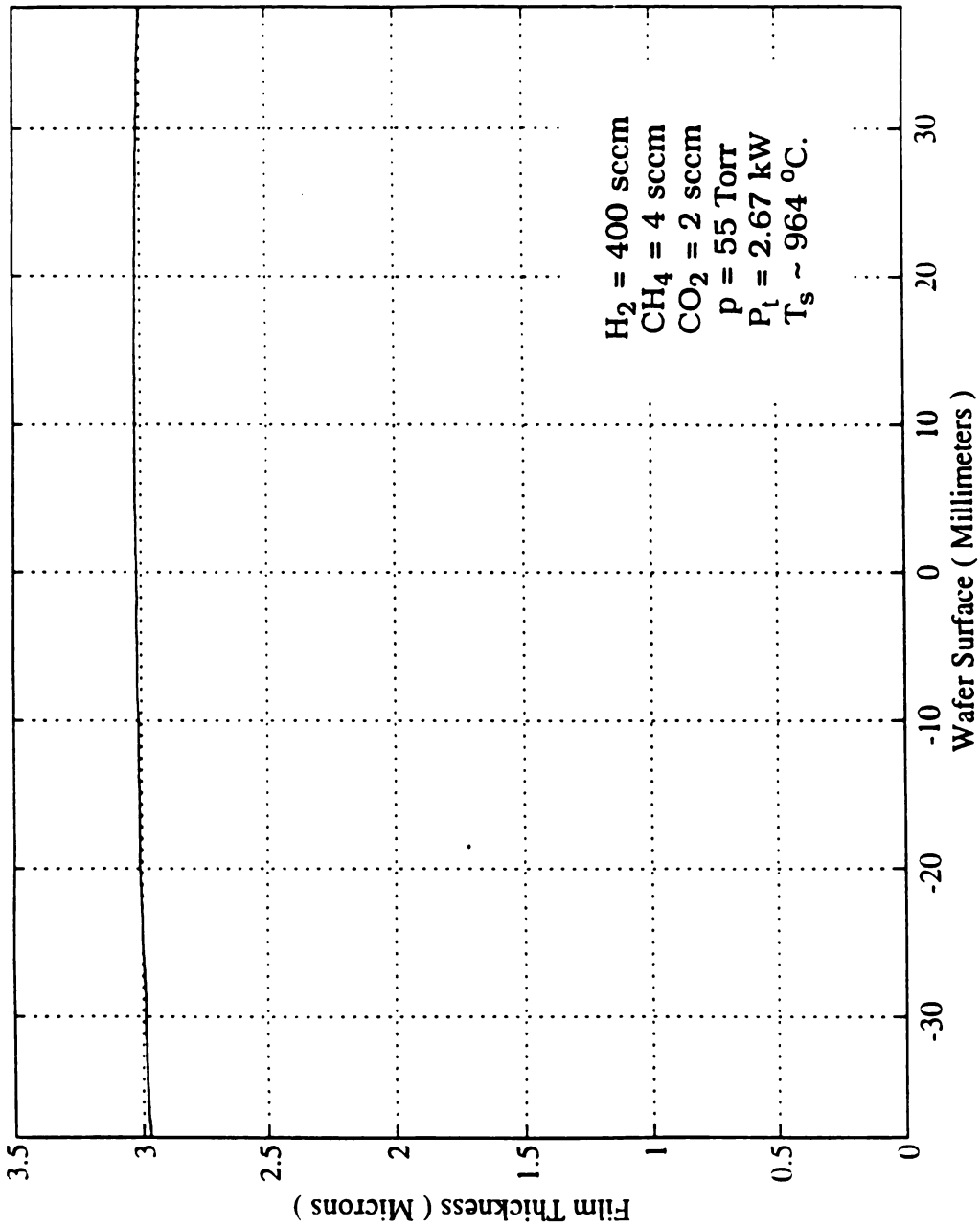

Figure 6.32 Cross-sectional Thickness Profile of a 3" Diamond Film

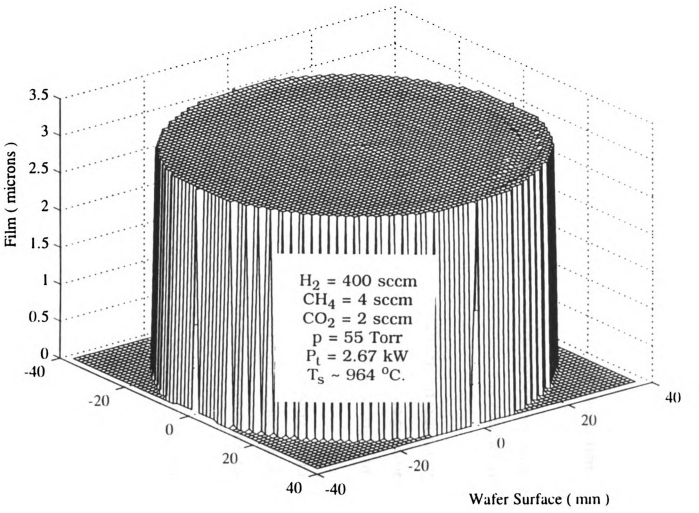

Figure 6.33 Three Dimensional Thickness Profile of a 3" Diamond Film

the following experimental conditions: H_2 flow rate = 400 sccm, CH_4 flow rate = 4 sccm, CO_2 flow rate = 2 sccm, pressure = 55 Torr, absorbed microwave power = 2.67 kW and substrate temperature ~ 964 ^oC.

6.4.6 Summary

From the parametric study of diamond film deposition on 3" silicon wafers, the results can be summarized as follows:

(1) There exists an optimum substrate temperature range for high rate diamond film growth with a suitable gas composition. The growth rate is gas composition dependent.

(2) There exists an optimum CH_4 concentration range for high rate diamond film growth at a suitable substrate temperature.

(3) Addition of CO_2 to a H_2/CH_4 discharge tends to dilute some of the reactive species in the discharge.

(4) The growth rate increases with increasing total flow rate in the region of 50 -200 sccm and saturates in the region of 300 - 400 sccm, keeping gas composition and substrate temperature constant. This suggests:

(i) at the low flow rates of 50 - 200 sccm, the deposition rate is limited by chemically active species hitting the substrate,

(ii) at the higher flow rates of 300 - 400 sccm, some of the input gas by-passes the deposition process.

(5) Carbon conversion efficiency decreases with increasing total flow rate and decreasing gas residence time.

(6) Film morphologies depend on substrate temperature, gas composition and total gas flow rate.

(7) Within all the CH_4 volume concentrations used, the average grain size of deposited films decreases as CH_4 volume concentration is increased.

(8) Within all the CO_2 volume concentrations used, the average grain size of deposited films increases as CO_2 volume concentration is increased.

(9) Raman spectrum exhibits the excellent characteristics of a diamond film deposited.

(10) Diamond film with excellent uniformity (better than 2%) has been deposited.

(11) Higher deposition rates may require changing the gas flow configuration.

(12) The maximum diamond film growth rate obtained on a 3" silicon wafer is ~ 0.67 μm/hour. The experimental conditions are: H_2 flow rate = 400 sccm, CH_4 flow rate = 6 sccm, absorbed microwave power = 2.34 kW, substrate temperature ~ 900 ^{o}C and pressure = 51 Torr.

6.5 Study of Experimental Set-ups with 4" Silicon Wafers

6.5.1 Introduction

When diamond films are deposited on 4" silicon wafers in the present reactor, the experimental set-ups affect the film growth rate, morphology and uniformity. Using growth rate and uniformity as judging criteria, a series of experiments are conducted to obtain optimum experimental set-ups for uniform diamond film deposition on 4" silicon wafers. The following independent input experimental parameters are

considered: (1) cavity shell geometry, (2) quartz dome geometry, (3) wafer holder material, (4) wafer location, (5) cavity excitation mode and (6) seeding mixtures.

In this study, diamond films are deposited on 4" silicon wafers using the forced flow configuration shown in Figure 3.16. Here the supporting quartz tube (28) has an inside diameter of 110 mm, an outside diameter of 115 mm.

The 4" silicon wafers used in these experiments have the following physical properties: prime grade, p-type, boron doped, <100> orientation, 24 - 36 ohm-cm in resistivity, 99.5 -100.5 mm in diameter, and 500 - 550 μm in thickness.

6.5.2 Cavity Shell Geometry

The two cavity shells shown in Figures 6.2 and 6.3 are used for diamond film deposition on 4" silicon wafers. Diamond films were deposited in the reactors employing the two cavity shells under the following experimental conditions: H_2 flow rate = 400 sccm, CH_4 flow rate = 4 sccm, CO_2 flow rate = 2 sccm, pressure = 47.5 Torr, absorbed microwave power = 2.58 kW, quartz tube length = 5.09 cm, and substrate holder material = graphite. The two reactors exhibit the following differences as displayed in Table 6.4.

Table 6.4 Comparison of Two Cavity Shells

	Cavity Shell (I)	Cavity Shell (II)
Coupling Efficiency	74.5%	82.8%
Growth Rate (mg/hour)	10.6	9.1

Hence, under otherwise the same experimental conditions, the microwave power coupling efficiency is higher but the diamond film growth rate is slower in the reactor employing cavity shell (II). It was also found that when diamond films are deposited on 4" diameter silicon wafers, the discharge created in the reactor employing cavity shell (II) tends to float toward the top surface of the quartz dome, which caused the quartz dome to be coated faster.

The reactor employing cavity shell (I) has been found to be a preferable choice for diamond film deposition on 4" silicon wafers with the present experimental configuration. It is used in all the experiments that follow.

6.5.3 Quartz Dome Geometry

With the same drawing, quartz domes made by different manufacturers and those constructed at different times by the same manufacturer present small differences in geometry. When diamond films are deposited on 4" silicon wafers, these small differences in geometry affect the optimum deposition conditions and the resulting film morphology, uniformity, and growth rate, etc.

Two quartz domes (Qd#1 and Qd#2) made by the same manufacture were used for diamond film deposition on 4" silicon wafers under the following experimental conditions: quartz tube length = 5.2 cm, substrate holder material = graphite, H_2 flow rate = 400 sccm, CO_2 flow rate = 2 sccm, CH_4 flow rate = 6 sccm, pressure = 35 Torr, absorbed microwave power = 2.15 kW and substrate temperature ~ 780 ^{o}C. The deposited films show differences in both growth rate and morphology as

displayed in Table 6.5 and Figure 6.34:

Table 6.5 Comparison of Two Quartz Domes

	Qd#1	Qd#2
Morphology	Figure 6.34 (a)	Figure 6.34 (b)
Growth Rate (mg/hour)	9.42	8.6

6.5.4 Substrate Location

Substrate location affects the substrate temperature and the resulting film properties, such as growth rate, morphology and uniformity, etc. In the present experimental configuration, the substrate location is varied by changing the length of quartz tube (28).

I Two experiments were conducted with quartz dome #1(Qd#1) and quartz tubes of lengths of 5.09 cm and 5.2 cm. The experimental conditions are: H_2 flow rate = 400 sccm, CH_4 flow rate = 6 sccm, CO_2 flow rate = 2 sccm, pressure = 35 Torr, substrate holder material = graphite, and absorbed microwave power = 2.12 kW

The effects of substrate location on substrate temperature T_s, growth rate and uniformity are displayed in Table 6.6, where the uniformity is judged by visual inspection.

Table 6.6 Effects of Substrate Location (I)

Substrate Location	T_s (°C)	Growth Rate	Uniformity
5.09 cm	790	10.9 mg/hour	good
5.20 cm	776	9.42 mg/hour	fair

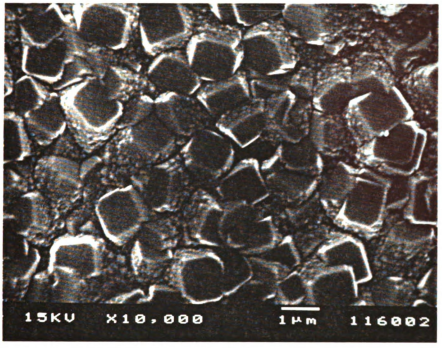

(a)

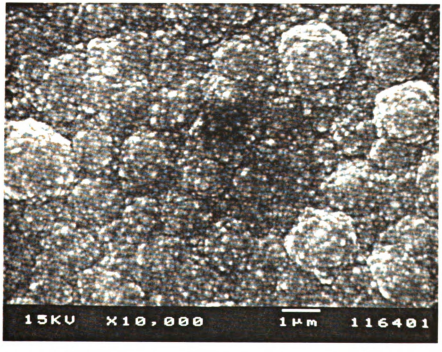

(b)

Figure 6.34 Effects of Quartz Dome Geometry on Film Morphology
H_2 = 400 sccm, CO_2 = 2 sccm, CH_4 = 6 sccm, p = 35 Torr
P_t = 2.15 kW, T_s ~ 780 °C, with (a) Qd#1 and (b) Qd#2.

As shown, the better choice of quartz tube lengths is 5.09 cm, judging from both growth rate and uniformity.

II. Three experiments were conducted with quartz dome #2 (Qd#2) and three quartz tubes of lengths of 5.05, 5.09, and 5.2 cm. The experimental conditions are as follows: H_2 flow rate = 400 sccm, CH_4 flow rate = 6 sccm, CO_2 flow rate = 2 sccm, pressure = 35 Torr, and absorbed microwave power = 2.16 kW.

The effects of substrate location on substrate temperature T_s, growth rate and uniformity are displayed in Table 6.7, where the uniformity was judged by visual inspection.

Table 6.7 Effects of Substrate Location (II)

Quartz tube length	T_s (°C)	Growth Rate	Uniformity
5.05 cm	791	8.7 mg/hour	fair
5.09 cm	784	9.3 mg/hour	good
5.20 cm	777	8.6 mg/hour	fair

As shown, the better choice of the quartz tube lengths is again 5.09 cm, judging from both growth rate and uniformity.

5.09 cm long quartz tube is most frequently used in the experiments where diamond films are deposited on 4" silicon wafers.

6.5.5 Cavity Mode Excitation

The microwave cavity applicator can be excited by TM_{01n} modes for diamond film deposition, where n is a positive integer. In the present

experimental reactor, the excitation of TM_{011} mode is not possible due to the conflict between cavity short length and excitation probe length requirements. TM_{012} and TM_{013} modes were investigated for their potentials in diamond film deposition experiments. When the cavity is excited with TM_{012} mode, the near field effect from the probe is slightly present, which causes the plasma to be attracted slightly towards the top of quartz dome. When the cavity is excited with TM_{013} mode, the near field effect is almost non-existent. Higher order modes, such as TM_{014} and TM_{015} modes, etc., were not used since microwave power loss on the cavity walls is of concern.

The following two experiments were conducted to quantitatively compare the effects of TM_{012} and TM_{013} modes. The experimental conditions were: quartz tube length = 5.09 cm, substrate material = graphite, H_2 flow rate = 400 sccm, CH_4 flow rate = 6 sccm, CO_2 flow rate = 2 sccm, pressure = 35 Torr, and absorbed microwave power = 2.06 kW. The effects of cavity mode excitation on substrate temperature, T_s, growth rate and uniformity are displayed in Table 6.8, where the uniformity is judged by visual inspection.

Table 6.8 Effects of Cavity Mode Excitation

Excitation Mode	T_s (°C)	Growth Rate	Uniformity
TM_{012}	806	12 mg/hour	good
TM_{013}	790	10.8 mg/hour	better

As shown, the diamond film deposited with TM_{013} mode is slightly more uniform than that with TM_{012} mode. But the average growth rate of the diamond film deposited with TM_{013} mode is slightly lower than that

with TM_{012} mode.

Comparing to TM_{012} mode excitation, TM_{013} mode excitation has the following advantages: (1) there is nearly no near field effect from the excitation probe, which means that the quartz dome is coated slower during the diamond film deposition process, and (2) the deposited diamond film is more uniform. Hence, TM_{013} mode excitation is used in most experiments described in this chapter.

6.5.6 Seeding Density

In the photo resist seeding method, different seeding densities result from different mixtures of diamond powder, photo resist and photo resist thinner. The effect of seeding density on diamond film growth was examined by depositing diamond films under otherwise identical experimental conditions. The two seeding mixtures examined are:

Seeding mixture #1: (a) mix 250 mg 0.1 μm diamond powder with 25 ml of photo resist, (b) ultrasonically mix the mixture for an hour, (c) apply the mixture onto a silicon wafer, (d) spin the wafer at 4000 rpm for 30 seconds, (e) bake the wafer at 135 ^{o}C for 30 minutes.

Seeding mixture #2: (a) mix 250 mg 0.1 μm diamond powder with 53 ml of photo resist and 20 ml of photo resist thinner, (b) ultrasonically mix the mixture for an hour, (c) apply the mixture onto a silicon wafer, (d) spin the wafer at 4000 rpm for 40 seconds, (e) bake the wafer at 135 ^{o}C for 30 minutes.

The deposition conditions are: H_2 flow rate = 400 sccm, CH_4 flow rate = 4 sccm, CO_2 flow rate = 2 sccm, pressure = 47.5 Torr, absorbed microwave power = 2.58 kW, quartz tube length = 5.2 cm, substrate

holder material = graphite and substrate temperature ~ 860 ^{o}C.

The average growth rates are similar with 9.46 mg/hour for seeding mixture #1 and 9.8 mg/hour for seeding mixture #2.

6.5.7 Summary

From the study of experimental set-ups for diamond film deposition on 4" silicon wafers, the results can be summarized as follows, in diamond film deposition on 4" silicon wafers,

(1) Cavity shell geometry influences diamond film growth. Cavity shell (I) is a preferable choice.

(2) Variation in quartz dome geometry influences diamond film growth rate and morphology.

(3) Substrate holder material influences discharge geometry and substrate heating.

(4) Substrate location influences film growth rate and uniformity. 5.09 cm long quartz tube is most frequently used substrate support tube.

(5) Cavity excitation modes influence film growth rate and uniformity. TM_{013} mode is a preferable choice.

(6) Diamond film growth is not sensitive to slight variation in seeding density.

6.6 Diamond Film Deposition on 4" Silicon Wafers

6.6.1 Introduction

Diamond films with various physical properties are deposited on 4" silicon wafers under various experimental conditions. In order to optimize the diamond film deposition process to achieve the objective of depositing diamond films with high growth rate and good uniformity (judged by visual inspection), it is useful to study the co-relation between the physical properties of the deposited diamond films and the experimental conditions. Hence a parametric study of diamond film deposition on 4" silicon wafers was conducted. In this study, the following experimental parameters are considered:

I The independent input experimental parameters:

(1) absorbed microwave power, P_t,

(2) pressure, p,

(3) gas (H_2, CH_4, CO_2) composition, and

(4) total flow rate, f_t.

II. The internal experimental parameters:

(1) substrate temperature T_s, and

(2) gas residence time, t_r.

III. The output experimental parameters:

(1) film linear growth rate (μm/hour),

(2) film weight gain u (mg/hour),

(3) film growth efficiencies:

(i) growth rate vs. power flux, i.e., u vs. S,

(ii) gas flow efficiency: k_4 (mg/liter) = u/f_t,

(iii) carbon conversion efficiency, k_5 (%).

(4) film morphology,

(5) typical film uniformity, and

(6) typical film Raman spectrum.

In this study, diamond films are deposited on 4" silicon wafers using the forced flow configuration displayed in Figure 3.16. The supporting quartz tube (28) has an inside diameter of 110 mm, an outside diameter of 115 mm and a length of 50.9 mm. The physical properties of the 4" silicon wafers are the same as that described in section 6.5.1.

Description of relevant experimental chemistry space is also included whenever possible.

6.6.2 Film Growth Rate and Growth Efficiency

6.6.2.1 Effects of Substrate Temperature

Figure 6.35 displays linear growth rate and weight gain vs. substrate temperature and power flux under the following experimental conditions: H_2 flow rate = 400 sccm, CH_4 flow rate = 6 sccm, and CO_2 flow rate = 2 sccm. The pressures and absorbed microwave powers used to achieve these temperatures are listed in Table 6.9 located above Figure 6.35.

As shown, the average linear growth rate and weight gain are increased as the substrate temperature is increased from 813 ^{o}C to 900 ^{o}C. But the film uniformity (from visual inspection) decreases as the substrate temperature is increased from 813 ^{o}C to 900 ^{o}C.

Table 6.9 Substrate Temperature Conditions (4")

Temperature, T_s (°C)	Pressure, p (Torr)	Power, P_t (kW)
900	45	2.43
836	40	2.28
825	40	2.24
813	37.5	2.2

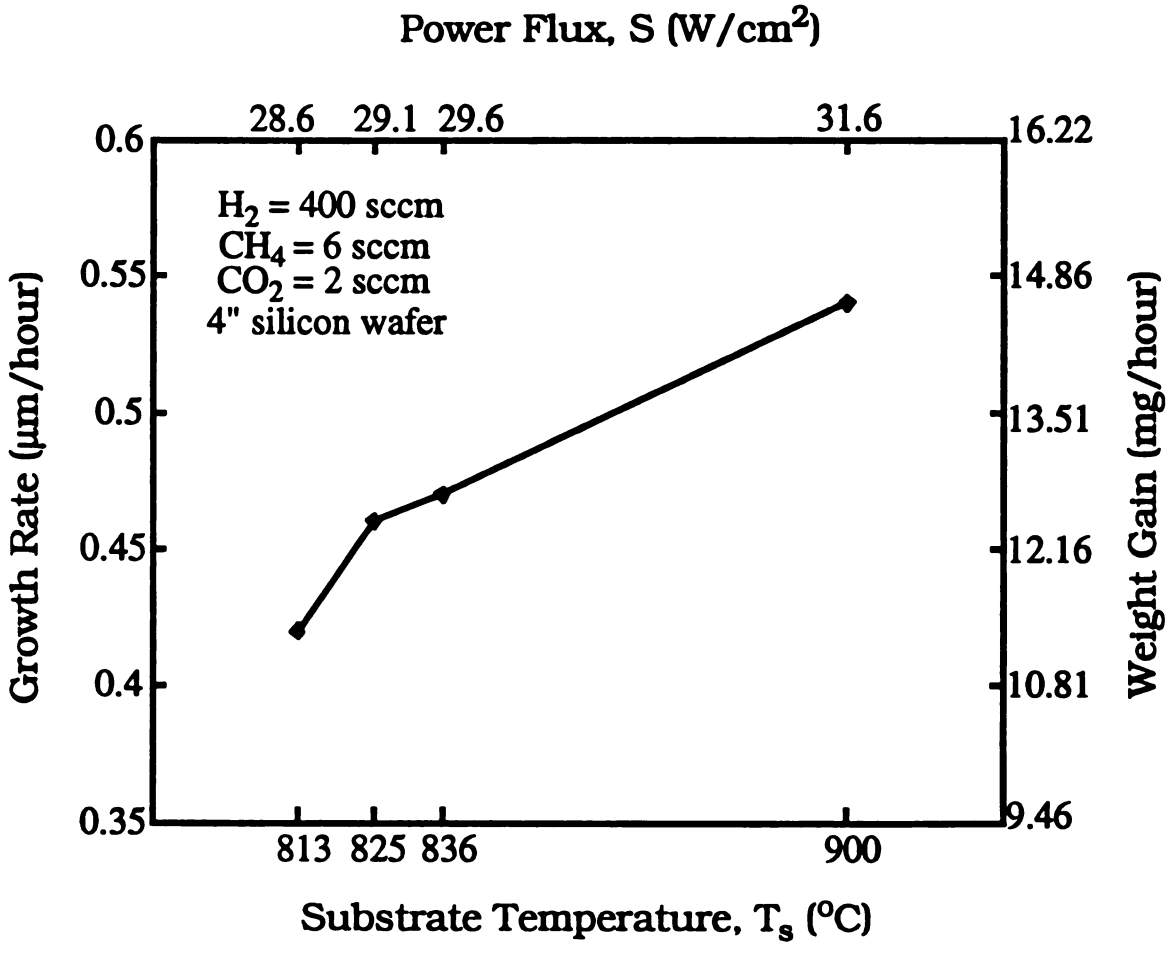

Figure 6.35 Linear Growth Rate and Weight Gain versus Substrate Temperature and Power Flux

Figure 6.36 displays carbon conversion efficiency and gas flow efficiency versus substrate temperature and power flux. The carbon conversion efficiency and gas flow efficiency are increased as substrate temperature is increased from 813 ^{o}C to 900 ^{o}C.

In the present reactor, there exists a compromise between the two objectives, i.e., high growth rate and good uniformity, in diamond film deposition on 4" silicon wafers. When a good uniformity is required, the upper limit on growth rate comes from the upper limit on the substrate temperature. The substrate temperature is primarily limited by the safety operation temperature limit and the coating speed of the quartz dome. As is shown in Figure 6.35, higher growth rate is achieved with higher substrate temperature. To improve the film uniformity in the higher substrate temperature case, more absorbed microwave power is required. The hot discharge is then in close contact with the quartz dome, heating the quartz dome up to its unsafe operation temperature region and coating the quartz dome at the same time. A compromise range for the substrate temperature to serve both objectives is between 800 ^{o}C to 850 ^{o}C.

In the growth rate vs. gas composition and total flow rate experiments that follow, the substrate temperature is chosen to be fixed at 845 ^{o}C. The CH_4 concentration is varied first in the growth rate vs. gas composition experiments.

6.6.2.2 Effects of CH_4 Concentration

Figure 6.37 displays the film linear growth rate, weight gain and carbon conversion efficiency vs. CH_4 gas concentration under the

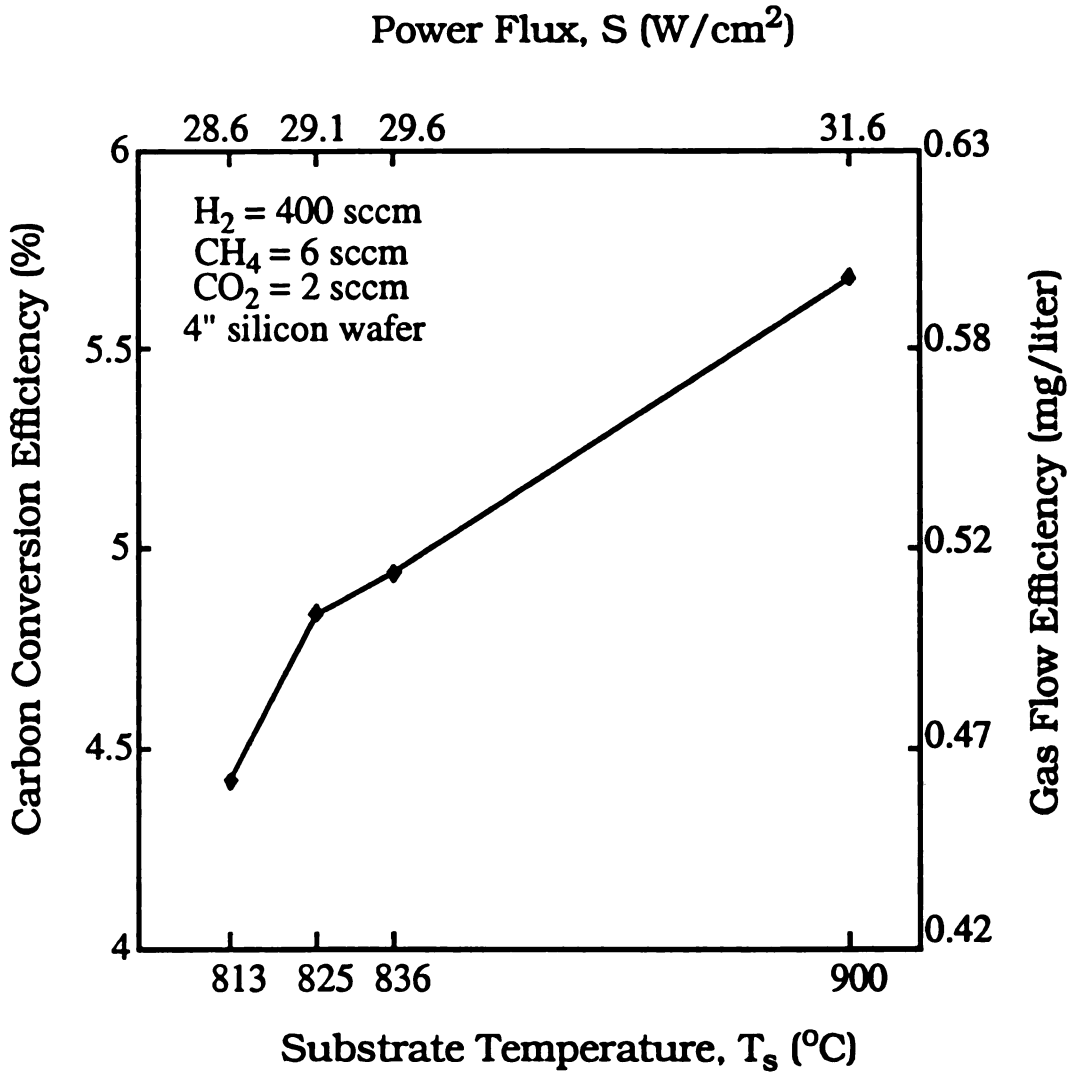

Figure 6.36 Carbon Conversion Efficiency and Gas Flow Efficiency versus Substrate Temperature and Power Flux

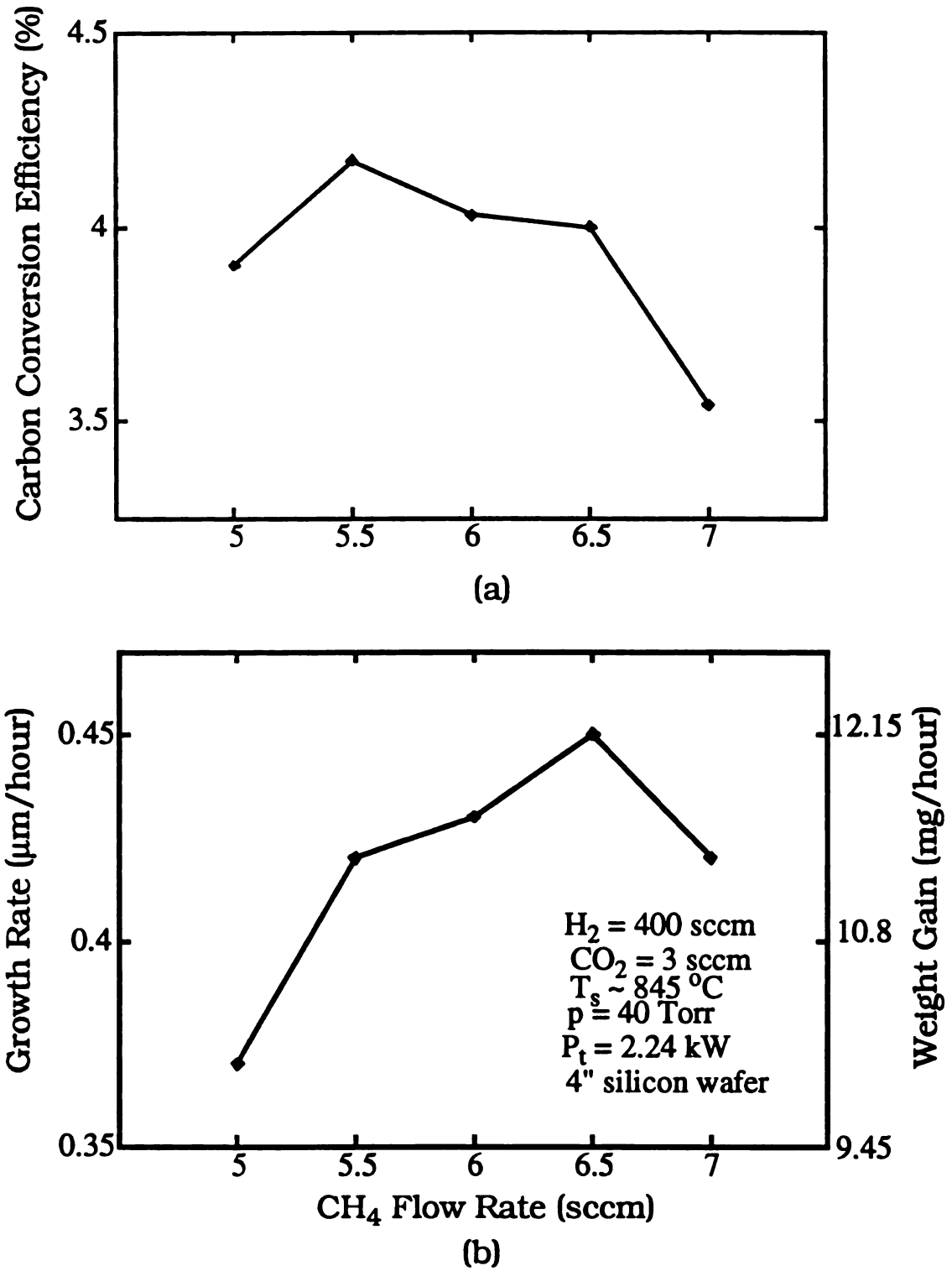

Figure 6.37 Linear Growth Rate, Weight Gain and Carbon Conversion Efficiency versus CH_4 concentration

following experimental conditions: H_2 flow rate = 400 sccm, CO_2 flow rate = 3 sccm, pressure = 40 Torr, absorbed microwave power = 2.24 kW, substrate temperature ~ 845 ^oC and deposition time = 8 hours.

As shown, the film linear growth rate and weight gain experience peak values with CH_4 to H_2 volume ratio of about 6.5/400 = 1.625%. But the film uniformity (judged by visual inspection) in this case is not as good as that in the case where the CH_4 to H_2 volume ratio is 6/400 = 1.5%. The following experiments of growth rate versus CO_2 concentration start from the gas composition of the later case. Also shown in Figure 6.37 is that the carbon conversion efficiency increases initially when CH_4 flow rate is increased from 5 to 5.5 sccm and decreases when CH_4 flow rate is further increased. The location of these gas compositions on the Bachmann C-H-O phase diagram is shown in Figure 6.38.

6.6.2.3 Effects of CO_2 Concentration

Figure 6.39 displays the film linear growth rate, weight gain and carbon conversion efficiency versus CO_2 gas concentration under the following experimental conditions: H_2 flow rate = 400 sccm, CH_4 flow rate = 6 sccm, pressure = 40 Torr, absorbed microwave power = 2.24 kW, substrate temperature ~ 845 ^oC and deposition time = 8 hours.

As shown, the film linear growth rate and weight gain experience peak values with CO_2 to H_2 volume ratio of about 2.5/400 = 0.625%. But the film uniformity (judged by visual inspection) in this case is not as good as that in the case where the CO_2 to H_2 volume ratio is 3/400 = 0.75%. The following experiments of growth rate vs. total flow rate start from the gas composition of the later case. Also shown in Figure 6.39 is

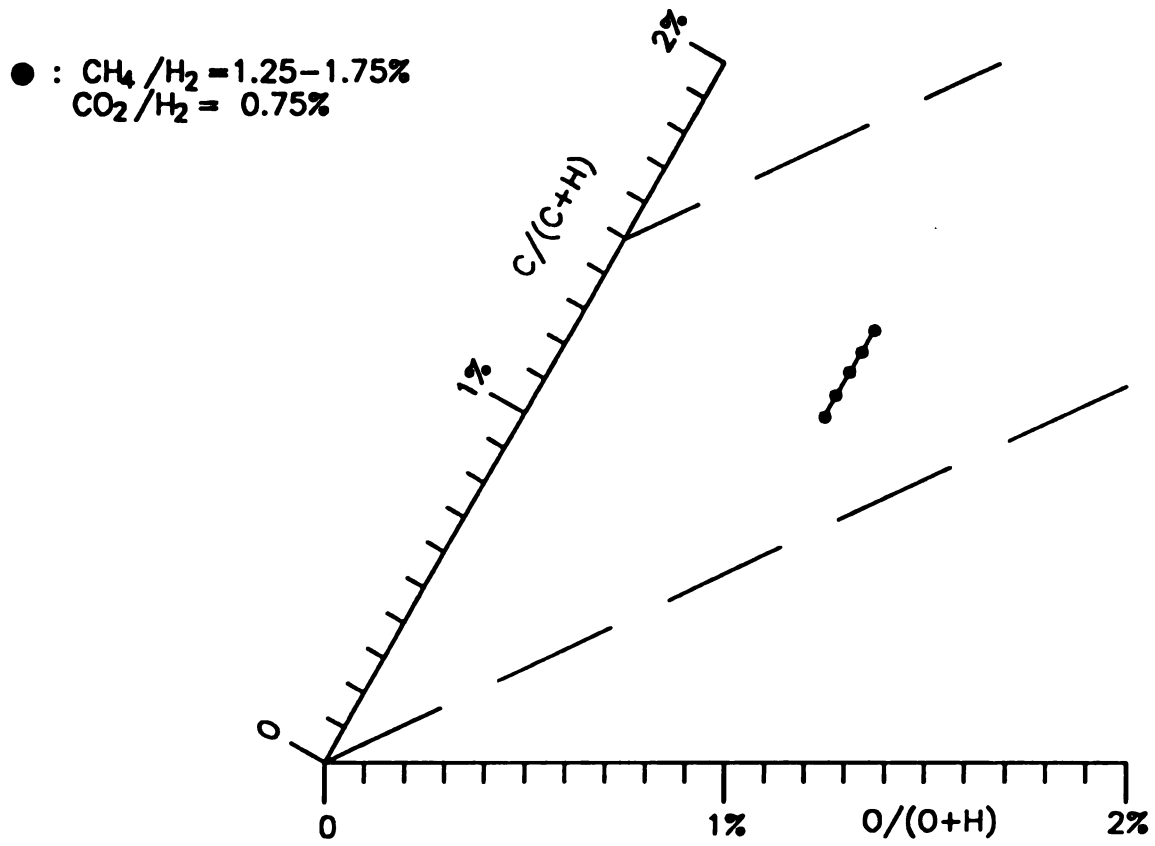

Figure 6.38 Location of Gas Compositions on the C-H-O Phase Diagram (IV)

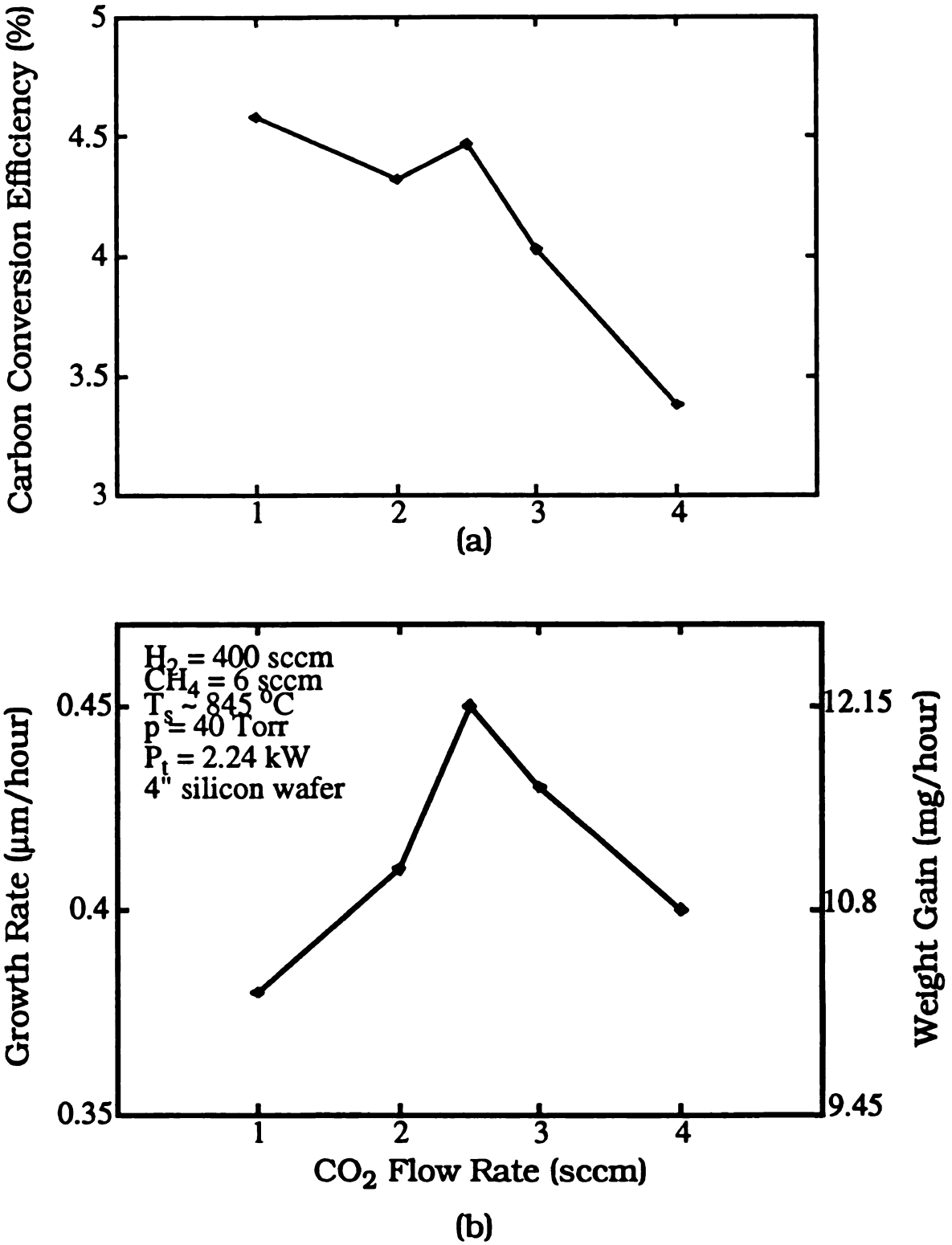

Figure 6.39 Linear Growth Rate, Weight Gain and Carbon Conversion Efficiency versus CO_2 concentration

that the carbon conversion efficiency experiences a peak value at the peak growth rate point and decreases as the CO_2 flow rate is further increased. The location of these gas compositions on the Bachmann C-H-O phase diagram is shown in Figure 6.40.

6.6.2.4 Effects of Total Flow Rate

Figure 6.41 displays the film linear growth rate, weight gain and carbon conversion efficiency versus total gas flow rate and gas residence time under the following experimental conditions: CH_4 to H_2 volume ratio = 1.5%, CO_2 to H_2 volume ration = 0.75%, pressure = 40 Torr, absorbed microwave power = 2.24 kW, substrate temperature ~ 845 ^oC and deposition time = 8 hours.

As shown, the film linear growth rate and weight gain initially experience an increase as the H_2 flow rate is increased from 100 to 300 sccm. They experience a slight decline as the H_2 flow rate is further increased from 300 to 400 sccm. Also shown in Figure 6.41 is that the carbon conversion efficiency decreases with increasing total gas flow rate and decreasing gas residence time.

6.6.3 Film Morphology

6.6.3.1 Introduction

Scanning Electron Microscopy (SEM) is used to identify the morphologies of films deposited under various experimental conditions. The films deposited under the various experimental conditions described

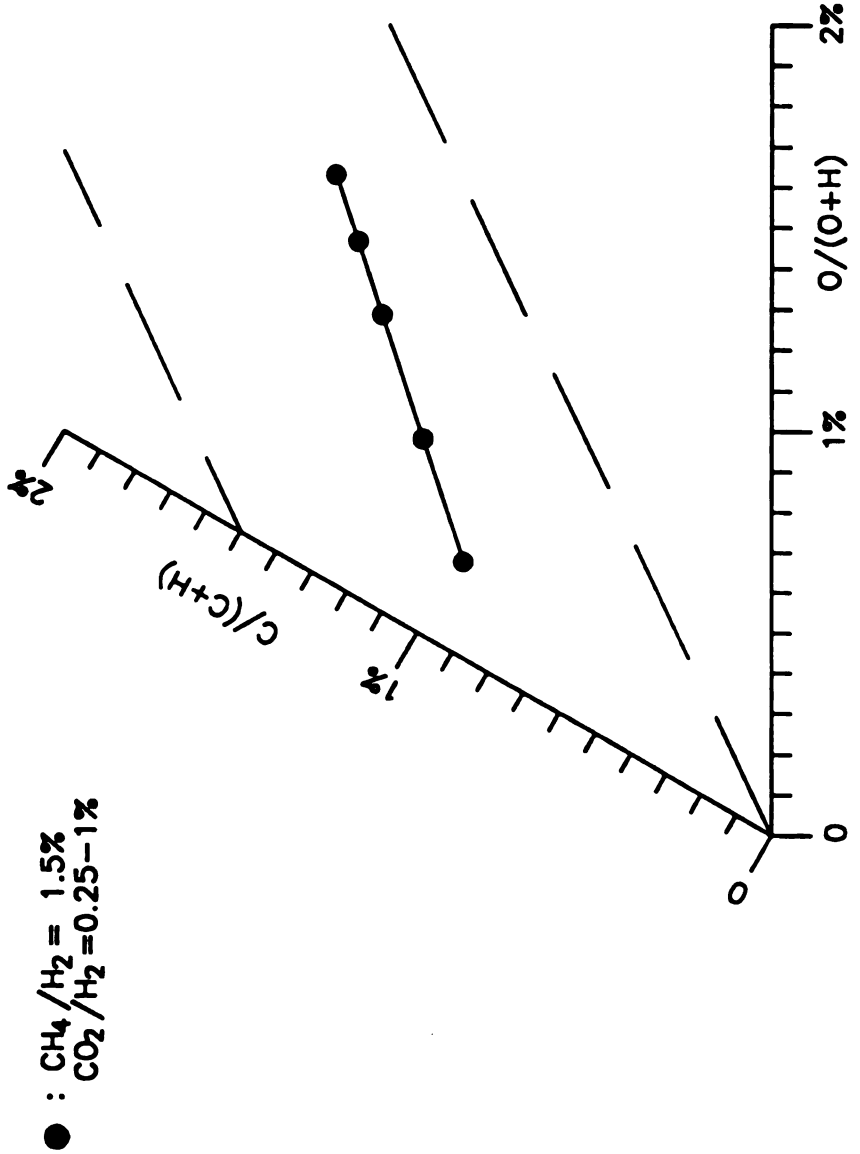

Figure 6.40 Location of Gas Compositions on the C-H-O Phase Diagram (V)

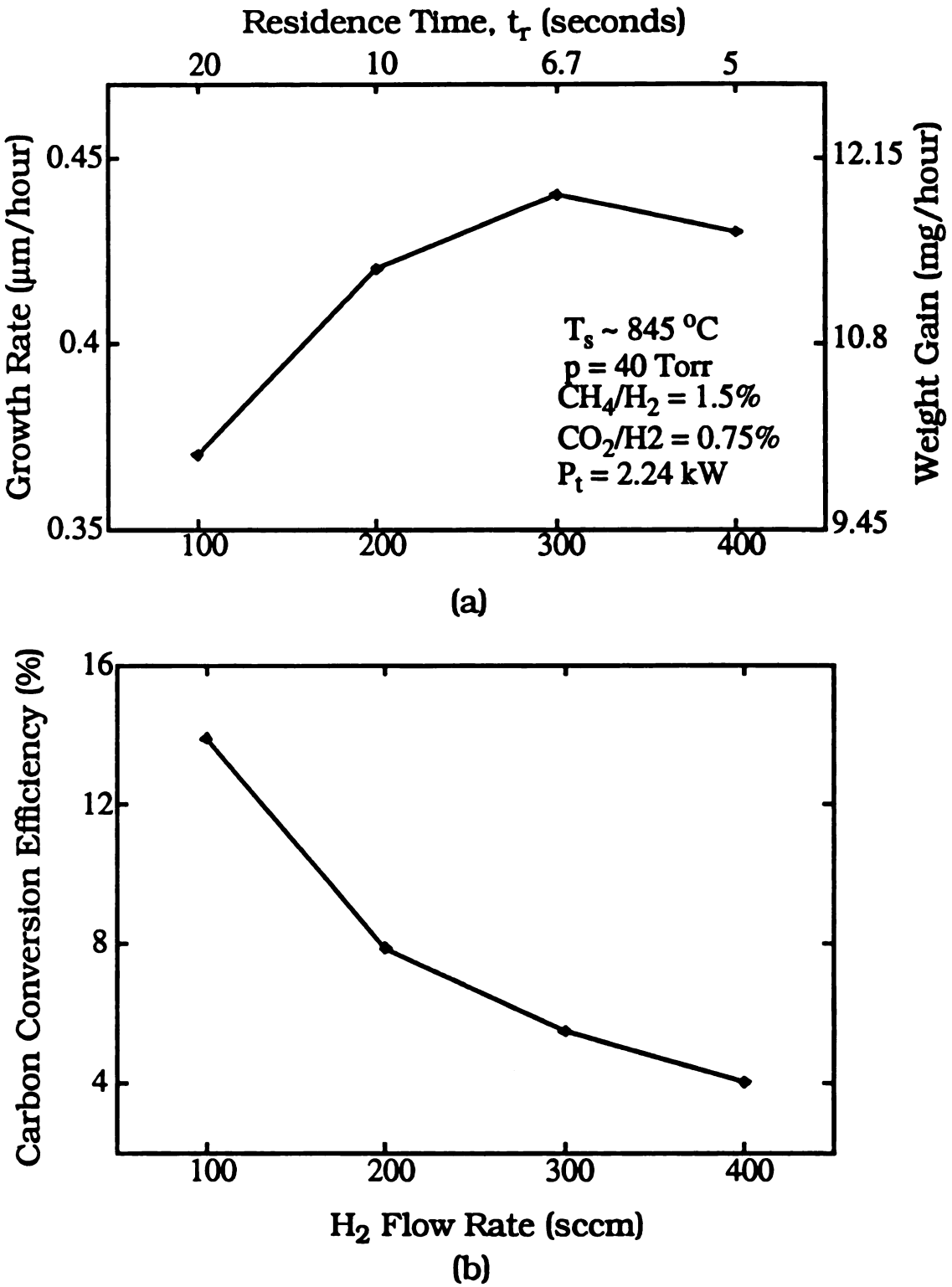

Figure 6.41 (a) Linear Growth Rate, Weight Gain and (b) Carbon Conversion Efficiency versus Total Flow Rate and Gas Residence Time

in section 6.6.2 are characterized.

6.6.3.2 Effects of Substrate Temperature

Figure 6.42 displays the SEM photographs of four films deposited with substrate temperatures: (a) 900 °C, (b) 836 °C, (c) 825 °C, and (d) 813 °C. The pressures and absorbed microwave powers used to achieve these temperatures are listed in Table 6.9 located above Figure 6.35. The other deposition conditions are: H_2 flow rate = 400 sccm, CH_4 flow rate = 6 sccm, CO_2 flow rate = 2 sccm, and deposition time = 8 hours.

As shown, the films deposited under these conditions are crystalline films with different average grain sizes. The film deposited at 900 °C has the largest average grain size and the film deposited at 813 °C has the smallest average grain size.

6.6.3.3 Effects of CH_4 Concentration

Film morphology versus CH_4 concentration is shown in Figure 6.43 where the SEM photographs of five films are displayed. These films are deposited under the following experimental conditions: H_2 flow rate = 400 sccm, CO_2 flow rate = 3 sccm, pressure = 40 Torr, absorbed microwave power = 2.24 kW, substrate temperature ~ 845 °C, deposition time = 8 hours and CH_4 flow rate (a) 7, (b) 6.5, (c) 6, (d) 5.5, and (e) 5.

As shown, the film deposited with 7 sccm CH_4 gas flow has very small average grain size. The average grain size jumps up when the CH_4 flow rate is reduced from 7 to 6.5 sccm. It then decreases gradually as the CH_4 flow rate is further reduced from 6.5 to 5 sccm.

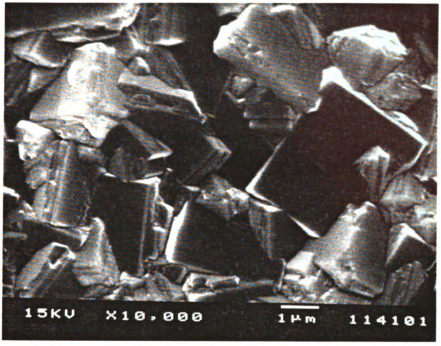

(a)

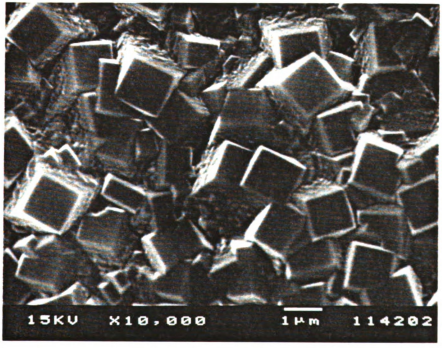

(b)

Figure 6.42 Effects of Substrate Temperature on Film Morphology H_2 = 400 sccm, CH_4 = 6 sccm, CO_2 = 2 sccm, and T_s = (a) 900, (b) 836, (c) 825 and (d) 813 °C.

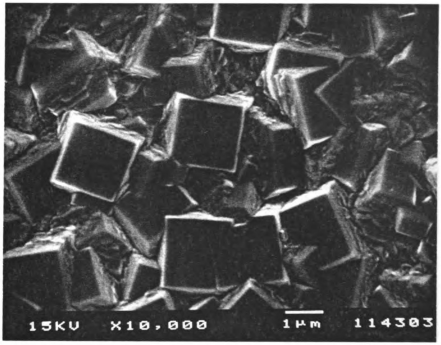

(c)

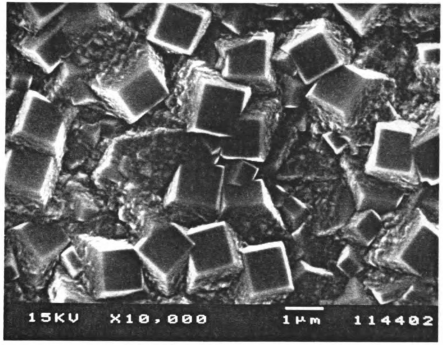

(d)

Figure 6.42 (cont'd)

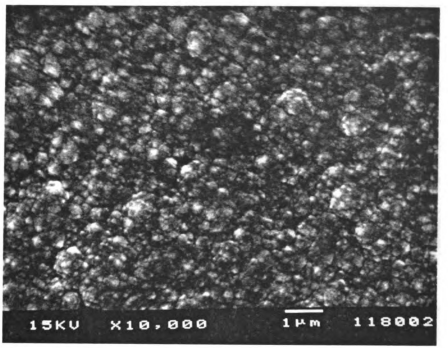

(a)

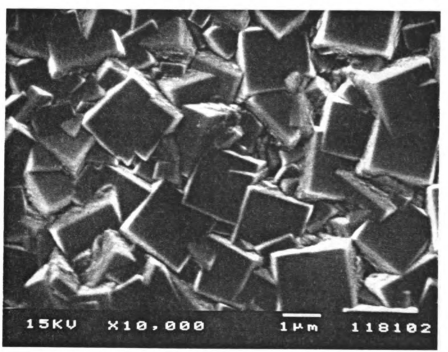

(b)

Figure 6.43 Effects of CH_4 Concentration on Film Morphology H_2 = 400 sccm, CO_2 = 3 sccm, p = 40 Torr, P_t = 2.24 kW, T_s = 845 °C, and CH_4 = (a) 7, (b) 6.5, (c) 6, (d) 5.5, (e) 5 sccm.

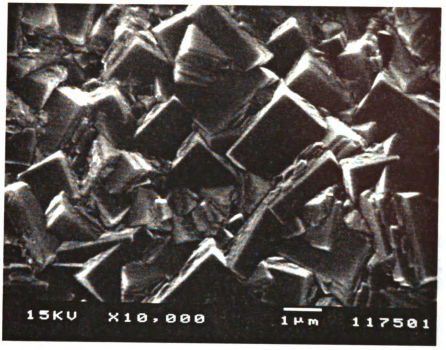

(c)

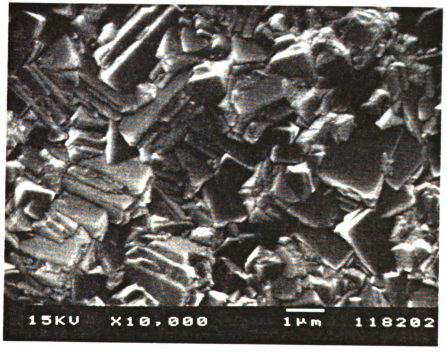

(d)

Figure 6.43 (cont'd)

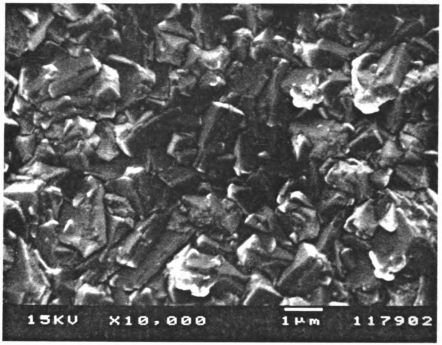

(e)

Figure 6.43 (cont'd)

6.6.3.4 Effects of CO_2 Concentration

Film morphology versus CO_2 concentration is shown in Figure 6.44 where the SEM photographs of five films are displayed. These films are deposited under the following experimental conditions: H_2 flow rate = 400 sccm, CH_4 flow rate = 6 sccm, pressure = 40 Torr, absorbed microwave power absorbed = 2.24 kW, substrate temperature ~ 845 ^oC, deposition time = 8 hours and CO_2 flow rate (a) 1, (b) 2, (c) 2.5, (d) 3 and (e) 4 sccm.

As shown, the films deposited with 1 and 2 sccm CO_2 gas flow have very small average grain size. The average grain size jumps up when CO_2 flow rate is increased to 2.5 sccm. It then experiences a gradual decline as the CO_2 flow rate is further increased to 4 sccm.

6.6.3.5 Effects of Total Flow Rate

Film morphology versus total flow rate is shown in Figure 6.45 where the SEM photographs of four films are displayed. These films are deposited under the following experimental conditions: CH_4 to H_2 volume ratio = 1.5%, CO_2 to H_2 volume ratio = 0.75%, pressure = 40 Torr, absorbed microwave power = 2.24 kW, substrate temperature ~ 845 ^oC, deposition time = 8 hours and H_2 flow rate (a) 400, (b) 300, (c) 200, and (d) 100 sccm.

As shown, the average grain size stays about the same when the H_2 flow rate is decreased from 400 to 300 sccm. It then experiences a gradual decline as the H_2 flow rate is further decreased from 300 to 100 sccm.

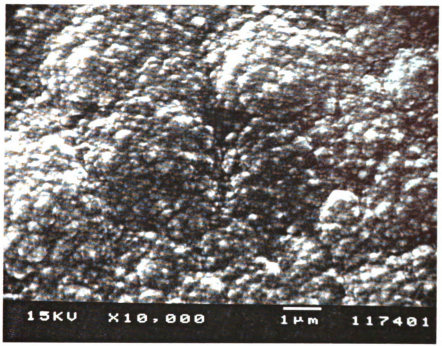

(a)

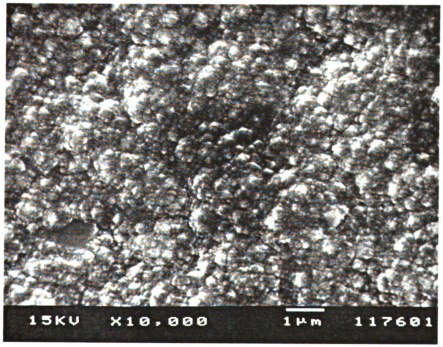

(b)

Figure 6.44 Effects of CO_2 Concentration on Film Morphology H_2 = 400 sccm, CH_4 = 6 sccm, p = 40 Torr, P_t = 2.24 kW, T_s ~ 845 °C, and CO_2 = (a) 1, (b) 2, (c) 2.5, (d) 3 and (e) 4 sccm.

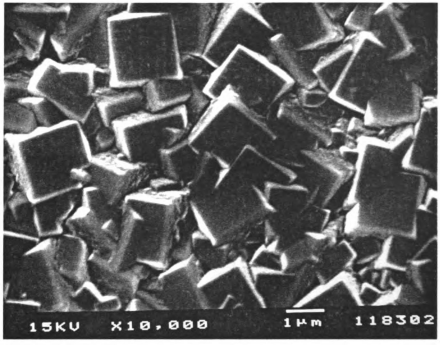

(c)

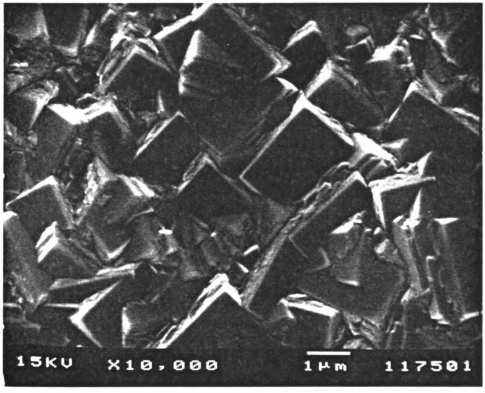

(d)

Figure 6.44 (cont'd)

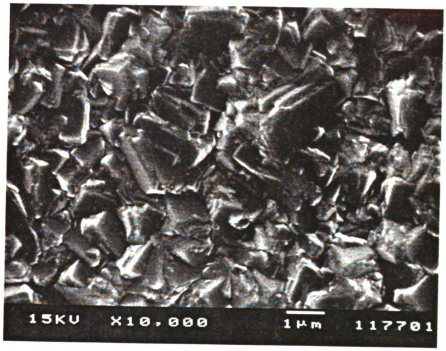

(e)

Figure 6.44 (cont'd)

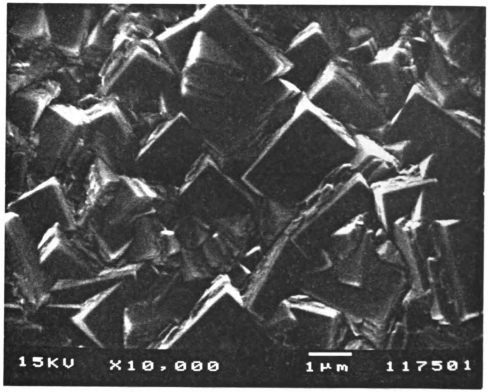

(a)

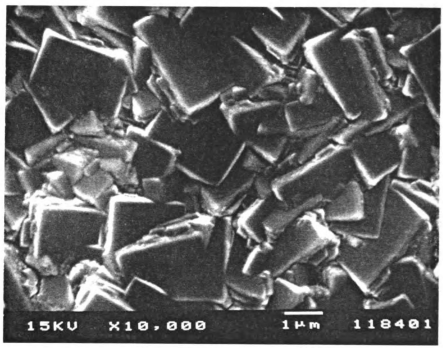

(b)

Figure 6.45 Effects of Total Flow Rate on Film Morphology CH_4/H_2 = 1.5%, CO_2/H_2 = 0.75%, p = 40 Torr, P_t = 2.24 kW, T_s ~ 845 ^{0}C, and H_2 = (a) 400, (b) 300, (c) 200 and (d) 100 sccm.

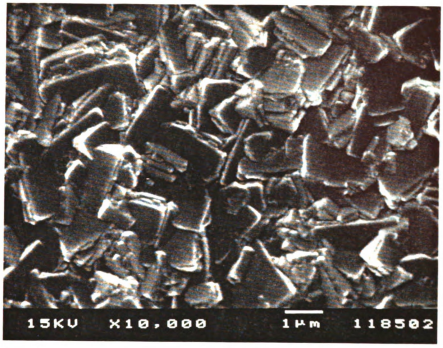

(c)

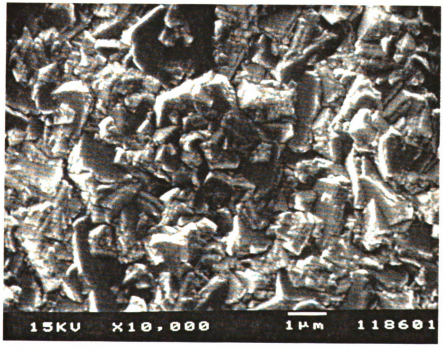

(d)

Figure 6.45 (cont'd)

6.6.4 Typical Raman Spectrum

Figure 6.46 displays the Raman spectrum[76] of a diamond film deposited on a 4" silicon wafer under the following experimental conditions: H_2 flow rate = 400 sccm, CH_4 flow rate = 6 sccm, CO_2 flow rate = 3 sccm, pressure = 40 Torr, absorbed microwave power = 2.24 kW and substrate temperature ~ 845 ^oC. The sharp peak near 1332 cm^{-1} indicates the excellent quality of the deposited diamond film.

6.6.5 Typical Uniformity Profile

The thickness profiles of a diamond film deposited on a 4" silicon wafer are displayed in Figures 6.47 and 6.48.[71] They were obtained by laser interference/reflection technique. The diamond film was deposited under the following experimental conditions: H_2 flow rate = 400 sccm, CH_4 flow rate = 6 sccm, CO_2 flow rate = 3 sccm, pressure = 40 Torr, absorbed microwave power = 2.24 kW and substrate temperature ~ 845 ^oC.

6.6.6 Summary

From the parametric study of diamond film deposition on 4" silicon wafers, the results can be summarized as follows:

(1) There exists a compromising substrate temperature range for diamond film deposition with high growth rate and good uniformity. When a good uniformity is required, the upper limit on film growth rate is primarily the safety operation temperature limit and the coating speed

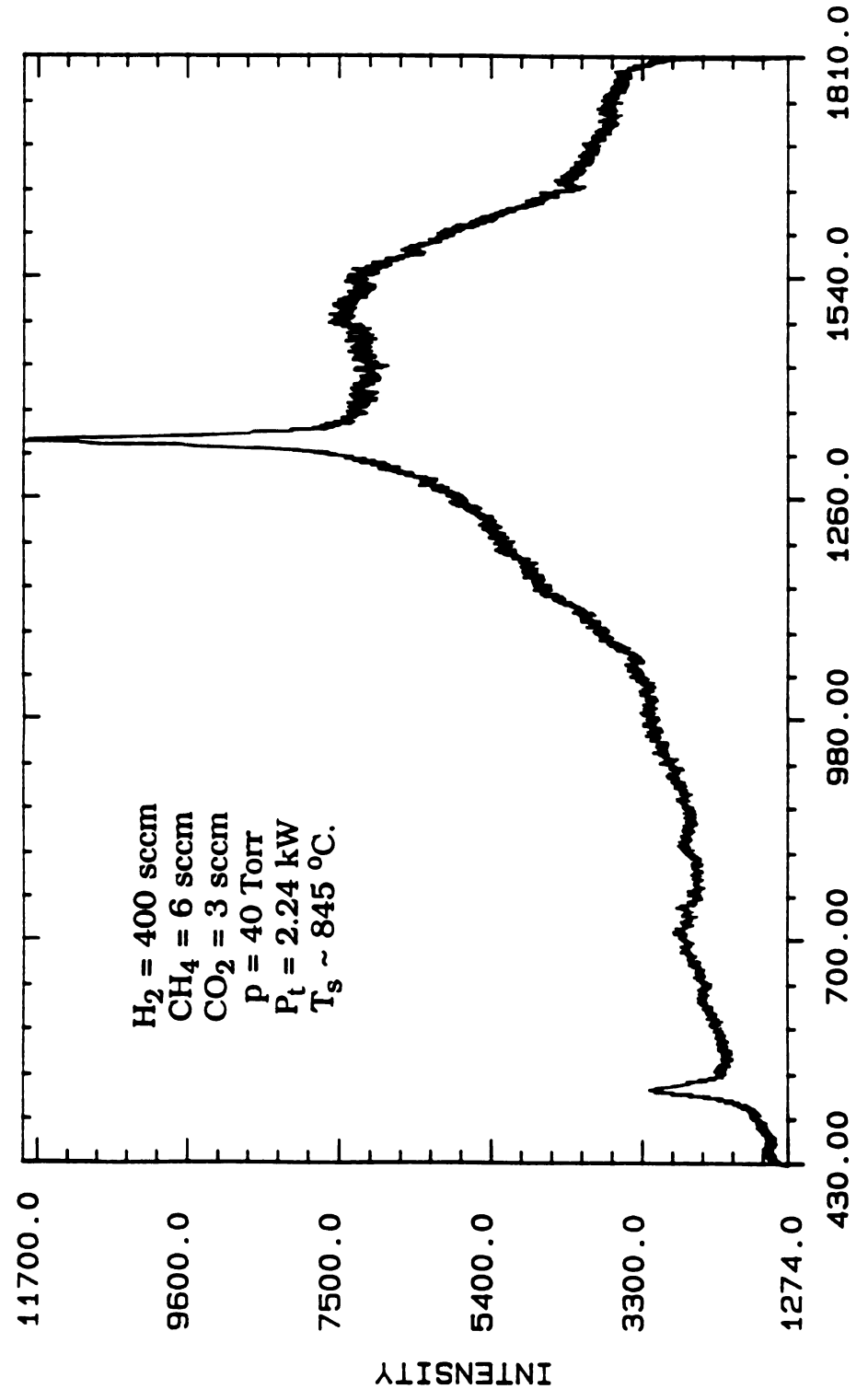

Figure 6.46 Raman Spectrum of a 4" Diamond Film Deposited in MCPR7-3

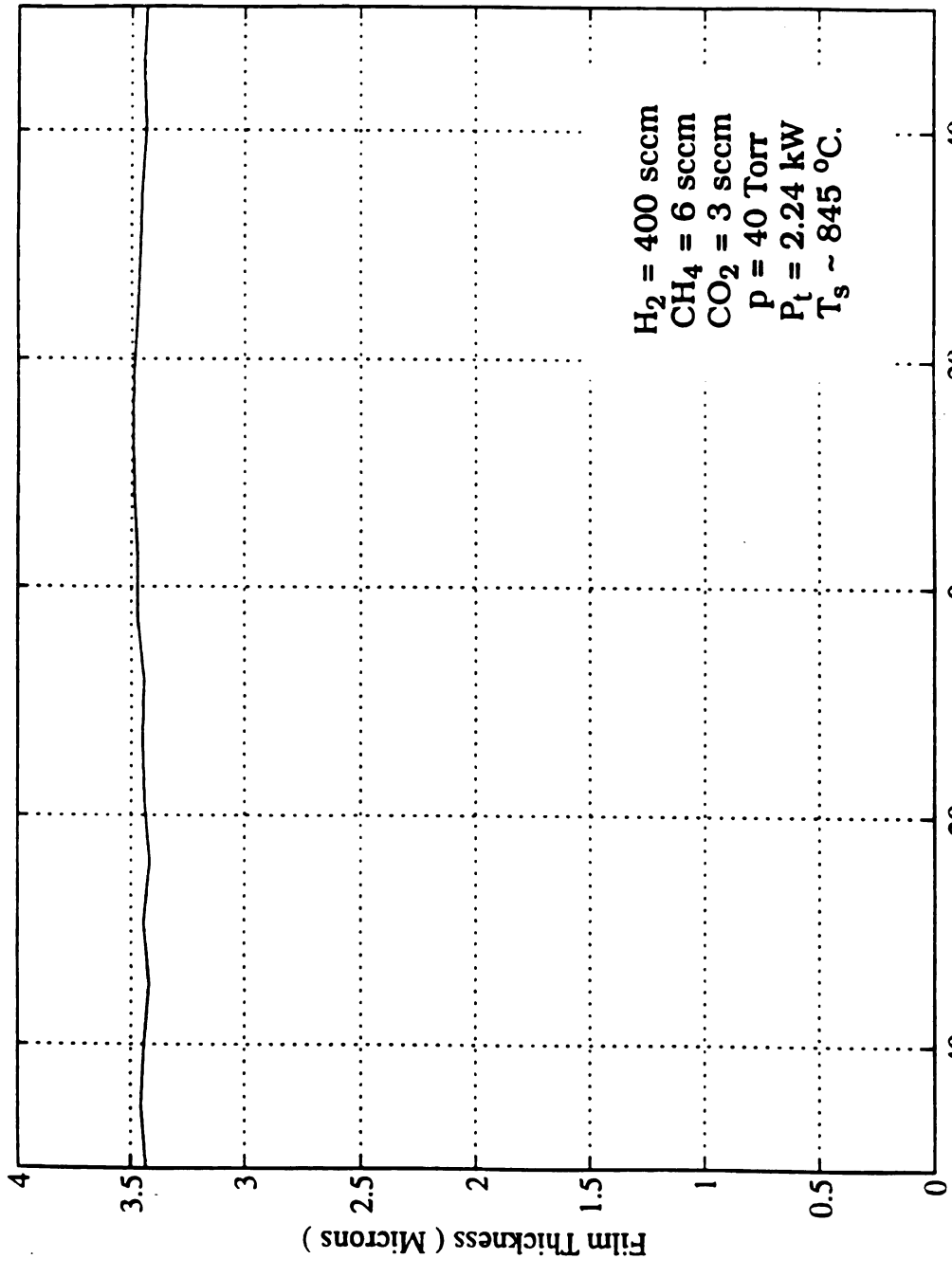

Figure 6.47 Cross-sectional Thickness Profile of a 4" Diamond Film

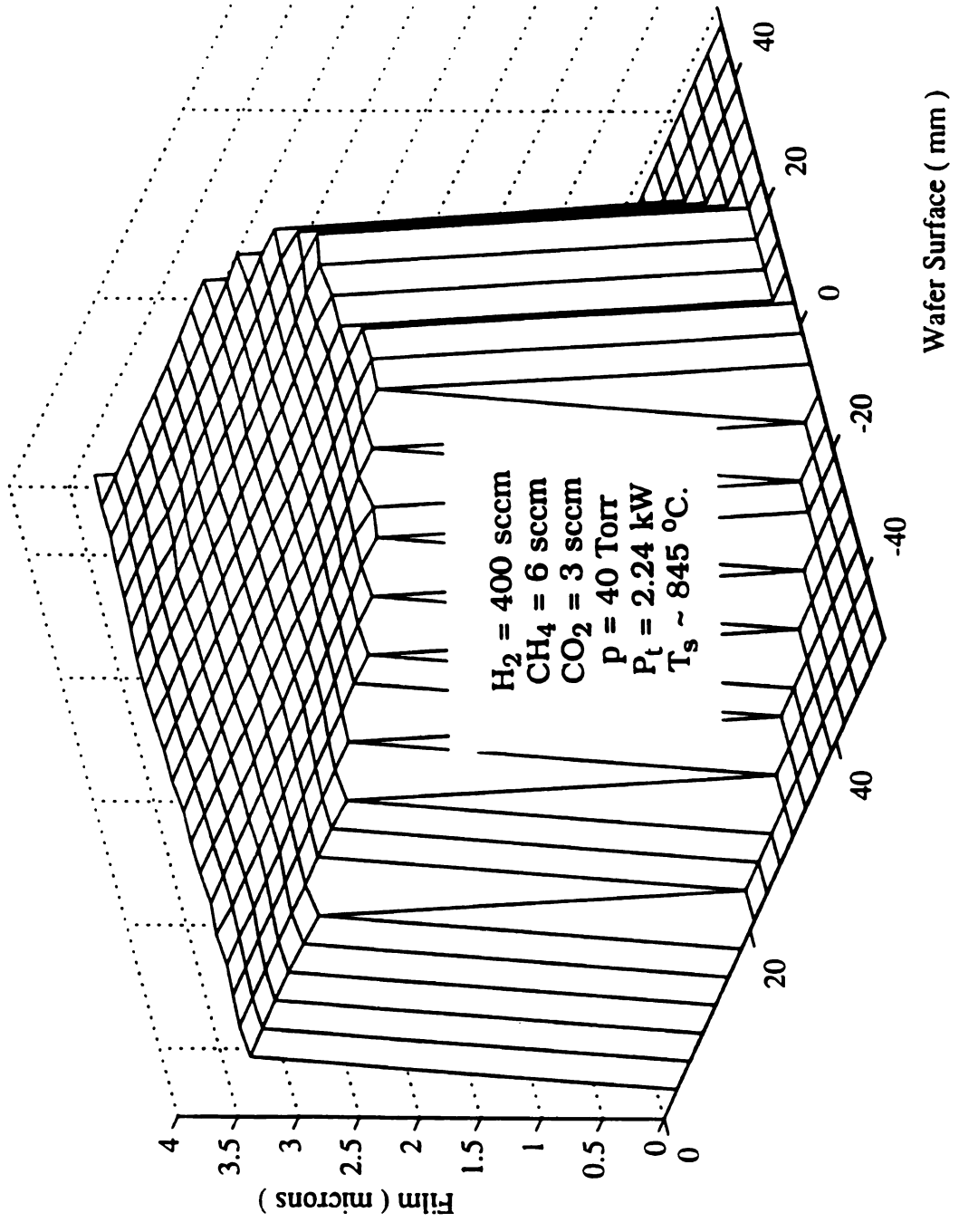

Figure 6.48 Three Dimensional Thickness Profile of a 4" Diamond Film

of the quartz dome.

(2) There exists an optimum CH_4 concentration range for high rate diamond film growth at a suitable substrate temperature.

(3) Addition of CO_2 to H_2/CH_4 discharge tends to dilute some of the reactive species in the discharge.

(4) The growth rate increases with increasing total flow rate in the region of 100 -200 sccm and saturates in the region of 300 - 400 sccm, keeping gas composition and substrate temperature constant. This suggests:

(i) at the low flow rates of 100 - 200 sccm, the deposition rate is limited by chemically active species hitting the substrate.

(ii) at the higher flow rate of 300 - 400 sccm, some of the input gas by-passes the deposition process.

(5) Carbon conversion efficiency decreases with increasing total flow rate and decreasing gas residence time.

(6) Film morphologies depend on substrate temperature, gas composition and total gas flow rate.

(7) Raman spectrum exhibits the excellent characteristics of a diamond film deposited.

(8) Diamond film with excellent uniformity (better than 2%) has been deposited.

(9) Diamond film with excellent uniformity and growth rate is deposited on a 4" silicon wafer under the following experimental conditions: H_2 flow rate = 400 sccm, CH_4 flow rate = 6 sccm, CO_2 flow rate = 3 sccm, absorbed microwave power = 2.24 kW, substrate temperature ~ 845 ^{o}C, pressure = 40 Torr and growth rate ~ 0.43 μm/ hour.

CHAPTER SEVEN

CONCLUSIONS AND RECOMMENDATIONS

7.1 Summary of Significant Results

7.1.1 Introduction

The research and development described in this dissertation have lead to the successful creation of a working prototype reactor (MCPR7-3) of an improved microwave cavity plasma reactor concept and a U. S. patent application[17]. Diamond films with uniformities better than 2% have been deposited on 3" and 4" silicon wafers with this prototype reactor. The linear growth rates obtained are 0.89 μm/hour on 2" silicon wafers, 0.67 μm/hour on 3" silicon wafers and 0.43 μm/hour on 4" silicon wafers. The performance "figures of merit" of diamond film deposition reactors were developed to compare the MCPRs and other reactors. Three generations (MCPR7-1, MCPR7-2 and MCPR7-3) of microwave cavity plasma reactors have been investigated and/or developed for diamond film deposition over larger substrate areas. Three generations (MCJR-1, MCJR-2 and MCJR-3) of microwave cavity jet reactors have also been developed and/or designed to deposit diamond films. These reactors have the potential to deposit diamond films with higher growth rates. A method to obtain the operational characteristics of

the MCPRs was developed. The diamond films deposited in the MCPR7-3 prototype reactor were investigated with respect to their growth rate and quality as the input experimental parameters were varied. The electric fields in the microwave cavity plasma reactor (MCPR7-1) were measured to develop a better understanding of the electromagnetic field/plasma interactions during diamond film deposition process. These important accomplishments are summarized in greater detail in the sections that follow.

7.1.2 MCPR Development

An improved microwave cavity plasma reactor was developed. This reactor uses the microwave plasma technology that was developed at MSU in earlier investigations. That is, the new reactor still employs single mode excitation and two internal independent tuning variables, i.e., cavity short and excitation probe length, are used to minimize the reflected microwave power from the cavity applicator.

Improvements over earlier microwave diamond film reactors are as follows:

(1) The excitation probe is placed on the sliding short end of the cavity applicator instead of on the side of the cavity. Near field effects are eliminated with the use of higher order axial modes. Only TM modes are excited and the interference from nearby TE modes is eliminated. TM_{012} and TM_{013} modes are used for diamond film deposition. The reactor operation is more reliable and the reactor is suitable for industrial applications.

(2) A resonance breaker was placed in the applicator to create a

stable discharge above the substrate surface.

(3) A larger (5") diameter quartz dome is used and discharges up to 12.5 cm in diameter are created.

(4) Higher power input (from 1.5 kW to 4.5 kW or more) capacity is achieved with this reactor.

(5) An improved internal gas flow configuration was developed. Reactive gases are forced to flow close to the substrates and the gas efficiencies are improved.

This reactor has been used to deposit diamond films in the 20 to 95 Torr pressure range. It can be used to deposit uniform diamond films on substrate surfaces up to 10 cm in diameter, even without substrate heating or cooling. Diamond film uniformity better than 2% over 10 cm diameter silicon wafer has been achieved.

The typical experimental conditions for diamond film deposition on 3" and 4" silicon wafers are as follows:

I. Diamond film deposition on 3" silicon wafers:

pressure = 51 Torr,

H_2 flow rate = 400 sccm, CH_4 flow rate = 6 sccm,

absorbed microwave power = 2.34 kW,

substrate temperature ~ 900 ^oC,

weight gain = 10.6 mg/hour and linear growth rate = 0.67 μm/hour.

II. Diamond film deposition on 4" silicon wafers:

pressure = 40 Torr,

H_2 flow rate = 400 sccm, CH_4 flow rate = 6 sccm, CO_2 flow rate = 3 sccm,

absorbed microwave power = 2.24 kW,

substrate temperature ~ 845 ^{o}C,

weight gain = 11.7 mg/hour and linear growth rate = 0.43 μm/hour.

7.1.3 Microwave Plasma Jet Reactor Development

7.1.3.1 Microwave Cavity Jet Reactors

Three generations of microwave cavity jet reactors have been developed for high rate diamond film deposition.

The first two generation reactors were investigated for diamond film deposition. One inch diameter quartz tubes were used as the plasma confinement chamber. The operating pressure and input microwave power were limited due to quartz tube over-heating. The total gas flow rate was limited by the pumping speed of the vacuum system.

The third generation reactor was designed in which the discharge confinement chamber was enlarged to be a dome. This design should overcome the confinement chamber over-heating problem. It was not built due to lack of funding.

7.1.3.2 Jet Configuration in MCPR

Preliminary investigation of diamond film deposition using a jet concept was conducted in the new MCPR7-3. Increased deposition rate (~ 1 μm/hour) over a 1.5 cm diameter area was obtained without substrate cooling. It is expected that higher deposition rates are possible with proper substrate cooling.

7.1.4 Reactor Operational Characteristics

A method to experimentally characterize a microwave plasma reactor was developed. It was described in sections 6.2 and 6.3 of this dissertation. This method probably can also be used to experimentally investigate other plasma reactors. It can be used to locate the required experimental conditions when diamond films with desired properties, such as film thickness, morphology, and uniformity, etc. are deposited.

When the discharge occupies only part of the quartz dome volume, the following conclusions were reached from the study of operational characteristics of MCPR:

(1) Substrate temperature, T_s, is primarily determined by operating pressure. Substrate temperature T_s increases sharply with increasing pressure (~ 6 ^oC/Torr) and at constant pressure, T_s increases gradually (~ 0.02 ^oC/W) with increasing absorbed microwave power. T_s is not sensitive to variation in gas composition and total flow rate.

(2) For a constant input power, the discharge volume, V_d, decreases with increasing pressure. At a constant pressure, V_d increases with increasing absorbed microwave power. V_d is not sensitive to variations in gas composition and total flow rate.

(3) Average discharge power density, w, increases with increasing pressure and at constant pressure, it is not sensitive to variation in absorbed microwave power. That is, under a constant pressure, as the absorbed microwave power increases, the discharge volume also increases, resulting in only small variations in absorbed power density. Power density is not sensitive to variations in gas composition and total flow rate.

(4) Power flux S to the substrate increases with increasing absorbed microwave power. It is not sensitive to variations in gas composition and total flow rate.

7.1.5 Diamond Film Deposition on 3" Silicon Wafers

A parametric study of diamond film deposition on 3" silicon wafers was conducted. The results of this study can be summarized as follows:

(1) There exists an optimum substrate temperature range (~ 800 - 1000 ^{o}C) for high rate diamond film growth with a suitable gas composition. The growth rate is gas composition dependent.

(2) There exists an optimum CH_4 concentration range for high rate diamond film growth at a suitable substrate temperature.

(3) Addition of CO_2 to H_2/CH_4 discharge tends to dilute some of the reactive species in the discharge.

(4) The growth rate increases with increasing total flow rate in the region of 50 -200 sccm and saturates in the region of 300 - 400 sccm, keeping gas composition and substrate temperature constant. This suggests:

(i) at the low flow rates of 50 - 200 sccm, the deposition rate is limited by chemically active species hitting the substrate,

(ii) at the higher flow rates of 300 - 400 sccm, some of the input gas by-passes the deposition process.

(5) Carbon conversion efficiency decreases with increasing total flow rate and decreasing gas residence time.

(6) Film morphologies depend on substrate temperature, gas composition and total gas flow rate.

(7) Within all the CH_4 concentrations used, the average grain size of deposited films decreases as CH_4 concentration is increased.

(8) Within all the CO_2 concentrations used, the average grain size of deposited films increases as CO_2 concentration is increased.

(9) Raman spectrum exhibits the excellent characteristics of a diamond film deposited.

(10) Diamond film with excellent uniformity (better than 2%) has been deposited.

(11) Higher deposition rates may require changing the gas flow configuration.

(12) The maximum diamond film growth rate obtained on a 3" silicon wafer is ~ 0.67 μm/hour. The experimental conditions are: H_2 flow rate = 400 sccm, CH_4 flow rate = 6 sccm, absorbed microwave power = 2.34 kW, substrate temperature ~ 900 ^{o}C and pressure = 51 Torr.

7.1.6 Diamond Film Deposition on 4" Silicon Wafers

7.1.6.1 Study of Experimental Set-ups

A study of experimental set-ups for diamond film deposition on 4" silicon wafers was conducted, the results of this study can be summarized as follows:

(1) A slight variation in cavity shell geometry influences diamond film growth. Cavity shell (I) is a preferable choice.

(2) A slight variation in quartz dome geometry influences diamond film growth rate and morphology.

(3) Substrate holder material influences discharge geometry and

substrate heating. Graphite is a preferable substrate holder material.

(4) Substrate location influences film growth rate and uniformity. 5.09 cm long quartz tube is most frequently used substrate support tube.

(5) Cavity excitation modes influence film growth rate and uniformity. TM_{013} mode is a preferable choice.

(6) Diamond film growth is not sensitive to slight variations in seeding density.

7.1.6.2 Diamond Film Deposition on 4" Silicon Wafers

A parametric study of diamond film deposition on 4" silicon wafers was conducted, the results of this study can be summarized as follows:

(1) There exists a compromising substrate temperature range for diamond film deposition with high growth rate and good uniformity. When a good uniformity is required, the upper limit on film growth rate is primarily the safe operating temperature limit and the coating rate on the quartz dome.

(2) There exists an optimum CH_4 concentration range for high rate diamond film growth at a suitable substrate temperature.

(3) Addition of CO_2 to H_2/CH_4 discharge tends to dilute some of the reactive species in the discharge.

(4) The growth rate increases with increasing total flow rate in the region of 100 -200 sccm and saturates in the region of 300 - 400 sccm, keeping gas composition and substrate temperature constant. This suggests:

(i) at the low flow rates of 100 - 200 sccm, the deposition

rate is limited by chemically active species hitting the substrate.

(ii) at the higher flow rate of 300 - 400 sccm, some of the input gas by-passes the deposition process.

(5) Carbon conversion efficiency decreases with increasing total flow rate and decreasing gas residence time.

(6) Film morphologies depend on substrate temperature, gas composition and total gas flow rate.

(7) Raman spectrum exhibits the excellent characteristics of a diamond film deposited.

(8) Diamond film with excellent uniformity (better than 2%) has been deposited.

(9) Diamond film with excellent uniformity and growth rate is deposited on a 4" silicon wafer under the following experimental conditions: H_2 flow rate = 400 sccm, CH_4 flow rate = 6 sccm, CO_2 flow rate = 3 sccm, absorbed microwave power = 2.24 kW, substrate temperature ~ 845 ^{o}C, pressure = 40 Torr and growth rate ~ 0.43 μm/ hour.

7.1.7 Reactor Performance "Figures of Merit"

7.1.7.1 Performance "Figures of Merit" of MCPR

Performance "figures of merit" were developed for comparison between different group of reactors and for comparison of the same reactor under different operating conditions.

I. The MCPRs have the following performance "figures of merit" as listed in Table 7.1.

Table 7.1 Summary of "Figures of Merit" of Diamond Film Deposition Experiments in MCPR

Exp. No.	Linear growth rate (μm/hr)	Dep. area (cm^2)	Weight gain (mg/hr)	Energy effic. (mg/ kW-hr)	Gas flow effic. (mg/ liter)	Carbon conv. effic. (%)
MCPR 7-1	0.4-0.8	16	2.25-4.5	4.5-9	0.19-0.38	3.5-7
MCPR 7-2	0.4-0.8	20	2.8-5.6	1.75-3.5	0.15-0.3	2.9-5.8
MCPR 7-3 NT#4	0.89	20	6.2	3.3	0.26	2.4
WT#27	0.67	45	10.6	4.5	0.44	5.5
WT#29	0.65	45	10.3	4.4	0.57	7.1
WT#30	0.62	45	9.75	4.2	0.81	10.1
WT#31	0.51	45	8	3.4	1.3	16.6
WF#75	0.43	78	11.7	5.2	0.49	4
WF#84	0.44	78	11.9	5.3	0.66	5.5
WF#85	0.42	78	11.4	5.1	0.95	7.9
WF#86	0.37	78	9.9	4.4	1.65	13.7

II. Comparing the experiments conducted in the MCPRs, the following conclusions can be reached:

(1) With the same deposition area, the diamond films deposited in MCPR7-3 have the highest linear growth rate and weight gain.

(2) Among the uniform diamond films deposited in MCPR7-3, as the deposition area increases, the linear growth rate decreases and the weight gain increases.

7.1.7.2 Comparison with other Reactors

Comparing with other reactor concepts reviewed in chapter 2 and referring to Table 2.1, the following conclusions can be reached:

(1) The linear growth rate in MCPR is lower than that in most high pressure (higher than 100 Torr) reactors.

(2) The uniform diamond film deposition area (78 cm^2) in MCPR is larger than that in the other reactors reported in the literature.

(3) The weight gain of the diamond films deposited in MCPR is higher than that in the other low pressure (less than 100 Torr) reactors. It is lower than that in some high pressure (more than 100 Torr) reactor.

(4) The energy efficiency of MCPR is comparable to most other diamond film deposition reactors.

(5) The gas flow efficiency of MCPR is higher than most high pressure diamond film deposition reactors.

(6) The carbon conversion efficiency of MCPR is higher than that of other diamond film deposition reactors.

(7) The excellent uniformity (better than 2%) of the diamond films deposited in MCPR is better than that in the other reactors reported

in the literature.

7.1.8 Measurement of Electric Fields in MCPR

The (relative) spatial variations of the exciting electromagnetic field patterns in MCPR7-1 under diamond film deposition conditions were measured. These spatial electric field measurements and intensities are related to other important experimental parameters such as gas mixture, flow rate, input power, substrate temperature, and discharge pressure, etc.

The following conclusions were reached from this study, under diamond film deposition condition in MCPR7-1:

(1) The excitation mode was identified to be discharge loaded TM_{011} mode.

(2) Maximum electric field intensity in the cavity was ~ 150 V/cm.

(2) Discharge loaded cavity quality factor was ~ 60.

(3) The tangential component of the $\vec{E}$ field is the main discharge excitation field.

(4) Average power density in the discharge was ~ 6 W/cm^3 at 20 Torr and 20 W/cm^3 at 70 Torr.

(5) Under a constant pressure, the square of the cavity electric field strength is approximately proportional to the power input and only slightly influenced by the variation in flow rates.

(6) At a constant gas flow, the square of the cavity electric field strength is approximately proportional to the power input and only slightly influenced by the variation in pressure.

(7) Under a constant pressure, the substrate temperature increases with the power input (~ 0.4 ^{o}C/W) and is only slightly influenced by the variation in flow rates.

(8) At a constant gas flow, the substrate temperature increases with the power input (~ 0.4 ^{o}C/W) under each working pressure. Also, at the constant gas flow and input power, the substrate temperature increases (~ 3.5 ^{o}C/Torr) with increasing pressure.

7.2 Recommendations for Future Research

(1) For diamond film deposition in MCPR7-3, higher growth rates may be achieved by using higher pressure (100 - 200 Torr), higher power (3 - 6 kW) and substrate cooling. A substrate cooling stage has been built. Different gas flow configurations should also be investigated for their potential to improve the diamond film growth rates.

(2) The MCPR concept may be scaled up to larger diameter (14 - 20 inch) cavities by dropping the microwave input power frequency to 915 MHz. Larger area substrates may be covered with increasing input microwave power. Also, with proper reactor design, the diameter of the cavity operated with 2.45 GHz power may be enlarged to 8-12 inches.

(3) The improved microwave cavity jet reactor (MCJR-3) should be built and investigated for its potential in diamond film deposition with higher growth rates.

(4) The jet configuration in MCPR7-3 offers an interesting alternative approach to deposit diamond films with higher growth rates. Experiments should be conducted to investigate this potential, using a substrate cooling system.

(5) In order to obtain a better understanding of the electromagnetic field/plasma interactions, electric field measurements in MCPR7-3 should be conducted. A new cavity with electric field measurement probe holes has been built.

(6) In order to improve the knowledge of the fundamental plasma/chemical reactions of diamond film deposition and to be able to better control the diamond film deposition process, it is necessary to identify the discharge species essential for diamond film deposition. It is helpful to characterize the microwave discharge under diamond film deposition conditions by emission spectroscopy, actinometry and laser induced fluorescence (LIF) spectroscopy. The knowledge obtained in this investigation will be beneficial to achieve single crystal diamond film growth which is essential for some industrial applications, such as diamond electronic and optical devices.

(7) For some industrial applications, it is necessary to deposit diamond film on substrates at low substrate temperature. The research on diamond film deposition at lower substrate temperatures and/or low pressures should be conducted.

(8) For different industrial applications, diamond films with different morphologies are required. Since only a preliminary investigation of diamond film morphologies versus experimental conditions was conducted, more detailed investigation of diamond film morphologies versus experimental conditions should be conducted.

(9) Alternative gas compositions, such as carbon monoxide (CO), oxygen (O_2), acetone (CH_3COCH_3) and acetylene (C_2H_2), etc., should be considered to improve the gas flow efficiency and diamond film growth rate.

LIST OF REFERENCES

LIST OF REFERENCES

[1] S. Tennant, "On the nature of the diamond," Phil. Trans. Roy. Soc. London, 87, 123 (1797).

[2] J.C. Angus and C.C. Hayman, Science 241, 913 (1988).

[3] R. Orr, "The impact of thin film diamond on advanced engineering systems," presented at the global business and technical outlook for high performance inorganic thin film coatings, Gorham advanced materials institute, Monterey, California, October 30 - November 1, 1988.

[4] F. P. Bundy, H. T. Hall, H. M. Strong, and R. H. Wentof, Jr., "Man-made diamond," Nature, 176, 51 (1955).

[5] W. G. Eversole, U. S. Patents 3030187 and 3030188.

[6] J. C. Angus, H. A. Will, and W. S. Stanko, J. Appl. Phys. 39, 2915 (1968).

[7] B. V. Deryaguin, D. V. Fedoseev, V. M. Lukyanovich, B. V. Spitsyn, V. A. Ryabov, and A. V. Lavrentyev, J. Cryst. Growth 2, 380 (1968).

[8] B. V. Spitsyn, L. L. Bouilov and B. V. Deryagin, J. Cryst. Growth 52, 219 (1981).

[9] S. Matsumoto, Y. Sato, M. Kamo, N. Setaka, Jpn. J. Appl. Phys. 21, part 2, 183 (1982).

[10] J. Rogers, "Properties of steady-state, high pressure argon discharges," Ph.D. Dissertation, Michigan State University,

1982.

[11] S. J. Whitehair, "Experimental development of a microwave electrothermal thruster," Ph.D. Dissertation, Michigan State University (1986).

[12] M. Dahimene, "Development of a microwave ion and plasma source immersed in a multicusp electron cyclotron resonant magnetic field," Ph.D. Dissertation, Michigan State University (1987).

[13] J. A. Hopwood, "Macroscopic properties of a multipolar electron cyclotron resonance microwave cavity plasma source for anisotropic silicon etching," Ph.D. Dissertation, Michigan State University (1990).

[14] J. Zhang, B. Huang, D. K. Reinhard and J. Asmussen, J. Vac. Sci. Technol. A 8, 2124 (1990).

[15] J. Zhang, G. King, T. Grotjohn, and J. Asmussen, "Diagnostic measurements of a resonant cavity microwave plasma diamond deposition reactor," presented at Third International Conference on the New Diamond Science and Technology, Heidelberg, Germany, August 31 - September 4, 1992.

[16] P. Mak, G. King, M. Ulczynski, J. Zhang, T. Grotjohn, and J. Asmussen, "Experimental diagnosis of low pressure microwave discharges during diamond thin film deposition," presented at Third International Conference on the New Diamond Science and Technology, Heidelberg, Germany, August 31 - September 4, 1992.

[17] J. Asmussen and J. Zhang, "Improved apparatus for the coating of material on a substrate using a microwave or UHF plasma," U. S. Patent Application, (May 28, 1992).

[18] S. Matsumoto, Y. Sato, M. Kamo and N. Setaka, Jpn. J. Appl. Phys. 21, 183 (1982).

[19] S. Matsumoto, Y. Sato, M. Tsutsumi and N. Setaka, J. Mater.

Sci., 17, 3106 (1982).

[20] Y. H. Lee, P. D. Richard, K. J. Bachmann, and J. T. Glass, Appl. Phys. Lett. 56, 620 (1990).

[21] K. Baba, Y. Aikawa, and N. Shobata, J. Appl. Phys. 69, 7313 (1991).

[22] A. Masood, "Technology of electronic properities of CVD diamond film microsensors for thermal signals," Ph.D. dissertation, Michigan State University (1992).

[23] K. Suzuki, A. Sawabe, H. Yasuda and T. Inuzuka, Appl. Phys. Lett. 50, 728 (1987).

[24] K. Suzuki, A. Sawabe, and T. Inuzuka, Jpn. J. Appl. Phys. 29, 153 (1990).

[25] S. Matsumoto, I. Hosoya and T. Chounan, Jpn. J. Appl. Phys. 29, 2082 (1990).

[26] K. V. Ravi, C. A. Koch, H. S. Hu, and A. Joshi, J. Mater. Res., 5, 2356 (1990).

[27] L. M. Hanssen, W. A. Carrington, J. E. Butler and K. A. Snail, Mater. Lett. 7, 289 (1988).

[28] S. Matsumoto, J. Mater. Sci. Lett., 4, 600 (1985).

[29] S. Matsumoto, M. Hino and T. Kobayashi, Appl. Phys. Lett., 51, 737 (1987).

[30] M. Kamo, Y. Sato, S. Matsumoto and N. Setaka, J. Cryst. Growth 62, 642 (1983).

[31] H. Kawarada, K. S. Mar and A. Hiraki, Jpn. J. Appl. Phys. 26, L1032 (1987).

[32] J. J. Chang, T. D. Mantei, R. Vuppuladhadium and H. E. Jackson, Appl. Phys. Lett. 59, 1170 (1991).

[33] T. D. Mantei, Third Diamond Workshop, Detroit, MI, March, 1992.

[34] Y. Liou, A. Inspektor, R. Weimer and R. Messier, Appl. Phys. Lett. 55, 631 (1989).

[35] P. K. Bachmann, W. Drawl, D. Knight, R. Weimer, and R. F. Messier, in Extended Abstracts Diamond and Diamond-like Materials Synthesis, edited by G. Johnson, A. Badzian, and M. Geis, Materials Research Society, Pittsburgh, PA, 1988, p. 99.

[36] P. Bachmann, D. Leers and H. Lydtin, Diamond and Related Materials, 1, 1 (1991).

[37] Y. Mitsuda, T. Yoshida and K. Akashi, Rev. Sci. Instrum. 60, 249 (1989).

[38] K. Takeuchi and T. Yoshida, J. Appl. Phys. 71, 2636 (1992).

[39] L. Mahoney, "The design and testing of a compact electron cyclotron resonant microwave-cavity ion source," M.S. Thesis, Michigan State University (1989).

[40] J. T. Salbert, "Anodic growth and cathodic removal of silicon dioxide layers utilizing an electron cyclotron resonant microwave plasma disk reactor," Ph.D. Dissertation, Michigan State University (1992)

[41] The computer monitor system was designed and built by Z. M. Rummler with help from M Ennis. The monior program was written by Z. M. Rummler at Michigan State University, East Lansing, Michigan.

[42] J. Asmussen, J. Root, "Ion generating apparatus and method for the use thereof," U. S. Patent No. 4,507,588, March 26, 1985.

[43] J. Asmussen, S. Nakanishi, J. Malinkey and S. Whitehair, "Microwave electrothruster," patent applied for by NASA-Lewis.

[44] J. Asmussen, D. K. Reinhard, "Method for treating a surface with a microwave plasma and improved apparatus," U. S. Patent No. 4,585,688, April 29, 1986.

[45] J. Asmussen, D. K. Reinhard, "Microwave or UHF plasma and improved apparatus," U. S. Patent No. 4,630,566, Dec. 23, 1986.

[46] T. Ropple, D. K. Reinhard and J. Asmussen, "Dual plasma microwave apparatus and method for treating a surface," U. S. Patent No. 4,691,662, Sept. 8, 1987.

[47] J. Asmussen, D. K. Reinhard and M. Dahimene, "Improved plasma generating apparatus using magnets and method," U. S. Patent No. 4,727, 293, Feb. 23, 1988.

[48] J. Asmussen, "Method for treating a material using radiofrequency waves," U. S. Patent No. 4,777,336, Oct. 11,1988.

[49] J. Asmussen, "Improved microwave apparatus," U. S. Patent No. 4,792,772, Dec. 20, 1988; also Canadian Letters Patent No. 1,287,666, Aug. 13, 1991.

[50] J. Asmussen, D. K. Reinhard, "Improved plasma reactor apparatus and method for treating a substrate," U. S. Patent No. 4,943,345, July 24, 1990.

[51] J. Root and J. Asmussen, Rev. Sci. Instrum., 56, 154 (1985).

[52] T. Roppel, D. K. Reinhard, and J. Asmussen, J. Vac. Sci. Technol., B4, 295 (1986)

[53] J. Asmussen and M. Dahimene, J. Vac. Sci. Technol., B5, 328 (1987).

[54] J. Asmussen, J. Vac. Sci. Technol., A7, 883 (1989).

[55] L. Mahoney, M. Dahimene, and J. Asmussen, Rev. Sci. Instrum., 59, 448 (1988).

[56] S. Whitehair, J. Asmussen and S. Nakanishi, J. Propul. Power, 3, 136 (1987).

[57] This figure was provided by J. Asmussen, Michigan State University, East Lansing, Michigan.

[58] B. Huang, "Electrical properties and physical characteristics of polycrystalline diamond films deposited in a microwave plasma disk reactor," Ph. D. Dissertation, Michigan State University (1992).

[59] Designed and built by W. Richardson in 1990 at Michigan State University, East Lansing, Michigan.

[60] Designed and built by Union Carbide Coatings Service Co., Cleveland, OH.

[61] Developed by Wavemat Inc., Plymouth, Michigan.

[62] Designed and built by F. C. Sze at Michigan State University, East Lansing, Michigan.

[63] J. Asmussen, R. Mallavarpu, J. R. Hamann, and H. C. Park, "The design of a microwave plasma cavity", Proc. IEEE, 109 (1974).

[64] R. Mallavarpu, M. C. Hawley and J. Asmussen, "Behavior of a microwave cavity discharge over a wide range of pressures and flow rates," IEEE Tran. on Plasma Science, PS-6, 341-354 (December, 1978).

[65] R. F. Harrington, Time-Harmonic Electromagnetic Fields (McGraw-Hill, New York, 1961)

[66] R. L. Kapitza, Sov. Phys. JETP 30, 973 (1970).

[67] L. M. Baltin, V. M. Batemin, I. I. Devyatkim, V. P. Lebedeva, N. I. Tsemko, High Temp. 9, 1019 (1971).

[68] Y. Arata, S. Miyake, A. Kubayashi, and S. Takuchi, Jpn. J.

Phys. 40, 1456 (1976).

[69] R. Chapman, J. Filpus, T. Morin, R. Snellenberger, J. Asmussen, M. Hawley, and R. Kerber, J. Spacecraft 19, 579 (1982).

[70] J. Asmussen, H. H. Lin, B. Manring, and R. Fritz, Rev. Sci. Instrum. 58, 1497 (1987).

[71] Film uniformity measurements by laser interference/reflection technique were conducted by T. Theissen at Michigan State University, East Lansing, Michigan.

[72] A. Masood, M. Aslam, M. A. Tamor and T. J. Potter, J. Electrochem. Soc. 138, L67 (1991)

[73] A. Masood, private communication, Michigan State University, East Lansing, Michigan.

[74] Amplex, 16 Britton drive, bloomfield, connecticut 06002

[75] Shipley company, 91 Bartlett Street, Marlboro, MA 02162

[76] The Raman spectra were provided by Scott Martin at Norton Diamond Film, Northboro, MA.